Intraprocedural Imaging of Cardiovascular Interventions

Michael H. Picard
Jonathan J. Passeri
Jacob P. Dal-Bianco
Editors

Springer

Intraprocedural Imaging of Cardiovascular Interventions

Michael H. Picard • Jonathan J. Passeri
Jacob P. Dal-Bianco
Editors

Intraprocedural Imaging of Cardiovascular Interventions

Springer

Editors
Michael H. Picard
Harvard Medical School
Massachusetts General Hospital
Boston, Massachusetts
USA

Jacob P. Dal-Bianco
Harvard Medical School
Massachusetts General Hospital
Boston, Massachusetts
USA

Jonathan J. Passeri
Harvard Medical School
Massachusetts General Hospital
Boston, Massachusetts
USA

ISBN 978-3-319-29426-1 ISBN 978-3-319-29428-5 (eBook)
DOI 10.1007/978-3-319-29428-5

Library of Congress Control Number: 2016938534

Printed on acid-free paper

This Springer imprint is published by Springer Nature
The registered company is Springer International Publishing AG Switzerland

Preface

While many forms of non-invasive cardiac imaging have been used in association with cardiac procedures for many years, their use gained prominence in the mid-1980s when transthoracic echocardiography became an important component of the percutaneous mitral valvotomy procedure, especially to identify appropriate patients for this procedure. Soon thereafter, the use of transesophageal echocardiography to exclude left atrial thrombus was shown to be a valuable procedure enabling safe DC cardioversion without the need to wait for weeks of pre-cardioversion therapeutic anticoagulation. Most recently, many new and complex transcatheter cardiovascular procedures have been introduced and are radically changing the face of clinical cardiology. A critical part of the success of these new treatments is their optimal intraprocedural guidance by non-invasive imaging. This guidance helps reduce complications and improves outcomes. In fact, a new specialty of "Interventional Non-Invasive Imaging" has evolved and these imagers are a vital member of the treatment team. Three-dimensional echocardiographic imaging is an important skill for these imagers.

In this book, we present a practical approach for the use of imaging in a variety of cardiovascular procedures. We are fortunate to have contributions from the leaders in this field.

We present a wide array of procedures. In addition to the newest techniques such as transcatheter aortic valve replacement and transcatheter mitral valve edge-to-edge repair, we have included guidance of more established procedures such as pericardiocentesis. Also in light of the accelerating use of mechanical circulatory devices in the treatment of advanced heart failure, we discuss the evolving role of imaging in association with these devices. We have also included the technique of optical coherence tomography which is gaining applications in diagnosis of coronary artery disease and as an adjunct to coronary artery interventions.

While we expect that this book will be of value to imagers, we hope that other clinicians and interventionalists can use this as a resource to understand imaging needs during various cardiovascular procedures.

Michael H. Picard, MD
Jonathan J. Passeri, MD
Jacob P. Dal-Bianco, MD

Contents

Contributors

David L. Ain, MD Cardiology Division, Massachusetts General Hospital, Boston, MA, USA

Reza Arsanjani, MD Medicine, Division of Cardiology, Cedars-Sinai Medical Center, Heart Institute, Los Angeles, CA, USA

Jorge Betancor, MD Department of Cardiovascular Medicine, Cleveland Clinic Foundation, Cleveland, OH, USA

Christina Chrysohoou, MD, PhD Division of Cardiology, Emory University School of Medicine, Atlanta, GA, USA

Hippokration Hospital, University of Athens, Athens, Greece

Jacob P. Dal-Bianco, MD, FACC, FASE Division of Cardiology, Department of Medicine, Massachusetts General Hospital, Harvard Medical School, Boston, MA, USA

David M. Dudzinski, MD, JD Divisions of Cardiology, Echocardiography, and Critical Care, Massachusetts General Hospital, Boston, MA, USA

Division of Cardiology, Division of Pulmonary/Critical Care, and Cardiac Ultrasonography Laboratory, Massachusetts General Hospital, Boston, MA, USA

Robert M. Gallagher, MD Cardiology Division, Massachusetts General Hospital, Interventional Cardiology, Boston, MA, USA

Richard A. Grimm, DO, FASE Department of Cardiovascular Medicine, Cleveland Clinic Foundation, Cleveland, OH, USA

Rebecca T. Hahn, MD, FACC, FASE Medicine, Division of Cardiology, The New York Presbyterian Hospital/Columbia University Medical Center, New York, NY, USA

Judy W. Hung, MD Division of Cardiology, Department of Medicine, Massachusetts General Hospital, Harvard Medical School, Boston, MA, USA

Ik-Kyung Jang, MD, PhD Cardiology Division, Harvard Medical School, Boston, MA, USA

Cardiology Division, Massachusetts General Hospital, Boston, MA, USA

Allan L. Klein, MD, FRCP (C), FACC, FAHA, FASE Cardiovascular Medicine, Heart and Vascular Institute, Cleveland Clinic Foundation, Cleveland, OH, USA

Stamatios Lerakis, MD, PhD Division of Cardiology, Emory University Hospital, Atlanta, GA, USA

Nino Mihatov, MD Department of Medicine, Massachusetts General Hospital, Boston, MA, USA

David B. Min, MD Heart and Vascular Institute, Cleveland Clinic Foundation, Cleveland, OH, USA

Ankit Parikh, MD Department of Internal Medicine, Emory University School of Medicine, Atlanta, GA, USA

Yong Hyun Park, MD Division of Cardiology, Department of Medicine, Massachusetts General Hospital, Harvard Medical School, Boston, MA, USA

Jonathan J. Passeri, MD Division of Cardiology, Department of Medicine, Corrigan Minehan Heart Center, Massachusetts General Hospital, Boston, MA, USA

Antonio Perez, MD Department of Cardiovascular Medicine, Cleveland Clinic Foundation, Cardiovascular Imaging, Cleveland, OH, USA

Matthew J. Price, MD Cardiac Catheterization Laboratory, Scripps Green Hospital, Scripps Clinic, La Jolla, CA, USA

Scripps Translational Science Institute, La Jolla, CA, USA

Division of Cardiovascular Diseases, Scripps Clinic, La Jolla, CA, USA

David S. Rubenson, MD Cardiovascular Diseases, Cardiac Non-Invasive Laboratory, Scripps Clinic, La Jolla, CA, USA

Danita M. Yoerger Sanborn, MD, MMSc Division of Cardiology, Department of Internal Medicine, Paul Dudley White Associates, Massachusetts General Hospital, Boston, MA, USA

Muhamed Saric, MD, PhD Department of Medicine, Leon H. Charney Division of Cardiology, New York University Langone Medical Center, New York, NY, USA

Robert J. Siegel, MD, FACC, FASE Division of Cardiology, Cedars-Sinai Medical Center, Heart Institute, Los Angeles, CA, USA

Nathaniel R. Smilowitz, MD Department of Medicine, Leon H. Charney Division of Cardiology, New York University Langone Medical Center, New York, NY, USA

Michael R. Smith, MD Division of Cardiovascular Diseases, Scripps Clinic, La Jolla, CA, USA

Transesophageal Echocardiographic-Guided Cardioversion

1

David B. Min and Allan L. Klein

Abstract

The incidence and prevalence of atrial fibrillation (AF) continues to grow especially as the population ages. The uncoordinated atrial activation and subsequent ineffective atrial contraction is a strong stimulus for left atrial (LA) thrombus formation especially in the LA appendage. AF is associated with increased risk of stroke, heart failure, and all-cause mortality. The presence of LA thrombus in AF portends a poor prognosis. Direct current cardioversion (DCCV) is the most effective method of restoring sinus rhythm and, with it there is relief of symptoms, improved LV filling, reversed atrial remodeling, and possibly reduced cardio-embolic risk. However, there are significant risks of systemic embolization following DCCV if LA thrombus is present. Transesophageal echocardiography (TEE) is an ideal non-invasive imaging modality to detect thrombus in the LA and especially in the LA appendage. Its proper use can lead to earlier DCCV for AF and improve safety of DCCV in AF. A key part of this strategy is proper use of anticoagulation therapy. This chapter illustrates the important role of TEE in patient evaluation and risk stratification prior to cardioversion.

Keywords

Optical coherence tomography • Intra-coronary imaging • Acute coronary syndrome • Coronary artery disease • Intravascular ultrasound • Percutaneous coronary intervention • Plaque rupture • Calcific nodule • Plaque erosion • Instent restneosis • Neointimal proliferation • Neoatherosclerosis

Introduction

Since Willem Einthoven's first electrocardiograph description of "pulsus inaqequalis et irregularis" in 1906 [1], atrial fibrillation (AF) is now recognized as the most common arrhythmia worldwide [2]. With the prevalence expected to rise to 5.6–12.0 million in the United States by 2050 [3], AF is a growing epidemic, with the greatest impact felt on the aging population [4]. Furthermore, the national financial liability of AF has been estimated to be $26.0 billion annually, with greater than $5 billion attributed to direct AF treatment costs [5, 6]. The magnitude of this public health problem is likely substantially underestimated, as AF often manifests little to no symptoms and can go unrecognized.

AF represents a common final phenotypic pathway resulting from a multitude of pathophysiologic processes [7] which alter atrial tissue thus promoting uncoordinated atrial activation and subsequently ineffective atrial contraction [8]. The resultant blood stasis within the left atrium (LA) and left

D.B. Min, MD
Heart and Vascular Institute, Cleveland Clinic Foundation, Cleveland, OH, USA
e-mail: mind@ccf.org

A.L. Klein, MD, FRCP (C), FACC, FAHA, FASE (✉)
Cardiovascular Medicine, Heart and Vascular Institute, Cleveland Clinic Foundation, Cleveland, OH, USA
e-mail: kleina@ccf.org

M.H. Picard et al. (eds.), *Intraprocedural Imaging of Cardiovascular Interventions*, DOI 10.1007/978-3-319-29428-5_1

atrial appendage (LAA) in conjunction with AF-associated endothelial and extracellular atrial abnormalities and inflammatory-mediated coagulation changes fulfill Virchow's triad for thrombogenesis [9]. It is in this hypercoagulable milieu that intra-atrial thrombi form. The Framingham Heart Study found that AF is associated with a four to fivefold increased risk of thromboembolic events [10]. Multiple studies have linked AF to increased long-term risks of stroke, heart failure, and all-cause mortality [11, 12]. More specifically, the identification of thrombus in AF portends a poor prognosis with studies showing an embolic risk of up to 10.4 % per year and an annual mortality rate of 15.8 % [13].

A variety of diagnostic and therapeutic paradigms have been deployed to understand and alter, if not prevent, the downstream consequences of AF, including systemic thromboembolism and impaired diastolic left ventricular function. First described by Dr. Bernard Lown in 1962 [14], direct current cardioversion (DCCV) has been utilized to restore normal sinus rhythm to relieve symptoms, improve LV filling, reverse atrial remodeling, and possibly reduce cardioembolic risk [15]. DCCV is the most effective method of restoring sinus rhythm with a reported short-term success rate of 75–93 % [16, 17]. However, DCCV is not completely benign; aside from the risks associated with sedation, there is significant a risk of systemic embolization after DCCV [18–21]. Since the 1930s [22], the LAA has known to be a location of thrombus formation. Since then, consideration effort has been made to detect the presence of thrombi within the LA and LAA and alter the risk of systemic embolization.

While transthoracic echocardiography (TTE) has excellent overall image quality, transesophageal echocardiography (TEE) offers superior spatial resolution to TTE [23] and is the reference standard for assessing the LAA for thrombus formation with high sensitivity (92–100 %), specificity (98–100 %), and negative predictive value (98–100 %) [8, 24–27]. Through case studies, this chapter aims to illustrate the important role of TEE in patient evaluation and risk stratification prior to cardioversion.

Left Atrial Appendage Structure and Function

Located lateral to the LA and extending over the atrioventricular groove towards the left circumflex artery in close proximity to the left ventricular free wall [28], the LAA is a blind, trabeculated cul-de-sac. The trabeculations (or pectinate muscles) reflect its embryological origins. Whereas the smooth-walled LA, with whom the LAA is contiguous, is formed from the primordial pulmonary veins, the LAA is a remnant of the embryonic LA [29, 30]. There is a fold of serous pericardium that forms a ridge between the LAA orifice and the left superior pulmonary vein; this structure is also known as the warfarin ridge, Q-tip sign, posterolateral ridge, and ligament (or fold) of Marshall [31]. This prominence can be mistaken for a tumor or thrombus due its undulating motion and/or side lobe artifacts arising from echoes reflecting off the ridge [32, 33].

The LAA has a highly variable morphology; an autopsy study noted that 90 % of the LAA examined had multiple lobes, with the presence of two (80 %) distinct lobes being the most common and some specimens having as many as five lobes [34]. Based on its lobular/angular morphology, the LAA shape has been classified as: "chicken wing" (48 %), "cactus" (30 %), "windsock" (19 %), and "cauliflower" (3 %). In a multimodality imaging study of AF-patients, LAA shape correlated with risk of stroke; patients with atrial fibrillation who had "chicken wing" morphology were 79 % less likely to have a stroke/TIA history compared to the other shapes [35]. Consistent with such lobular heterogeneity, the LAA has great variation in length (ranging from 16 to 51 mm) and volume (0.7–19.2 mL) [36]. Likewise, the orifice connecting the LA and LAA, which typically lies superiorly and laterally, is an eccentric, elliptical structure with a minimal diameter ranging from 4 to 27 mm and a maximum diameter from 10 to 40 mm [36, 37]. The complexity and variability of LAA shape, size, and number of lobes underscores the importance of fully interrogating the LAA from multiple different angles/planes to detect possible thrombus prior to cardioversion.

Whereas the key function of the LA in modulating left ventricular filling as a reservoir, conduit, and pump is well recognized [38], the role of the LAA is less clear. It has been postulated given its increased distensibility, the LAA may serve as a decompression chamber during ventricular systole and in states of increased LA pressure and volume overload [39]. The LAA may further regulate volume homeostasis by secreting atrial natriuretic peptide and b-type natriuretic peptide in response to activation of stretch receptors within the LAA that ultimately results in diuresis [30, 40–43].

The trabeculated pectinate musculature of the LAA actively contracts in young, healthy individuals with normal intracardiac conduction with a distinctive pattern [34, 39]. LAA flow velocities can be assessed using pulsed wave Doppler by placing the sample volume 1–2 cm from the orifice within the LAA chamber, ideally in the midesophageal 0° or 90° planes [31]. In patients with a normal sinus rhythm, the characteristic pattern is quadriphasic (Fig. 1.1), as described below [44–46]:

- Early diastolic LAA emptying: In early diastole, a low-velocity positive wave occurs following the mitral-inflow E wave that represents the drop in LA pressure following opening of the MV and external compression of the LAA due to LA distension. The average early diastolic emptying velocity is 20–40 cm/s and is related to mitral E and PV diastolic velocities.

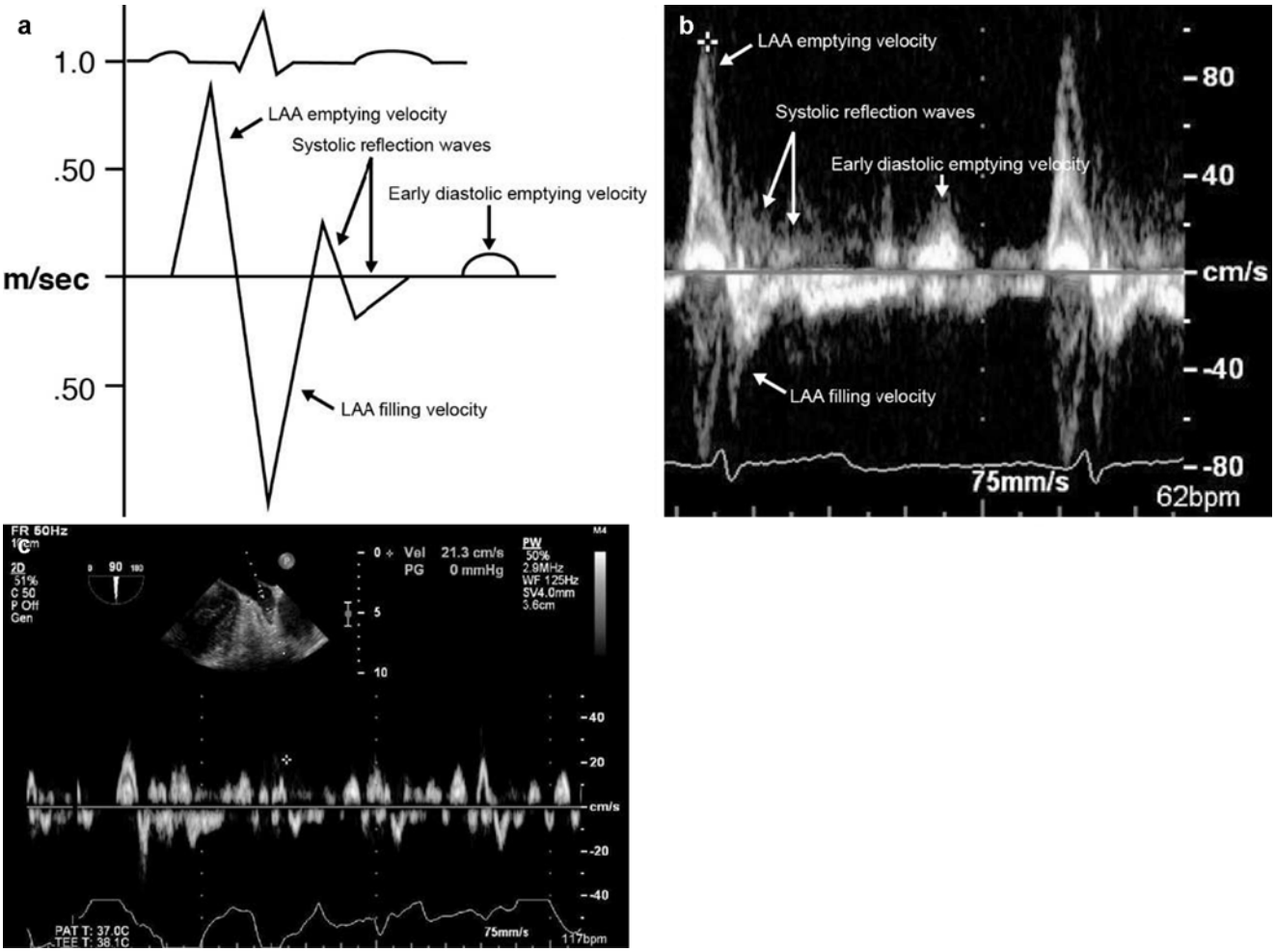

Fig. 1.1 LAA flow pattern in sinus rhythm (**a**, **b**) and AF (**c**)

- Late diastolic LAA emptying: Starts in late diastole immediately after the p-wave and represents LAA contraction and emptying. The late diastolic emptying velocity, which is typically 50–60 cm/s, is the largest wave in sinus rhythm and is a marker of LAA contractile function. This velocity correlates with LAA ejection fraction, LA size, and LA pressure.
- LAA filling: The retrograde velocity wave following late diastolic emptying in early systolic reflects LAA elastic recoil and relaxation. The average LAA filling velocity is 40–50 cm/s; the magnitude of the LAA filling velocity is inversely related to velocity of LAA contraction.
- Systolic reflection waves: After LAA filling in early systole, multiple low-velocity alternating inflow-outflow waves are seen; the functional significance of these waves has yet to be definitively determined.

In AF, the LAA develops endocardial thickening with fibrosis and loses pectinate muscle; this negative remodeling results in stretching, dilation, and decreased LAA contractility predisposing it to stagnant blood flood and thrombosis [47]. Some of most devastating consequences of AF including thromboembolic sequelae; over 90 % of thrombi in non-valvular AF have been localized to the LAA [48]. Thrombi have been found in patients who have had AF for <3 days [49] as well as patients who had been receiving oral anticoagulant therapy for 4 weeks [50]. Point scoring systems such as $CHADS_2$ and CHA_2DS_2-VASc have been developed and validated assessing the risk of ischemic stroke in non-valvular AF patients [51, 52]. A subgroup analysis of a transesophageal study found that patients who had a $CHADS_2$ score ≥3 had significantly higher mortality than those with lower scores; however, the $CHADS_2$ scoring system was not reliable in predicting risk for left atrial appendage thrombus formation, especially in patients with low $CHADS_2$ scores [53]. Given the significant stakes involved, careful scrutiny of the LAA using TEE and/or other non-invasive modalities is often necessary to exclude thrombi prior to cardioversion.

Transesophageal Echocardiography Evaluation of LA/LAA

Indications for TEE in AF

Given the risk of clinical significant thromboembolism in AF, risk reduction strategies have been employed to reduce the chance of an embolic event before and after DCCV through the use of anticoagulation and/or imaging modalities [54, 55]. Up until the early 1990s, the conventional strategy to reduce the risk of thromboembolic events after DCCV for AF or atrial flutter ≥48 h was to anticoagulate with warfarin for at least 3 weeks before DCCV [56, 57]; this strategy is still a Class I recommendation from the AHA/ACC/HRS [8]. Anticoagulation post-cardioversion is necessary for AF of >48 h duration (and AF <48 h with risk factors for thromboembolism) due to the variability of return of coordinated atrial function ("atrial stunning"); retrospective analysis of pooled data from 32 studies found that 98 % of embolic events occurred within 10 days of DCCV [54].

With the advent of TEE and through the landmark study entitled Assessment of Cardioversion Using Transesophageal Echocardiography (ACUTE), TEE was shown to be effective in guiding and expediting DCCV with short-term anticoagulation [58]. This large, multicenter, randomized, prospective trial of 1,222 patients undergoing DCCV for AF of >48 h duration compared a TEE-guided short-term anticoagulation strategy prior to DCCV to a conventional (3 week) anticoagulation strategy and found no significant difference in embolic events. The TEE-guided group had less hemorrhagic events and shorter time to DCCV, thus reducing the time for possible adverse atrial remodeling due to delays in the return of atrial function. Similarly, the follow-up ACUTE II trial investigated the safety of TEE-guided DCCV using low-molecular weight heparin (enoxaparin) versus unfractionated heparin [59]. The study found that there were no differences in safety (embolic events, bleeding, or deaths) between the two groups but that the enoxaparin TEE-guided approach had a shorter median length of hospitalization. The Anticoagulation in Cardioversion using Enoxaparin (ACE) trial also similarly showed non-inferiority of enoxaparin to unfractionated heparin plus a vitamin K antagonist in reducing significant events post TEE-guided DCCV [60].

Since the ACUTE I trial, TEE-guided cardioversion has become increasingly popular; in the setting of increasing costs of general diagnostic imaging, appropriateness criteria were developed. In 2011, a multi-society writing committee, including the ACC, AHA and American Society of Echocardiography (ASE), published updated appropriate use guidelines regarding the use of TEE-guided cardioversion: TEE is appropriate to "facilitate clinical decision making with regards to anticoagulation, cardioversion, and/or radiofrequency ablation"; TEE is inappropriate when "the decision has been made to anticoagulate and not to perform cardioversion" [61]. An analysis by Grewal et al. in 2012 found that the vast majority of TEEs performed before DCCV were appropriate (only 2.7 % were found to be inappropriate); the most common indications were symptomatic AF and CHF/hemodynamic compromise [62]. The 2014 AHA/ACC/Heart Rhythm Society (HRS) Guideline for the Management of Patients with Atrial Fibrillation provides further recommendations on the evaluation and treatment of AF, including guidance on direct-current cardioversion. Per this set of guidelines, TEE prior to cardioversion is appropriate (Class IIa recommendation) for patients with AF or atrial flutter of 48 h or longer who have not been anticoagulated for the proceeding 3 weeks, provided that anticoagulation is achieved before TEE and can be maintained after potential cardioversion for at least 4 weeks [8].

Performing TEE in AF

Despite being considered a semi-invasive procedure that is generally performed with conscious sedation, the safety profile of TEE has been well documented with a <0.02 % major complication rate when performed by an experienced clinician [63–65]. The American College of Cardiology (ACC) and American Heart Association (AHA) have published guidelines establishing TEE competence [66]. To help guide the sonographer, the American Society of Echocardiography and the Society of Cardiovascular Anesthesiologists have published joint guidelines on performing a comprehensive TEE examination that provides recommendations on TEE indications, patient selection, monitoring during sedation, and general imaging views [31]. One caveat to consider when monitoring sedated patients with atrial fibrillation is that blood pressure (BP) measurements may fluctuate due to high beat-to-beat variability in ventricular filling time, stroke volume, and contractility [67].

Once the TEE probe is safely intubated into the mid-esophagus in a neutral position, the LA is the near-field structure, which will make it difficult to image the entire structure from a single plane [31]. Thus, multi-planar assessment and sweeping from the inter-atrial septum to lateral wall (rotating clockwise to counterclockwise) looking for potential thrombi or masses is needed. The LA is a muscular structure with small pits and troughs; abnormal increases in wall thickness may be sequelae of mural thrombus or endocarditis [31, 68].

The LAA is frequently best visualized in the mid-esophageal window starting at 0°. As a lateral structure, it may require slight counterclockwise rotation and flexion or withdrawal of the probe to a more cranial position to center

the LAA within the plane [69]. Given the complexity of its shape and the importance of excluding a potential thrombus, it is imperative that the LAA be systematically imaged from multiple imaging planes (i.e. mid-esophageal 0°, 45°, 90°, 120°, 160°); often the additional lobe(s) of the LAA will only be appreciated at angles >100° [69] (Fig. 1.2). Simultaneous, multiple-plane assessment modalities (such as biplane or multiplane) can be very helpful in assessing the LAA for abnormalities from orthogonal views.

In evaluating possible thromboembolic sources in AF, the TEE should not be limited solely to the LA and LAA. Complex aortic plaque (4 mm and the presence of mobile components) has been linked to increased stroke risk; furthermore, aortic atheroma or plaque is prevalent in patients with AF [70–72] (Fig. 1.3a). While assessment of the LV via TEE is limited due to foreshortening of the apical segments, abnormal findings on TEE may prompt assessment via alternative modalities. Thorough evaluation of the MV and AV is also indicated, for rheumatic valvular heart disease is a well-recognized stroke risk factor, as is the presence of a mechanical prosthetic valve, even in the absence of atrial fibrillation [73]. For patients with atrial fibrillation who may undergo pulmonary vein isolation in the future, one can also assess the pulmonary vein anatomy at time of TEE prior to DCCV to guide potential electrophysiology procedures; the Role of Transeosphageal Echocardiography Compared to Computed Tomography in Evaluation of Pulmonary Vein Ablation for Atrial Fibrillation (ROTEA) study showed that TEE provided both anatomical and function information that complemented CT [74]. Other major sources of cardioembolic strokes are infective and non-infective endocarditis, atrial myxomas, atrial and ventricular septal defects, and mitral annular calcification; thus a detailed TEE prior to DCCV can further identify potentially relevant sources of embolism beyond the LAA that can significant impact clinical management [75] (Fig. 1.3b–e).

The LAA is often surgically excised or excluded at time of concomitant open-heart surgery procedures in an attempt to prevent future thromboembolic events. However, TEE studies have reported patent flow between the LA and the residual LAA following surgical LAA intervention, up to 60 % [76–78]. Patients who had high persistent flow into the LAA after exclusion were also found to have a high prevalence of LAA thrombus [77]. Furthermore, differences in LAA patency rates have been found depending on technique and that the differences can been seen in the early (<30 day) post-operative period [77]. Given reports of early thrombus formation <48 h of onset of atrial fibrillation in patients following open-heart surgery [79], it is important not to assume that a history of "LAA ligation" is protective. Careful scrutiny of the structure, function, and flow characteristics of the remnant LAA is needed to exclude the presence of thromboembolic risks.

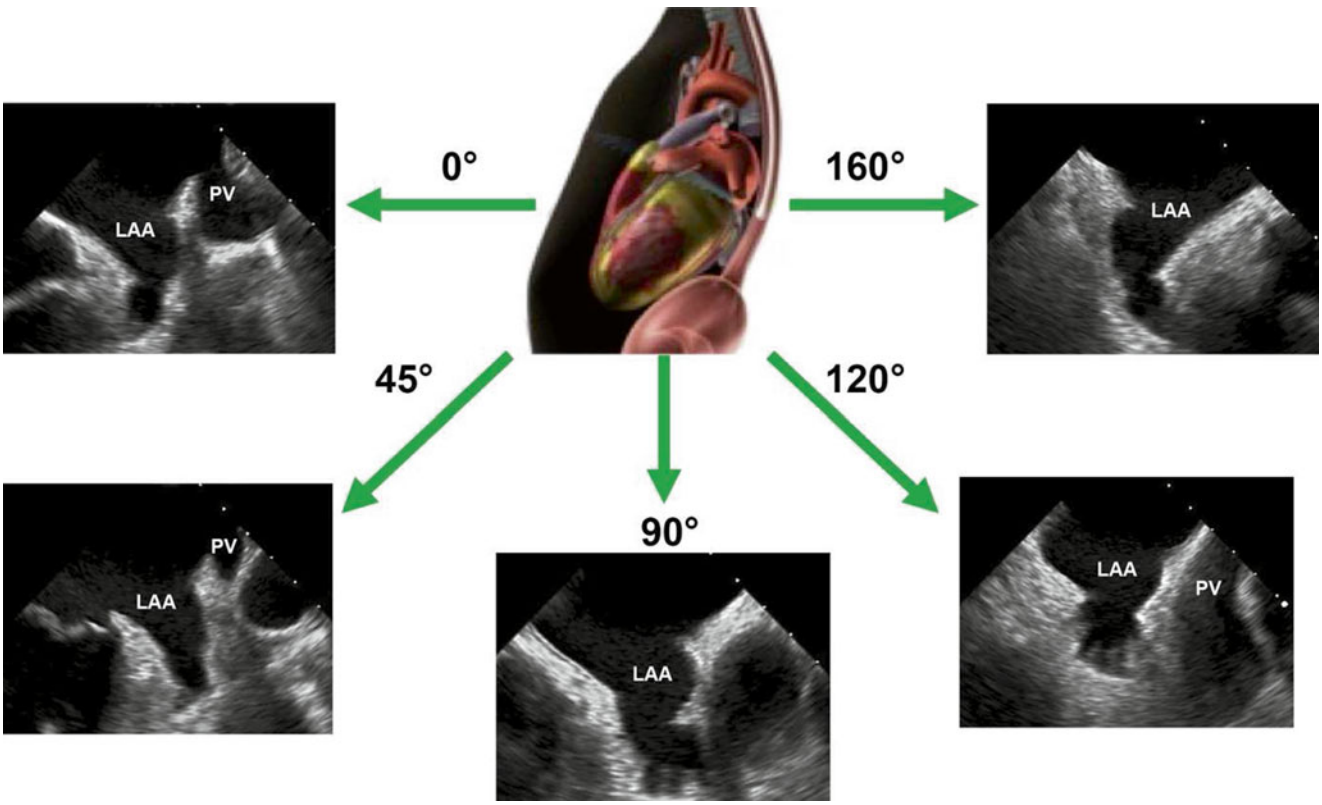

Fig. 1.2 Multiplanar imaging of LAA at different angles

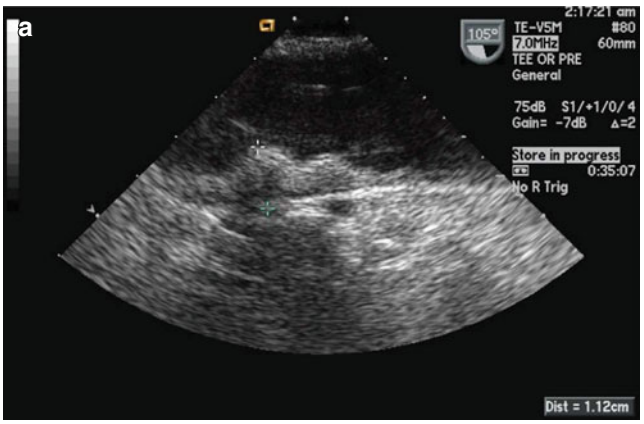
a
2:17:21 am
TE-V5M
7.0MHz
TEE OR PRE
General
75dB S1/+1/0/4
Gain= -7dB
Store in progress
0:35:07
No R Trig
Dist = 1.12cm

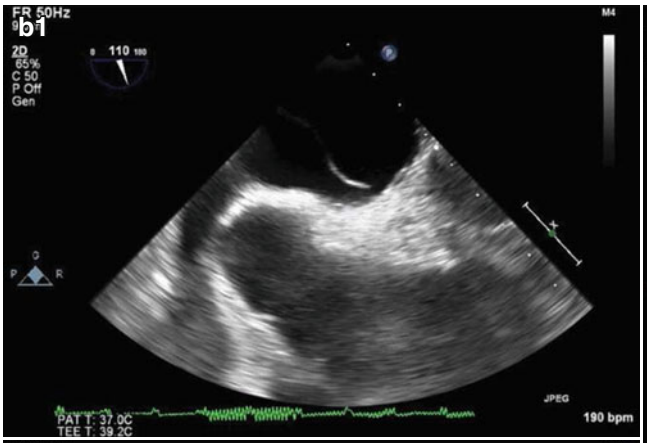
b1
FR 50Hz
2D
65%
C 50
P Off
Gen
JPEG
PAT T: 37.0C
TEE T: 39.2C
190 bpm

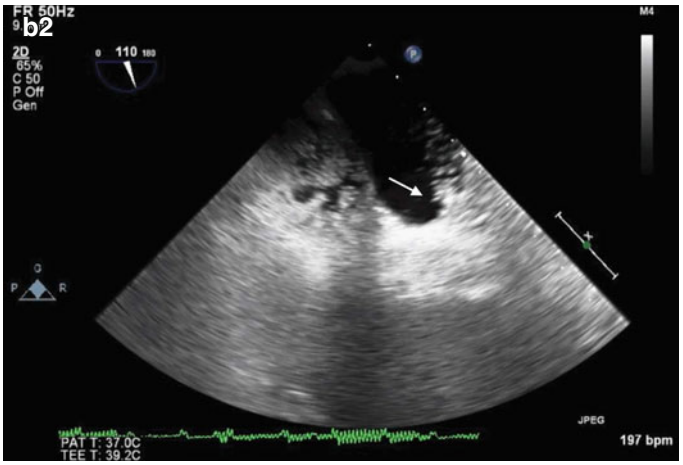
b2
FR 50Hz
2D
65%
C 50
P Off
Gen
JPEG
PAT T: 37.0C
TEE T: 39.2C
197 bpm

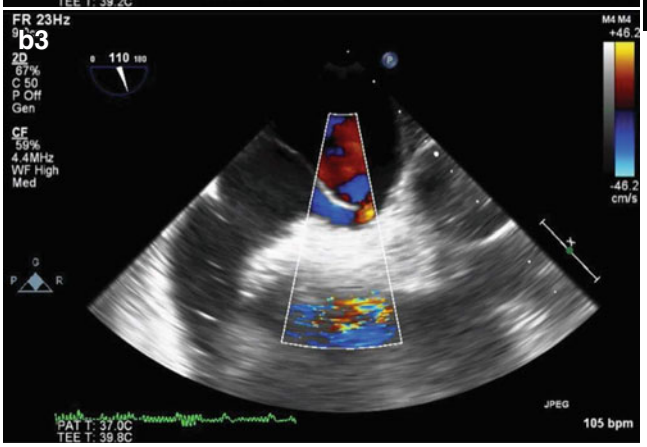
b3
FR 23Hz
2D
67%
C 50
P Off
Gen
CF
59%
4.4MHz
WF High
Med
cm/s
JPEG
PAT T: 37.0C
TEE T: 39.8C
105 bpm

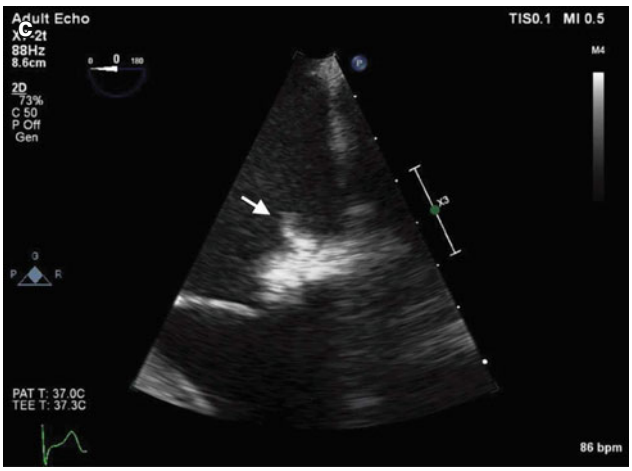
c
Adult Echo
TIS0.1 MI 0.5
88Hz
8.6cm
2D
73%
C 50
P Off
Gen
PAT T: 37.0C
TEE T: 37.3C
86 bpm

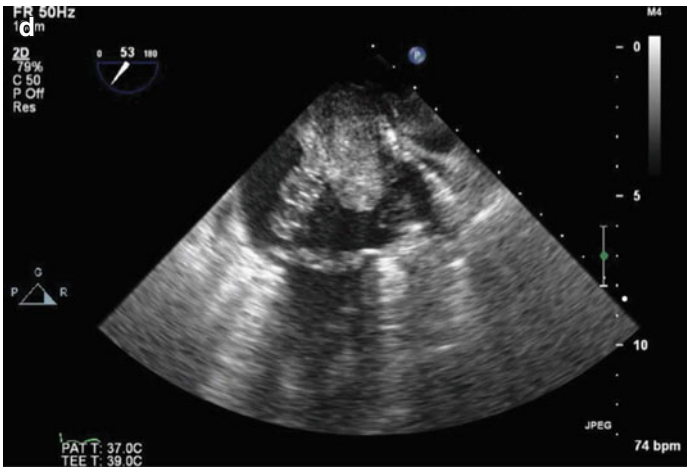
d
FR 50Hz
2D
79%
C 50
P Off
Res
JPEG
PAT T: 37.0C
TEE T: 39.0C
74 bpm

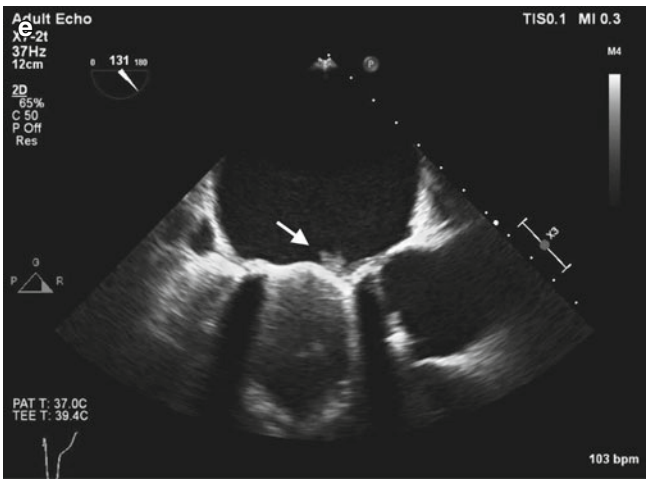

Fig. 1.3 (continued)

TEE Abnormalities in AF

Blood stasis secondary to ineffective LAA contraction in AF can be visualized on two-dimensional (2D) TEE as a spectrum ranging from spontaneous echocontrast (SEC) to sludge to thrombus formation [80, 81] (Fig. 1.4). SEC, also known as "smoke", has a slow, swirling motion of variable echodensity that represents non-laminar, low blood flow velocities [82, 83]. Reflecting increased erythrocyte aggregation, and presence of fibrinogen, SEC has been seen in up to 60 % of patients with AF [84–86]. A precursor of thrombus formation, SEC has been strongly associated with subsequent thrombotic events [58, 87]. However, the use of aspirin or warfarin does not influence the presence of SEC as the underlying hemodynamic abnormalities are persistent despite anticoagulation therapy [88]. Despite attempts to quantitative the degree of

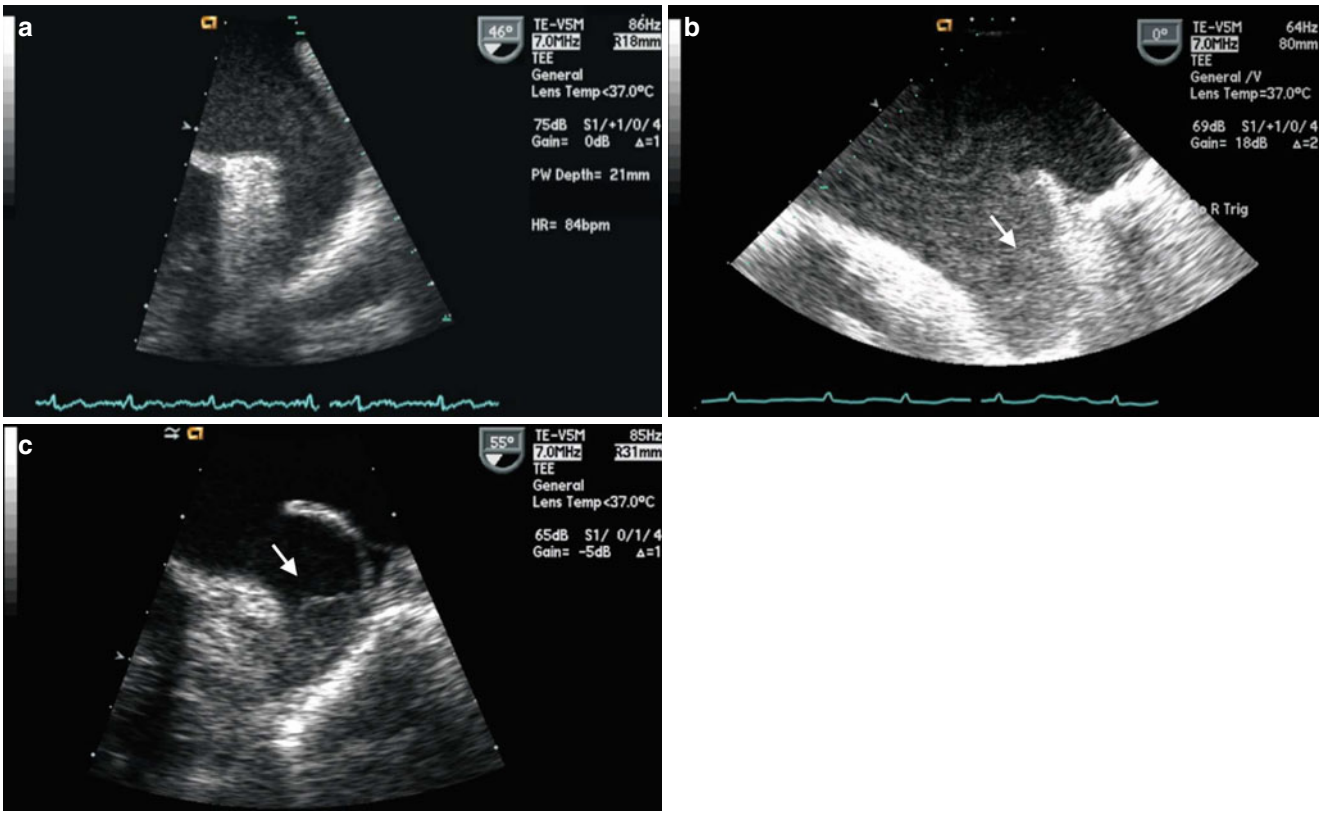

Fig. 1.4 Spectrum of LAA Thrombogenic Milieu (**a**) shows severe spontaneous echocontrast (*SEC*) in the LAA. (**b**) Shows severe SEC and layered sludge within the LAA. (**c**) Shows thrombus that has formed in the LAA

Fig. 1.3 Potential sources of emboli. (**a**) Shows severe atheroma (1.2 cm) in the mid-aortic arch. (**b**1) Shows a patent foramen ovale (PFO). (**b**2) Shows agitated saline flowing through the PFO. (**b**3) Shows color flow through the PFO. (**c**) Shows mobile mitral annular calcification. (**d**) Shows a large mass in the LA that on pathology was revealed to be sarcoma. (**e**) Shows a vegetation on a prosthetic mitral valve consistent with prosthetic endocarditis

spontaneous echo contrast [89–91], it is general graded as absent, mild, or severe [69].

Sludge represents a progression of SEC in the continuum towards thrombus formation. As a thrombus in situ, sludge has a gelatinous, layered quality, and is seen throughout the cardiac cycle but is not well circumscribed [92]. It differs from thrombus, which is defined as a well circumscribed, uniformly echodense, highly reflective mass that is distinct from the LA or LAA endocardium and is present throughout the cardiac cycle [31, 93]. It can be difficult to differentiate sludge from thrombus; prolonged single or simultaneous multi-planar observation may be necessary. While the clinical implications of sludge remains debated, there has been recent evidence that suggests that sludge has prognostic implications [94]. Lowe et al. followed 340 patients at the Cleveland Clinic for 6.7 ± 3.7 years who underwent TEE prior to DCCV or radiofrequency pulmonary vein isolation (PVI); those who were found to have sludge were found to have high rates of thromboembolism and death comparable with patients with LAA thrombus. Sludge was also found to be independently associated with subsequent thromboembolic events and all-cause mortality [92]. While the presence of thrombus is an absolute contraindication to DCCV or PVI, it remains debated whether identification of sludge precludes safe DCCV [95].

Pectinate muscles, reverberation artifact from the warfarin ridge, septa between multiple LAA lobes, and severe SEC can mimic LAA thrombi [96, 97] and cause false positive TEE results. The use of simultaneous multi-planar and/or three-dimensional imaging, echocontrast agents, and other adjunctive TEE techniques can assist in distinguishing between true LAA thrombi, artifacts, and intrinsic structures.

Adjunctive TEE Techniques

Given that in spite of multiplanar 2D interrogation of the LAA, small thrombi (<2 mm) can be missed [31], clinicians may elect to further assess the LAA utilizing adjunctive TEE techniques.

Three-Dimensional TEE

While 3D TEE does not have the temporal or spatial resolution of 2D TEE, the lobular morphology of the LAA is well suited to 3D TEE imaging and its ability to visualize and reconstruct cardiac structures from multiple vantage points [98, 99]. Since it provides a more comprehensive assessment of the multiple LAA lobes, 3D TEE has shown to be more accurate in estimating LAA geometry and size. 3D TEE may be less influenced by artifacts, such as reverberations off of the warfarin ridge, and more easily differentiate adjacent structures, such as pectinate muscles versus thrombi [100]. Real-time 3D TEE has been valuable in assessment of the LAA for closure devices and placement of the device within the LAA orifice [101]. Since 3D TEE is in its relative infancy, data regarding the sensitivity and specificity for detecting LAA thrombi is still needed.

Echocontrast Agents

Dense SEC and reverberation artifacts can limit the assessment of the LAA cavity and/or mimic thrombi. Ultrasound contrast agents can enhance imaging of the LAA by suppressing SEC and uncovering true filling defects due to underlying thrombi within the LAA [102, 103]. By completely opacifying the LAA cavity, an echocontrast-enhanced TEE can improve the structural assessment of a multilobular LAA. Thus, in the setting of inconclusive TEE images, contrast enhancement can improve the ability to identify or exclude LA and LAA thrombi with minimal risk, although it does add incremental cost and time to the TEE examination [104].

Doppler

In addition to evaluating the anatomy of the LAA, evaluating the contractile activity of the LAA by pulsed Doppler can assist in assessing the risk of thrombus formation. Replacing the characteristic quadriphasic Doppler pattern in sinus rhythm, the LAA emptying velocities can be either an irregular sawtoothed pattern or absent [105–107]. In the sawtooth pattern, two types of emptying waves can be seen: a high frequency, highly variable, low amplitude wave during systole and a higher velocity wave in early diastole before the QRS. The low amplitude fibrillatory wave is a marker of the AF cycle length, while the diastolic LAA emptying wave reflects mitral valve opening and suction secondary to LV relaxation [44] and should be measured at time of TEE assessment. Low diastolic LAA emptying velocities reflect poor LAA mechanical function and have been associated with presence of SEC and risk of thromboembolism; velocities <20 cm/s has been associated with LAA thrombus and strongly correlated with higher incidence of stroke [11, 108, 109]. LAA diastolic flow velocities >40 cm/s has been shown to predict greater likelihood of sustained normal sinus rhythm for 1 year after cardioversion [110].

Additional Echo Assessment Techniques

Given the prevalence of atrial fibrillation, there are a number of different studies exploring novel methods of further assessing the LA, LAA, and the risk of thrombus formation.

Strain-based techniques, including tissue Doppler imaging and speckle tracking, have been shown to correlate to presence of LAA thrombus, reflecting poor LAA contractile function and low emptying velocities [90, 111–116]. Motoki et al. and others have also assessed the relationship between left atrial strain, LA contractile function, and the maintenance of sinus rhythm for atrial fibrillation [117–119]. Further validation of these techniques is needed before widespread adoption, but significant interest remains in further development of non-invasive echo parameters.

Summary

TEE has become widely adopted in assessment of patients with atrial fibrillation prior to cardioversion. From assessment of the multilobular structure of the LAA to evaluating its contractile function, TEE provides a valuable tool in detecting the presence of LAA thrombus and assessing the risk of stroke. Given the growing epidemic of atrial fibrillation and the clinical significance of thromboembolism, TEE will continue to develop as a tool for clinicians as a screening and diagnostic modality.

Acknowledgement The authors acknowledge the invaluable secretarial assistance of Marie Campbell.

TEE-Guided Direct Current Cardioversion Cases

Case 1: Thrombus (Fig. 1.5a–g)

A 70 year-old woman presents to the emergency department with shortness of breath. She has a past medical history significant for hypertension, heart failure with preserved ejection fraction, and apical variant hypertrophic cardiomyopathy. She states that she was in her usual state of health when she drifted off to sleep while watching TV. She woke up short of breath but denies any chest pain, fevers, or cough. She intermittently takes her heart failure medications, including her diuretic. She was taken by a family member to the emergency room, where on arrival, she was in respiratory distress, hypertensive, and tachycardic, with a blood pressure of 182/90 mmHg, heart rate of 126 beats per minute, and respiratory rate of 44 breaths per minute, with a oxygen saturation of 100 % on room air. Her initial exam as noted for irregular, tachycardic heart rate, bilateral crackles over her lung fields, and mild lower extremity edema. Her chest x-ray was consistent with pulmonary edema and her laboratory work-up was unremarkable, including negative cardiac enzymes, except for an elevated beta-naturetic pepitide level. Her ECG showed atrial fibrillation, which was a new diagnosis. She was started on a nitroglycerin infusion, placed on a non-invasive positive pressure ventilator (NIPPV), and given IV furosemide. With diuresis, she was quickly weaned off NIPPV and the nitroglycerin drip less than 24 h after presentation. Given her new diagnosis of atrial fibrillation, she was also started on IV heparin with plan for TEE-guided DCCV.

Her TEE revealed severe SEC in her LA and LAA, which had a large primary lobe and smaller adjacent lobe. There was a large, mobile echodensity in the LAA, which prolapsed into the left atrium, which was consistent with thrombus. Her LAA peak emptying velocity was 38 cm/s. Of note, a TTE performed prior to her TEE showed spontaneous echocontrast but did not detect any thrombus in the LA.

Her elective DCCV was canceled and she was bridged on IV heparin and started on warfarin therapy until her INR was >2. She was discharged with outpatient follow-up; at her clinic visit, she was noted to have self-converted into normal sinus rhythm. There were no obvious clinical manifestations of thromboembolism on history or physical exam.

Clinical Pearl

Regarding utilizing TTE to detect thrombus, the Comprehensive Left Atrial Appendage Optimization of Thrombus (CLOTS) multicenter pilot study demonstrated that TTE may be useful in detecting thrombus when utilizing harmonic imaging combined with IV echocontrast. In that study, LAA wall tissue Doppler velocities also correlated to the presence of sludge or thrombus (apical E velocity ≤9.7 cm/s, anterior S velocity ≤5.2 cm/s) [120]. TEE, however, remains the gold standard for LAA thrombus detection. While a majority of patients have a multilobular appendage, which has been shown to be independently associated with thrombus formation, 20 % of subjects in an autopsy study had a single lobe [34, 121]. Simultaneous multiplanar imaging can be essential in determine the lobular structure of the LAA and detecting possible thrombus.

Case 2: SEC/Sludge/Thrombus (Fig. 1.6)

A 69 year-old man presents to outpatient clinic with increasing fatigue. He has a past medical history significant for atrial fibrillation, hypertension, hyperlipidemia, sleep apnea, congestive heart failure, and diabetes. He has a known non-ischemic cardiomyopathy with left ventricular systolic ejection fraction of 20 %. He has an ICD that was placed for primary prevention of sudden cardiac death. He has been compliant with his medications, including his warfarin for CVA prevention ($CHADS_2$ risk score = 3, 5.9 %/year risk of thromboembolic event, CHA_2DS_2-VASc risk score = 4, 9.3 %/year risk of stroke) as well as his heart failure regimen. He was diagnosed with atrial fibrillation 6 months prior to

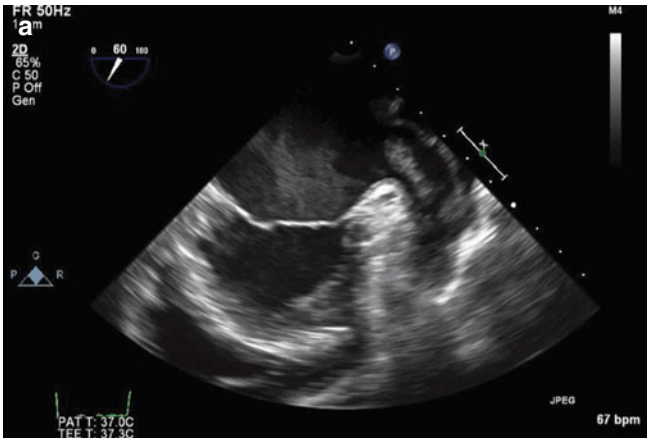
a
FR 50Hz
2D
65%
C 50
P Off
Gen
PAT T: 37.0C
TEE T: 37.3C
67 bpm

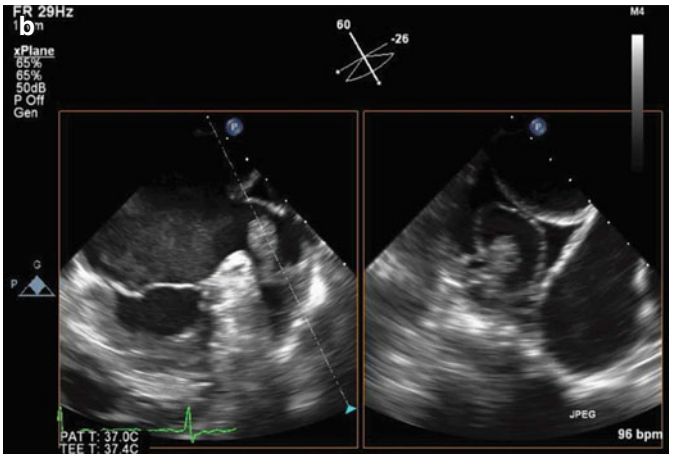
b
FR 29Hz
xPlane
85%
65%
50dB
P Off
Gen
60
-26
PAT T: 37.0C
TEE T: 37.4C
96 bpm

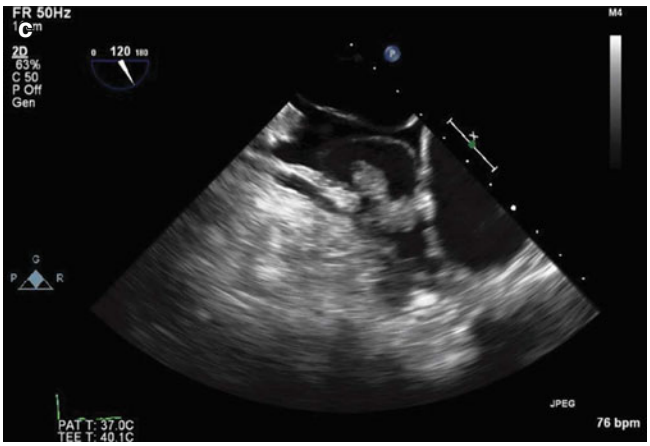
c
FR 50Hz
2D
63%
C 50
P Off
Gen
PAT T: 37.0C
TEE T: 40.1C
76 bpm

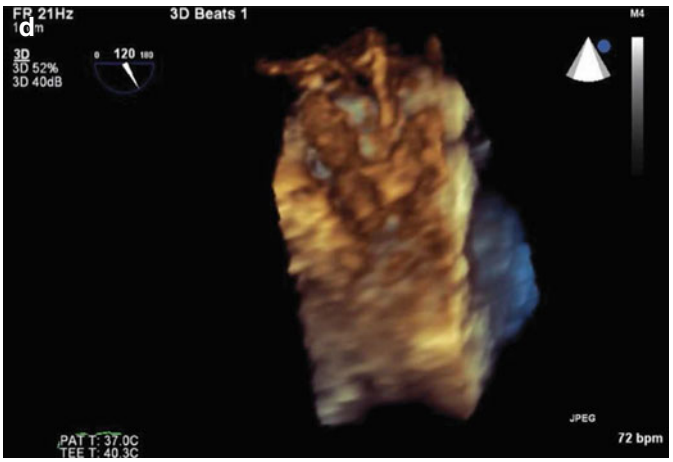
d
FR 21Hz
3D Beats 1
3D
3D 52%
3D 40dB
PAT T: 37.0C
TEE T: 40.3C
72 bpm

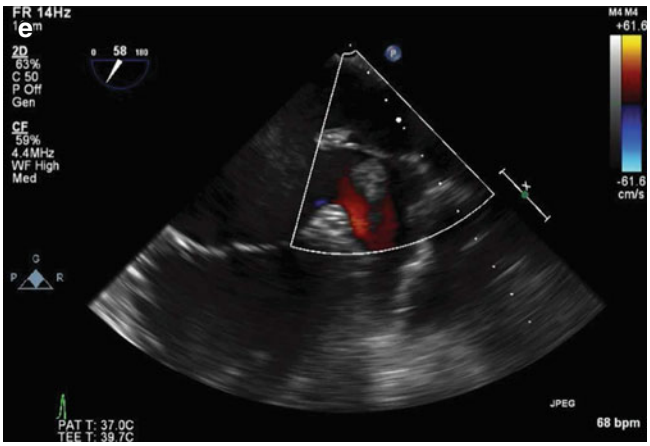
e
FR 14Hz
2D
63%
C 50
P Off
Gen
CF
59%
4.4MHz
WF High
Med
PAT T: 37.0C
TEE T: 39.7C
68 bpm

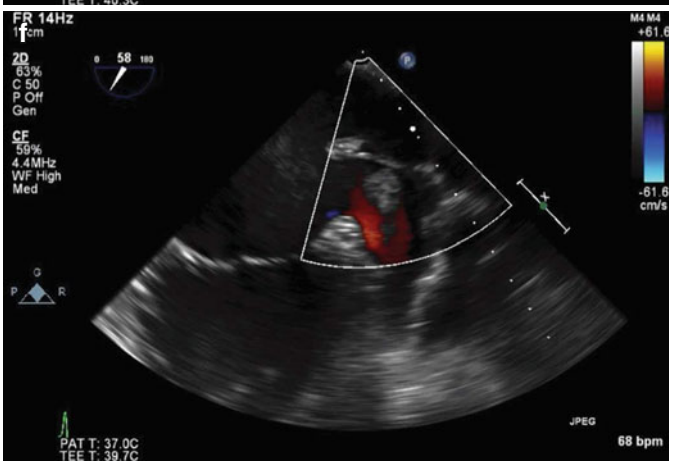
f
FR 14Hz
2D
63%
C 50
P Off
Gen
CF
59%
4.4MHz
WF High
Med
PAT T: 37.0C
TEE T: 39.7C
68 bpm

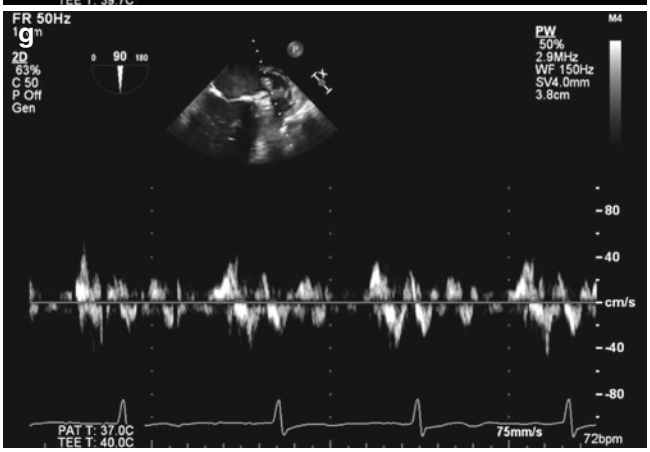
g
FR 50Hz
2D
63%
C 50
P Off
Gen
PW
50%
2.9MHz
WF 150Hz
SV4.0mm
3.8cm
80
40
cm/s
-40
-80
PAT T: 37.0C
TEE T: 40.0C
75mm/s
72bpm

presentation and underwent an uneventful TEE-guided cardioversion and was placed on dofetilide. However, his antiarrhythmic regimen was changed to amiodarone due to patient preference several months later. On exam, his vital signs were acceptable and he clinically appeared euvolemic with flat neck veins and no peripheral edema. His heart sounds were notable for an irregular rhythm; atrial fibrillation was confirmed on ECG. His INR was therapeutic at 2.3. On interrogation of his ICD, it was found that his atrial fibrillation burden was 2 %. There was concern that the loss of atrial kick or heart rate changes secondary to atrial fibrillation was worsening his heart failure symptoms, thus it was decided that the patient should have a TEE-guided DCCV.

His TEE revealed no left atrial appendage thrombus but the presence of severe spontaneous echo contrast (Fig. 1.6a–d).

He underwent successful DCCV and his heart failure was well controlled for 2 years; however, he again returned to clinic with increasing fatigue and was found to be back in atrial fibrillation. His INR again was therapeutic and he underwent a TEE for possible DCCV.

His TEE this time showed again showed severe SEC in the LAA with a peak emptying velocity of 16 cm/s. There is no thrombus, but a layer of sludge in the LAA (Fig. 1.6e–h).

Given the presence of sludge, the elective DCCV was canceled and patient was maintained on anticoagulation but subsequently was admitted to the hospital 3 weeks later in decompensated heart failure. Following stabilization of his volume status, he underwent interval TEE to evaluate whether he could again be converted to sinus rhythm.

His interval TEE now showed the presence of a LAA thrombus despite documented adequate anticoagulation between the echocardiographic studies. His elective DCCV was canceled and he remained on anticoagulation (Fig. 1.6i–j).

Clinical Pearl

SEC is seen in 50 % of patients with AF and in 2 % of patients with NSR. Furthermore, SEC was present in 90 % of patients with LAA thrombus. In a subgroup analysis of the Stroke Prevention in Atrial Fibrillation (SPAF-III) trial, dense SEC was an independent predictor of thromboembolic events [122]. Furthermore, despite anticoagulant therapy, patients with AF and dense SEC have a high likelihood of cerebral embolism and/or death [123]. In a separate study, the presence of sludge has also been independently associated with thromboembolic events and all-cause mortality [92]. The decision to DCCV in the setting of dense SEC or sludge, however, is controversial and remains highly debated.

Case 3: NOAC Case (Fig. 1.7)

A 50-year old man with palpitations presented to clinic for evaluation. He has a past medical history for hypertension and diabetes. He denies any chest pain but describes an irregular heart rhythm most notable with activity but can occur at rest. He had a negative exercise stress test earlier in the year as part of an insurance physical exam. On physical exam, he has an irregular heart rhythm and no cardiac murmurs. An ECG confirms atrial fibrillation with a controlled rate. A TTE was performed that showed a mildly enlarged left atrium but no significant valvular abnormalities. He also had no metabolic dearrangement on laboratory testing, including normal renal function. He dislikes frequent blood tests; thus, after discussion of the risks and benefits with his physician, he is started on dabigatran for stroke prophylaxis. Following 3-weeks of anticoagulation, he presented for TEE-guided cardioversion for trial of sinus rhythm restoration.

His TEE revealed a bilobed LAA with no SEC, no sludge, and no thrombus. Doppler of the LAA orifice revealed a fibrillatory patter with high emptying velocities (61 cm/s). He underwent successful DCCV without any immediate complications.

Clinical Pearl

A number of new non-vitamin K oral anticoagulants (NOAC) have been developed and approved for thromboembolic prophylaxis. Direct thrombin inhibitor, dabigatran through the RE-LY trial [124], and factor Xa inhibitors: rivaroxaban through the ROCKET AF trial [125], apixaban through the ARISTOTLE trial [126], and edoxaban through the ENGAGE AF-TIMI 48 trial [127], have been shown to be non-inferior to conventional warfarin therapy for the prevention of embolic events in the setting of atrial fibrillation. Post-hoc, subgroup analyses of RE-LY, ROCKET AF, and ARISTOTLE, have similar shown at least non-inferiority of dabigatran [128], rivaroxaban [129], and apixaban [130] for embolic events compared to warfarin for subjects who underwent cardioversion. There is a prospective, randomized, open-label, blinded endpoint evaluation (PROBE) trial currently enrolling that compares edoxaban to warfarin in subjects undergoing DCCV for AF [131]. Given the lack of direct head-to-head comparisons of the NOACs, it is not clear that a particular NOAC is superior. There have been

Fig. 1.5 (**a**–**g**) Case of LAA thrombus (Case 1) (**a**–**d**) demonstrate a large mobile echodensity within the primary lobe of the LAA that prolapses in the LA. (**b**) Depicts the simultaneous, multiplanar view of the thrombus. (**e**) Shows a 3D reconstruction of the thrombus. (**f**) Shows color flow around the thrombus, offering additional evidence that the echodensity was indeed thrombus and not an echo artifact. (**g**) Shows the erratic emptying velocities of the LAA in atrial fibrillation, with an emptying velocity of 38 cm/s

several meta-analyses pooling the data from the NOAC-trials that have shown similar or lower rate of embolic events, major bleeding, and/or all-cause mortality with NOACs compared to warfarin [132–137]. The results of these analyses and the convenience of no required monitoring (i.e. unlike blood draws for INR with warfarin) must be weighed against the lack of reversal agents and safety data to come with long-term use of these newer agents.

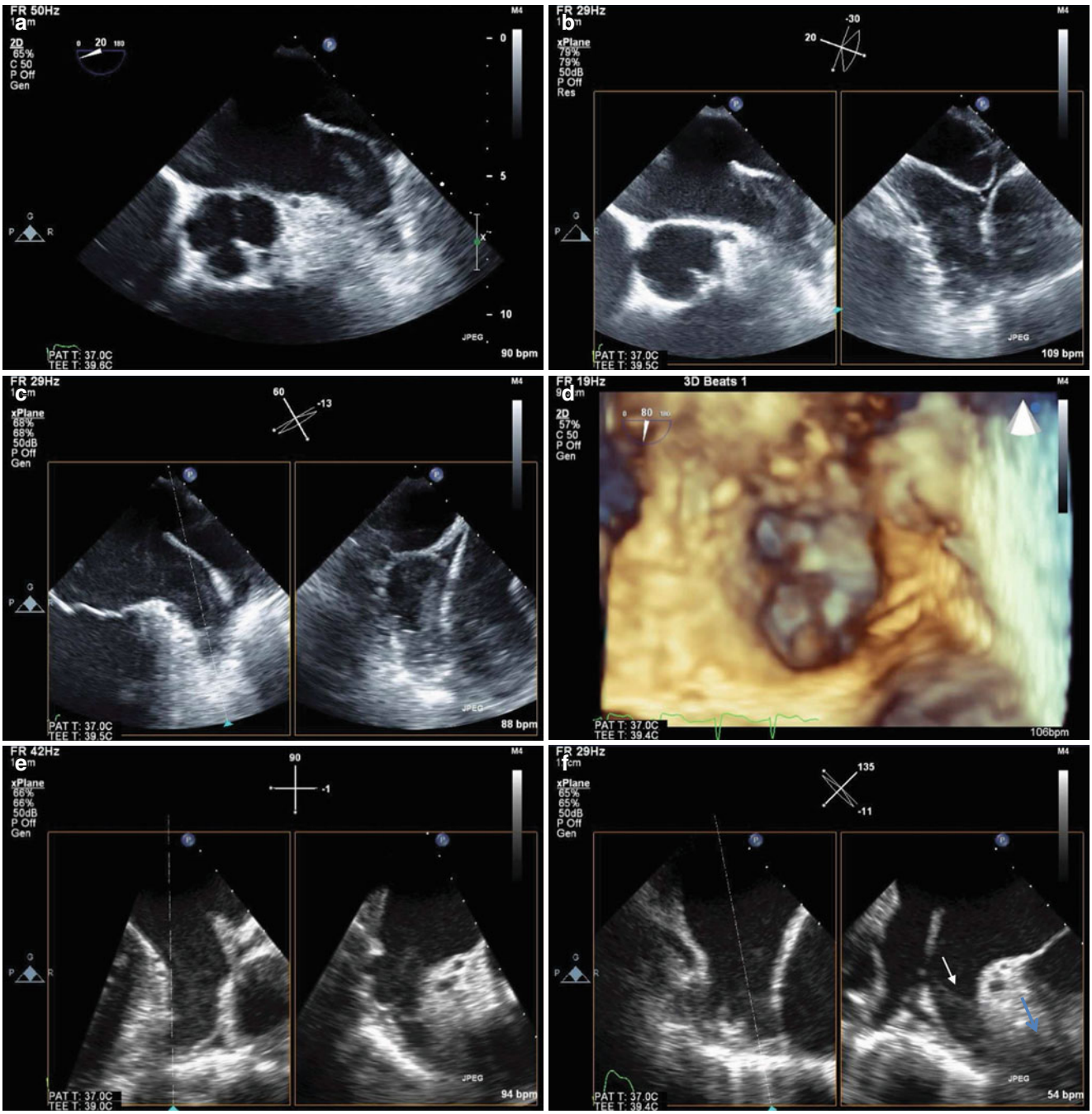

Fig. 1.6 (**a**–**d**) Spontaneous echocontrast (Case 2) (**a**–**c**) demonstrate severe echocontrast within the LAA but no LAA thrombus. Simultaneous multiplanar imaging was used to evaluate for possible thrombus. (**d**) Shows the SEC that appears within the lumen of the LAA in (**d**). (**e**–**h**) Sludge (Case 2) (**e**–**f**) demonstrate severe echocontrast within the LAA as well as layered sludge. (**g**) Shows that color flow Doppler to the apex of the LAA. (**h**) Shows reduced LAA emptying velocities. (**i**–**j**) Thrombus (Case 2) (**i**–**j**) demonstrate formation of a thrombus in the apex of the LAA. (**j**) Shows marking of the thrombus by the sonographer. Overall, the Figures in Case 2 highlight the progression of SEC to sludge to thrombus formation in a patient with LAA and low emptying velocities

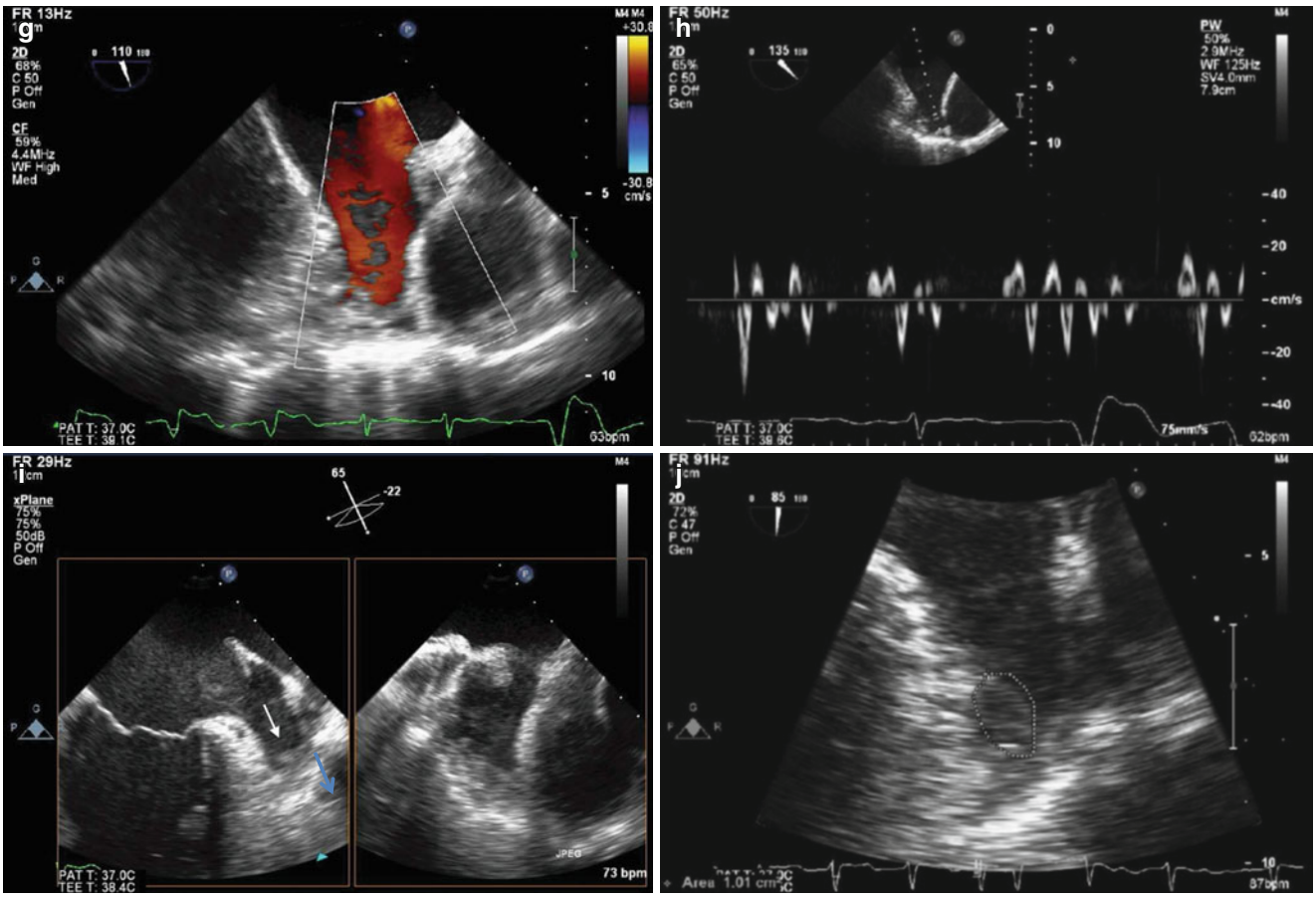

Fig. 1.6 (continued)

The current AHA/ACC/HRS guidelines recommend at least 3 weeks of anticoagulation before DCCV for AF ≥48 h in duration (or when duration is unknown); may proceed with DCCV sooner than 3 weeks of therapeutic anticoagulation if TEE is performed prior to DCCV to rule out LA thrombus [8]. In the cardioversion subgroup analyses of RE-LY (dabigatran), ROCKET-AF (rivaroxaban), and ARISTOTLE (apixaban), the patients had received long-term anti-coagulation (>3 weeks) at time of DCCV. In the Rivaroxaban vs. Vitamin K antagonists (VKAs) for Cardioversion in Atrial Fibrillation (X-VeRT) trial, the investigators prospectively evaluated the efficacy and safety of rivaroxaban versus VKAs undergoing early (1–5 days of anticoagulation) versus delayed (3–8 weeks of anticoagulation) DCCV, with or without TEE-guidance [138]. While underpowered for statistical significance, the study showed similar incidence of adverse events in those receiving rivaroxaban versus VKAs in both the early and delayed cardioversion arms, suggesting that early DCCV with rivaroxaban may be comparable to the standard VKA paradigm. The current AHA/ACC/HRS guidelines do not specify the type of anticoagulation needed if proceeding with TEE-guided DCCV prior to achieving 3 weeks of anticoagulation.

Case 4: Artifact (Fig. 1.8)

A 72 year old woman was referred for another opinion regarding a left atrial appendage thrombus. She has a past medical history significant for severe aortic stenosis, atrial fibrillation s/p DCCV in the past and on chronic anticoagulation, hypertension, hyperlipidemia, CAD, and a TIA. She is symptomatic from her severe AS with significant shortness of breath performing activities of daily living; however, due to her comorbidities, she was felt to be too high risk to undergo open heart surgery. She subsequently underwent a TEE for preoperative planning prior to possible transcatheter aortic valve replacement (TAVR) when she was reported to have a LAA thrombus. Her TAVR planning was halted, her anticoagulation was continued, and she was referred to another medical center for further evaluation.

She underwent a repeat TEE for further assessment of her left atrial appendage. An echodensity was visualized within the LAA between the membranous band of the left upper pulmonary vein and the LAA wall without any clear connection to the wall. It had a fully dependent motion with respect to the LAA and heart motion. Simultaneous multiplanar

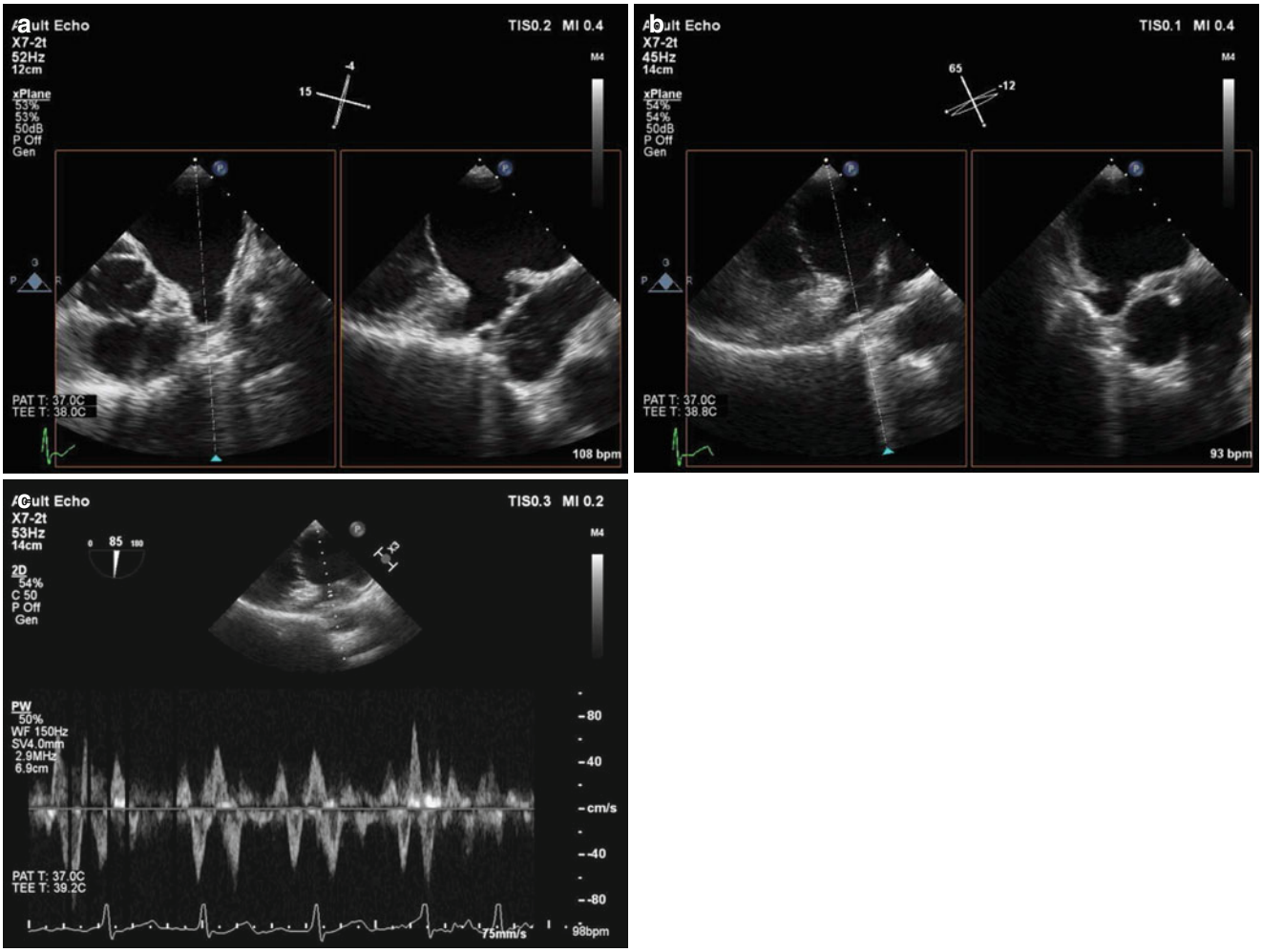

Fig. 1.7 (**a**–**c**) NOACs (Case 3) (**a**–**c**) demonstrate a bi-lobed LAA with no SEC, no sludge, and no thrombus after 3 weeks of anticoagulation with dabigatran, a NOAC. (**c**) Shows high LAA emptying velocities in AF, 61 cm/s

imaging, in addition to echocontrast, was utilized to confirm suspicions that the visualized density was an artifact from the warfarin ridge.

She underwent successful TAVR; of note, TEE at time of TAVR again confirmed the presence of a reverberation artifact within the LAA.

Clinical Pearl

Reverberation artifacts and pectinate muscles are often mistaken for LAA thrombi during TEE. In a series of patients undergoing TEE-guided DCCV, 23 % of patients had LAA artifacts. Reverberation artifacts from the warfarin ridge are located twice the distance from the transducer to the ridge, have a fully dependent motion with respect to the heart, and are morphologically consistent with the ridge. Thrombi have an independent motion, often-rounded morphology, attached to the LAA, often associated with SEC, and are distinct in echogenicity from the surrounding walls. Pectinate muscles are confined to the body of the LAA, have a fully dependent motion, and have the same echogenicity as the LAA walls. The use of echocontrast, simultaneous multiplanar imaging, and 3D techniques can help distinguish between true LAA thrombus, artifact, and intrinsic structures.

Case 5: LAA Exclusion (Fig. 1.9)

A 74 year old woman presented for TEE prior to anti-arrhythmic drug load (sotalol) for atrial fibrillation. She had a past medical history significant for hypertension, hyperlipidemia, interstitial lung disease, and atrial fibrillation. At the time of thoracic surgery for recurrent pleural effusions, her left atrial appendage was surgically oversewn with suture. She continued on anticoagulation therapy for stroke prophylaxis. She was admitted for anti-arrhythmic therapy due to symptomatic palpitations that was felt to be due to atrial fibrillation.

Her TEE showed a large mobile thrombus within the LAA with residual communication from the appendage to

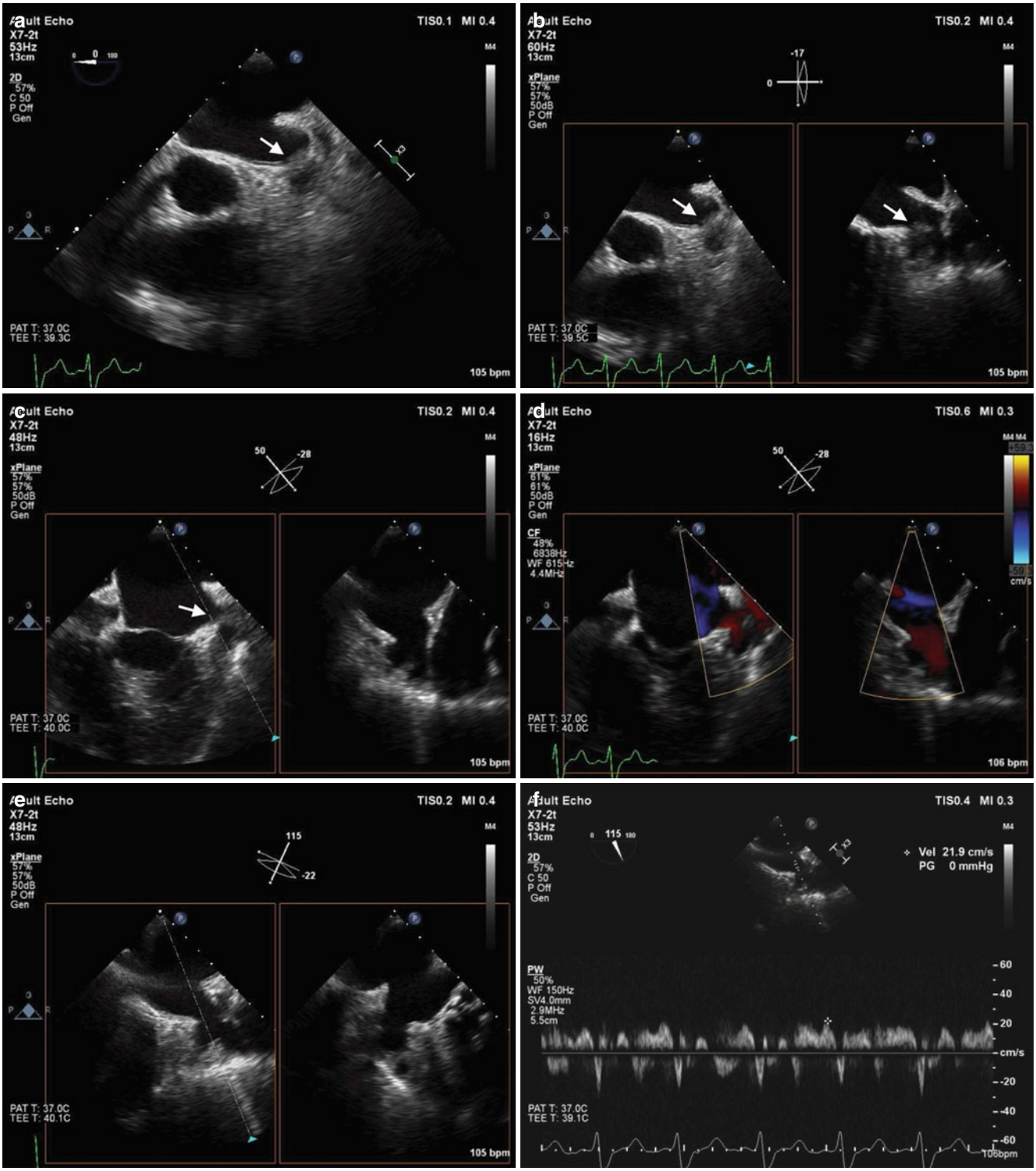

Fig. 1.8 (**a**–**h**) Artifact (Case 4) (**a**–**b**) demonstrate an echodensity in the middle of the LAA orifice that is concerning for possible thrombus. Of note, the echodensity is two times the distance from the warfarin ridge. (**c**) Demonstrates that simultaneous multiplanar imaging through the echodensity does not reveal any density in the perpendicular plane. (**d**) Shows that color flow does not respect the echodensity seen on 2D imaging. (**e**) Shows another multiplanar image of the same LAA from different angles does not reveal the same echodensity. (**f**) Shows a typical quadriphasic LAA emptying pattern in sinus rhythm, although the late diastolic emptying velocity is low at 21 cm/s. (**g**–**h**) Show the use of echocontrast to confirm that the echodensity is reverberation artifact from the warfarin ridge due to the lack of a filling defect

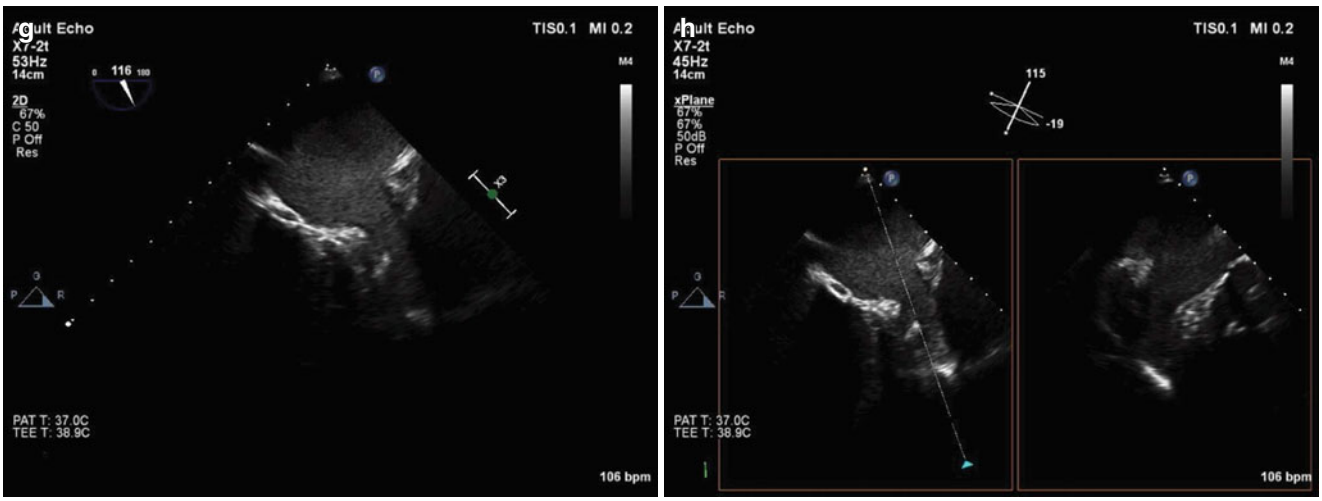

Fig. 1.8 (continued)

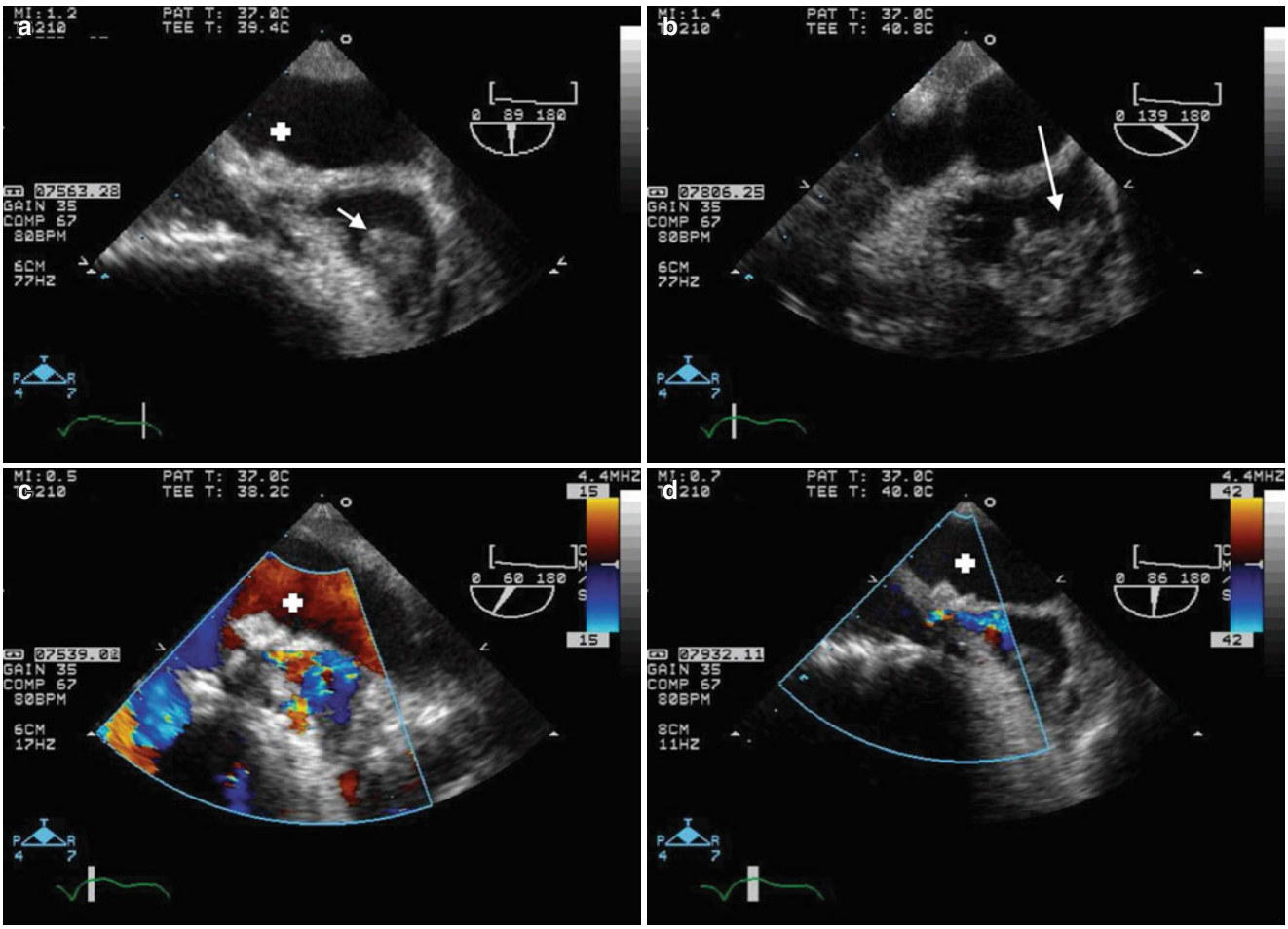

Fig. 1.9 (**a**–**d**) LAA surgical oversewing (Case 5) (**a**–**b**) demonstrate formation of a thrombus (marked with an *arrow*) within a LAA that has been surgical oversewn. (**c**–**d**) Demonstrate residual communication between the LAA and the LA. There is suggestion of thrombus formation in the LA where the LAA was surgical oversewn (marked with a + in **a**, **c**, **d**)

the LA. She was not started on anti-rhythmic therapy and a rate control strategy was adopted with continued anticoagulation.

Clinical Pearl

While the LAA is often surgically excised or excluded at time of concomitant thoracic surgery, multiple TEE studies have demonstrated flow between the LA and residual LAA [76–78]. A study performed at the Cleveland Clinic reviewing 137 patients who had LAA closure and subsequent TEE evaluation, showed that only 55 of 137 (40 %) of closures were successful and that LAA thrombus was found in 41 % of patients with patent communication between the LA and LAA. From the study, it appeared that of the various LAA interventional techniques, surgical excision was more successful than exclusion (suture or stapler) [77]. With the advent to newer percutaneous LAA closure techniques, TEE evaluation of residual flow and/or thrombus formation should not be overlooked.

References

1. Fye WB. Tracing atrial fibrillation – 100 years. N Engl J Med. 2006;355(14):1412–4.
2. Chugh SS, Roth GA, Gillum RF, Mensah GA. Global burden of atrial fibrillation in developed and developing nations. Global Heart. 2014;9(1):113–9.
3. Go AS, Hylek EM, Phillips KA, Chang Y, Henault LE, Selby JV, et al. Prevalence of diagnosed atrial fibrillation in adults: national implications for rhythm management and stroke prevention: the AnTicoagulation and Risk Factors in Atrial Fibrillation (ATRIA) study. JAMA J Am Med Assoc. 2001;285(18):2370–5.
4. Tsang TS, Gersh BJ. Atrial fibrillation: an old disease, a new epidemic. Am J Med. 2002;113(5):432–5.
5. Kim MH, Johnston SS, Chu BC, Dalal MR, Schulman KL. Estimation of total incremental health care costs in patients with atrial fibrillation in the United States. Circ Cardiovasc Qual Outcome. 2011;4(3):313–20.
6. Coyne KS, Paramore C, Grandy S, Mercader M, Reynolds M, Zimetbaum P. Assessing the direct costs of treating nonvalvular atrial fibrillation in the United States. Values Health J Int Soc Pharmacoecon Outcomes Res. 2006;9(5):348–56.
7. Wakili R, Voigt N, Kääb S, Dobrev D, Nattel S. Recent advances in the molecular pathophysiology of atrial fibrillation. J Clin Invest. 2011;121(8):2955–68.
8. January CT, Wann LS, Alpert JS, Calkins H, Cigarroa JE, Cleveland Jr JC, et al. 2014 AHA/ACC/HRS guideline for the management of patients with atrial fibrillation: a report of the American College of Cardiology/American Heart Association Task Force on Practice Guidelines and the Heart Rhythm Society. Circulation. 2014;130(23):e199–267.
9. Watson T, Shantsila E, Lip GY. Mechanisms of thrombogenesis in atrial fibrillation: virchow's triad revisited. Lancet. 2009;373(9658):155–66.
10. Wolf PA, Abbott RD, Kannel WB. Atrial fibrillation as an independent risk factor for stroke: the Framingham study. Stroke. 1991;22(8):983–8.
11. Risk factors for stroke and efficacy of antithrombotic therapy in atrial fibrillation. Analysis of pooled data from five randomized controlled trials. Arch Intern Med. 1994;154(13):1449–57.
12. Stewart S, Hart CL, Hole DJ, McMurray JJ. A population-based study of the long-term risks associated with atrial fibrillation: 20-year follow-up of the Renfrew/Paisley study. Am J Med. 2002;113(5):359–64.
13. Leung DY, Davidson PM, Cranney GB, Walsh WF. Thromboembolic risks of left atrial thrombus detected by transesophageal echocardiogram. Am J Cardiol. 1997;79(5):626–9.
14. Lown BA, Neuman J. New method for terminating cardiac arrhythmias: use of synchronized capacitor discharge. JAMA J Am Med Assoc. 1962;182:548–55.
15. Wazni OM, Tsao HM, Chen SA, Chuang HH, Saliba W, Natale A, et al. Cardiovascular imaging in the management of atrial fibrillation. J Am Coll Cardiol. 2006;48(10):2077–84.
16. Gallagher MM, Guo XH, Poloniecki JD, Guan Yap Y, Ward D, Camm AJ. Initial energy setting, outcome and efficiency in direct current cardioversion of atrial fibrillation and flutter. J Am Coll Cardiol. 2001;38(5):1498–504.
17. Elhendy A, Gentile F, Khandheria BK, Hammill SC, Gersh BJ, Bailey KR, et al. Predictors of unsuccessful electrical cardioversion in atrial fibrillation. Am J Cardiol. 2002;89(1):83–6.
18. Fatkin D, Kuchar DL, Thorburn CW, Feneley MP. Transesophageal echocardiography before and during direct current cardioversion of atrial fibrillation: evidence for "atrial stunning" as a mechanism of thromboembolic complications. J Am Coll Cardiol. 1994;23(2):307–16.
19. Stein B, Halperin JL, Fuster V. Should patients with atrial fibrillation be anticoagulated prior to and chronically following cardioversion? Cardiovasc Clin. 1990;21(1):231–47; discussion 48–9.
20. Grimm RA, Stewart WJ, Black IW, Thomas JD, Klein AL. Should all patients undergo transesophageal echocardiography before electrical cardioversion of atrial fibrillation? J Am Coll Cardiol. 1994;23(2):533–41.
21. Hansen ML, Jepsen RM, Olesen JB, Ruwald MH, Karasoy D, Gislason GH, et al. Thromboembolic risk in 16 274 atrial fibrillation patients undergoing direct current cardioversion with and without oral anticoagulant therapy. Europace. 2015;17:18–23.
22. Weiss S, Davis D. Rheumatic heart disease: III. Embolic manifestations. Am Heart J. 1933;9(1):45–52.
23. Silvestry FE, Kerber RE, Brook MM, Carroll JD, Eberman KM, Goldstein SA, et al. Echocardiography-guided interventions. J Am Soc Echocardiogr. 2009;22(3):213–31; quiz 316–7.
24. Aschenberg W, Schluter M, Kremer P, Schroder E, Siglow V, Bleifeld W. Transesophageal two-dimensional echocardiography for the detection of left atrial appendage thrombus. J Am Coll Cardiol. 1986;7(1):163–6.
25. Fatkin D, Scalia G, Jacobs N, Burstow D, Leung D, Walsh W, et al. Accuracy of biplane transesophageal echocardiography in detecting left atrial thrombus. Am J Cardiol. 1996;77(4):321–3.
26. Manning WJ, Weintraub RM, Waksmonski CA, Haering JM, Rooney PS, Maslow AD, et al. Accuracy of transesophageal echocardiography for identifying left atrial thrombi. A prospective, intraoperative study. Ann Intern Med. 1995;123(11):817–22.
27. Olson JD, Goldenberg IF, Pedersen W, Brandt D, Kane M, Daniel JA, et al. Exclusion of atrial thrombus by transesophageal echocardiography. J Am Soc Echocardiogr. 1992;5(1):52–6.
28. Syed TM, Halperin JL. Left atrial appendage closure for stroke prevention in atrial fibrillation: state of the art and current challenges. Nat Clin Pract Cardiovasc Med. 2007;4(8):428–35.
29. Moore KL, Persaud TVN. The developing human: clinically oriented embryology. 7th ed. Philadelphia: Saunders; 2003, xv, 560 p.
30. Kanmanthareddy A, Reddy YM, Vallakati A, Earnest MB, Nath J, Ferrell R, et al. Embryology and anatomy of the left atrial appendage: why does thrombus form? Interv Cardiol Clin. 2014;3(2):191–202.
31. Hahn RT, Abraham T, Adams MS, Bruce CJ, Glas KE, Lang RM, et al. Guidelines for performing a comprehensive transesophageal

echocardiographic examination: recommendations from the American Society of Echocardiography and the Society of Cardiovascular Anesthesiologists. J Am Soc Echocardiogr. 2013;26(9):921–64.
32. Maltagliati A, Pepi M, Tamborini G, Muratori M, Celeste F, Doria E, et al. Usefulness of multiplane transesophageal echocardiography in the recognition of artifacts and normal anatomical variants that may mimic left atrial thrombi in patients with atrial fibrillation. Ital Heart J Off J Ital Fed Cardiol. 2003;4(11):797–802.
33. Klein AL, Asher CR. Clinical echocardiography review: a self-assessment tool. Philadelphia: Wolters Kluwer/Lippincott Williams & Wilkins Health; 2011, xvii, 476 p.
34. Veinot JP, Harrity PJ, Gentile F, Khandheria BK, Bailey KR, Eickholt JT, et al. Anatomy of the normal left atrial appendage: a quantitative study of age-related changes in 500 autopsy hearts: implications for echocardiographic examination. Circulation. 1997;96(9):3112–5.
35. Di Biase L, Santangeli P, Anselmino M, Mohanty P, Salvetti I, Gili S, et al. Does the left atrial appendage morphology correlate with the risk of stroke in patients with atrial fibrillation? Results from a multicenter study. J Am Coll Cardiol. 2012;60(6):531–8.
36. Ernst G, Stollberger C, Abzieher F, Veit-Dirscherl W, Bonner E, Bibus B, et al. Morphology of the left atrial appendage. Anat Rec. 1995;242(4):553–61.
37. O'Brien J, Al-Hassan D, Ng J, Joshi M, Hague C, Chakrabarti S, et al. Three-dimensional assessment of left atrial appendage orifice geometry and potential implications for device closure. Int J Cardiovasc Imaging. 2014;30(4):819–23.
38. Hoit BD. Left atrial size and function: role in prognosis. J Am Coll Cardiol. 2014;63(6):493–505.
39. Al-Saady NM, Obel OA, Camm AJ. Left atrial appendage: structure, function, and role in thromboembolism. Heart. 1999;82(5):547–54.
40. Davis 3rd CA, Rembert JC, Greenfield Jr JC. Compliance of left atrium with and without left atrium appendage. Am J Physiol. 1990;259(4 Pt 2):H1006–8.
41. Hoit BD, Shao Y, Gabel M. Influence of acutely altered loading conditions on left atrial appendage flow velocities. J Am Coll Cardiol. 1994;24(4):1117–23.
42. Inoue S, Murakami Y, Sano K, Katoh H, Shimada T. Atrium as a source of brain natriuretic polypeptide in patients with atrial fibrillation. J Card Fail. 2000;6(2):92–6.
43. Rodeheffer RJ, Naruse M, Atkinson JB, Naruse K, Burnett Jr JC, Merrill WH, et al. Molecular forms of atrial natriuretic factor in normal and failing human myocardium. Circulation. 1993;88(2):364–71.
44. Donal E, Yamada H, Leclercq C, Herpin D. The left atrial appendage, a small, blind-ended structure: a review of its echocardiographic evaluation and its clinical role. Chest. 2005;128(3):1853–62.
45. Mugge A, Kuhn H, Nikutta P, Grote J, Lopez JA, Daniel WG. Assessment of left atrial appendage function by biplane transesophageal echocardiography in patients with nonrheumatic atrial fibrillation: identification of a subgroup of patients at increased embolic risk. J Am Coll Cardiol. 1994;23(3):599–607.
46. Tabata T, Oki T, Fukuda N, Iuchi A, Manabe K, Kageji Y, et al. Influence of left atrial pressure on left atrial appendage flow velocity patterns in patients in sinus rhythm. J Am Soc Echocardiogr. 1996;9(6):857–64.
47. Shirani J, Alaeddini J. Structural remodeling of the left atrial appendage in patients with chronic non-valvular atrial fibrillation: implications for thrombus formation, systemic embolism, and assessment by transesophageal echocardiography. Cardiovasc Pathol Off J Soc Cardiovasc Pathol. 2000;9(2):95–101.
48. Blackshear JL, Odell JA. Appendage obliteration to reduce stroke in cardiac surgical patients with atrial fibrillation. Ann Thorac Surg. 1996;61(2):755–9.
49. Stoddard MF, Dawkins PR, Prince CR, Ammash NM. Left atrial appendage thrombus is not uncommon in patients with acute atrial fibrillation and a recent embolic event: a transesophageal echocardiographic study. J Am Coll Cardiol. 1995;25(2):452–9.
50. Scherr D, Dalal D, Chilukuri K, Dong J, Spragg D, Henrikson CA, et al. Incidence and predictors of left atrial thrombus prior to catheter ablation of atrial fibrillation. J Cardiovasc Electrophysiol. 2009;20(4):379–84.
51. Gage BF, Waterman AD, Shannon W, Boechler M, Rich MW, Radford MJ. Validation of clinical classification schemes for predicting stroke: results from the National Registry of Atrial Fibrillation. JAMA J Am Med Assoc. 2001;285(22):2864–70.
52. Lip GY, Nieuwlaat R, Pisters R, Lane DA, Crijns HJ. Refining clinical risk stratification for predicting stroke and thromboembolism in atrial fibrillation using a novel risk factor-based approach: the euro heart survey on atrial fibrillation. Chest. 2010;137(2):263–72.
53. Yarmohammadi H, Varr BC, Puwanant S, Lieber E, Williams SJ, Klostermann T, et al. Role of CHADS2 score in evaluation of thromboembolic risk and mortality in patients with atrial fibrillation undergoing direct current cardioversion (from the ACUTE Trial Substudy). Am J Cardiol. 2012;110(2):222–6.
54. Berger M, Schweitzer P. Timing of thromboembolic events after electrical cardioversion of atrial fibrillation or flutter: a retrospective analysis. Am J Cardiol. 1998;82(12):1545–7, A8.
55. Airaksinen KE, Gronberg T, Nuotio I, Nikkinen M, Ylitalo A, Biancari F, et al. Thromboembolic complications after cardioversion of acute atrial fibrillation: the FinCV (Finnish CardioVersion) study. J Am Coll Cardiol. 2013;62(13):1187–92.
56. Jaber WA, Prior DL, Thamilarasan M, Grimm RA, Thomas JD, Klein AL, et al. Efficacy of anticoagulation in resolving left atrial and left atrial appendage thrombi: a transesophageal echocardiographic study. Am Heart J. 2000;140(1):150–6.
57. You JJ, Singer DE, Howard PA, Lane DA, Eckman MH, Fang MC, et al. Antithrombotic therapy for atrial fibrillation: antithrombotic therapy and prevention of thrombosis, 9th ed: American College of Chest Physicians Evidence-Based Clinical Practice Guidelines. Chest. 2012;141(2 Suppl):e531S–75.
58. Klein AL, Grimm RA, Murray RD, Apperson-Hansen C, Asinger RW, Black IW, et al. Use of transesophageal echocardiography to guide cardioversion in patients with atrial fibrillation. N Engl J Med. 2001;344(19):1411–20.
59. Klein AL, Jasper SE, Katz WE, Malouf JF, Pape LA, Stoddard MF, et al. The use of enoxaparin compared with unfractionated heparin for short-term antithrombotic therapy in atrial fibrillation patients undergoing transoesophageal echocardiography-guided cardioversion: assessment of Cardioversion Using Transoesophageal Echocardiography (ACUTE) II randomized multicentre study. Eur Heart J. 2006;27(23):2858–65.
60. Stellbrink C, Nixdorff U, Hofmann T, Lehmacher W, Daniel WG, Hanrath P, et al. Safety and efficacy of enoxaparin compared with unfractionated heparin and oral anticoagulants for prevention of thromboembolic complications in cardioversion of nonvalvular atrial fibrillation: the Anticoagulation in Cardioversion using Enoxaparin (ACE) trial. Circulation. 2004;109(8):997–1003.
61. American College of Cardiology Foundation Appropriate Use Criteria Task F, American Society of E, American Heart A, American Society of Nuclear C, Heart Failure Society of A, Heart Rhythm S, et al. ACCF/ASE/AHA/ASNC/HFSA/HRS/SCAI/SCCM/SCCT/SCMR 2011 appropriate use criteria for echocardiography. A report of the American College of Cardiology Foundation Appropriate Use Criteria Task Force, American Society of Echocardiography, American Heart Association, American Society of Nuclear Cardiology, Heart Failure Society of America, Heart Rhythm Society, Society for Cardiovascular Angiography and Interventions, Society of Critical Care

Medicine, Society of Cardiovascular Computed Tomography, and Society for Cardiovascular Magnetic Resonance Endorsed by the American College of Chest Physicians. J Am Coll Cardiol. 2011;57(9):1126–66.
62. Grewal GK, Klosterman TB, Shrestha K, Yarmohammadi H, Zurick AO, Varr BC, et al. Indications for TEE before cardioversion for atrial fibrillation: implications for appropriateness criteria. J Am Coll Cardiol Img. 2012;5(6):641–8.
63. Daniel WG, Erbel R, Kasper W, Visser CA, Engberding R, Sutherland GR, et al. Safety of transesophageal echocardiography. A multicenter survey of 10,419 examinations. Circulation. 1991;83(3):817–21.
64. Khandheria BK, Seward JB, Tajik AJ. Transesophageal echocardiography. Mayo Clin Proc. 1994;69(9):856–63.
65. Hilberath JN, Oakes DA, Shernan SK, Bulwer BE, D'Ambra MN, Eltzschig HK. Safety of transesophageal echocardiography. J Am Soc Echocardiogr. 2010;23(11):1115–27; quiz 220–1.
66. Quinones MA, Douglas PS, Foster E, Gorcsan 3rd J, Lewis JF, Pearlman AS, et al. ACC/AHA clinical competence statement on echocardiography: a report of the American College of Cardiology/American Heart Association/American College of Physicians-American Society of Internal Medicine Task Force on Clinical Competence. J Am Coll Cardiol. 2003;41(4):687–708.
67. Stergiou GS, Kollias A, Destounis A, Tzamouranis D. Automated blood pressure measurement in atrial fibrillation: a systematic review and meta-analysis. J Hypertens. 2012;30(11):2074–82.
68. Holmes DR, Reddy VY, Turi ZG, Doshi SK, Sievert H, Buchbinder M, et al. Percutaneous closure of the left atrial appendage versus warfarin therapy for prevention of stroke in patients with atrial fibrillation: a randomised non-inferiority trial. Lancet. 2009;374(9689):534–42.
69. Wheeler R, Masani ND. The role of echocardiography in the management of atrial fibrillation. Eur J Echocardiogr J Work Group Echocardiogr Eur Soc Cardiol. 2011;12(10):i33–8.
70. Blackshear JL, Pearce LA, Hart RG, Zabalgoitia M, Labovitz A, Asinger RW, et al. Aortic plaque in atrial fibrillation: prevalence, predictors, and thromboembolic implications. Stroke. 1999;30(4):834–40.
71. Toyoda K, Yasaka M, Nagata S, Yamaguchi T. Aortogenic embolic stroke: a transesophageal echocardiographic approach. Stroke. 1992;23(8):1056–61.
72. Meissner I, Khandheria BK, Sheps SG, Schwartz GL, Wiebers DO, Whisnant JP, et al. Atherosclerosis of the aorta: risk factor, risk marker, or innocent bystander? A prospective population-based transesophageal echocardiography study. J Am Coll Cardiol. 2004;44(5):1018–24.
73. Arboix A, Alio J. Cardioembolic stroke: clinical features, specific cardiac disorders and prognosis. Curr Cardiol Rev. 2010;6(3):150–61.
74. To AC, Gabriel RS, Park M, Lowe BS, Curtin RJ, Sigurdsson G, et al. Role of transesophageal echocardiography compared to computed tomography in evaluation of pulmonary vein ablation for atrial fibrillation (ROTEA study). J Am Soc Echocardiogr. 2011;24(9):1046–55.
75. Khariton Y, House JA, Comer L, Coggins TR, Magalski A, Skolnick DG, et al. Impact of transesophageal echocardiography on management in patients with suspected cardioembolic stroke. Am J Cardiol. 2014;114(12):1912–6.
76. Garcia-Fernandez MA, Perez-David E, Quiles J, Peralta J, Garcia-Rojas I, Bermejo J, et al. Role of left atrial appendage obliteration in stroke reduction in patients with mitral valve prosthesis: a transesophageal echocardiographic study. J Am Coll Cardiol. 2003;42(7):1253–8.
77. Kanderian AS, Gillinov AM, Pettersson GB, Blackstone E, Klein AL. Success of surgical left atrial appendage closure: assessment by transesophageal echocardiography. J Am Coll Cardiol. 2008;52(11):924–9.
78. Katz ES, Tsiamtsiouris T, Applebaum RM, Schwartzbard A, Tunick PA, Kronzon I. Surgical left atrial appendage ligation is frequently incomplete: a transesophageal echocardiograhic study. J Am Coll Cardiol. 2000;36(2):468–71.
79. Verhaert D, Puwanant S, Gillinov AM, Klein AL. Atrial fibrillation after open heart surgery: how safe is early conversion without anticoagulation? J Am Soc Echocardiogr. 2009;22(2):212.e1–3.
80. Merino A, Hauptman P, Badimon L, Badimon JJ, Cohen M, Fuster V, et al. Echocardiographic "smoke" is produced by an interaction of erythrocytes and plasma proteins modulated by shear forces. J Am Coll Cardiol. 1992;20(7):1661–8.
81. Sigel B, Coelho JC, Spigos DG, Flanigan DP, Schuler JJ, Kasprisin DO, et al. Ultrasonography of blood during stasis and coagulation. Investig Radiol. 1981;16(1):71–6.
82. Black IW. Spontaneous echo contrast: where there's smoke there's fire. Echocardiography. 2000;17(4):373–82.
83. Castello R, Pearson AC, Fagan L, Labovitz AJ. Spontaneous echocardiographic contrast in the descending aorta. Am Heart J. 1990;120(4):915–9.
84. Goldman ME, Pearce LA, Hart RG, Zabalgoitia M, Asinger RW, Safford R, et al. Pathophysiologic correlates of thromboembolism in nonvalvular atrial fibrillation: I. Reduced flow velocity in the left atrial appendage (The Stroke Prevention in Atrial Fibrillation [SPAF-III] study). J Am Soc Echocardiogr. 1999;12(12):1080–7.
85. Zotz RJ, Muller M, Genth-Zotz S, Darius H. Spontaneous echo contrast caused by platelet and leukocyte aggregates? Stroke. 2001;32(5):1127–33.
86. Mahony C, Ferguson J, Fischer PL. Red cell aggregation and the echogenicity of whole blood. Ultrasound Med Biol. 1992;18(6–7):579–86.
87. Kleemann T, Becker T, Strauss M, Schneider S, Seidl K. Prevalence of left atrial thrombus and dense spontaneous echo contrast in patients with short-term atrial fibrillation <48 hours undergoing cardioversion: value of transesophageal echocardiography to guide cardioversion. J Am Soc Echocardiogr. 2009;22(12):1403–8.
88. Black IW, Hopkins AP, Lee LC, Walsh WF. Left atrial spontaneous echo contrast: a clinical and echocardiographic analysis. J Am Coll Cardiol. 1991;18(2):398–404.
89. Bashir M, Asher CR, Schaffer K, Murray RD, Apperson-Hansen C, Jasper SE, et al. Left atrial appendage spontaneous echo contrast in patients with atrial arrhythmias using integrated backscatter and transesophageal echocardiography. Am J Cardiol. 2001;88(8):923–7, A9.
90. Donal E, Sallach JA, Murray RD, Drinko JK, Jasper SE, Thomas JD, et al. Contrast-enhanced tissue Doppler imaging of the left atrial appendage is a new quantitative measure of spontaneous echocardiographic contrast in atrial fibrillation. Eur J Echocardiogr J Work Group Echocardiogr Eur Soc Cardiol. 2008;9(1):5–11.
91. Klein AL, Murray RD, Black IW, Chandra S, Grimm RA, DS DA, et al. Integrated backscatter for quantification of left atrial spontaneous echo contrast. J Am Coll Cardiol. 1996;28(1):222–31.
92. Lowe BS, Kusunose K, Motoki H, Varr B, Shrestha K, Whitman C, et al. Prognostic significance of left atrial appendage "Sludge" in patients with atrial fibrillation: a new transesophageal echocardiographic thromboembolic risk factor. J Am Soc Echocardiogr. 2014;27:1176–83.
93. Seward JB, Khandheria BK, Oh JK, Freeman WK, Tajik AJ. Critical appraisal of transesophageal echocardiography: limitations, pitfalls, and complications. J Am Soc Echocardiogr. 1992;5(3):288–305.
94. Troughton RW, Asher CR, Klein AL. The role of echocardiography in atrial fibrillation and cardioversion. Heart. 2003;89(12):1447–54.
95. Hajjiri M, Bernstein S, Saric M, Benenstein R, Aizer A, Dym G, et al. Atrial fibrillation ablation in patients with known sludge

in the left atrial appendage. J Interv Card Electrophysiol Int J Arrhythmias Pacing. 2014;40(2):147–51.
96. Mizuguchi KA, Burch TM, Bulwer BE, Fox AA, Rizzo RJ, Shernan SK. Thrombus or bilobar left atrial appendage? Diagnosis by real-time three-dimensional transesophageal echocardiography. Anesth Analg. 2009;108(1):70–2.
97. Solomon SD, Bulwer BE. Essential echocardiography: a practical handbook with DVD. Totowa: Humana Press; 2007, xiv, 458 p.
98. Nakajima H, Seo Y, Ishizu T, Yamamoto M, Machino T, Harimura Y, et al. Analysis of the left atrial appendage by three-dimensional transesophageal echocardiography. Am J Cardiol. 2010;106(6):885–92.
99. Khan GN, Dairywala IT, Liu Z, Li P, Carroll J, Vannan MA. Three-dimensional echocardiography of left atrial appendage thrombus. Echocardiography. 2001;18(2):163–6.
100. Karakus G, Kodali V, Inamdar V, Nanda NC, Suwanjutah T, Pothineni KR. Comparative assessment of left atrial appendage by transesophageal and combined two- and three-dimensional transthoracic echocardiography. Echocardiography. 2008;25(8):918–24.
101. Nucifora G, Faletra FF, Regoli F, Pasotti E, Pedrazzini G, Moccetti T, et al. Evaluation of the left atrial appendage with real-time 3-dimensional transesophageal echocardiography: implications for catheter-based left atrial appendage closure. Circ Cardiovasc Imaging. 2011;4(5):514–23.
102. von der Recke G, Schmidt H, Illien S, Luderitz B, Omran H. Use of transesophageal contrast echocardiography for excluding left atrial appendage thrombi in patients with atrial fibrillation before cardioversion. J Am Soc Echocardiogr. 2002;15(10 Pt 2):1256–61.
103. Yao SS, Ilercil A, Meisner JS, Strom JA, Shirani J. Improved Doppler echocardiographic assessment of the left atrial appendage by peripheral vein injection of sonicated albumin microbubbles. Am Heart J. 1997;133(4):400–5.
104. Jung PH, Mueller M, Schuhmann C, Eickhoff M, Schneider P, Seemueller G, et al. Contrast enhanced transesophageal echocardiography in patients with atrial fibrillation referred to electrical cardioversion improves atrial thrombus detection and may reduce associated thromboembolic events. Cardiovasc Ultrasound. 2013;11(1):1.
105. Fatkin D, Feneley M. Stratification of thromboembolic risk of atrial fibrillation by transthoracic echocardiography and transesophageal echocardiography: the relative role of left atrial appendage function, mitral valve disease, and spontaneous echocardiographic contrast. Prog Cardiovasc Dis. 1996;39(1):57–68.
106. Jue J, Winslow T, Fazio G, Redberg RF, Foster E, Schiller NB. Pulsed Doppler characterization of left atrial appendage flow. J Am Soc Echocardiogr. 1993;6(3 Pt 1):237–44.
107. Manning WJ, Silverman DI. Atrial anatomy and function postcardioversion: insights from transthoracic and transesophageal echocardiography. Prog Cardiovasc Dis. 1996;39(1):33–46.
108. Handke M, Harloff A, Hetzel A, Olschewski M, Bode C, Geibel A. Left atrial appendage flow velocity as a quantitative surrogate parameter for thromboembolic risk: determinants and relationship to spontaneous echocontrast and thrombus formation – a transesophageal echocardiographic study in 500 patients with cerebral ischemia. J Am Soc Echocardiogr. 2005;18(12):1366–72.
109. Heppell RM, Berkin KE, McLenachan JM, Davies JA. Haemostatic and haemodynamic abnormalities associated with left atrial thrombosis in non-rheumatic atrial fibrillation. Heart. 1997;77(5):407–11.
110. Antonielli E, Pizzuti A, Palinkas A, Tanga M, Gruber N, Michelassi C, et al. Clinical value of left atrial appendage flow for prediction of long-term sinus rhythm maintenance in patients with nonvalvular atrial fibrillation. J Am Coll Cardiol. 2002;39(9):1443–9.
111. Uretsky S, Shah A, Bangalore S, Rosenberg L, Sarji R, Cantales DR, et al. Assessment of left atrial appendage function with transthoracic tissue Doppler echocardiography. Eur J Echocardiogr J Work Group Echocardiogr Eur Soc Cardiol. 2009;10(3):363–71.
112. Parvathaneni L, Mahenthiran J, Jacob S, Foltz J, Gill WJ, Ghumman W, et al. Comparison of tissue Doppler dynamics to Doppler flow in evaluating left atrial appendage function by transesophageal echocardiography. Am J Cardiol. 2005;95(8):1011–4.
113. Ono K, Iwama M, Kawasaki M, Tanaka R, Watanabe T, Onishi N, et al. Motion of left atrial appendage as a determinant of thrombus formation in patients with a low CHADS2 score receiving warfarin for persistent nonvalvular atrial fibrillation. Cardiovasc Ultrasound. 2012;10:50.
114. Kaya EB, Tokgozoglu L, Aytemir K, Kocabas U, Tulumen E, Deveci OS, et al. Atrial myocardial deformation properties are temporarily reduced after cardioversion for atrial fibrillation and correlate well with left atrial appendage function. Eur J Echocardiogr J Work Group Echocardiogr Eur Soc Cardiol. 2008;9(4):472–7.
115. Providencia R, Faustino A, Ferreira MJ, Goncalves L, Trigo J, Botelho A, et al. Evaluation of left atrial deformation to predict left atrial stasis in patients with non-valvular atrial fibrillation – a pilot-study. Cardiovasc Ultrasound. 2013;11:44.
116. Arslan S, Simsek Z, Gundogdu F, Aksakal E, Kalkan ME, Gurlertop Y, et al. Can left atrial strain and strain rate imaging be used to assess left atrial appendage function? Cardiology. 2012;121(4):255–60.
117. Motoki H, Negishi K, Kusunose K, Popovic ZB, Bhargava M, Wazni OM, et al. Global left atrial strain in the prediction of sinus rhythm maintenance after catheter ablation for atrial fibrillation. J Am Soc Echocardiogr. 2014;27(11):1184–92.
118. Motoki H, Dahiya A, Bhargava M, Wazni OM, Saliba WI, Marwick TH, et al. Assessment of left atrial mechanics in patients with atrial fibrillation: comparison between two-dimensional speckle-based strain and velocity vector imaging. J Am Soc Echocardiogr. 2012;25(4):428–35.
119. To AC, Flamm SD, Marwick TH, Klein AL. Clinical utility of multimodality LA imaging: assessment of size, function, and structure. J Am Coll Cardiol Img. 2011;4(7):788–98.
120. Sallach JA, Puwanant S, Drinko JK, Jaffer S, Donal E, Thambidorai SK, et al. Comprehensive left atrial appendage optimization of thrombus using surface echocardiography: the CLOTS multicenter pilot trial. J Am Soc Echocardiogr. 2009;22(10):1165–72.
121. Yamamoto M, Seo Y, Kawamatsu N, Sato K, Sugano A, Machino-Ohtsuka T, et al. Complex left atrial appendage morphology and left atrial appendage thrombus formation in patients with atrial fibrillation. Circ Cardiovasc Imaging. 2014;7(2):337–43.
122. Transesophageal echocardiographic correlates of thromboembolism in high-risk patients with nonvalvular atrial fibrillation. The Stroke Prevention in Atrial Fibrillation Investigators Committee on Echocardiography. Ann Intern Med. 1998;128(8):639–47.
123. Bernhardt P, Schmidt H, Hammerstingl C, Luderitz B, Omran H. Patients with atrial fibrillation and dense spontaneous echo contrast at high risk a prospective and serial follow-up over 12 months with transesophageal echocardiography and cerebral magnetic resonance imaging. J Am Coll Cardiol. 2005;45(11):1807–12.
124. Connolly SJ, Ezekowitz MD, Yusuf S, Eikelboom J, Oldgren J, Parekh A, et al. Dabigatran versus warfarin in patients with atrial fibrillation. N Engl J Med. 2009;361(12):1139–51.
125. Patel MR, Mahaffey KW, Garg J, Pan G, Singer DE, Hacke W, et al. Rivaroxaban versus warfarin in nonvalvular atrial fibrillation. N Engl J Med. 2011;365(10):883–91.
126. Granger CB, Alexander JH, McMurray JJ, Lopes RD, Hylek EM, Hanna M, et al. Apixaban versus warfarin in patients with atrial fibrillation. N Engl J Med. 2011;365(11):981–92.
127. Giugliano RP, Ruff CT, Braunwald E, Murphy SA, Wiviott SD, Halperin JL, et al. Edoxaban versus warfarin in patients with atrial fibrillation. N Engl J Med. 2013;369(22):2093–104.

128. Nagarakanti R, Ezekowitz MD, Oldgren J, Yang S, Chernick M, Aikens TH, et al. Dabigatran versus warfarin in patients with atrial fibrillation: an analysis of patients undergoing cardioversion. Circulation. 2011;123(2):131–6.
129. Piccini JP, Stevens SR, Lokhnygina Y, Patel MR, Halperin JL, Singer DE, et al. Outcomes after cardioversion and atrial fibrillation ablation in patients treated with rivaroxaban and warfarin in the ROCKET AF trial. J Am Coll Cardiol. 2013;61(19):1998–2006.
130. Flaker G, Lopes RD, Al-Khatib SM, Hermosillo AG, Hohnloser SH, Tinga B, et al. Efficacy and safety of apixaban in patients after cardioversion for atrial fibrillation: insights from the ARISTOTLE Trial (apixaban for reduction in stroke and other thromboembolic events in atrial fibrillation). J Am Coll Cardiol. 2014;63(11):1082–7.
131. Lip GYH, Merino J, Ezekowitz M, Ellenbogen K, Zamoryakhin D, Lanz H, et al. A prospective evaluation of edoxaban compared to warfarin in subjects undergoing cardioversion of atrial fibrillation: the EdoxabaN vs. warfarin in subjectS UndeRgoing cardiovErsion of Atrial Fibrillation (ENSURE-AF) study. Am Heart J. 2015:169:597–604
132. Dentali F, Riva N, Crowther M, Turpie AG, Lip GY, Ageno W. Efficacy and safety of the novel oral anticoagulants in atrial fibrillation: a systematic review and meta-analysis of the literature. Circulation. 2012;126(20):2381–91.
133. Adam SS, McDuffie JR, Ortel TL, Williams Jr JW. Comparative effectiveness of warfarin and new oral anticoagulants for the management of atrial fibrillation and venous thromboembolism: a systematic review. Ann Intern Med. 2012;157(11):796–807.
134. Ntaios G, Papavasileiou V, Diener HC, Makaritsis K, Michel P. Nonvitamin-K-antagonist oral anticoagulants in patients with atrial fibrillation and previous stroke or transient ischemic attack: a systematic review and meta-analysis of randomized controlled trials. Stroke. 2012;43(12):3298–304.
135. Ruff CT, Giugliano RP, Braunwald E, Hoffman EB, Deenadayalu N, Ezekowitz MD, et al. Comparison of the efficacy and safety of new oral anticoagulants with warfarin in patients with atrial fibrillation: a meta-analysis of randomised trials. Lancet. 2014;383(9921):955–62.
136. Bruins Slot KM, Berge E. Factor Xa inhibitors versus vitamin K antagonists for preventing cerebral or systemic embolism in patients with atrial fibrillation. Cochrane Database Syst Rev. 2013;8:CD008980.
137. Salazar CA, del Aguila D, Cordova EG. Direct thrombin inhibitors versus vitamin K antagonists for preventing cerebral or systemic embolism in people with non-valvular atrial fibrillation. Cochrane Database Syst Rev. 2014;3:CD009893.
138. Cappato R, Ezekowitz MD, Klein AL, Camm AJ, Ma CS, Le Heuzey JY, et al. Rivaroxaban vs. vitamin K antagonists for cardioversion in atrial fibrillation. Eur Heart J. 2014;35:3346–55.

Echo Guided Pericardiocentesis

2

Robert J. Siegel and Reza Arsanjani

Abstract

In this chapter we discuss the indications, as well as the echocardiographic/Doppler diagnosis of pericardial tamponade. We provide an in depth description of how to perform an echocardiographic guided pericardiocentesis. A detailed description is given on how to prepare for performing pericardiocentesis, equipment needed, use of local analgesia, exclusion criteria, and the optimal site for pericardial puncture as dictated by echocardiographic guidance. We explain different approaches for pericardial access, how to identify the angle for needle insertion and to determine the depth of needle penetration that is both safe and required. We describe the use of pericardial catheter drainage, laboratory studies that should be performed on the pericardial fluid and management of pericardial drain, as well as when the drain should be removed. We outline our use of medications before (local analgesia), and after the procedure (anti-staphlococcal coverage while the pericardial catheter is in place and the use of colchicine and non-steroidal anti-inflammatory agents). Detailed imaging is provided for the echocardiographic findings as well as step-by-step photo demonstration of the pericardiocentesis procedure.

Keywords

Pericardial effusion • Pericardial tamponade • Ultrasound guidance • Echocardiography • Doppler • Pericardial drainage

Historical Perspective

Hippocrates first identified the pericardium as a sac around the heart containing a small amount of yellow fluid. Some 600 years later Galen, the Greek physician to Roman gladiators, was the first to describe pericardial effusion due to cardiac trauma. The first open drainage of a traumatic pericardial effusion was performed by the surgeon Dominque Larrey in 1810. A soldier in the French army had stabbed himself in the chest and was progressively deteriorating. Forty-days after the self – inflicted wound, Larrey surgically drained more than a liter of fluid and clot. Initially the patient made a remarkable recovery, only to succumb to infection about 3 weeks later. The first percutaneous drainage of the pericardium was done in Vienna by Frank Schuh in 1840, to treat a 24 year old woman suffering from severe dyspnea. Schuh inserted a trocar between her ribs and removed over a liter of blood tinged effusion. His patient had prompt improvement in her breathing, but succumbed to an intra-thoracic neoplasm. In 1896, the German physician Ludvig Rehn performed the first successful treatment of pericardial tamponade by draining the effusion and suturing an RV laceration due to a stab wound. In 1911 Antoine Marfan in France described

R.J. Siegel, MD, FACC, FASE (✉)
Division of Cardiology,
Cedars-Sinai Medical Center, Heart Institute,
127 S. San Vicente, AHSP Building,
Los Angeles, CA 90048, USA
e-mail: Robert.Siegel@cshs.org

R. Arsanjani, MD
Medicine, Division of Cardiology,
Cedars-Sinai Medical Center, Heart Institute,
127 S. San Vicente Blvd, A3100, Los Angeles, CA 90025, USA
e-mail: arsanjanir@gmail.com

M.H. Picard et al. (eds.), *Intraprocedural Imaging of Cardiovascular Interventions*, DOI 10.1007/978-3-319-29428-5_2

the subcostal approach for pericardiocentesis. This became the standard approach for decades, and is still used as the primary site for access when the pericardiocentesis procedure is done without echocardiographic guidance.

Indications for Pericardiocentesis

The indications for pericardiocentesis can be categorized as elective, urgent, or emergent. Elective pericardiocenteses are often indicated for diagnostic purposes in the setting of an effusion to assess for metastatic disease or to diagnose purulent pericarditis. Emergent pericardiocentesis is usually performed when there is acute hemodynamic compromise with hypotension. This may occur in the cardiac catheterization and electrophysiology (EP) laboratories when there is a cardiac perforation resulting in the rapid accumulation of 50–100 cc of blood in the pericardial space. Even with echo equipment readily available for guidance, deterioration in some cases may so be rapid that an immediate subcostal needle puncture is required to relieve possible tamponade to prevent complete cardiovascular collapse.

The most frequent clinical setting in which a significant pericardial effusion is detected in our hospital are: an increase in the cardiac silhouette on chest X-ray, post cardiac procedures such as open heart surgery or percutaneous cardiac intervention, hypotension and/or tachycardia. In these settings an echocardiogram is done to confirm the clinical suspicion of a pericardial effusion. In addition, some effusions are found "incidentally". These patients often have shortness of breath, tachycardia, chest pain or other non-specific symptoms. Post-cardiac surgical patients may develop asymptomatic and large pericardial effusions – especially if they are receiving anticoagulation. Effusions that develop rapidly generally manifest clinically with symptoms and/or hemodynamic compromise. With effusions that develop slowly, the echo findings of tamponade or "pre- tamponade" moderate to large effusions often precede symptoms or clinical signs of hypotension or hypoperfusion. As shown in Fig. 2.1, a large pericardial effusion is circumferential and greater than 1 cm [1]. Multiple echocardiographic signs of cardiac tamponade are shown in the following Figs. 2.2, 2.3, and 2.4. Right atrial systolic collapse (LV systole) as shown in Fig. 2.2 – is an early sign of tamponade. However when there are signs of an elevated right atrial pressure as demonstrated in Fig. 2.3 – (a dilated and non-collapsing IVC) or diastolic collapse of the RV seen in Fig. 2.4 – signs and symptoms of tamponade are generally present. Additionally, Doppler inspiratory variation of the tricuspid and mitral inflow as well as LVOT pulsed wave (PW) Doppler could indicate tamponade physiology. It should be kept in mind however that certain clinical findings will prevent the development of tamponade physiology and may thus delay the diagnosis. These findings include intracardiac shunts such as an ASD, elevated LV filling pressures

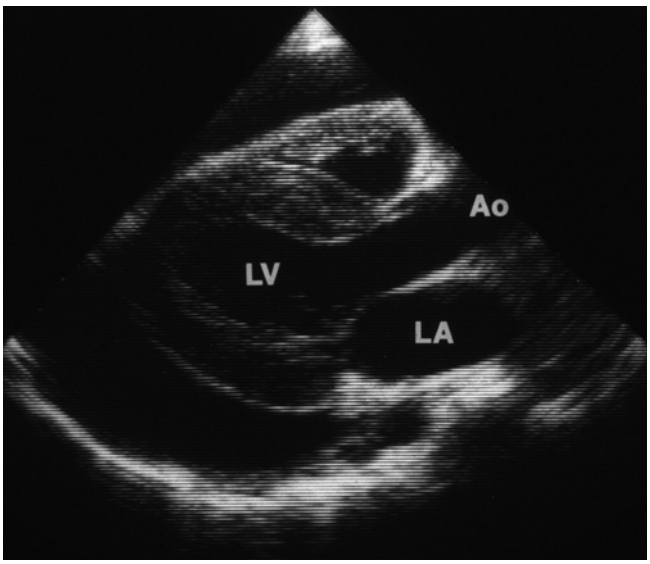

Fig. 2.1 Parasternal long axis echocardiographic window demonstrating a large, circumferential pericardial effusion

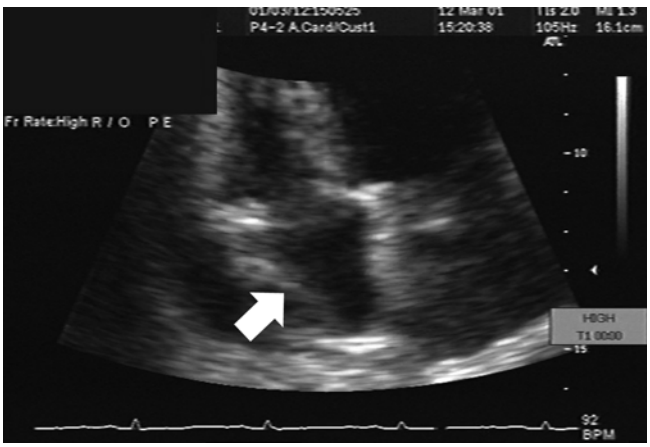

Fig. 2.2 Echocardiographic images demonstrating right atrial collapse, which is an early sign of tamponade

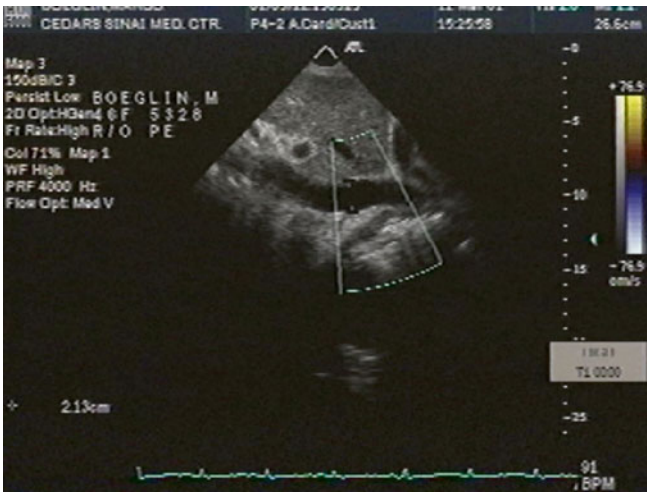

Fig. 2.3 Subcostal images demonstrating inferior vena cava plethora, which is a very sensitive (97 %) but non-specific (40 %) sign of tamponade

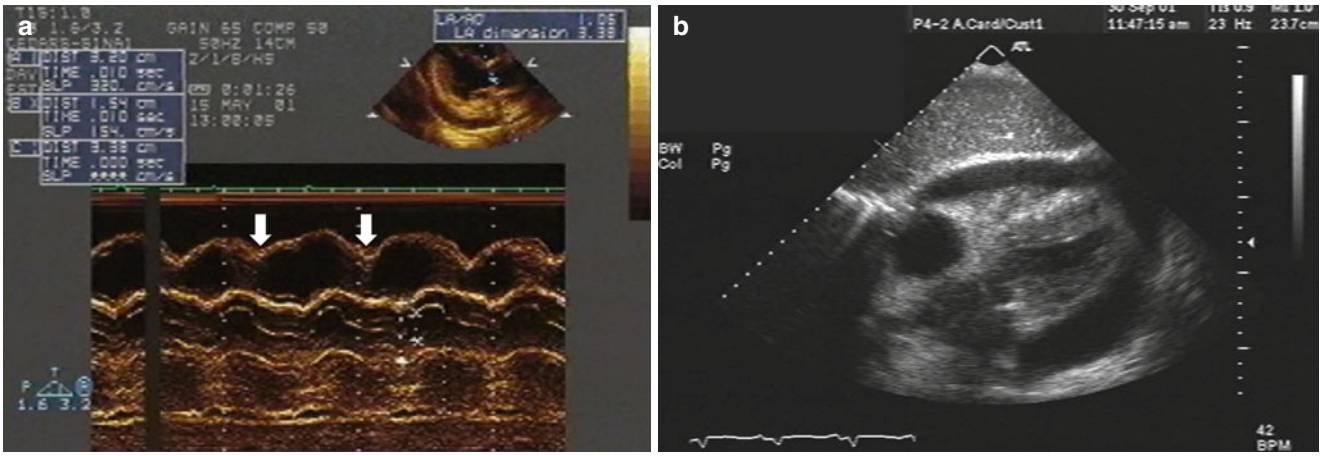

Fig. 2.4 (**a**) M-mode (*arrows*) and (**b**) subcostal images demonstrating right ventricular diastolic collapse

that preclude the RVEDP equalizing with the LVEDP (i.e. >20 mmHg), and aortic regurgitation that allows LV filling, independent of respiratory hemodynamic changes. Very large effusions in excess of 2000 ml can accumulate if the fluid build-up is slow. Thus the hemodynamic changes as a consequence of the effusion – emergent vs. urgent and even elective pericardiocentesis is generally more related to the rate of fluid accumulation than to effusion size.

Pericardiocentesis Without Echocardiographic Guidance

Pericardiocentesis without echocardiographic guidance is usually done in the emergent setting, and almost always employs a subcostal approach to try to enter the pericardial space. It may be preferable to angulate the needle toward the left shoulder as this is away from the lung and closer to the heart, however the needle can also be pointed towards the right shoulder to avoid puncturing the left anterior descending coronary artery. Some interventional cardiologists utilize fluoroscopy which allows visualization of the enlarged cardiac silhouette but does not permit precise delineation of the pericardial effusion or differentiate the epicardial surface from the limits of the pericardium. Consequently, using fluoroscopy is limited for finding the safest and easiest site to enter the pericardial effusion. Without echo guidance, complication rates range between 20 % and 50 % and the mortality is 6 % [2]. Complications include cardiac penetration, coronary artery laceration, pneumothorax, and penetration or laceration of viscera in the path of the pericardiocentesis needle [3].

Echocardiographic Guided Pericardiocentesis

The Mayo Clinic group, especially Callahan, Seward, Tsang and Nishimura [4] were early proponents for echo guided pericardiocentesis.

Their publications demonstrated that echo guidance improves the safety and feasibility of percutaneous pericardiocentesis. Over a 21 year period of performing pericardiocentesis on nearly 1,000 patients (n = 977), their success rate of obtaining fluid and draining the effusion was 97 %; major complications were only 1.2 % and minor complications occurred in 3.5 %. Their results reflect a substantial improvement over pericardiocentesis without echo guidance [2]. In our experience at Cedars Sinai Medical Center over the past 15 years with more than 500 patients, the major complication rate was 0.2 % with 1 patient having a pneumothorax and no mortality or need for urgent surgery [5, 6].

We prefer to perform pericardiocentesis in the ICU at the patient's bedside which allows for continuous monitoring of heart rate, blood pressure, and oxygen saturation. This avoids moving a potentially hemodynamically unstable patient to and from the catheterization laboratory or procedure room. In addition, keeping the patient in the same room reduces infection risk and the potential for catheter dislodgement during patient transfers (Tables 2.1a and 2.1b)

Preparations Prior to Pericardiocentesis

1. Obtain patient consent for the pericardiocentesis procedure.
2. Check platelet count and coagulation status.
3. Perform a 2D echo to find the largest effusion site, which is easiest to access.
4. Exclude patients with aortic dissection and/or a dilated aorta which suggests the possibility of an aortic dissection. While pericardiocentesis in the setting of a dissection may alleviate hypotension, it may also extend the dissection and/or promote aortic rupture.
5. Determine the optimal site for the pericardial puncture, avoiding lung, liver or other viscera. In addition the distance from the skin to the effusion should be measured

Table 2.1a Equipment for the pericardiocentesis

1. Echo machine
2. Mask, gowns, sterile gloves, surgical tape
3. Pericardiocentesis kit containing a large bore 19 gauge Cook needle, a 0.35 cm J-tipped guide wire, an 8 or 9 Fr dilator, a pig-tailed Pericardiocentesis catheter with side holes, sterile gauze
4. Sterile drapes
5. A sterile blade to incise the skin at the catheter insertion site
6. A hemostat, sterile scissors
7. Suture (0 or 00 silk or chromic) with a curved needle
8. A sterile sheath and gel for the ultrasound probe
9. A micro-puncture needle[a]
10. An angio-catheter[a]

[a]Optional- the pericardial puncture may be done with a 19 gauge needle that allows advancement of an 0.35 guide wire or with a micro puncture needle set – which is less traumatic than the standard needle or an angiocatheter of sufficient length can be used which is large enough to allow passage of a guide wire through it

Table 2.1b Medications for the pericardiocentesis

1. 1 % xylocaine without epinephrine
2. Atropine – opened or at the bedside in case the patient has a vasovagal reaction during or immediately after the Pericardiocentesis
3. Post- procedure treat with anti-staphlococcal medication until the pericardial catheter has been removed
4. Post-procedure anti-inflamatory drugs colchicine, and NSAIDs and or aspirin (never give corticosteroids as this increase recurrence rate of pericarditis)

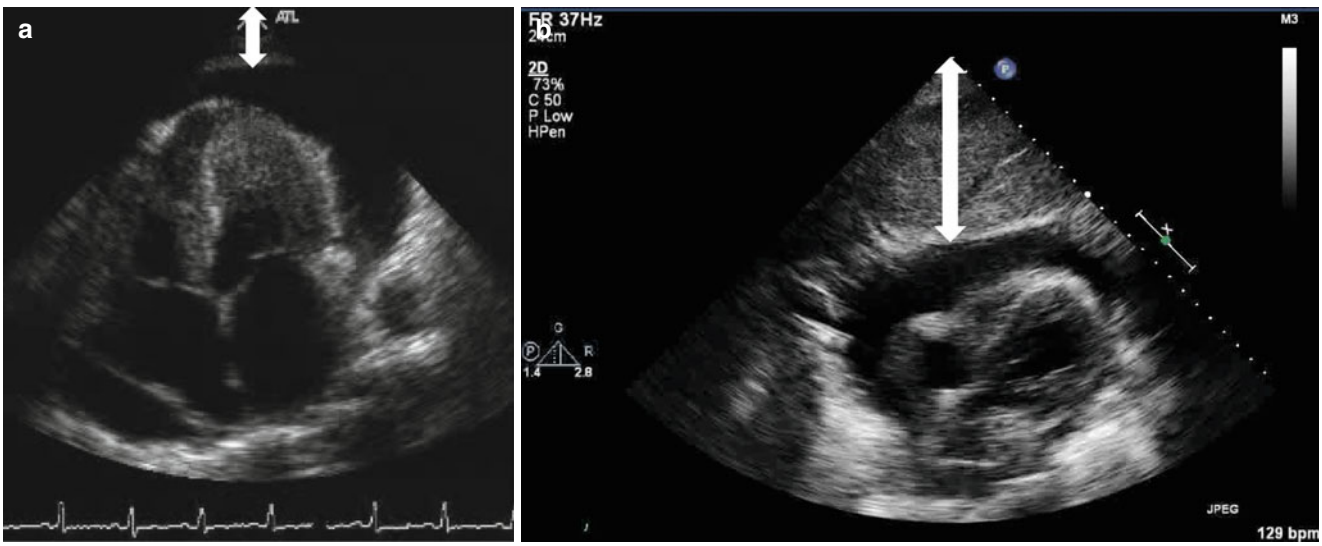

Fig. 2.5 (**a**) Apical 4-chamber and (**b**) Subcostal images are demonstrated. In each case the *arrows* indicate the distance between the skin and pericardial effusion

and it should be confirmed that the needle length is sufficient to access the effusion (Figs. 2.5a, b).

6. Measure the distance from the chest wall (Fig. 2.5a) or subcostal space to the effusion (Fig. 2.5b). A transapical access may be preferable, but this decision is dictated by effusion size and location. We use the ultrasound transducer to determine the optimal entry site into the thorax, and also to set the angle of incidence for the needle and the chest wall that will be used when entering the chest and advancing the needle. Thus the operator performing the pericardiocentesis should image the pericardial effusion from the planned site of needle entry to set the best angle of needle insertion. The ultrasound transducer should be tilted medial and laterally as well as in the anterior and posterior directions to see where there is sufficient amount of pericardium for safe needle access to the pericardial effusion.

The Pericardiocentesis Procedure

1. Explain each aspect of the procedure to the patient. This helps to reassure the patient and keeps patient movement to a minimum which is important to avoid complications.
2. Position the patient in the supine position close to the edge of the bed with the head at 0–30° and even as high as 45° to avoid respiratory distress. Positioning is important to facilitate ease of the procedure.
3. Mark the puncture site. This may be done with "permanent ink" however this sometimes disappears with the sterile preparation solution. It can be preferable to gently scratch the skin to create a mark which is easily seen as in Fig. 2.6a. This mark is not affected by the skin prep solution.
4. Prepare the puncture site with a very thorough and meticulous skin preparation to avoid the introduction of any bacteria into the pericardial space. Drape the area as seen in the Fig. 2.6b.
5. Infiltrate the site with 1 % xylocaine without epinephrine (1st with a 25 gauge and then with a 22 gauge needle) as shown in Fig. 2.6c. It has become our habit to use 20–30 ml of xylocaine so that the procedure is painless, the patient is comfortable, and does not move during the procedure. With adequate local xylocaine analgesia additional pain medication is not necessary. A patient with a hemodynamically significant effusion should never receive sedation as this may reduce adrenergic drive and result in profound hypotension
6. Make a skin incision (Fig. 2.6d) at the planned site of needle entry and dilate that site with a hemostat (Fig. 2.6e). Figure 2.7 shows the various sites used at our institution for needle insertion which include subxiphoid, trans-apical, parasternal, apical lateral and high lateral sites. The trans apical and subxiphoid approaches are most common. We avoid the subxiphoid approach if the liver or other viscera are in the way. However, a report by Lindenberger describes pericardial access through the liver. They reported no complications even in anti-coagulated patients [7]. As we almost uniformly leave a pericardial drain in place, this could be problematic with a trans-hepatic stick potentially leading to a hepatic fistula, bleeding or other problems.
7. Monitoring:
   (a) During advancement of the 18 gauge 15 cm in length pericardiocentesis needle as shown in Fig. 2.8a, ECG is monitored, along with blood pressure every 1–2 min
   (b) A surface 2D echo using a regular probe from a location outside of the surgical field to prevent contamination (e.g. parasternal view, apical view for a subcostal approach and a subcostal view for an apical approach). Alternatively, a sterile sheath or ultrasound probe cover may be placed over a 2D transthoracic transducer, using standard ultrasonic gel with in the sheath and sterile gel on the surface of the probe cover. In addition, there are specially manufactured acoustically reflective procedure needles that may be used to visualize the needle with ultrasound imaging during insertion.
   (c) The sub-xiphoid approach is monitored by echo from a parasternal or apical window. Measuring the distance from the skin to the effusion is important in this approach because the distance to the effusion is generally greater than with the transthoracic puncture.
   (d) With a trans-thoracic puncture care should be taken to ensure that there is no intervening lung between the chest wall and puncture site. As shown in Fig. 2.5a, this is readily confirmed by echo showing the effusion extending to the chest wall.
   (e) For transapical approaches in women, one should not go through the breast tissue. If the left breast is in the surgical field, we securely tape it upwards as demonstrated in Fig. 2.6a so that the breast remains out of the sterile field during the procedure.
   (f) In cases in which there is a relatively small or loculated effusion in which the pericardiocentesis is being done for diagnostic evaluation (cancer or infection) ECG monitoring via the pericardiocentesis needle itself can be helpful to avoid myocardial puncture. To do this, an alligator clamp is attached to the pericardial needle and to an ECG electrode. The electrode is then attached to an ECG machine or the bedside ECG monitor. If during the procedure the needle comes into contact with the ventricular epicardium ST segment elevation will appear on the ECG tracing. If this occurs, the needle should be pulled back slowly until ST segment elevation disappears.
8. During needle insertion (Fig. 2.8b) we advance in 2–3 mm movements at the angle determined by the pre-procedure bedside echo.
9. When non-sanguinous fluid is aspirated we generally remove 10 cc of fluid to decompress the pericardial sac, and then carefully detach the syringe from the needle without changing the needle location and/or angle. A guide wire is then advanced thru the needle into the pericardial space as shown in Fig. 2.8c. The guide wire should advance easily; if it does not, the wire should be removed and the needle redirected. When the pericardial aspirate is free flowing the guide wire should be re-advanced. If the effusion is bloody, discharge some of the aspirate on to a gauze pad and check for the presence of small blood clots. If the aspirate clots, the needle is

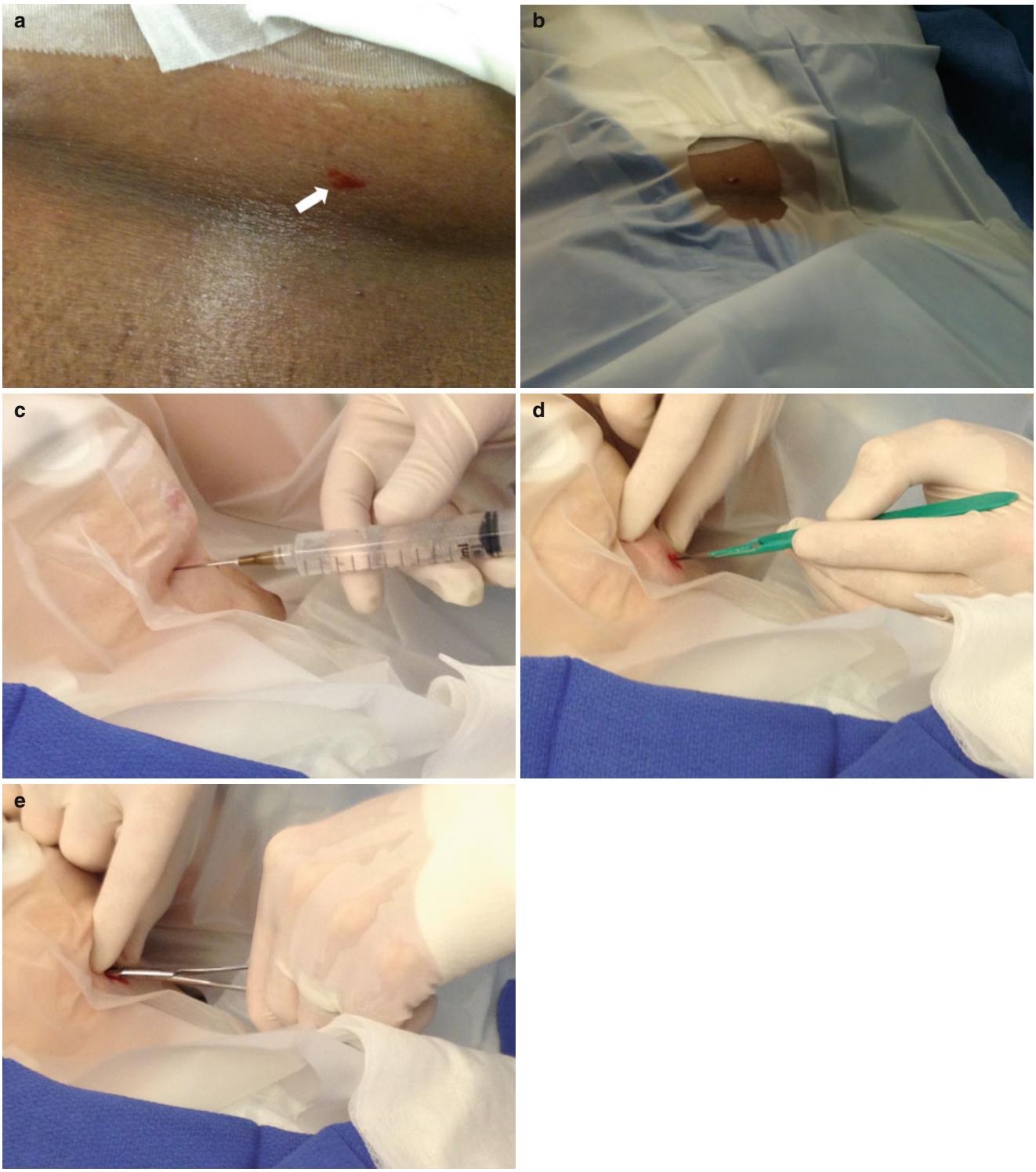

Fig. 2.6 (**a**) The puncture site could be marked by permanent ink or by scratching the skin as shown below. In this female patient the breast tissue is taped to hold the breast out of the plane of access for pericardiocentesis. (**b**) The pericardiocentesis site is prepared and draped in usual sterile fashion. (**c**) The access site is anesthesized using 1 % xylocaine without epinephrine. (**d**) A skin incision is made using a scalpel at the planned site of needle entry. (**e**) The entry site is dilated using a hemostat

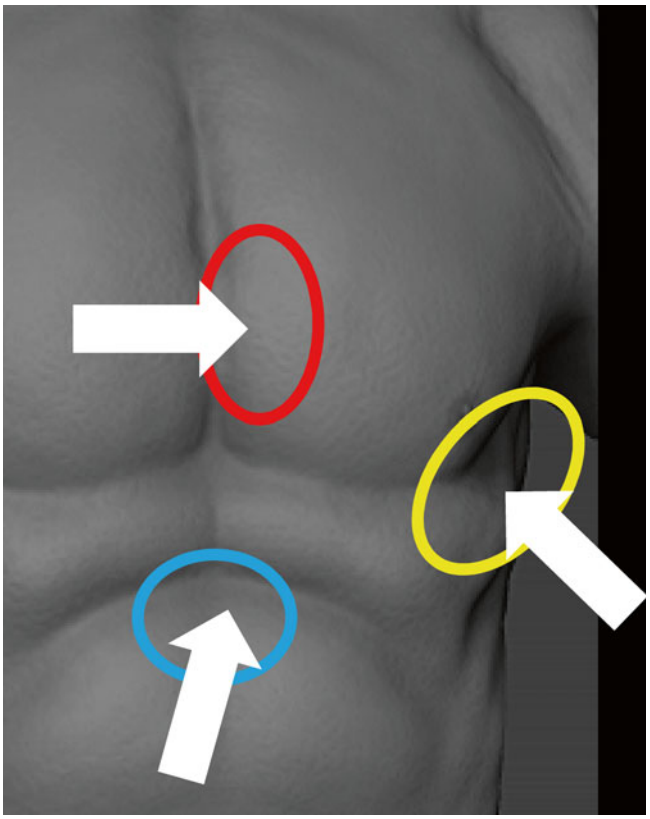

Fig. 2.7 Various sites used for needle insertion during pericardiocentesis. These sites include parasternal (*red*), apical (*yellow*), and subcostal (*blue*) with the *arrows* indicating potential the sites of access

not in the pericardial space or it is very fresh blood from a ruptured heart or aortic dissection with leakage of blood into the pericardial space. This is an emergent situation and aspiration of blood should be immediately stopped as relief of tamponade in this setting will allow systemic pressure to rise and lead to further ventricular or aortic rupture or dissection. Such patients should be taken urgently to the OR and a TEE done to confirm the diagnosis.

If the bloody fluid is non-clotting one needs to determine if the source of the blood is the heart or the pericardial space. This may be done by injecting agitated saline into the pericardial space. As demonstrated in Fig. 2.9. our preference is to aspirate the patient's blood admix it between two syringes with a three way stopcock and re-inject it through the catheter, resulting in a robust echo-contrast image allowing determination of whether the needle is intra-pericardial as in Fig. 2.9 or intra-cardiac if the echo contrast would be seen within the heart itself.

10. After confirmation that the needle is in the pericardial space in which case the dilator is passed over a guidewire as seen in Fig. 2.8d. We generally dilate the space three times to allow for easy passage of the pericardial catheter.
11. The pericardial catheter is then advanced into the pericardial space at least 20 cm (Fig. 2.8e). The catheter is sutured in place and the pericardial fluid is aspirated and transferred to drainage bag until there is no further drainage.
12. We attach the pericardial catheter to a Jackson Pratt drain (Fig. 2.8f) and keep the intra-pericardial catheter in place for generally more than 36 h and until the drainage is less than 50 ml in a 24 h period and there is concomitantly no more than a trivial pericardial effusion on echo.
13. Pericardial fluid is sent for analysis. The tests which are ordered depend on the clinical setting. When it is clearly a traumatic etiology, we generally only send for culture, gram stain, cell count and glucose to ensure that no secondary infection is present. If there is a potential for a neoplastic process, in addition to the above, we send most of the fluid for cytology. We have found that distinguishing between transudate and exudate by LDH or total protein has little diagnostic or prognostic value. A transudate does not exclude a neoplastic etiology [8]. When there is a potential for infection especially in elderly or immune compromised patients, we assess not only for bacteria but also for fungi and for TB by PCR and AFB stain.
14. Patients are treated with an antibiotic prophylaxis that provides anti- staphylococcal coverage until the pericardial catheter is removed. If there are no contraindications, it is also our practice to place the patients on anti-inflammatory therapy with colchicine and NSAIDS or ASA.
15. Following removal of a large pericardial effusion, the heart rate usually improves (Fig. 2.10). In addition, echocardiographic images demonstrate improvement in right atrial pressure (IVC collapsibility), resolution of inspiratory variation of the tricuspid and mitral inflow (Fig. 2.11), as well as the respiratory variation seen on a pulse oximeter, these all reflect the resolution of pulsus paradoxus which is caused by cardiac tamponade.

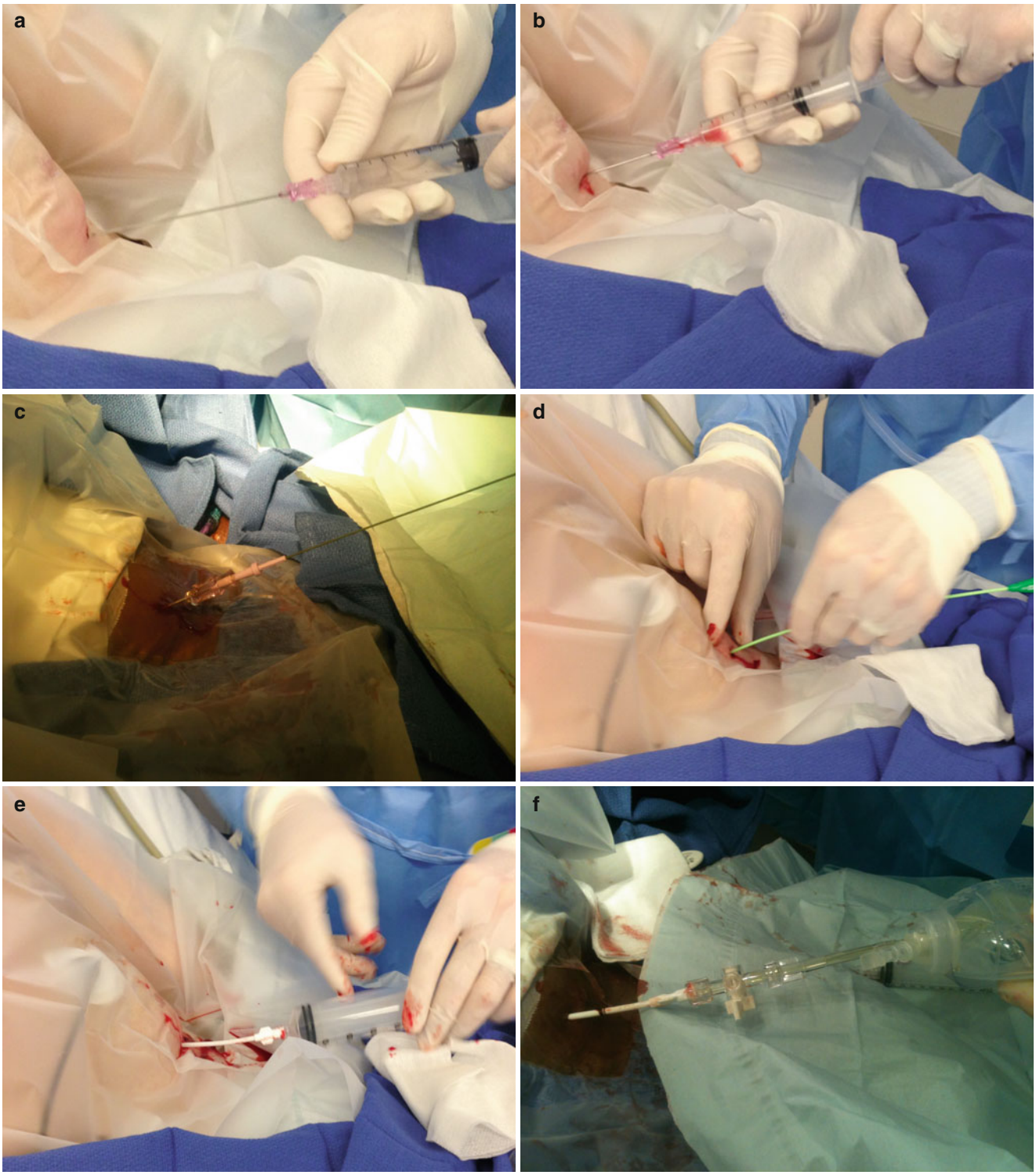

Fig. 2.8 (**a**) A Cook needle is used to gain access to the pericardial space. (**b**) The Cook needle is slowly advanced until small amount of pericardial fluid is aspirated. (**c**) The guide wire is advanced thru the needle into the pericardial space. (**d**) A dilator is passed over the guidewire to allow for easy passage of the pericardial catheter. (**e**) The pericardial catheter is advanced over the guidewire into the pericardial space for at least 20 cm. (**f**) The pericardial catheter is attached to a Jackson Pratt drain and kept in place for generally more than 36 h

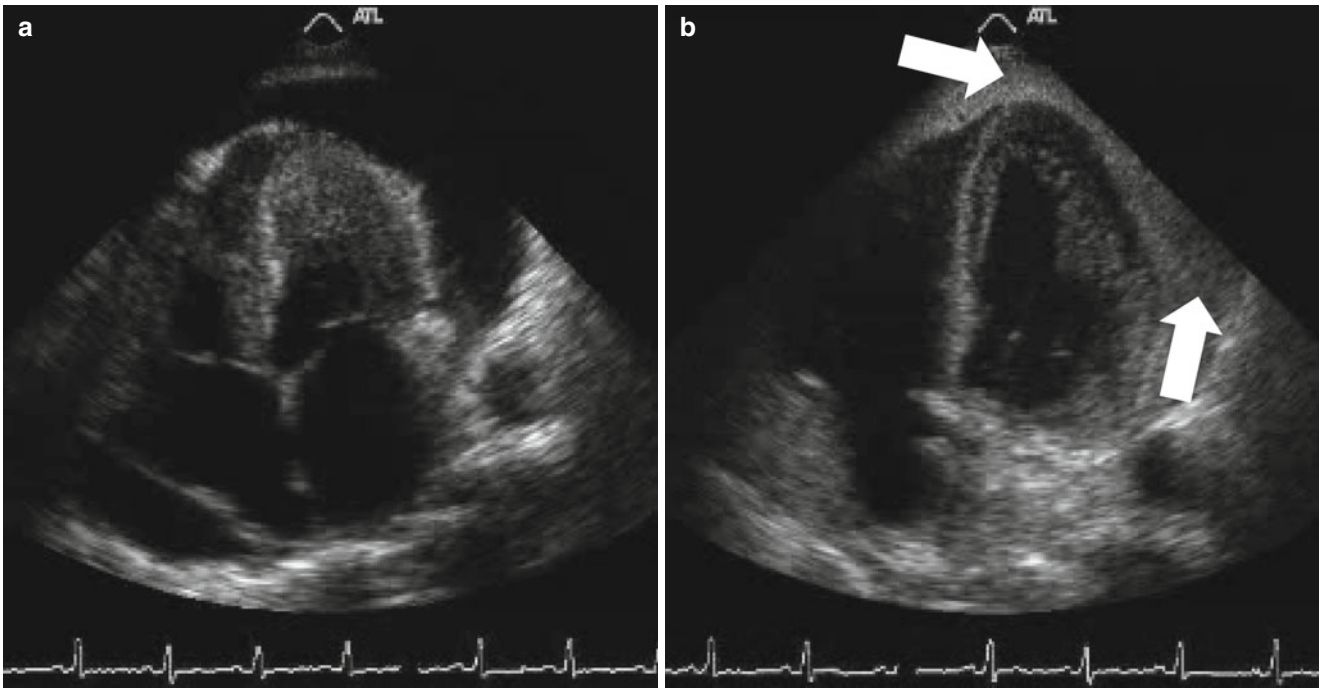

Fig. 2.9 (**a**) Apical 4-chamber echocardiographic image demonstrating pericardial effusion. (**b**) *Arrows* demonstrate saline echo-contrast injected into pericardial space confirming the location of pericardial catheter

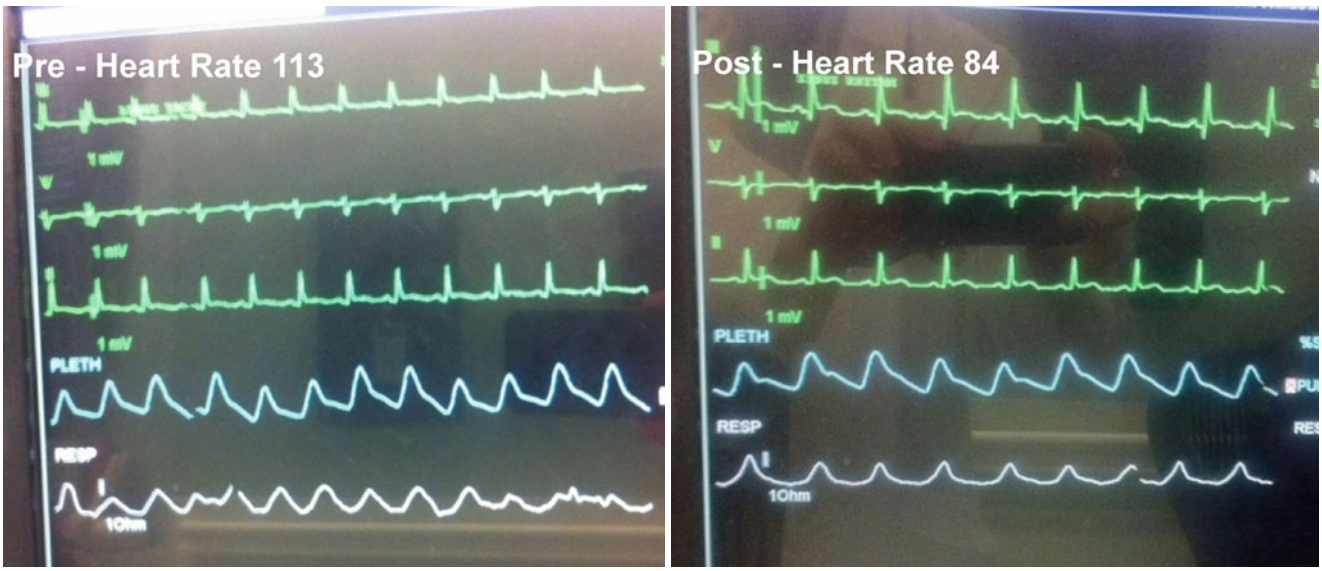

Fig. 2.10 Vital signs pre- and post- pericardiocentesis demonstrating significant improvement in heart rate

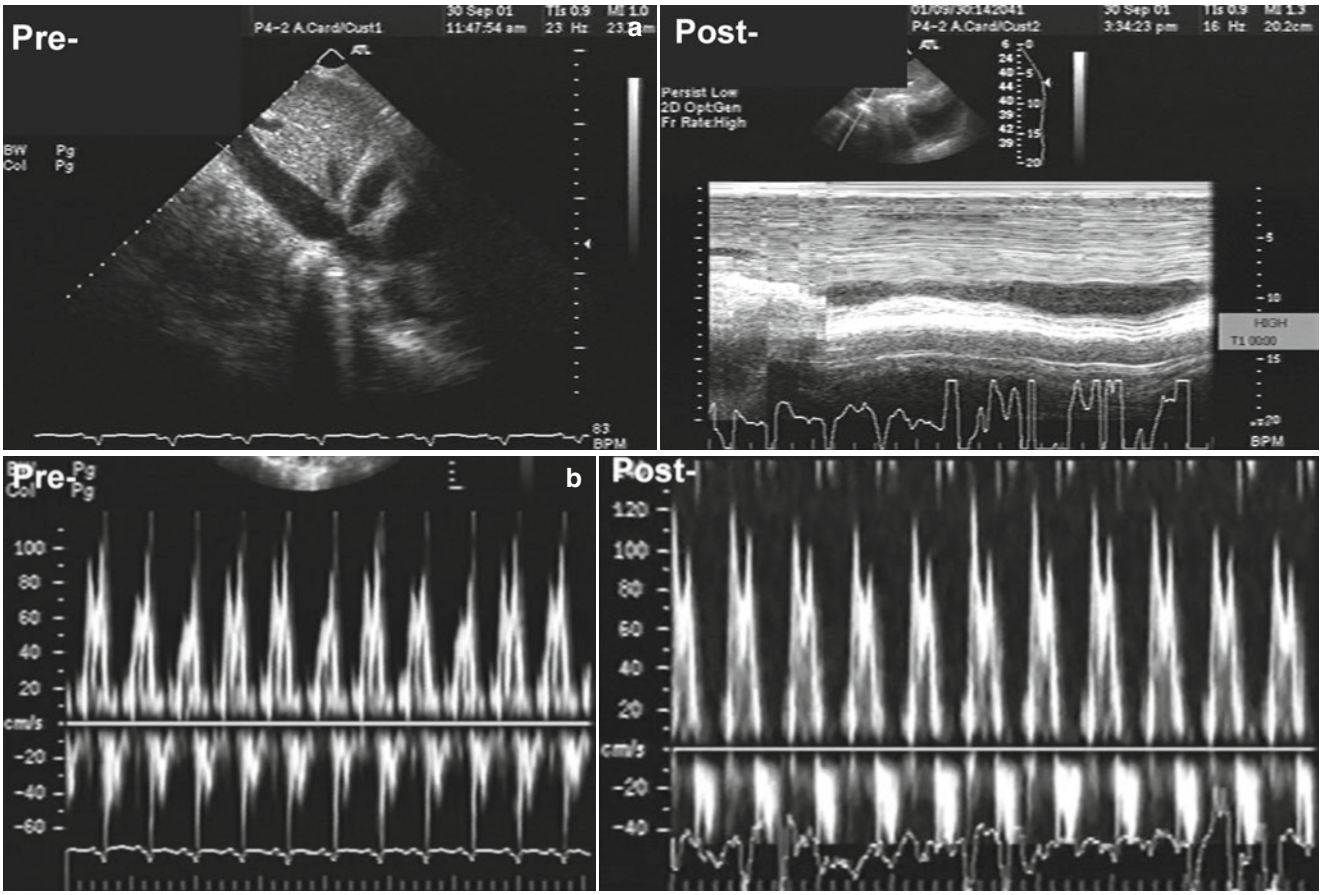

Fig. 2.11 (**a**) Following pericardiocentesis the IVC collapses and (**b**) the inspiratory variation across the mitral valve is no longer present

References

1. Weitzman LB, Tinker WP, Kronzon I, Cohen ML, Glassman E, Spencer FC. The incidence and natural history of pericardial effusion after cardiac surgery – an echocardiographic study. Circulation. 1984;69(3):506–11.
2. Tsang TSM, Enriquez-Sarano M, Freeman WK, Barnes ME, Sinak LJ, Gersh BJ, Bailey KR, Seward JB. Consecutive 1127 therapeutic echocardiographically guided pericardiocenteses: clinical profile, practice patterns, and outcomes spanning 21 years. Mayo Clin Proc. 2002;77(5):429–36.
3. Silvestry FE, Kerber RE, Brook MM, Carroll JD, Eberman KM, Goldstein SA, Herrmann HC, Homma S, Mehran R, Packer DL, Parisi AF, Pulerwitz T, Seward JB, Tsang TSM, Wood MA. Echocardiography-guided interventions. J Am Soc Echocardiogr Off Publ Am Soc Echocardiogr. 2009;22(3):213–31; quiz 316–317.
4. Callahan JA, Seward JB, Nishimura RA, Miller FA, Reeder GS, Shub C, Callahan MJ, Schattenberg TT, Tajik AJ. Two-dimensional echocardiographically guided pericardiocentesis: experience in 117 consecutive patients. Am J Cardiol. 1985;55(4):476–9.
5. Patel N, Rafique AM, Eshaghian S, Mendoza F, Biner S, Cercek B, Siegel RJ. Retrospective comparison of outcomes, diagnostic value, and complications of percutaneous prolonged drainage versus surgical pericardiotomy of pericardial effusion associated with malignancy. Am J Cardiol. 2013;112(8):1235–9.
6. Rafique AM, Patel N, Biner S, Eshaghian S, Mendoza F, Cercek B, Siegel RJ. Frequency of recurrence of pericardial tamponade in patients with extended versus nonextended pericardial catheter drainage. Am J Cardiol. 2011;108(12):1820–5.
7. Lindenberger M, Kjellberg M, Karlsson E, Wranne B. Pericardiocentesis guided by 2-D echocardiography: the method of choice for treatment of pericardial effusion. J Intern Med. 2003;253(4):411–7.
8. Atar S, Chiu J, Forrester JS, Siegel RJ. Bloody pericardial effusion in patients with cardiac tamponade: is the cause cancerous, tuberculous, or iatrogenic in the 1990s? Chest. 1999;116(6):1564–9.

Percutaneous Mitral Valvulotomy

3

Judy W. Hung and Yong Hyun Park

Abstract

Rheumatic mitral stenosis remains a common mitral valve disorder in the developing world. Percutaneous Mitral Valvotomy is an important therapy for rheumatic mitral stenosis. This chapter will review the critical role that echocardiography plays in the diagnosis, assessment of suitability and guidance of percutaneous mitral valvotomy.

Keywords

Mitral valve • Stenosis • Balloon • Valvulotomy • Echocardiography

Introduction

Rheumatic mitral stenosis (RMS) remains a common mitral valve disorder internationally, with the highest prevalence in developing countries [1, 2]. RMS results from an inflammatory process affecting the mitral valve following an episode of rheumatic fever. The pathophysiological mechanism involves inflammation of primarily the subvalvular chords and leaflet tips resulting in narrowing of the mitral orifice at the leaflet tips and fusion of the commissures. This leads to characteristic imaging features of rheumatic MS which are (1) Doming of the anterior leaflet, where the narrowest orifice occurs at the leaflet tips creating a "hockey stick" deformity of the anterior leaflet (2) Posterior leaflet immobility (3) "fish mouth" opening appearance of the mitral valve orifice due to fusion of the commissures and (4) Subvalvular thickening (Fig. 3.1). Percutaneous mitral valvotomy (PMV) is an effective treatment for RMS [3–7]. Echocardiography plays an important role in all aspects of PMV. From the initial diagnosis of RMS, to determination of suitability for PMV, guidance of PMV and assessment of post PMV results. This section will demonstrate the important role of echo in PMV through case based examples.

Role of Echocardiography in Guidance of Percutaneous Mitral Valvotomy

Echocardiographic Features of Rheumatic Mitral Stenosis

Patient is a 45 year old female who presents with dyspnea on exertion. She was born in Brazil and came to US as a young adult. She has no prior history of rheumatic fever. Figure 3.2 shows her transthoracic echocardiogram demonstrating rheumatic mitral stenosis. Mitral valve area (MVA) is calculated to be 1.0 cm^2 by direct planimetry and pressure half time. Peak and mean transmitral gradients are 16 and 10 mmHg at a heart rate of 72 bpm. When reporting gradients for MS, it is important to include the heart rate as diastolic gradients are particularly dependent on trans mitral valve (MV) flow. Pulmonary artery systolic pressure (PASP) is estimated to be 46 mmHg.

Because she is symptomatic with severe MS by valve area, she is considered for PMV. Morphological features of the MV by echo have been shown to predict success of PMV [8]. A common scoring system to predict success of PMV, called the Wilkins Score, is based on echo morphological features (Table 3.1) [8].

Electronic supplementary material The online version of this chapter (doi:10.1007/978-3-319-29428-5_3) contains supplementary material, which is available to authorized users.

J.W. Hung, MD (✉) • Y.H. Park, MD
Division of Cardiology, Department of Medicine, Massachusetts General Hospital, Harvard Medical School,
55 Fruit Street, Blake 256, Boston, MA 02114-2696, USA
e-mail: jhung@mgh.harvard.edu; ypark7@mgh.harvard.edu

M.H. Picard et al. (eds.), *Intraprocedural Imaging of Cardiovascular Interventions*, DOI 10.1007/978-3-319-29428-5_3

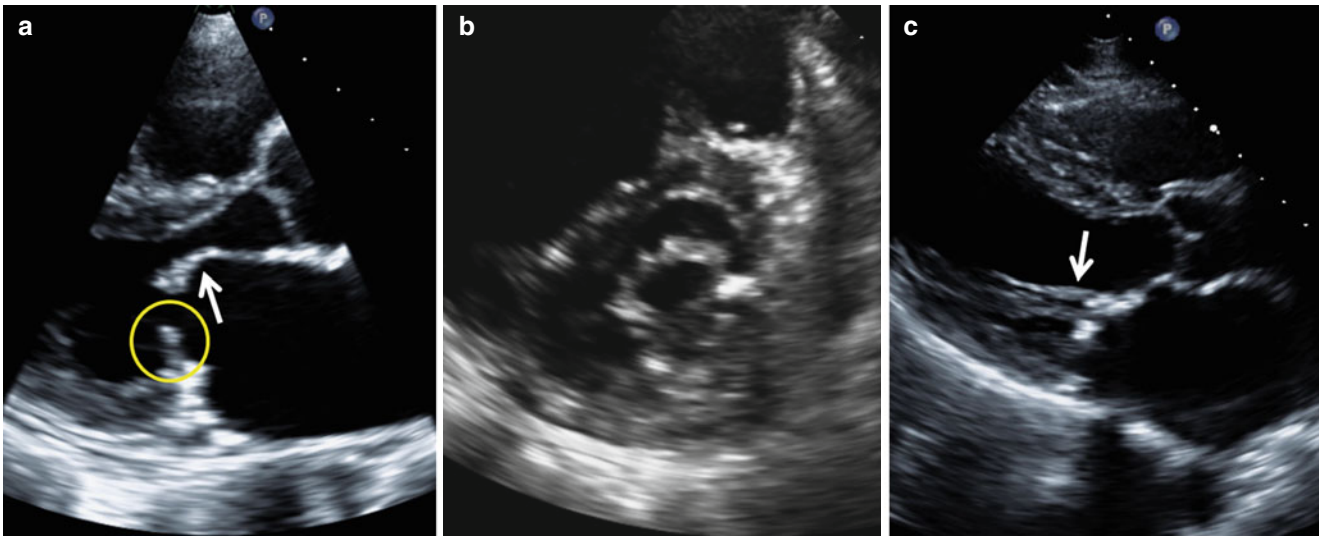

Fig. 3.1 Echo features of rheumatic mitral stenosis; (**a**) *arrow* points to doming of the anterior leaflet, resulting in characteristic "hockey stick" configuration of the anterior leaflet. *Yellow circle* outlines a rigid and immobile posterior leaflet. (**b**) "Fish mouth" appearance of the mitral orifice due to fusion of the commissures. (**c**) Subvalvular thickening (*arrow*)

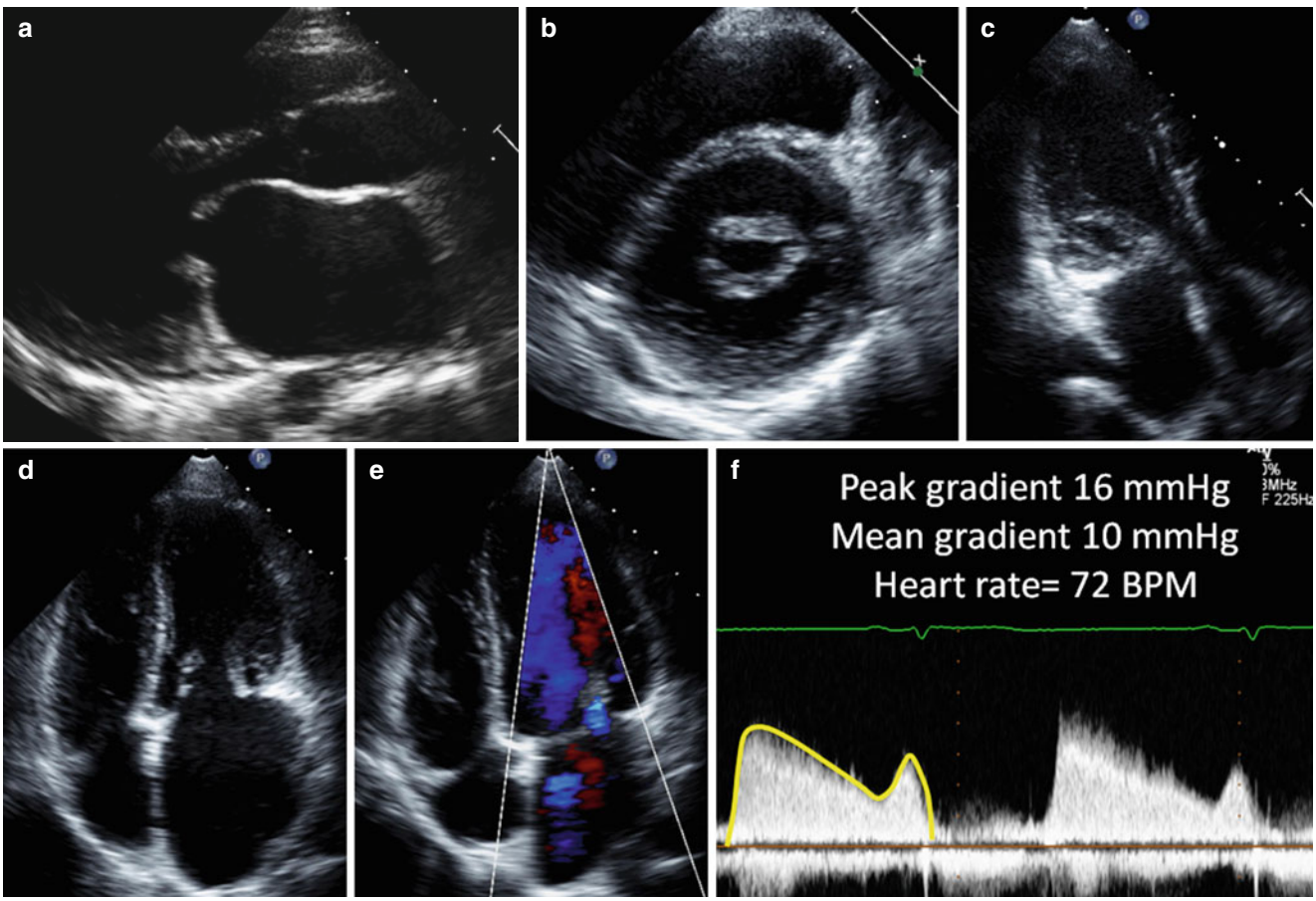

Fig. 3.2 Transthoracic echocardiogram demonstrating rheumatic mitral stenosis. (**a**) Parasternal long axis view with typical diastolic leaflet doming. (**b**) "Fish mouth" appearance of the mitral orifice due to fusion of the commissures. (**c**) Subvalvular thickening. (**d**) Apical 4 chamber view in diastole and (**e**) systole with Color Doppler. (**f**) Transmitral Doppler indicating severe mitral stenosis hemodynamics at a relatively low heart

Four morphological features of the mitral valve apparatus (leaflet mobility, leaflet thickening, leaflet calcification, and subvalvular thickening) are each assigned a score from 0 to 4 for a total score ranging from 0 to 16. The higher the number, the worse the outcome of PMV. Scores of 8 or below have favorable PMV outcomes. Figure 3.3 (Videos 3.1, 3.2, 3.3,

Table 3.1 Grading of mitral valve characteristics from the echocardiographic examination

Grade	Mobility	Subvalvar thickening	Thickening	Calcification
1	Highly mobile valve with only leaflet tips restricted	Minimal thickening just below the mitral leaflets	Leaflets near normal in thickness (4–5 mm)	A single area of increased echo brightness
2	Leaflet mid and base portions have normal mobility	Thickening of chordal structures extending up toone third of thechordal length	Mid-leaflets normal considerable thickening of margins (5–8 mm)	Scattered areas of brightness confined to leaflet margins
3	Valve continues to move forward in diastole mainly from the base	Thickening extending to the distal third of the chords	Thickening extending through the entire leaflet (5–8 mm)	Brightness extending into the mid-portion of the leaflets
4	No or minimal forward movement of the leaflets in diastole	Extensive thickening and shortening of all chordal structures extending down to the papillary muscles	Considerable thickening of all leaflet tissue (>8–10 mm)	Extensive brightness throughout much of the leaflet tissue

The total echocardiographic score was derived from an analysis of mitral leaflet mobility, valvar and subvalvar thickening, and calcification which were graded from 0 to 4 according to the above criteria. This gave a total score of 0–16. Adapted from Ref. [8]

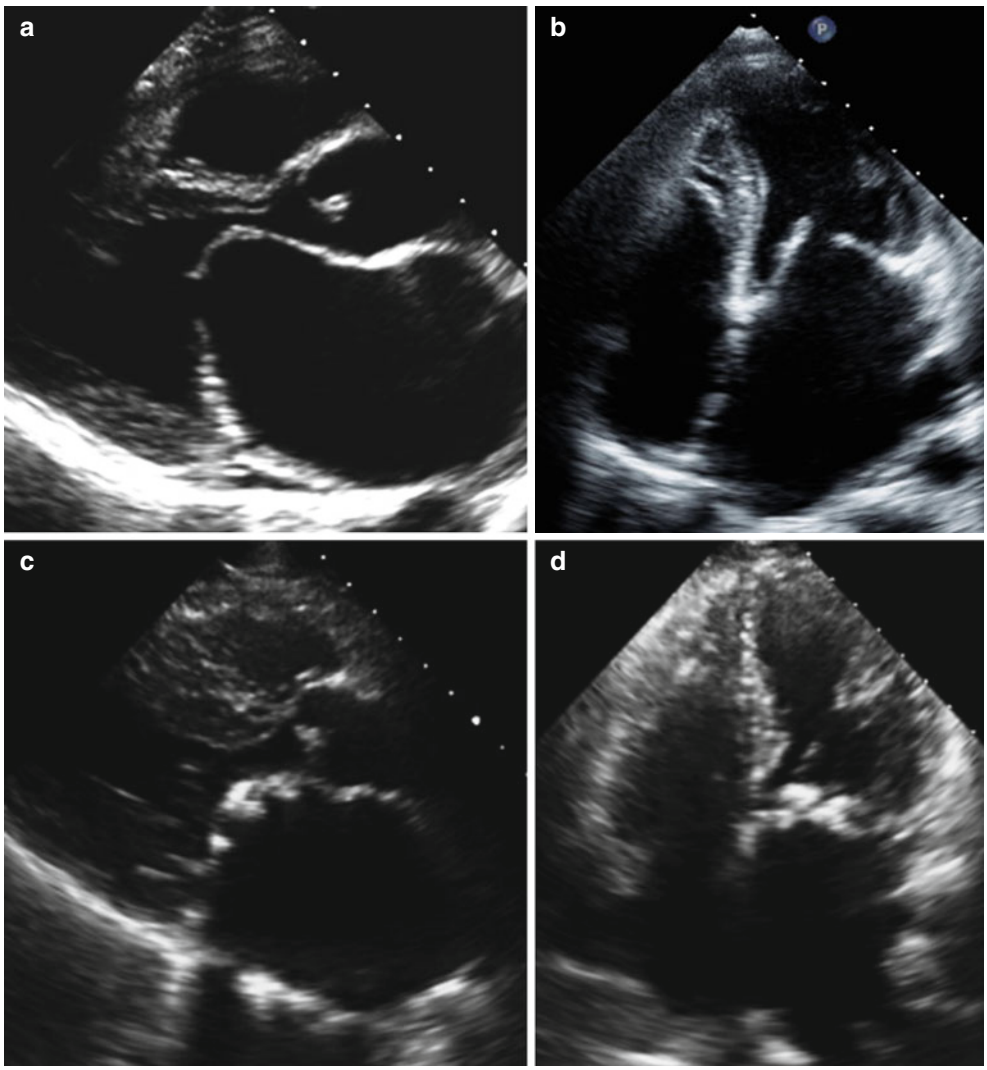

Fig. 3.3 Example of low Wilkins Score (5) associated with successful PMV outcome (*top* panel **a** and **b**) and high Wilkins Score (13) associated with poor PMV outcome (*lower* panel **c** and **d**). Note the difference in leaflet thickening/calcification comparing panels (**a**) vs (**c**) and (**b**) vs (**d**)

and 3.4) shows case of low Wilkins and high Wilkins score respectively. An important cause of morbidity and mortality is development of severe MR following PMV. Padial et al. [9] refined the Wilkins score to incorporate commissural calcium pattern to predict severe MR post PMV (Table 3.2; Fig. 3.4). Significant bilateral or asymmetric calcium patterns in the commissures are associated with significant MR post PMV [9, 10]. Both the Wilkins and Padial scores are based on semi-quantitative assessment of MV morphologic features which are subject to observer variability and have been less reliable for scores in the mid-range. Nunes et al. [11] recently demonstrated improved accuracy for predicting

Table 3.2 Echocardiographic score for severe mitral regurgitation after percutaneous mitral calvulotomy

I–II. Valvular thickening (score each leaflet separately)
1. Leaflet near normal (4–5 mm) or with only a thick segment
2. Leaflet fibrotic and/or calcified evenly; no thin areas
3. Leaflet fibrotic and/or calcified with uneven distribution; thinner segments are mildly thickened (5–8 mm)
4. Leaflet fibrotic and/or calcified with uneven distribution; thinner segments are near normal (4–5 mm)
III. Commissural calcification
1. Fibrosis and/or calcium in only one commissure
2. Both commissures mildly affected
3. Calcium in both commissures, one markedly affected
4. Calcium in both commissures, both markedly affected
IV. Subvatvular disease
1. Minimal thickening of chordal structures just below the valve
2. Thickening of chordae extending up to one-third of chordal length
3. Thickening to the distal third of the chordae
4. Extensive thickening and shortening of all chordae extending down to the papillary muscle

The total score is the sum of these echocardiographic features (maximum 16). Adapted from Ref. [9]

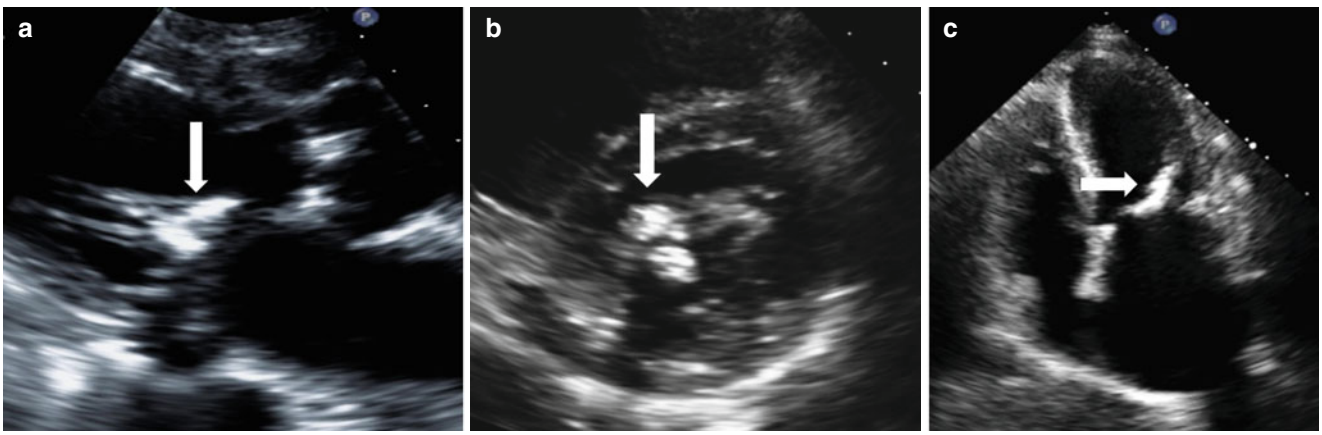

Fig. 3.4 Example of high Padial score; a high Padial Score is associated with increased risk of severe MR post PMV. (**a**) *Arrow points* to diffuse and uneven thickening (5–8 mm) of the mitral leaflets; (**b**) *Arrow points* to asymmetric calcification of the commissures; (**c**) *Arrow points* to extensive thickening and shortening of the chordae extending to papillary muscle

PMV success and development of severe MR using Commissural Area ratio (Fig. 3.5a) and Leaflet Displacement (Fig. 3.5b) which are quantitative MV functional and morphological criteria that incorporate both functional and morphological features of rheumatic MS. A commissural area ratio of greater 1.25 than and leaflet displacement of ≤12 mm are associated with poor PMV success. Figure 3.6 shows transthoracic echocardiographic findings of a patient with high Nunes score.

Echocardiographic evaluation of this patient demonstrated a low echo (Wilkins) score of 5 with trace MR (Fig. 3.2). She was felt to be a good candidate for PMV.

Intraprocedure Guidance During PMV

Prior to PMV, a complete transthoracic echocardiogram should be obtained to evaluate suitability for PMV. It is also important to evaluate for left atrial or left appendage thrombus prior to PMV by transesophageal echocardiogram (TEE) [12]. Patients with left atrial thrombus should not undergo PMV or only be performed under special circumstances. Figure 3.7 shows a thrombus seen in left atrial appendage (Video 3.5).

During PMV, echocardiography (usually transthoracic) is used after each balloon inflation to assess for MR, the change in mitral valve gradients and the mitral valve leaflet anatomy and mobility.

This patient underwent two balloon inflations with increase in mitral valve area from 1.0 to 1.5 cm^2 and a change in mean gradient from 10 to 5 mmHg. The degree of MR increased from trace to mild (Fig. 3.8).

TEE or alternatively intracardiac echo (ICE) guidance for trans-septal puncture can be useful, especially in patients with large atria or abnormal interatrial anatomy (thickened or redundant interatrial septum). An optimal location for the

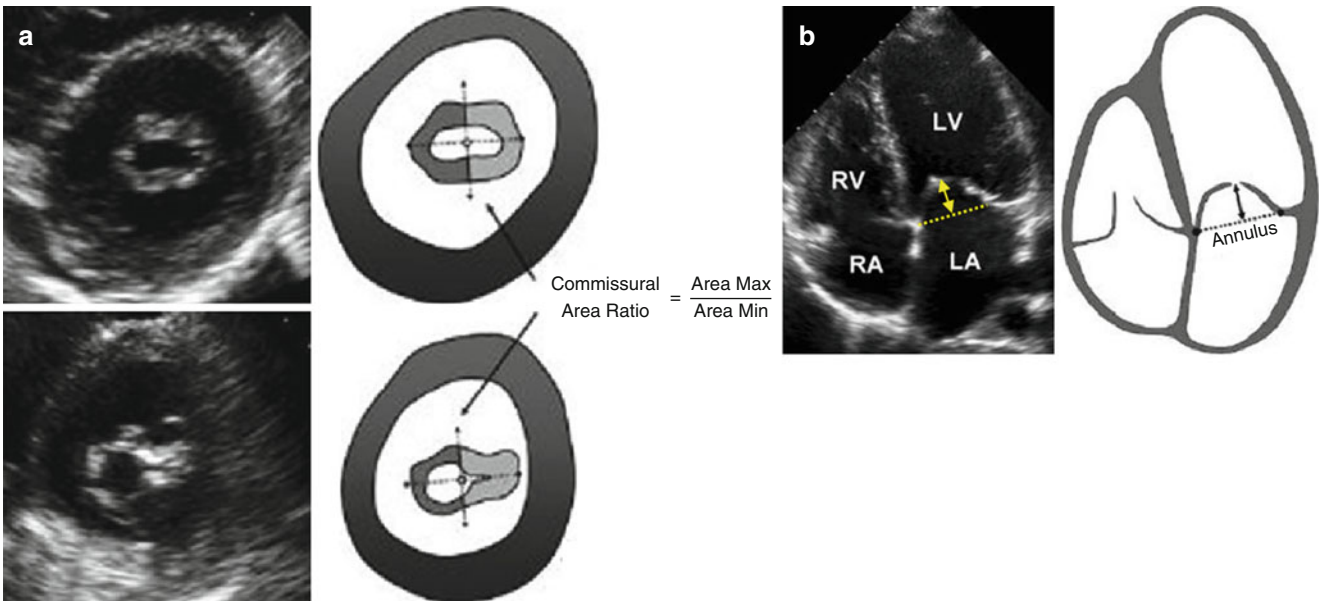

Fig. 3.5 Commissural Area ratio (**a**) and Leaflet Displacement (**b**) incorporate both functional and morphological features of rheumatic MS to predict both PMV success and development of severe MR. *Left* panel displays short axis image of mitral valve showing commissural area ratio measurement. Right panel displays apical 4 chamber view showing maximum leaflet displacement (*yellow arrow*) relative to the annular plane (*yellow dashed line*). *LA* left atrium, *RA* right atrium, *LV* left ventricle, *RV* right ventricle (Adapted from Nunes et al. Circulation 2014)

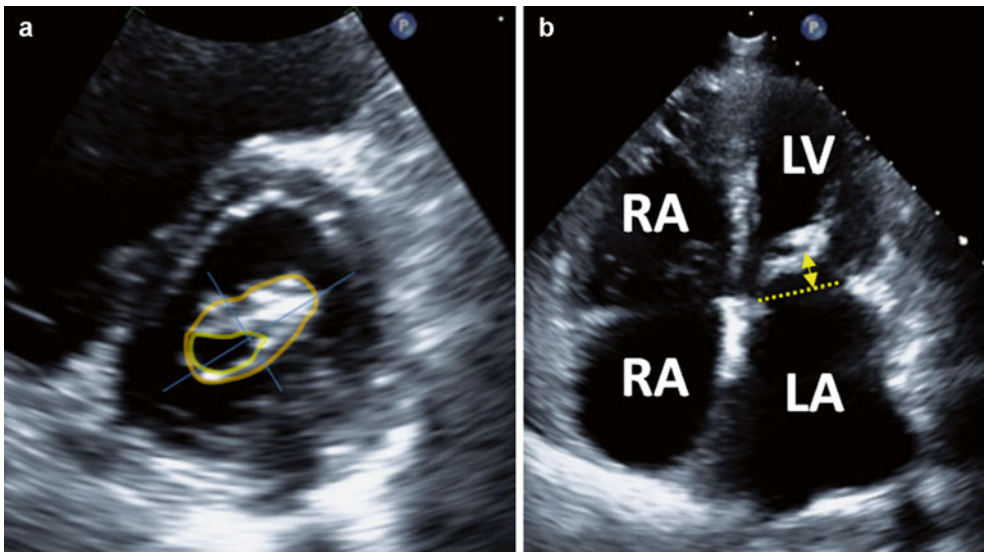

Fig. 3.6 Transthoracic echocardiography showing high commissural area ratio (**a**) and decreased maximal leaflet displacement (**b**, *yellow arrow*) relative to the annular plane (*yellow dashed line*). *LA* left atrium, *RA* right atrium, *LV* left ventricle, *RV* right ventricle

trans-septal puncture is in the middle to slightly posterior location of the fossa ovalis with care to avoid being too anterior (near aortic root) or posterior (near atrial wall) (Fig. 3.9). Typically, the trans-septal needle or catheter can be visualized in the left atrium to confirm successful puncture (Fig. 3.10). On occasion, 2D TEE imaging is unable to visualize the catheter as the catheter is not in the same plane of the imaging beam. 3D TEE echocardiography can often provide better visualization of the catheter in these instances (Fig. 3.11, Video 3.6).

This patient underwent PMV with single balloon technique as demonstrated by TEE in Fig. 3.12. TEE can assist in guidance of catheters and wires across the MV and positioning of the balloon within the mitral valve orifice. Balloon inflation should be avoided in the subvalvular region as this may lead to leaflet, chordal, or papillary muscle rupture. As shown in Fig. 3.13, the mitral valve orifice is occluded during balloon inflation as demonstrated by stasis in the left atrium (Video 3.7). Close hemodynamic monitoring is critical during balloon inflation.

Post PMV Imaging

Following PMV, echocardiography should be performed to assess for severe MR of which there is a reported incidence of 1–9 % [13, 14]. The mechanism of severe MR post PMV is most often due to leaflet tears. An assessment of leaflet mobility and morphology, MV area and transmitral gradients should also be performed. Evaluations for pericardial effusion and of the transseptal puncture site should also be performed. In the acute setting after PMV, the MV area is calculated by planimetry rather than pressure half time method because the pressure half time method immediately after PMV has been shown to be inaccurate until the net LA-LV compliance adjusts [15].

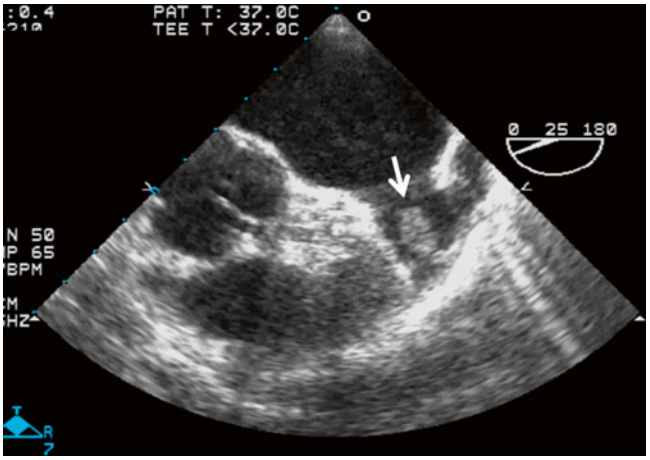

Fig. 3.7 Transesophageal echocardiogram showing left atrial appendage thrombus (*white arrow*)

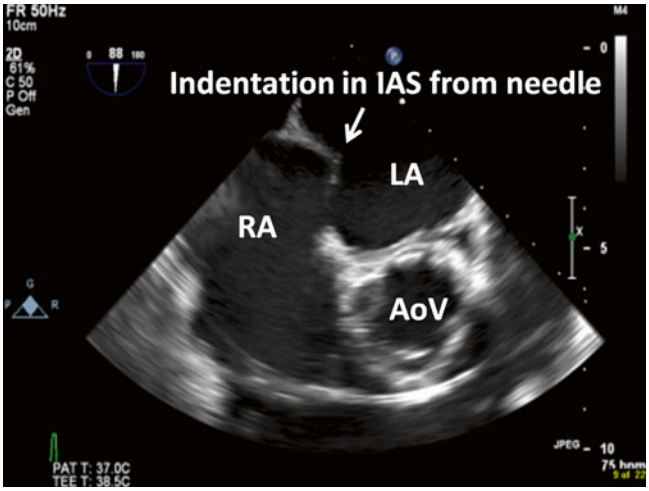

Fig. 3.9 Location of trans-septal needle is noted by indentation of the inter-atrial septum (IAS; *white arrow*). The location of needle is well-positioned in the middle of the fossa ovalis, away from aortic valve (AoV); *RA* right atrium, *LA* left atrium

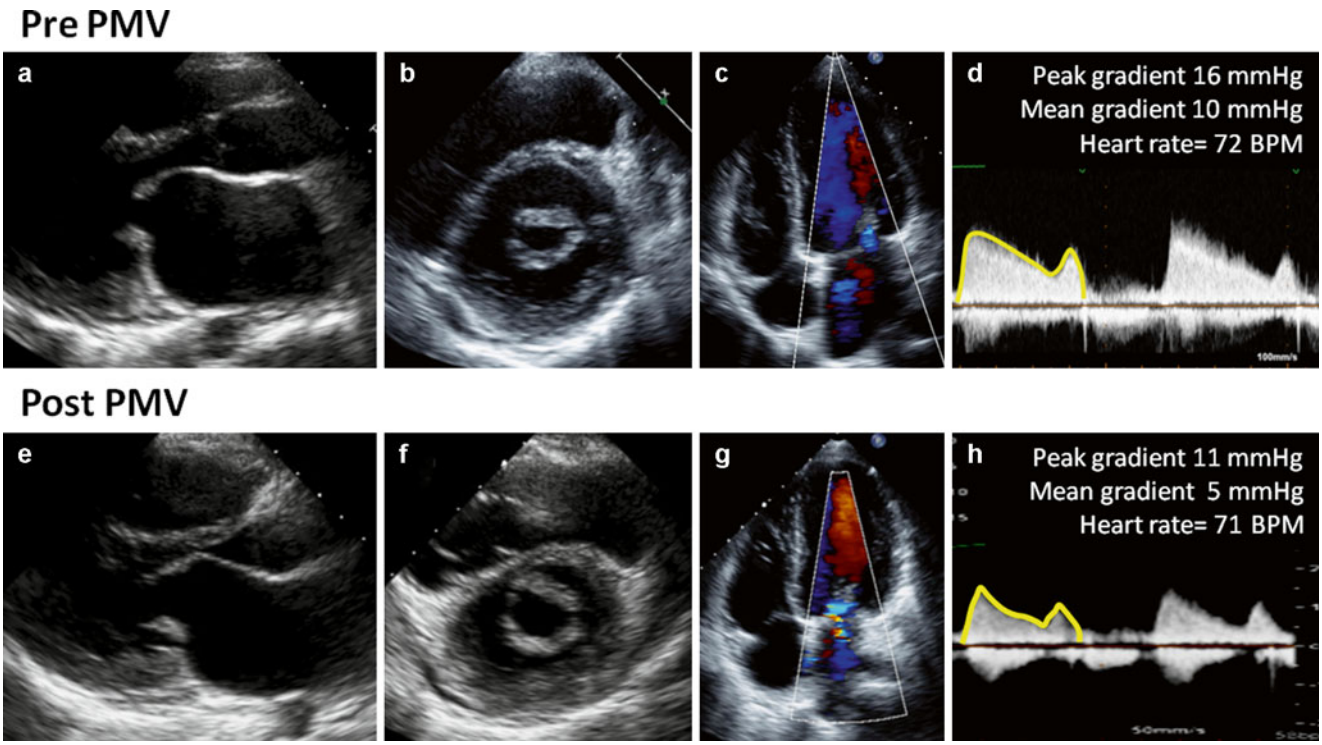

Fig. 3.8 Pre percutaneous mitral valvotomy (PMV) echo images indicating severe MS (**a**–**d**). The echo images after successful PMV show improved MV opening (**e** and **f**) with only mild MR (**g**) and significantly lower trans MV gradients in the setting of a similar heart rate (**h**)

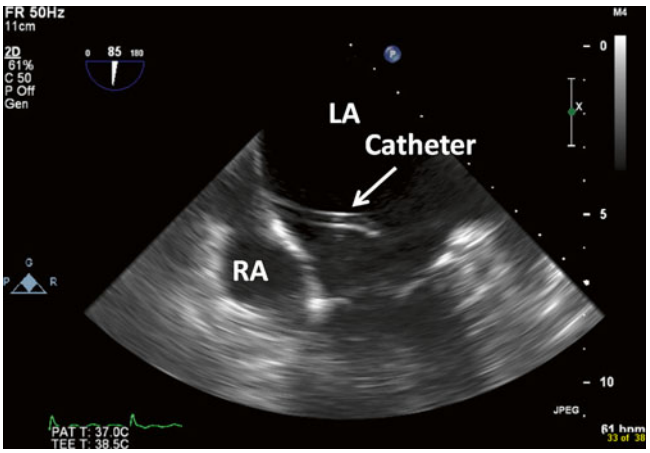

Fig. 3.10 Location of trans-septal catheter can be confirmed in the left atrium (*white arrow*); *RA* right atrium, *LA* left atrium

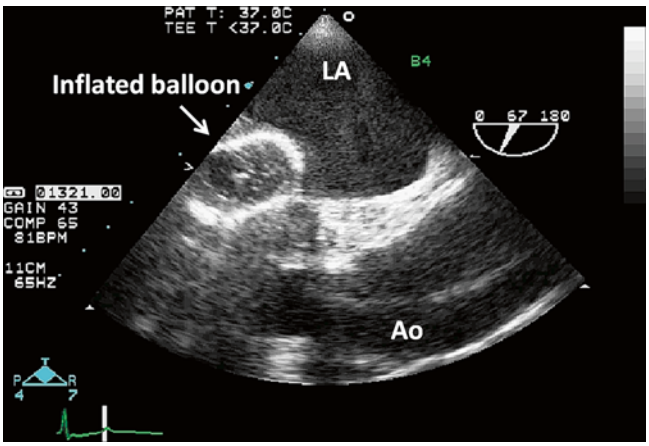

Fig. 3.13 The mitral valve orifice is occluded during balloon inflation as demonstrated by stasis in the left atrium: *LA* left atrium, *Ao* aorta

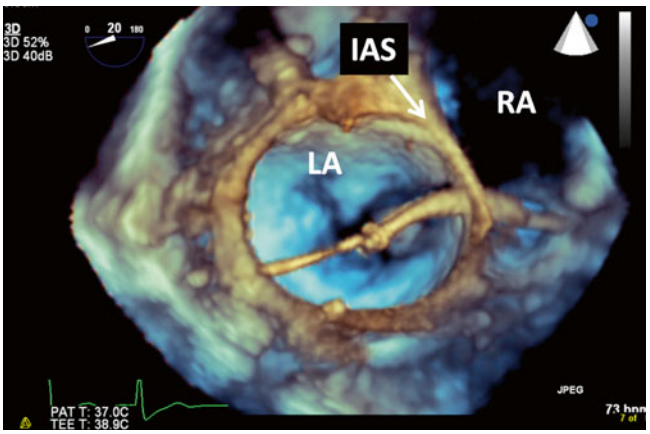

Fig. 3.11 3D TEE enface image left atrium (LA), right atrium (RA) showing catheter across inter-atrial septum (IAS)

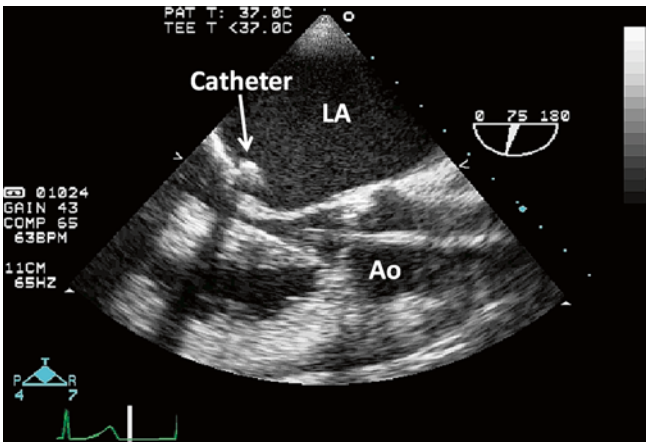

Fig. 3.12 TEE demonstrating catheter in the left atrium: *LA* left atrium, *Ao* aorta

Conclusion

PMV offers an effective therapy for rheumatic mitral stenosis. Echocardiography plays an important part in all aspects of PMV clinical decision making, including accurate diagnosis of rheumatic MS, suitability for PMV, assessment of high risk features, peri-procedural guidance and post procedural assessment of PMV results.

References

1. Iung B, Baron G, Butchart EG, Delahaye F, Gohlke-Barwolf C, Levang OW, et al. A prospective survey of patients with valvular heart disease in Europe: the Euro Heart Survey on Valvular Heart Disease. Eur Heart J. 2003;24(13):1231–43.
2. Carapetis JR, Steer AC, Mulholland EK, Weber M. The global burden of group A streptococcal diseases. Lancet Infect Dis. 2005;5(11):685–94.
3. Reyes VP, Raju BS, Wynne J, Stephenson LW, Raju R, Fromm BS, et al. Percutaneous balloon valvuloplasty compared with open surgical commissurotomy for mitral stenosis. N Engl J Med. 1994;331(15):961–7.
4. Ben Farhat M, Ayari M, Maatouk F, Betbout F, Gamra H, Jarra M, et al. Percutaneous balloon versus surgical closed and open mitral commissurotomy: seven-year follow-up results of a randomized trial. Circulation. 1998;97(3):245–50.
5. Iung B, Garbarz E, Michaud P, Helou S, Farah B, Berdah P, et al. Late results of percutaneous mitral commissurotomy in a series of 1024 patients. Analysis of late clinical deterioration: frequency, anatomic findings, and predictive factors. Circulation. 1999;99(25):3272–8.
6. de Souza JA, Martinez Jr EE, Ambrose JA, Alves CM, Born D, Buffolo E, et al. Percutaneous balloon mitral valvuloplasty in comparison with open mitral valve commissurotomy for mitral stenosis during pregnancy. J Am Coll Cardiol. 2001;37(3):900–3.
7. Iung B, Nicoud-Houel A, Fondard O, Hafid A, Haghighat T, Brochet E, et al. Temporal trends in percutaneous mitral commissurotomy over a 15-year period. Eur Heart J. 2004;25(8):701–7.

8. Wilkins GT, Weyman AE, Abascal VM, Block PC, Palacios IF. Percutaneous balloon dilatation of the mitral valve: an analysis of echocardiographic variables related to outcome and the mechanism of dilatation. Br Heart J. 1988;60(4):299–308.
9. Padial LR, Freitas N, Sagie A, Newell JB, Weyman AE, Levine RA, et al. Echocardiography can predict which patients will develop severe mitral regurgitation after percutaneous mitral valvulotomy. J Am Coll Cardiol. 1996;27(5):1225–31.
10. Cannan CR, Nishimura RA, Reeder GS, Ilstrup DR, Larson DR, Holmes DR, et al. Echocardiographic assessment of commissural calcium: a simple predictor of outcome after percutaneous mitral balloon valvotomy. J Am Coll Cardiol. 1997;29(1):175–80.
11. Nunes MC, Tan TC, Elmariah S, do Lago R, Margey R, Cruz-Gonzalez I, et al. The echo score revisited: Impact of incorporating commissural morphology and leaflet displacement to the prediction of outcome for patients undergoing percutaneous mitral valvuloplasty. Circulation. 2014;129(8):886–95.
12. Nishimura RA, Otto CM, Bonow RO, Carabello BA, Erwin 3rd JP, Guyton RA, et al. 2014 AHA/ACC guideline for the management of patients with valvular heart disease: a report of the American College of Cardiology/American Heart Association Task Force on Practice Guidelines. Circulation. 2014;129(23):e521–643.
13. Palacios IF, Sanchez PL, Harrell LC, Weyman AE, Block PC. Which patients benefit from percutaneous mitral balloon valvuloplasty? Prevalvuloplasty and postvalvuloplasty variables that predict long-term outcome. Circulation. 2002;105(12):1465–71.
14. Chen CR, Cheng TO. Percutaneous balloon mitral valvuloplasty by the Inoue technique: a multicenter study of 4832 patients in China. Am Heart J. 1995;129(6):1197–203.
15. Thomas JD, Wilkins GT, Choong CYP, Abascal VM, Palacios IF, Block PC, et al. Inaccuracy of mitral pressure half-time immediately after percutaneous mitral valvotomy. Circulation. 1988;78:980–93.

Echocardiographic Guidance of Alcohol Septal Ablation for Hypertrophic Obstructive Cardiomyopathy

4

Danita M. Yoerger Sanborn

Abstract

Alcohol septal ablation (ASA) has become an established treatment option for patients with refractory symptoms due to the obstructive variant of hypertrophic cardiomyopathy (HCM) (Fifer and Sigwart, Eur Heart J 32(9):1059–1064, 2011; Fifer, Circulation 116(2):207–216, 2007; Holmes et al., Catheter Cardiovasc Interv 66(3):375–389, 2005; El Masry and Breall, Curr Cardiol Rev 4(3):193–197, 2008). Trans-thoracic echocardiography is often the initial modality performed when a diagnosis of HCM is suspected and results are typically used to help determine which treatments might be appropriate to help relieve obstruction. A multidisciplinary team approach to procedure selection and guidance is an ideal management strategy for patients with obstructive HCM. Once the decision has been made to proceed with ASA, real-time intra-procedural echocardiography is the ideal imaging modality to help define the anatomy and mechanism of the obstruction and contrast echocardiography is used to guide the selection of the appropriate septal perforator into which the alcohol will be infused. Imaging during and after ASA is useful to predict procedural success and to monitor for complications.

Keywords

Echocardiography • Hypertrophic obstructive cardiomyopathy • Alcohol septal ablation

Introduction

Successful management of patients with obstructive HCM ideally employs an interdisciplinary approach. At our center, decision making regarding which interventional treatment option is best for medical therapy-refractory disease typically involves a clinical cardiologist specialized in HCM, an interventional cardiologist skilled in the ASA procedure, an echocardiographer experienced in ASA procedural guidance, a cardiac surgeon and sometimes an electrophysiologist. A detailed review of the baseline trans-thoracic echocardiographic images performed with the patient on maximally tolerated medical therapy is required to determine if a particular patient is a suitable candidate for the ASA procedure [1–4]. Approximately 25% of patients with HCM have resting gradients but it has been estimated that up to 70% of patients with HCM develop gradients with activity [5, 6]. When patients are symptomatic in the absence of a resting gradient, attempts to provoke a gradient while imaging with echocardiography, such as with an exercise stress echo or Valsalva maneuver can be undertaken. Dobutamine stress echocardiography should generally not be used as a provocative test because of the ability of dobutamine to provoke gradients of questionable significance, even in normal individuals [7]. Intra-procedurally, our team always includes an HCM cardiologist, an interventional cardiologist experienced in ASA and an echocardiography attending with expertise in ASA guidance.

D.M.Y. Sanborn, MD, MMSc
Division of Cardiology, Department of Internal Medicine,
Paul Dudley White Associates, Massachusetts General Hospital,
55 Fruit Street, Yaw 5B-5916, Boston, MA 02114, USA
e-mail: dysanborn@mgh.harvard.edu

Before the Procedure

Prior to a planned ASA procedure, the echocardiographer who will guide the procedure must perform a detailed review of available imaging. This is extremely important to help

M.H. Picard et al. (eds.), *Intraprocedural Imaging of Cardiovascular Interventions*, DOI 10.1007/978-3-319-29428-5_4

determine if the anatomy is suitable for ASA as well as to screen for other coexisting lesions that might make surgery preferable. Interpretable image quality is an important prerequisite, and may impact choice of imaging modality to guide the procedure. Although either trans-thoracic (TTE) or trans-esophageal (TEE) imaging can be used to guide the ASA procedure, our center has exclusively used TTE imaging during ablation procedures. Since immediate procedural success is determined by successful reduction of left ventricular outflow tract (LVOT) gradient, we have used TTE in order to avoid the need for general anesthesia, with its inherent effects on cardiovascular hemodynamics that might make interpretation of gradient reduction difficult. We have had an excellent imaging success rate using TTE guidance.

Appropriate anatomy for ASA includes the presence of LVOT obstruction due to significant basal interventricular septal hypertrophy and systolic anterior motion (SAM) of the mitral valve. The septal thickness at the level of the obstruction must be ≥16 mm in order to avoid the theoretical risk of excessive septal thinning resulting in post-procedure ventricular septal rupture. There are many different patterns of left ventricular (LV) hypertrophy in HCM that should be excluded, including midventricular and apical variants, which would not be expected to benefit from ASA. Complete assessment of mitral valve anatomy is essential. Because of the dynamic nature of LVOT obstruction in this disease, mitral regurgitation severity may vary from trace to severe depending on loading conditions. It is important to exclude coexisting significant organic mitral valve disease (prolapse, flail, calcification, stenosis), that would be unlikely to be improved after septal ablation and may adversely impact symptom resolution after ASA [3, 8]. It is also important to carefully screen for mimickers of obstructive HCM, including coexisting subaortic membrane that may be masked by reactive hypertrophy of the septum and sometimes even SAM just below the membrane [9, 10]. While ASA might reduce the septal thickness and improve the SAM, the fixed obstruction caused by a membrane will not be relieved by ASA. Presence of significant aortic insufficiency should raise suspicion of this condition and prompt a more detailed assessment of the outflow tract. Cardiac amyloidosis can also mimic HCM and lead to dynamic obstruction and should be excluded prior to determining appropriate invasive therapy [11].

During the Procedure

As is the case in all procedures that utilize echocardiographic guidance, recording a detailed set of baseline images is important to both monitor for success as well as screen for complications. Since the patient is supine on the catheterization table and under sterile draping, TTE images from the apical view are the most often utilized views (Fig. 4.1).

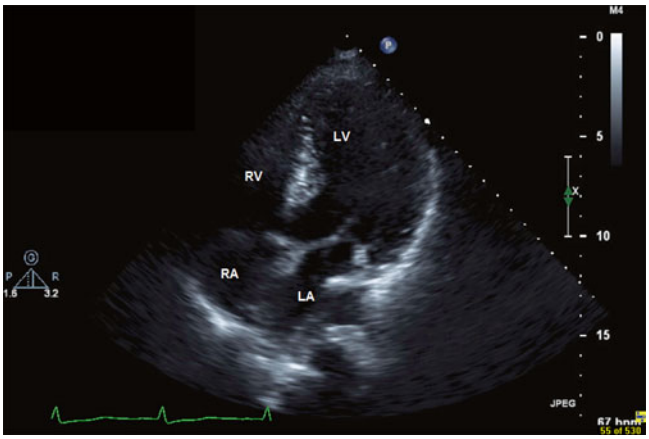

Fig. 4.1 Intraprocedural imaging from an apical window demonstrating typical image quality from a supine patient on the catheterization table. *LV* left ventricle, *LA* left atrium, *RV* right ventricle, *RA* right atrium

Baseline apical four chamber, apical five chamber, apical two chamber and apical long axis views are be recorded using both two-dimensional and color Doppler imaging. The echocardiographer should obtain images with adequate visualization of the myocardium and endocardial border and perform an assessment of baseline regional wall motion from these views. Additionally, care should be taken to visualize the pericardial space from these baseline views, as well as the entire length of the RV free wall and inferior wall of the LV. Pulse wave and continuous wave Doppler interrogation should be performed and recorded from the apex through the LVOT and aortic valve to confirm the level of maximal obstruction. Typically the obstruction is dynamic (peaking late in systole) and occurs at the site of SAM contact (Fig. 4.2a). Early peaking or parabolic shaped gradients should raise suspicion of a fixed obstruction that would not be expected to improve with ASA (Fig. 4.2b). Color Doppler should be used to assess mitral regurgitation severity as well as for flow patterns across the LVOT and aortic valve. These images will be used for comparison during contrast injection to determine the perfusion area 'at risk' prior to administration of ethanol as well as to monitor for complications. Occasionally, ASA will be performed in a patient with provocable but no resting LVOT gradients. Additional baseline images during provocation (with dobutamine or nitroglycerin infusion, with Valsalva maneuver or post-PVC) should be recorded for later comparison.

Use of intracoronary contrast echocardiography has been shown to improve procedural outcome and decrease complications of ASA [12–14]. Contrast agents that have been reported to be used for ASA in the United States include those commercially available, including Optison™, Definity™ and agitated angiographic contrast. Our center originally used Optison™, which must be drawn up in a ster-

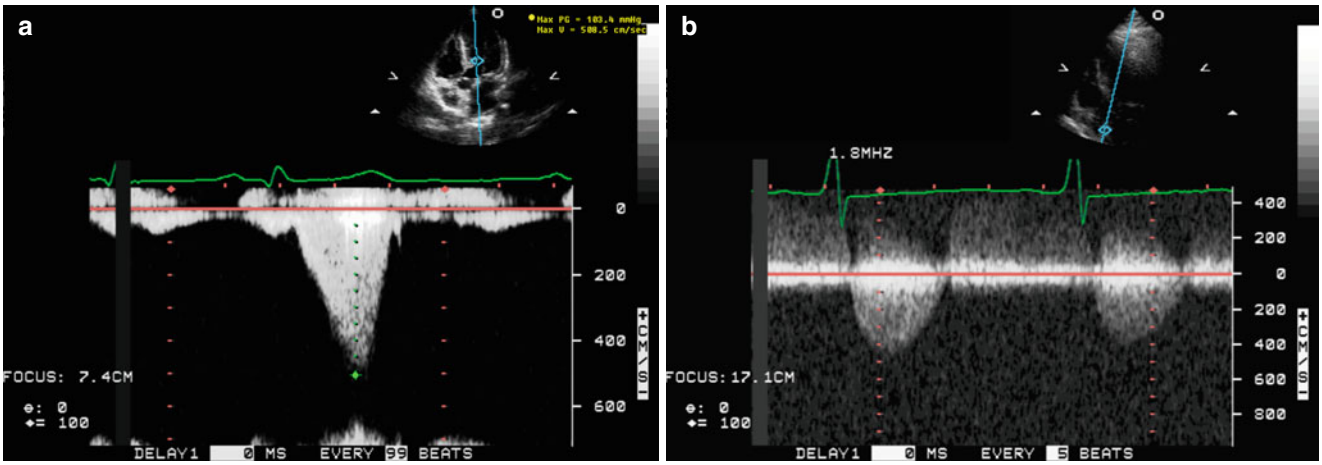

Fig. 4.2 (**a**) Classic "dagger-shaped" late peaking LVOT gradient. (**b**) Parabolic gradient of fixed stenosis from a subaortic membrane

ile fashion and diluted by the interventionalist prior to use. Typically 3 milliliters (ml) of Optison™ are mixed with 7 ml of sterile normal saline to create the contrast solution. The amount of contrast solution needed to define the anatomy can vary, but usually 0.5–2 ml of the contrast solution should be injected distal to the inflated balloon while echo images are being recorded. Use of too much contrast or administering the contrast with too strong an injection can cause blooming and spillage of contrast into the cardiac chambers, which can make determination of the target perfusion area more difficult. Over the past several years during a time when Optison™ was not commercially available and Definity™ did not have intracoronary labeling, our center switched to using agitated angiographic contrast as our myocardial contrast agent. We had previously been advised by other centers that they used this technique and we had also noted that while imaging during angiography to confirm balloon placement, we often saw the perfusion area enhance during angiographic contrast administration and confirmed in several serial patients that the area detected by agitated angiographic contrast was the same as the area we were defining with echocardiographic contrast. Since we have made this change in contrast agent, we have had excellent experience and procedural success with the use of agitated angiographic contrast.

A potential target septal perforator coronary artery is isolated by the interventional cardiologist using a perfusion balloon. Once the position is confirmed angiographically, an intracoronary injection of a diluted echo contrast agent such as Optison™, Definity™ or of agitated angiographic contrast, is performed distal to the balloon during real-time imaging. The echocardiographer's role is to confirm contrast enhancement of the target area (upper septum at the site of SAM contact) and in no other areas. Using TTE, imaging is from an apical five chamber view during the injection (Fig. 4.3). Additional images should quickly be obtained of the RV free wall, inferior wall of the LV and the LV apex to insure that there are no coronary collateral communications or spillage around the balloon that could signal a risk of inadvertently infarcting these remote areas during the ethanol injection, since the ethanol is expected to distribute in the coronary circulation in the same pattern that the contrast distributes. Figure 4.4 shows examples of contrast appearing in remote and/or undesired territories during septal perforator contrast injection.

Decision making regarding which septal perforator will be injected with ethanol is in real-time, integrating data from angiography and echocardiography, and thus we have found it important to have both the experienced attending echocardiographer and interventional cardiologist members of our multidisciplinary team present during the imaging and injections. Though rare, if an appropriate septal perforator cannot be identified because of a perforator supplying the wrong perfusion bed or too large a perfusion bed or if there is an inability to isolate a desired perforator branch, then the procedure is aborted and other treatment options are considered.

Typically the 1st septal perforator is the target of therapy in an ASA because it is most often the coronary artery that supplies the basal septum at the site of SAM contact. Because of wide variability in coronary anatomy, ASA is sometimes performed in more than one septal perforator, or in subbranches of septal perforators (Fig. 4.5). Taking the time to choose the perforator or branch that preferentially supplies the septum at the level of obstruction and no other areas is critical to increase likelihood of procedural success and reduce risk of complications. Reported doses and rates of ethanol infusion were initially variable across centers and it was eventually reported that slower rates of ethanol infusion were associated with less complete heart block [3, 15, 16]. Higher total ethanol dose created a larger infarct area and was thus felt to contribute to high rate of permanent pace-

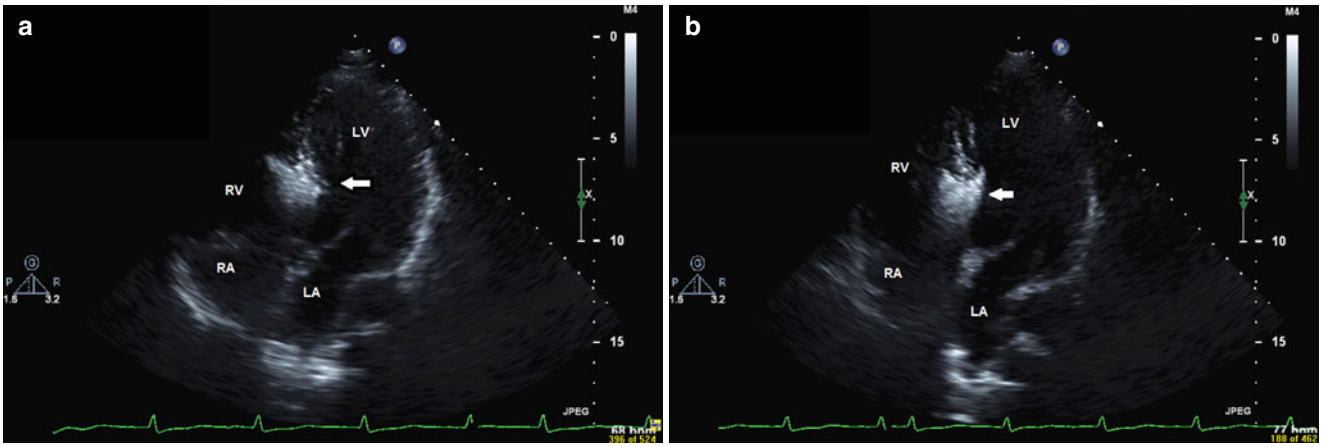

Fig. 4.3 (**a**) Intraprocedural image showing contrast enhancement in the basal septum at the site of SAM contact (*arrow*). *LV* left ventricle, *LA* left atrium, *RV* right ventricle, *RA* right atrium. (**b**) Intraprocedural image from the same patient showing ethanol enhancement in the basal septum at the site of SAM contact in the same patient (*arrow*). *LV* left ventricle, *LA* left atrium, *RV* right ventricle, *RA* right atrium

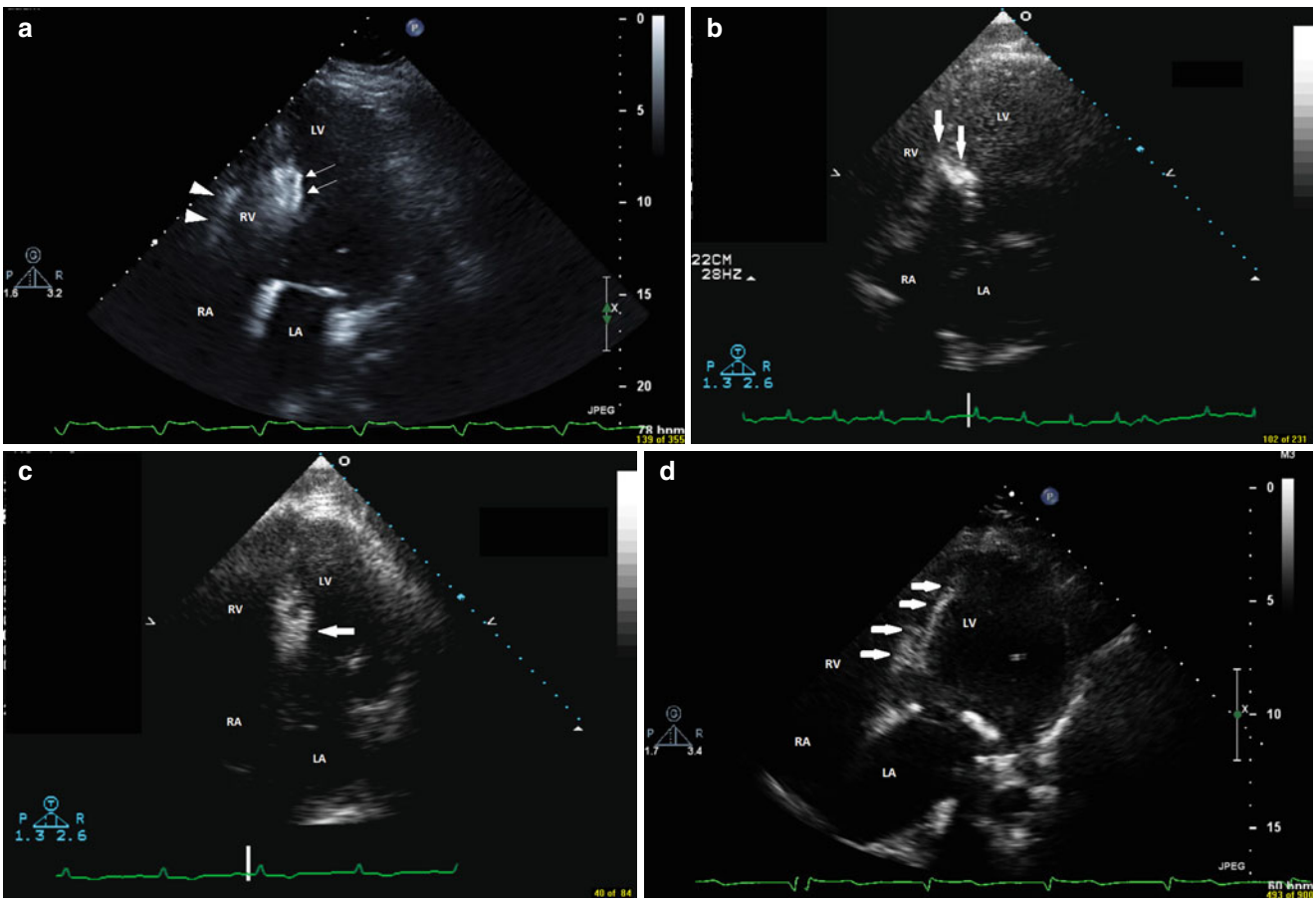

Fig. 4.4 (**a**) contrast enhancement of the RV free wall (*arrow heads*) as well as the basal septum (*arrows*) from a large second septal perforator branch. *LV* left ventricle, *LA* left atrium, *RV* right ventricle, *RA* right atrium. (**b**) Contrast injection into what was thought to be the first septal perforator. Note that the contrast enhances the midportion of the septum and the RV moderator band (*arrows*). *LV* left ventricle, *LA* left atrium, *RV* right ventricle, *RA* right atrium. (**c**) Contrast injection in the same patient as (**b**). This time the injection was into the true first septal perforator which happened to originate off the first diagonal branch, and contrast is seen in the desired portion of the basal septum (*arrow*). *LV* left ventricle, *LA* left atrium, *RV* right ventricle, *RA* right atrium. (**d**) Contrast enhancement of almost the entire length of the septum from an injection into the first septal perforator (*arrows*). There were no subbranches to isolate so the ablation procedure was not performed because the risk area was too large. *LV* left ventricle, *LA* left atrium, *RV* right ventricle, *RA* right atrium

maker implantation [13, 14], and lower doses were subsequently found to be associated with similar success rates as measured by gradient relief and symptom reduction [17].

Immediate procedural success necessitates adequate coverage of the 'risk area' by the ethanol, which will appear echo-bright during and for up to hours after the ethanol injection (Fig. 4.3b). This is typically accompanied by new regional LV dysfunction in the ethanol-perfused area. Often but not always, the degree of SAM may be diminished or absent at the end of the procedure and MR severity may be similar or reduced. The LVOT gradient should be reduced and typically is no longer late-peaking in profile at the end of the case (Fig. 4.6).

It is not uncommon to need to administer ethanol into more than one septal perforator branch in order to completely infarct the septum contributing to the LVOT obstruction.

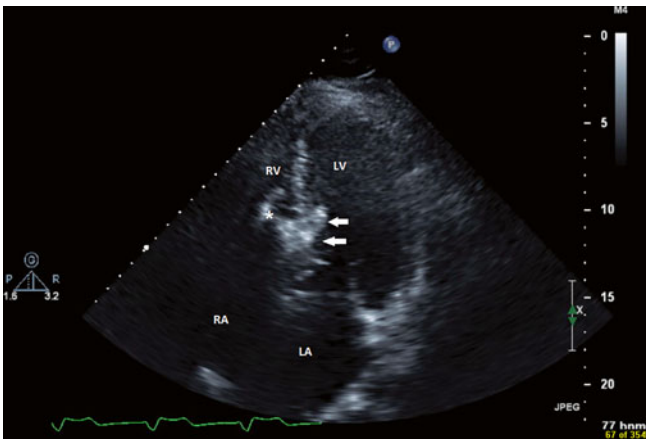

Fig. 4.5 Example the subsequent contrast injection into the proximal subdivision of the second septal perforator from the same patient as in Fig. 4.4. Note that contrast now only enhances the basal septum (*arrows*) and no longer enhances the RV free wall. The * indicates a pacemaker wire in the RV cavity. *LV* left ventricle, *LA* left atrium, *RV* right ventricle, *RA* right atrium

Contrast imaging prior to a second ethanol injection can be challenging because the initial ethanol infusion will cause a persistent echo-bright area and thus it may be difficult to delineate a new contrast-enhanced area adjacent to an acutely ablated area. Careful interpretation by an experienced echocardiographer of the real-time images during the subsequent injections is required to distinguish the newly enhanced risk area perfused by the second perforator (Fig. 4.7).

Echocardiography is a very useful tool to assess for the variety of complications that can occur during any interventional coronary procedure. Instrumentation for catheter placement can lead to coronary dissection, and echocardiography allows for immediate assessment for new regional myocardial dysfunction should this complication occur. Perforation of a cardiac structure either by catheters or from the temporary pacemaker wire that most patients require can lead to pericardial effusion and tamponade. The echocardiogram can provide immediate visualization of the pericardial space in these situations and comparison with baseline images can be useful to help guide rapid therapy.

After the Procedure

Post-procedure imaging is typically performed in similar fashion to the baseline imaging and the two sets of images should be compared. Echo-bright enhancement of the site of ethanol perfusion can persist for hours after the procedure. Regional wall motion assessment and Doppler interrogation of the LV cavity and LVOT should again be performed. The pattern of LVOT gradient response after ASA can be triphasic, with acute reduction in gradient, followed by early rise back to pre-ablation levels in the days following the procedure, only to decline again by 3 months following ASA [18, 19]. Thus, the mechanism of acute and persistent gradient

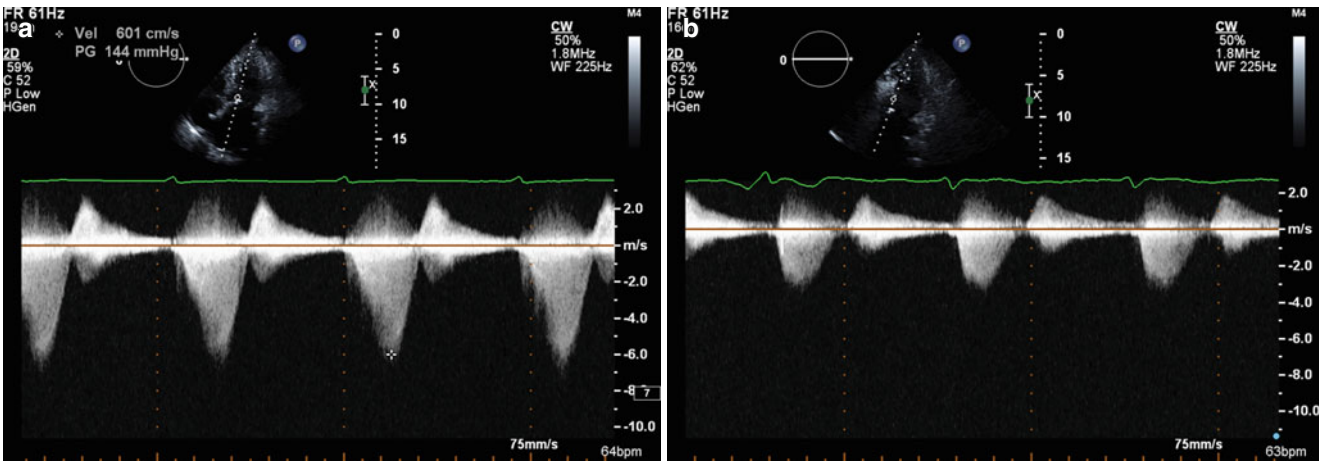

Fig. 4.6 (**a**) Late peaking LVOT gradient immediately prior to ablation procedure. (**b**) Final gradient after ablation procedure. Note that not only has the gradient decreased but that the Doppler profile is no longer late peaking

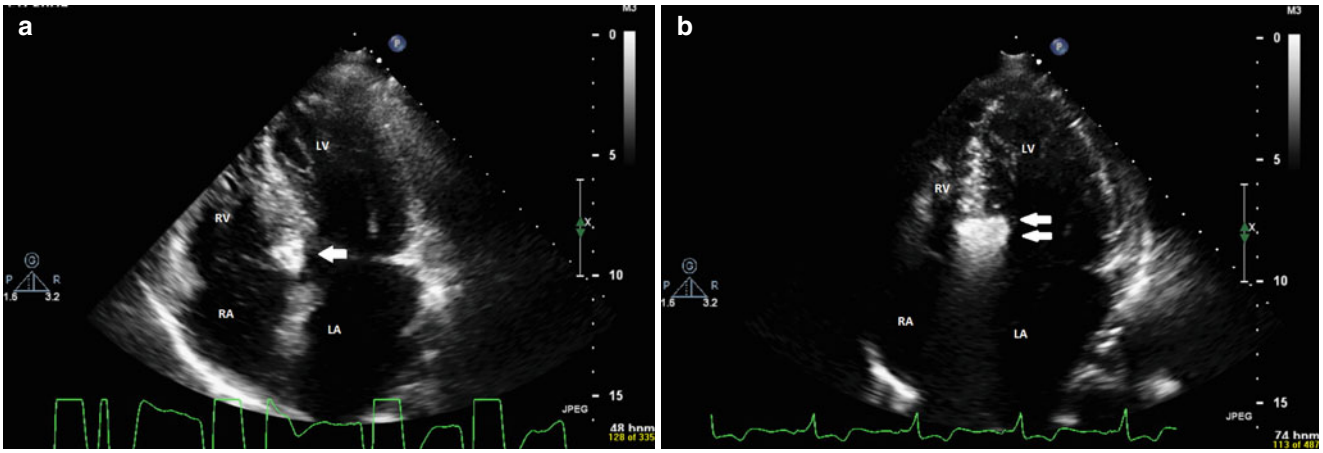

Fig. 4.7 (**a**) Enhancement of basal septum (*arrow*) from ethanol injection into the first septal perforator branch. *LV* left ventricle, *LA* left atrium, *RV* right ventricle, *RA* right atrium. (**b**) In the same patient, enhancement of a slightly more distal territory (*arrows*) of the septum from injection of contrast into the proximal portion of the second septal perforator after ethanol was already given into the first septal perforator *LV* left ventricle, *LA* left atrium, *RV* right ventricle, *RA* right atrium

reduction are believed to differ, in that acute gradient reduction is felt to be due to acute regional LV dysfunction caused by the ethanol. Some areas in the periphery of the infarcted area may exhibit stunning that will ultimately recover function and can lead to early return of LVOT obstruction in some. Long-term gradient and symptom relief is felt to be achieved due to remodeling of the infarcted area with decrease in LV mass, and septal and remote wall thickness [20, 21], enlargement of the LVOT outflow tract [22], improved diastolic function [23, 24] and lessening or resolution of SAM [25]. If provocation was required at baseline to induce LVOT obstruction, repeat post-procedure imaging should be performed during attempts at provocation to insure that relief of obstruction persists both at rest and with provocation.

Heart block and need for pacing are common complications after the procedure and may impact gradient assessment [26, 27]. The scar that results in the upper septal myocardium may be a substrate for ventricular ectopy and sustained ventricular arrhythmias both early and late after the procedure [28–30] Additionally continued progression of hypertrophy of the areas around the infarcted territory can cause redevelopment of SAM and LVOT obstruction (Fig. 4.8). Depending on the septal perforator anatomy and patient preference, this may be successfully treated with repeat ablation or surgical septal myectomy [31].

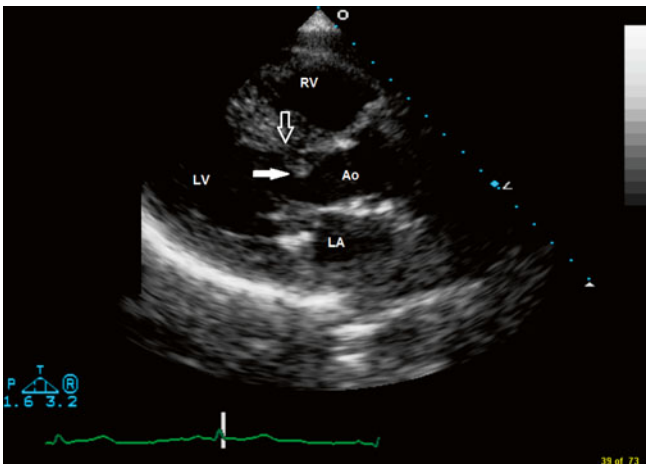

Fig. 4.8 Parasternal long axis view from a patient 6 months after ablation. Note the thinned area of remodeled septum (*open arrow*) and the hypertrophied regrowth of septal tissue closer to the aortic valve, now causing LVOT obstruction (*solid arrow*). *LV* left ventricle, *LA* left atrium, *RV* right ventricle, *Ao* aorta

Summary

Echocardiography is an essential tool for the diagnosis and treatment of patients with HCM. While many imaging modalities can provide structural and functional information that can help guide choice of invasive treatment, the portability, low-cost, safety and ease of serial examinations makes echocardiography an ideal tool for procedural guidance during alcohol septal ablation. The presence of an experienced echocardiographer on the procedural team can enhance success of ASA, limit some complications and rapidly diagnose treatable adverse events.

References

1. Fifer MA, Sigwart U. Controversies in cardiovascular medicine. Hypertrophic obstructive cardiomyopathy: alcohol septal ablation. Eur Heart J. 2011;32(9):1059–64.
2. Fifer MA. Controversies in cardiovascular medicine. Most fully informed patients choose septal ablation over septal myectomy. Circulation. 2007;116(2):207–16; discussion 16.

3. Holmes Jr DR, Valeti US, Nishimura RA. Alcohol septal ablation for hypertrophic cardiomyopathy: indications and technique. Catheter Cardiovasc Interv. 2005;66(3):375–89.
4. El Masry H, Breall JA. Alcohol septal ablation for hypertrophic obstructive cardiomyopathy. Curr Cardiol Rev. 2008;4(3):193–7.
5. Maron MS, Olivotto I, Zenovich AG, Link MS, Pandian NG, Kuvin JT, et al. Hypertrophic cardiomyopathy is predominantly a disease of left ventricular outflow tract obstruction. Circulation. 2006;114(21):2232–9.
6. Shah JS, Esteban MT, Thaman R, Sharma R, Mist B, Pantazis A, et al. Prevalence of exercise-induced left ventricular outflow tract obstruction in symptomatic patients with non-obstructive hypertrophic cardiomyopathy. Heart (British Cardiac Society). 2008;94(10):1288–94.
7. Luria D, Klutstein MW, Rosenmann D, Shaheen J, Sergey S, Tzivoni D. Prevalence and significance of left ventricular outflow gradient during dobutamine echocardiography. Eur Heart J. 1999;20(5):386–92.
8. Maron BJ, Dearani JA, Ommen SR, Maron MS, Schaff HV, Gersh BJ, et al. The case for surgery in obstructive hypertrophic cardiomyopathy. J Am Coll Cardiol. 2004;44(10):2044–53.
9. Anderson MJ, Arruda-Olson A, Gersh B, Geske J. Subaortic membrane mimicking hypertrophic cadiomyopathy. BMJ Case Rep. 2015. pii: bcr2015212321. doi: 10.1136/bcr-2015-212321.
10. Ahn KT, Lee YD, Choi UL, Jin SA, Park SJ, Kim JH, et al. Flail subaortic membrane mimicking left ventricular outflow tract obstruction in hypertrophic cardiomyopathy. J Cardiovasc Ultrasound. 2013;21(2):90–3.
11. Allen RD, Edwards WD, Tazelaar HD, Danielson GK. Surgical pathology of subaortic septal myectomy not associated with hypertrophic cardiomyopathy: a study of 98 cases (1996–2000). Cardiovasc Pathol. 2003;12(4):207–15.
12. Faber L, Ziemssen P, Seggewiss H. Targeting percutaneous transluminal septal ablation for hypertrophic obstructive cardiomyopathy by intraprocedural echocardiographic monitoring. J Am Soc Echocardiogr. 2000;13(12):1074–9.
13. Monakier D, Woo A, Puri T, Schwartz L, Ross J, Jamorski M, et al. Usefulness of myocardial contrast echocardiographic quantification of risk area for predicting postprocedural complications in patients undergoing septal ethanol ablation for obstructive hypertrophic cardiomyopathy. Am J Cardiol. 2004;94(12):1515–22.
14. Faber L, Seggewiss H, Welge D, Fassbender D, Schmidt HK, Gleichmann U, et al. Echo-guided percutaneous septal ablation for symptomatic hypertrophic obstructive cardiomyopathy: 7 years of experience. Eur J Echocardiogr. 2004;5(5):347–55.
15. Kuhn H, Lawrenz T, Lieder F, Leuner C, Strunk-Mueller C, Obergassel L, et al. Survival after transcoronary ablation of septal hypertrophy in hypertrophic obstructive cardiomyopathy (TASH): a 10 year experience. Clin Res Cardiol. 2008;97(4):234–43.
16. Bhagwandeen R, Woo A, Ross J, Wigle ED, Rakowski H, Kwinter J, et al. Septal ethanol ablation for hypertrophic obstructive cardiomyopathy: early and intermediate results of a Canadian referral centre. Can J Cardiol. 2003;19(8):912–7.
17. Veselka J, Prochazkova S, Duchonova R, Bolomova-Homolova I, Palenickova J, Tesar D, et al. Alcohol septal ablation for hypertrophic obstructive cardiomyopathy: lower alcohol dose reduces size of infarction and has comparable hemodynamic and clinical outcome. Catheter Cardiovasc Interv. 2004;63(2):231–5.
18. Yoerger DM, Picard MH, Palacios IF, Vlahakes GJ, Lowry PA, Fifer MA. Time course of pressure gradient response after first alcohol septal ablation for obstructive hypertrophic cardiomyopathy. Am J Cardiol. 2006;97(10):1511–4.
19. Veselka J, Duchonova R, Prochazkova S, Homolova I, Palenickova J, Zemanek D, et al. The biphasic course of changes of left ventricular outflow gradient after alcohol septal ablation for hypertrophic obstructive cardiomyopathy. Kardiol Pol. 2004;60(2):133–6; discussion 7.
20. van Dockum WG, Beek AM, ten Cate FJ, ten Berg JM, Bondarenko O, Gotte MJ, et al. Early onset and progression of left ventricular remodeling after alcohol septal ablation in hypertrophic obstructive cardiomyopathy. Circulation. 2005;111(19):2503–8.
21. van Dockum WG, Kuijer JP, Gotte MJ, Ten Cate FJ, Ten Berg JM, Beek AM, et al. Septal ablation in hypertrophic obstructive cardiomyopathy improves systolic myocardial function in the lateral (free) wall: a follow-up study using CMR tissue tagging and 3D strain analysis. Eur Heart J. 2006;27(23):2833–9.
22. Schulz-Menger J, Strohm O, Waigand J, Uhlich F, Dietz R, Friedrich MG. The value of magnetic resonance imaging of the left ventricular outflow tract in patients with hypertrophic obstructive cardiomyopathy after septal artery embolization. Circulation. 2000;101(15):1764–6.
23. Jassal DS, Neilan TG, Fifer MA, Palacios IF, Lowry PA, Vlahakes GJ, et al. Sustained improvement in left ventricular diastolic function after alcohol septal ablation for hypertrophic obstructive cardiomyopathy. Eur Heart J. 2006;27(15):1805–10.
24. Nagueh SF, Lakkis NM, Middleton KJ, Killip D, Zoghbi WA, Quinones MA, et al. Changes in left ventricular diastolic function 6 months after nonsurgical septal reduction therapy for hypertrophic obstructive cardiomyopathy. Circulation. 1999;99(3):344–7.
25. Delling FN, Sanborn DY, Levine RA, Picard MH, Fifer MA, Palacios IF, et al. Frequency and mechanism of persistent systolic anterior motion and mitral regurgitation after septal ablation in obstructive hypertrophic cardiomyopathy. Am J Cardiol. 2007;100(11):1691–5.
26. Chang SM, Nagueh SF, Spencer 3rd WH, Lakkis NM. Complete heart block: determinants and clinical impact in patients with hypertrophic obstructive cardiomyopathy undergoing nonsurgical septal reduction therapy. J Am Coll Cardiol. 2003;42(2):296–300.
27. Chen AA, Palacios IF, Mela T, Yoerger DM, Picard MH, Vlahakes G, et al. Acute predictors of subacute complete heart block after alcohol septal ablation for obstructive hypertrophic cardiomyopathy. Am J Cardiol. 2006;97(2):264–9.
28. Hori Y, Ueda M, Nakayama T, Saegusa N, Uehara M, Lee K, et al. Occurrence of de novo sustained monomorphic ventricular tachycardia induced after percutaneous transluminal alcohol septal myocardial ablation for hypertrophic obstructive cardiomyopathy. Int J Cardiol. 2007;119(3):403–7.
29. Boltwood Jr CM, Chien W, Ports T. Ventricular tachycardia complicating alcohol septal ablation. N Engl J Med. 2004;351(18):1914–5.
30. Simon RD, Crawford 3rd FA, Spencer 3rd WH, Gold MR. Sustained ventricular tachycardia following alcohol septal ablation for hypertrophic obstructive cardiomyopathy. Pacing Clin Electrophysiol. 2005;28(12):1354–6.
31. Fernandes VL, Nagueh SF, Wang W, Roberts R, Spencer 3rd WH. A prospective follow-up of alcohol septal ablation for symptomatic hypertrophic obstructive cardiomyopathy--the Baylor experience (1996–2002). Clin Cardiol. 2005;28(3):124–30.

Catheter-Based Atrial Septal Defect Closure

5

Nathaniel R. Smilowitz and Muhamed Saric

Abstract

Atrial septal defects (ASDs) are among the most common congenital heart defects in adults. Ostium secundum type ASDs account for 70 % of all defects and the majority are amenable to percutaneous closure. At present, non-secundum ASDs require surgical repair. Echocardiography has emerged as an essential imaging tool to characterize defect anatomy, measure ASD dimensions, identify candidates for percutaneous closure, and facilitate appropriate device selection. Intra-procedural echocardiographic guidance is critical to transcatheter closure. 3D transesophageal echocardiography offers significant advantages over 2-dimensional imaging by providing highly accurate representations of septal defects in the en face views.

Keywords

Atrial septal defect • Percutaneous • Transcatheter • Closure • Repair • Congenital heart disease • Echocardiography • Transesophageal, septal occluder

Background

Atrial septal defects (ASD) account for 13 % of all congenital heart diagnoses with a prevalence of 1.6 out of 1,000 individuals at birth [1]. ASDs frequently remain asymptomatic until adulthood, when atrial arrhythmias, paradoxical embolization, or pulmonary hypertension can develop. ASDs are the most common congenital heart lesion in adults aside from the bicuspid aortic valve. Echocardiography plays an instrumental role in the diagnosis of ASDs and is commonly used to guide catheter-based closure.

Electronic supplementary material The online version of this chapter (doi:10.1007/978-3-319-29428-5_5) contains supplementary material, which is available to authorized users.

N.R. Smilowitz • M. Saric, MD, PhD (✉)
Department of Medicine, Leon H. Charney Division of Cardiology, New York University Langone Medical Center, New York, NY 10106, USA
e-mail: Nathaniel.Smilowitz@nyumc.org; Muhamed.Saric@nyumc.org

Embryology and Pathology

The atrial septum is a complex convex structure that develops within a primitive single atrium during early embryonic life. In normal development, septation of the atria begins in the fifth week of gestation, when the septum primum (primary septum) grows from the roof of the common atrium towards the endocardial cushions of the atrioventricular (AV) canal. The opening between the leading edge of the septum primum and the endocardial cushions is referred to as the ostium primum. Fusion of the septum primum with the endocardial cushion closes the ostium primum, but a second orifice, the ostium secundum, develops via partial resorption of the central portion of the septum primum.

In the 12th week of development, tissue from the roof of the right atrium forms the septum secundum by growing caudally to cover the right side of the ostium secundum to form the foramen ovale. In neonatal life, this conduit permits oxygenated blood from the umbilical vein to pass directly from the right atrium to the left atrium, bypassing the pulmonary circulation. At birth, when pulmonary vascular resistance drops, right atrial pressures decline and the foramen ovale closes. Closure of the

M.H. Picard et al. (eds.), *Intraprocedural Imaging of Cardiovascular Interventions*, DOI 10.1007/978-3-319-29428-5_5

foramen ovale reroutes deoxygenated blood through the pulmonary circuit, completing the transition to normal adult circulation. In the majority of individuals, the septum secundum subsequently fuses with the septum primum after birth, permanently sealing the foramen ovale. However, in 25–30 % of adults, fusion of the septum primum and secundum fails to occur and a patent foramen ovale remains [2, 3].

Failure of the complex developmental sequence of atrial septation leads to persistent communications between the atria. There are four major sub-types of ASDs. Ostium secundum ASDs, which result from excessive resorption of the septum primum or inadequate growth of the septum secundum, account for 70 % of all ASDs and are the only subtype currently amenable to percutaneous closure. Less common subtypes, listed in order of decreasing frequency, are primum ASD (15–20 %), superior vena cava type sinus venosus ASD (3–10 %), inferior vena cava type sinus venosus ASD (1 %), and unroofed coronary sinus (<1 %) [4]. While these defects are surgically correctable, they are frequently not isolated and can involve other cardiac structures. Primum ASDs, for example, are associated with endocardial cushion defects that often require extensive surgical repair. Due to complex permutations of developmental abnormalities, significant anatomic variations can occur. Thus, careful evaluation of cardiac anatomy is essential to plan surgical or percutaneous repair.

Indications for ASD Closure

According to the 2008 American College of Cardiology/American Heart Association (ACC/AHA) guidelines for the management of adults with congenital heart disease, the principal indication for ASD closure is the presence of right-sided atrial or ventricular enlargement, regardless of symptoms (Class I, Level of Evidence B) [5]. Closure can also be considered in the setting of: (a) paradoxical emboli from the venous to systemic circulation via a right to left intracardiac shunt (Class IIa; Level of Evidence C); (b) platypnea-orthodeoxia, when arterial oxygen desaturation occurs when changing from a recumbent to an upright position (Class IIa; Level of Evidence B); (c) left-to-right shunting, with pulmonary vascular resistance less than two-thirds systemic resistance, pulmonary artery pressure less than two-thirds systemic pressure, or when elevated pulmonary vascular resistance is responsive to vasodilators (Class IIb; Level of Evidence C). ASD closure is contraindicated in the setting of irreversible, severe pulmonary arterial hypertension when left to right shunt is absent. The European Society of Cardiology (ESC) provides similar guidance. The ESC guidelines also specifically endorse device closure as the preferred method for secundum ASD repair (Class I, Level of Evidence C) [6].

Approaches to ASD Repair

Surgical Techniques for ASD closure were pioneered in the 1950s, prior to the development of cardiopulmonary bypass [7]. The first successful ASD closure (and first open heart surgery) was performed in 1952 by F John Lewis at the University of Minnesota [8]. Today, surgeons with expertise in congenital heart disease can safely achieve surgical closure of all types of ASDs [5]. Modern surgical approaches employ direct suture closure, pericardial patch, or polyethylene terephthalate (Dacron®) patch placement for septal repair.

Percutaneous techniques for secundum ASD closure emerged as an alternative to surgery in 1975, when King and Mills performed the first successful transcatheter closure at the Ochsner Medical Center in New Orleans, LA [9]. Since that time, a dramatic rise in the frequency of secundum ASD closure has been documented, with the percutaneous approach as the dominant method of repair [10]. Minimally invasive transcatheter techniques offer reduced periprocedural morbidity and shorter hospital stays. However, not all secundum ASDs are amenable to percutaneous closure. Anatomic features, such as the maximal ASD diameter and the dimensions of the circumferential tissue rim, are important determinants of the feasibility of percutaneous intervention, device selection, and technical and procedural success. Additional factors, such as associated anomalous pulmonary venous connections, may also preclude percutaneous secundum ASD closure. Surgery remains the only appropriate method to close ostium primum, sinus venosus, and unroofed coronary sinus ASDs.

Role of Echocardiography

Echocardiography has emerged as an essential imaging tool for ASD diagnosis, to characterize defect anatomy and measure ASD dimensions, identify candidates for percutaneous closure, and provide intra-procedural imaging guidance. Historically, ASD dimensions were obtained from invasive balloon catheter occlusion techniques prior to percutaneous closure in conjunction with color Doppler echocardiography. In this method, sizing balloons are placed across the ASD and inflated until complete cessation of flow across the ASD as determined by color Doppler imaging is achieved. Unfortunately, dimensions obtained from this "stop-flow" approach reflected distorted ASD anatomy and often fail to accurately delineate the sizes and shapes of complex or fenestrated ASDs.

More recently, two-dimensional (2D) transesophageal echocardiography (TEE) has been used to characterize ASD anatomy. Maximum ASD dimensions should be measured in atrial diastole in multiple orthogonal views. The anatomic

ASD tissue rims should be measured to confirm a sufficient width to anchor a closure device [11, 12].

There are six conventional ASD tissue rims that should be visualized by 2D TEE. The midesophageal four-chamber view at 0° provides visualization of atrioventricular rim (adjacent to the tricuspid and mitral valves) and posterosuperior rim of the ASD. Aortic (anterior) and posteroinferior rims can be seen in the short axis view at 60°. The bicaval view at 120° permits visualization of the superior vena cava (SVC) and inferior vena cava (IVC) rims. Accurate dimensions of circumferential ASD tissue rims are critical to guide device selection (Fig. 5.1).

Although 2D TEE imaging can provide reasonably accurate measurements of circular or oval ASDs, complex defect shapes are notoriously difficult to measure by this method. 2D-TEE images can also underestimate ASD dimensions when geometric chords, rather than maximal short- and long-axis diameters, are visualized [13]. Although 2D multiplane reconstructions have been used to enhance visualization of ASD anatomy, the ease and performance of 3D-TEE imaging may render these techniques obsolete.

Three-dimensional (3D) transesophageal echocardiographic (TEE) is becoming the new gold standard for visualization of ASD anatomy in preparation for percutaneous closure [13–15]. Modern 3D-TEE imaging systems have matrix-array transducers with 3,000 elements that acquire a pyramid-shaped volume of echocardiographic data and can reconstruct 3D zoom views from both the right atrial and left atrial perspectives. The en face septal views provide accurate visualization of the shape (circular, triangular, ovoid, or fenestrated) and size of ASDs (Fig. 5.2) as well as the dimensions of the circumferential tissue rims, and anatomic relationships of the ASD to surrounding cardiac structures. 3D-TEE can also rapidly identify other associated structural anomalies, such as atrial septal aneurysms.

The three-step TUPLE (Tilt-Up-Then-Left) maneuver can be utilized to achieve a standardized, anatomically correct orientation of the septum in the en face view (Fig. 5.3) [16]. To begin, optimal 2D-TEE midesophageal images should be obtained at 0° to visualize the interatrial septum. After generating a 3D zoom image, the interatrial septum should be tilted up along the horizontal axis to provide the en face view from the right atrial perspective. Rotation of the interatrial septum 180° (degrees) counterclockwise around the vertical Z-axis completes the TUPLE sequence, yielding an en face view from the left atrial perspective. As a rule of thumb, TUPLE sequences obtained from 2D-TEE imaging angles greater than 0° will require additional counterclockwise rotation of the resulting 3D images by a similar degree. Images acquired at 60° on 2D-TEE, for example, will require an additional 60° counterclockwise rotation in the Z-axis to achieve the appropriate en face view. Once the en face view of the atrial septum has been obtained in atrial diastole (Fig. 5.4), a rectangular grid of known proportions can be superimposed on the resulting images to permit semi-quantitative

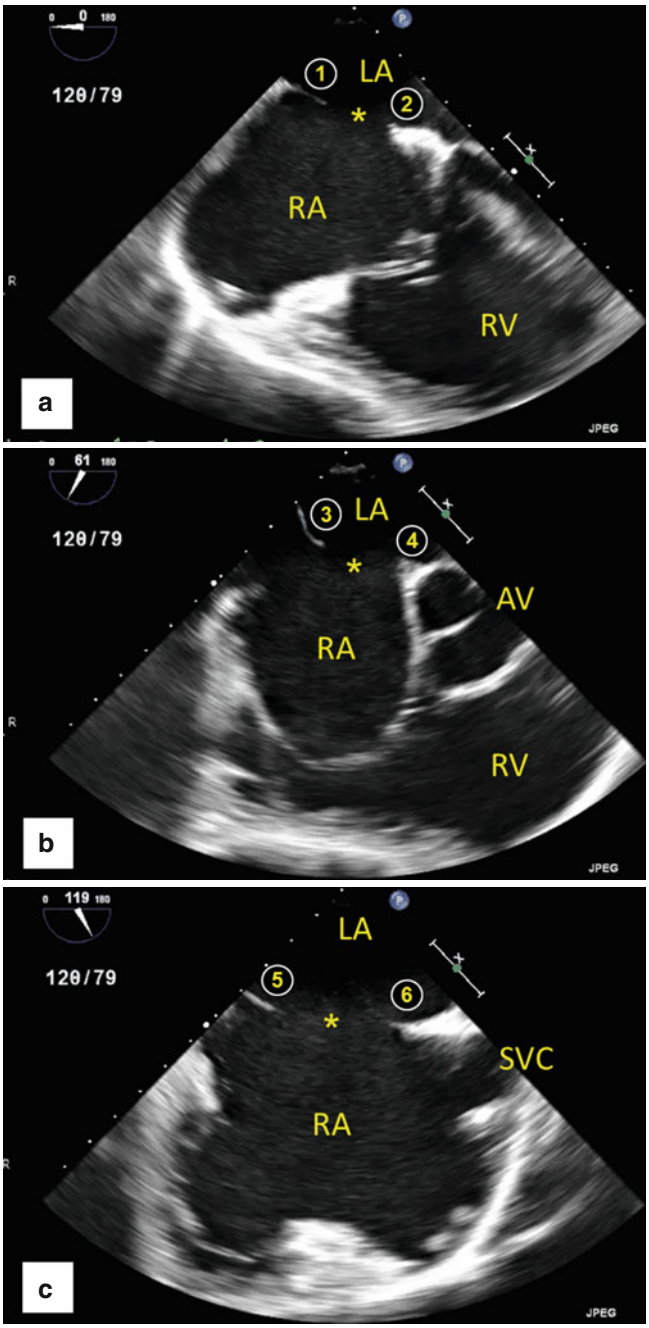

Fig. 5.1 ASD tissue rims that should be visualized by 2D TEE. The midesophageal four-chamber view at 0° (Panel **a**, Video 5.1) provides visualization of the (*1*) posterosuperior rim of the ASD and (*2*) the atrioventricular rim adjacent to the tricuspid and mitral valves and. The (*3*) posteroinferior and (*4*) anterior aortic rims can be seen in the short axis view at 60° (Panel **b**, Video 5.2). The bicaval view at 120° permits visualization of the (*5*) inferior vena cava and (*6*) superior vena cava rims (Panel **c**, Video 5.3). *AV* aortic valve, *LA* left atrium, *RA* right atrium; *RV* right ventricle, *SVC* superior vena cava

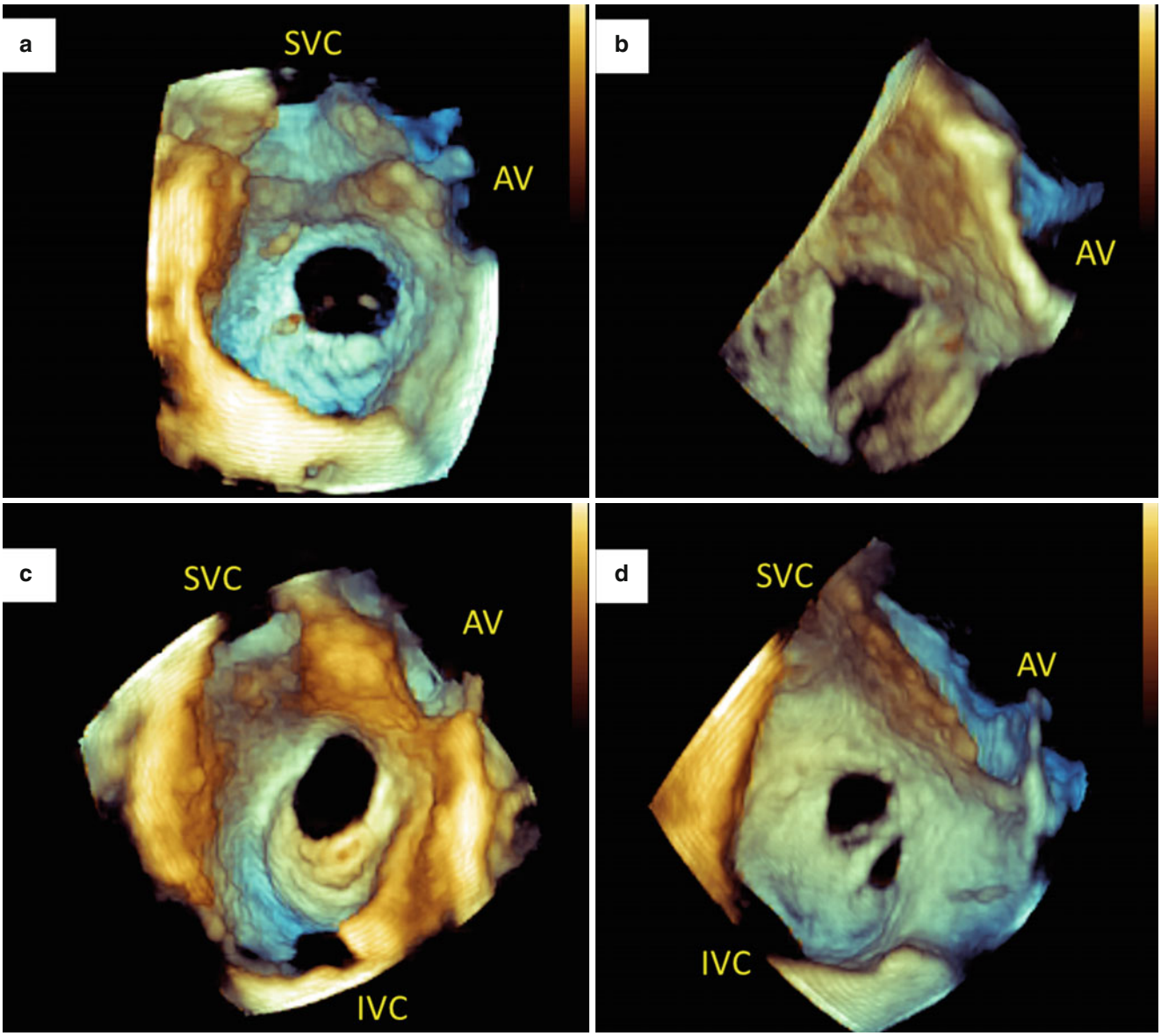

Fig. 5.2 Morphologic variants of secundum ASD. *Circular* (Panel **a**), *triangular* (Panel **b**), *ovoid* (Panel **c**), or *fenestrated* (Panel **d**) ASDs visualized by 3D TEE. *AV* aortic valve, *IVC* inferior vena cava, *SVC* superior vena cava

measurements. Alternatively, direct caliper measurement of structures in the en face views can provide dimensions with a high degree of accuracy (Fig. 5.5).

There are some limitations to peri-procedural 3D-TEE evaluation of ASDs. 3D zoom modes that can yield anatomically accurate en face views are limited to relatively low frame rates. The presence of stitch artifacts can degrade overall image quality during multi-beat acquisition sequences. The size of current 3D-TEE transducers may limit the application of this imaging modality to adults and larger pediatric patients (weighing ≥20 kg). Still, 3D-TEE represents a leap forward in accurate imaging of ASDs.

Device Selection

A number of transcatheter devices are available for ASD closure in the United States (US) (Fig. 5.6). All the devices share a similar basic structure of two disks with an interconnecting shaft. While most devices are approved for repair of simple secundum ASDs with a solitary defect, others can repair complex fenestrated or cribriform (sieve-like) ASDs. The most commonly used devices approved for use in the US include the Amplatzer Septal Occluder, the Amplatzer Multifenestrated Septal Occluder (St Jude Medical, St Paul, MN, USA), and the Gore-Helix Atrial Septal Occluder (W L Gore & Associates, Inc., Flagstaff, AZ, USA).

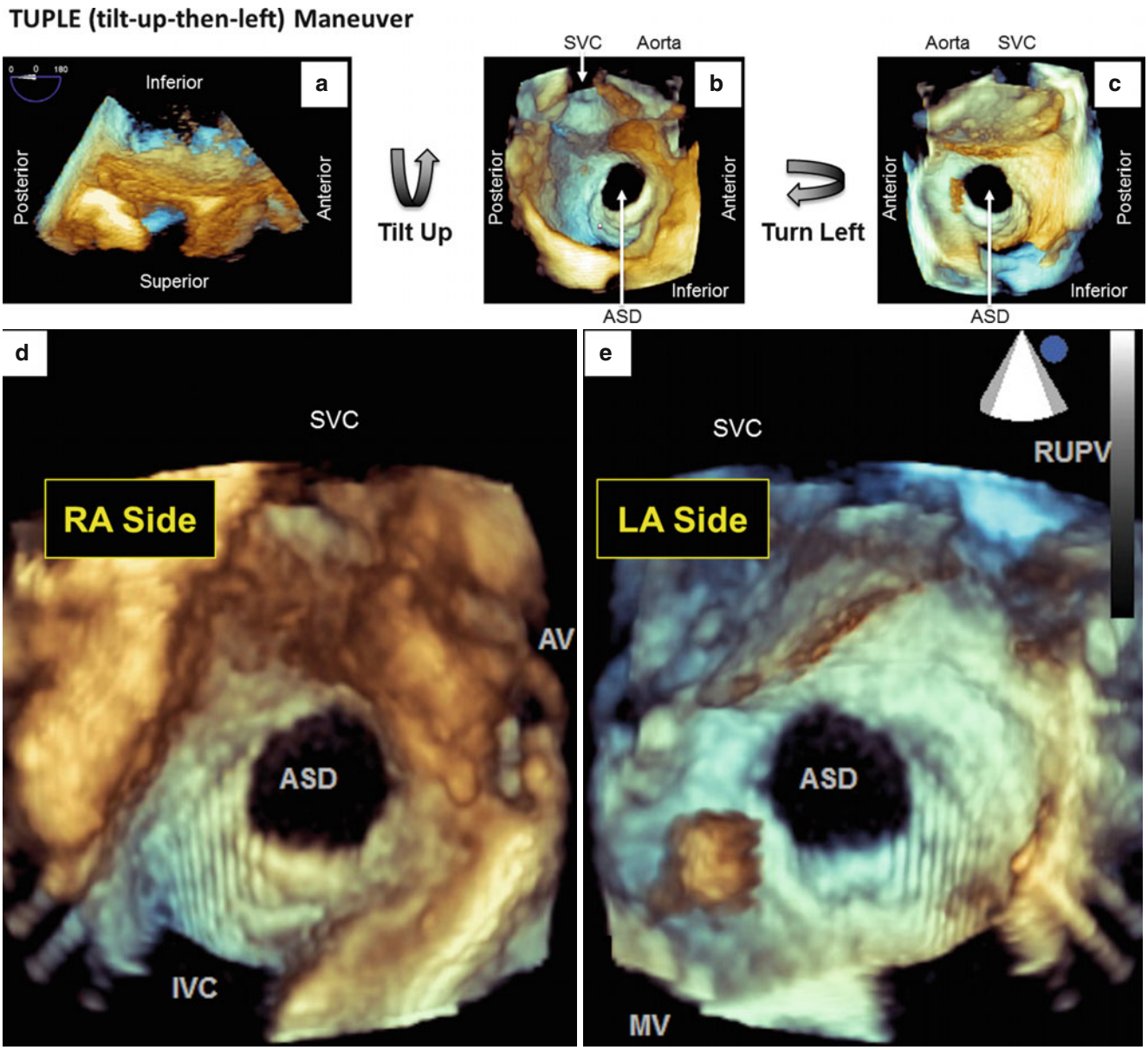

Fig. 5.3 The three-step TUPLE (Tilt-Up-Then-Left) maneuver. The 3D TEE TUPLE maneuver achieves anatomically correct views of the septum in the en face view. The resulting right atrial (Panel **d**) and left atrial (Panel **e**) aspect of the atrial septum (See Video 5.4). *ASD* atrial septal defect, *AV* aortic valve, *IVC* inferior vena cava, *LA* left atrium, *MV* mitral valve, *RA* right atrium, *RUPV* right upper pulmonary vein, *SVC* superior vena cava

Device selection depends largely on ASD anatomy, as it requires a match between measurements of the septal defect and the dimensions available for each closure device. For example, the Amplatzer Septal Occluder, named after the Austrian-born American radiologist Kurt Amplatz, consists of two nitinol (nickel and titanium alloy) wire mesh round disks – a larger left atrial disk and a smaller right atrial disk – connected by a short waist. The nitinol waist ranges from 4 to 38 mm in diameter and should correspond to the diameter of the ASD to ensure adequate percutaneous closure. In contrast, the Gore-Helex device consists of two equal sized disks with a diameter ranging from 15 to 36 mm covered with an ultra-thin polytetrafluoro-ethylene membrane with an interconnecting spiral shaft. A disk diameter at least twice the ASD diameter is required for optimal Gore-Helex closure. Thus, the maximum ASD diameter should not exceed device-specific cutoff values of 38 mm for Amplatzer and 18 mm for the Gore-Helex septal occluder. The Amplatzer Multifenestrated Septal Occluder consists of two equal sized disks (diameter ranges from 18 to 35 mm) connected by a thin shaft intended for use with cribriform ASDs when disk diameter is sufficient to cover the entire defect.

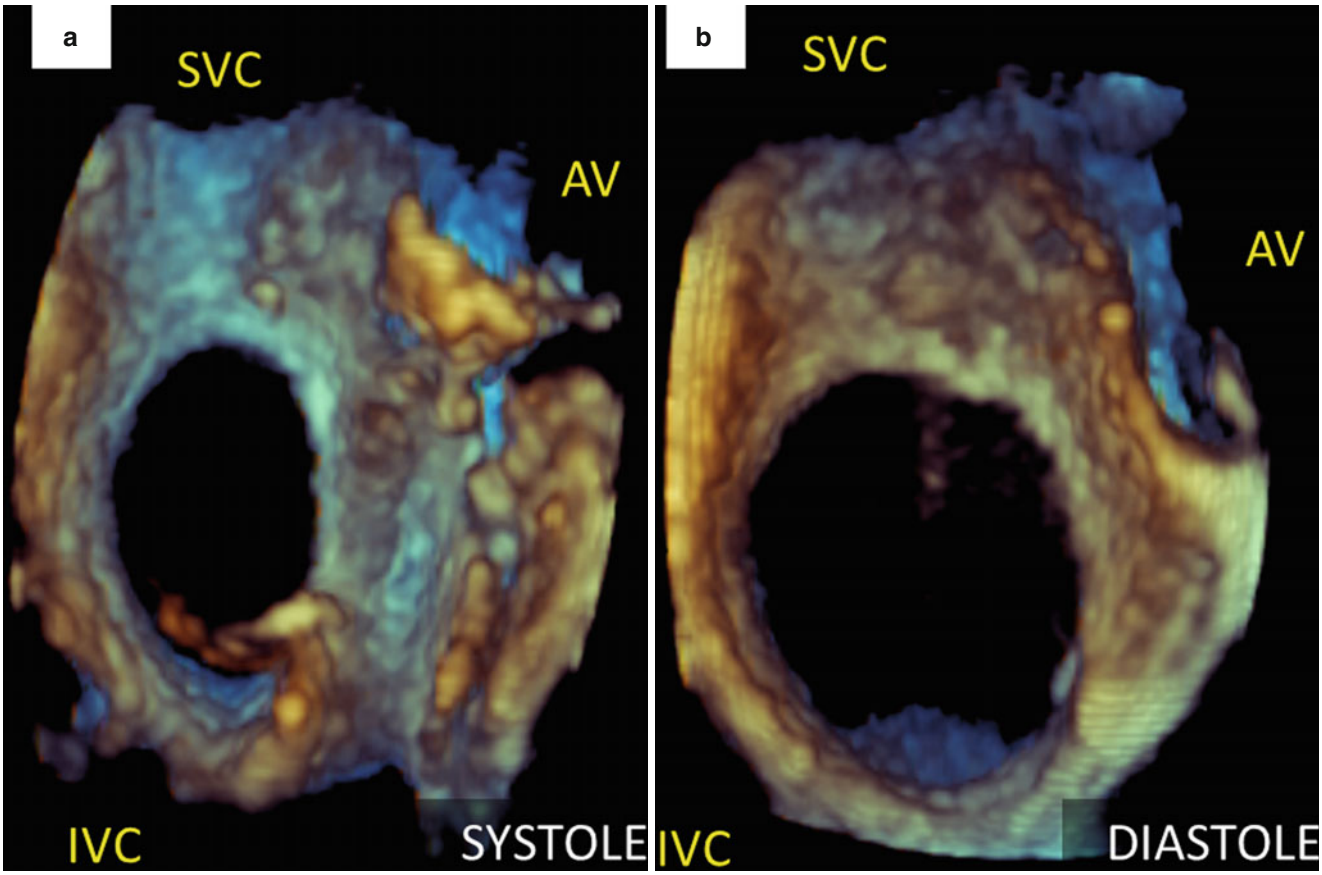

Fig. 5.4 The atrial septum in systole and diastole. Atrial septal defect dimensions vary considerably during the cardiac cycle. ASD dimensions are smallest in early systole (Panel **a**) and largest in early diastole (Panel **b**). *AV* aortic valve, *IVC* inferior vena cava, *SVC* superior vena cava

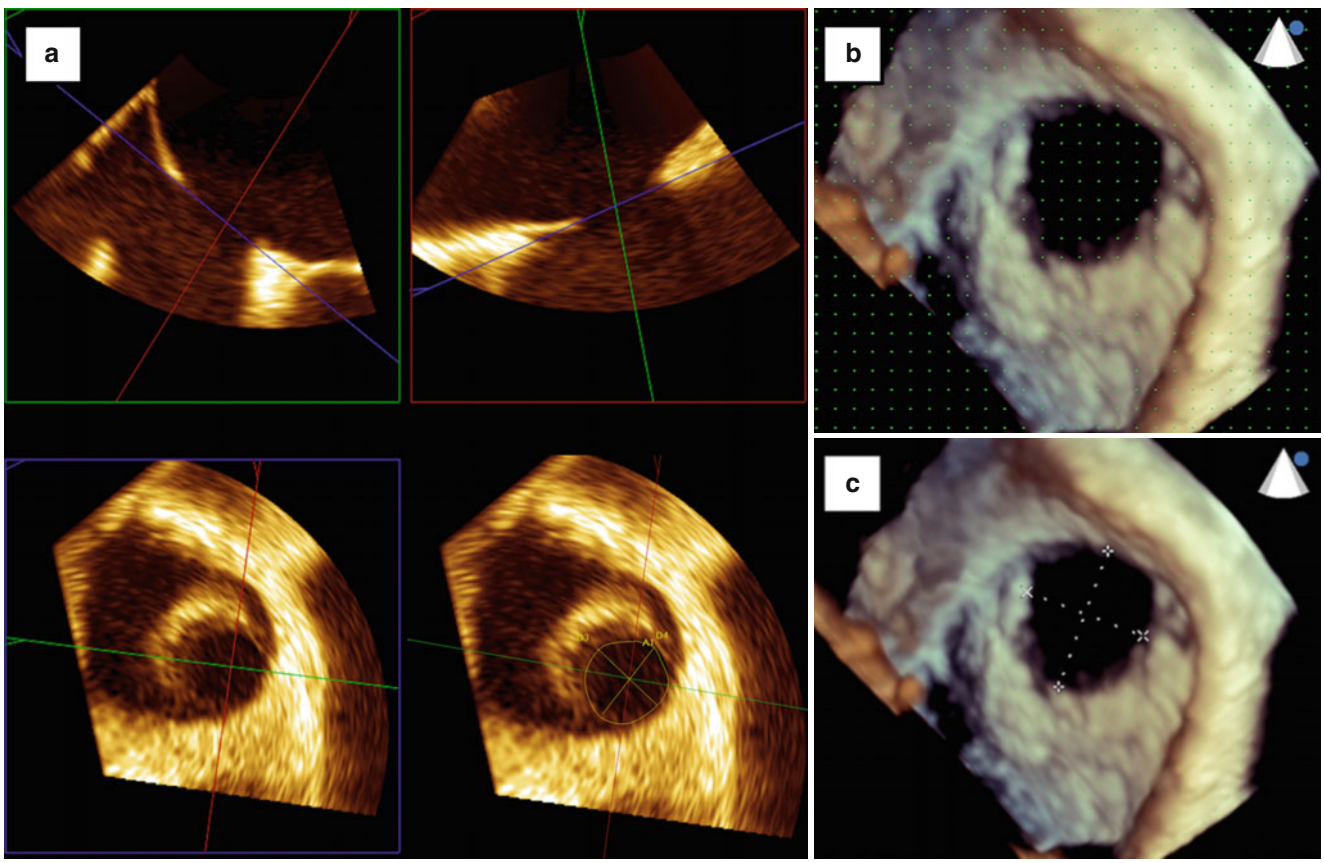

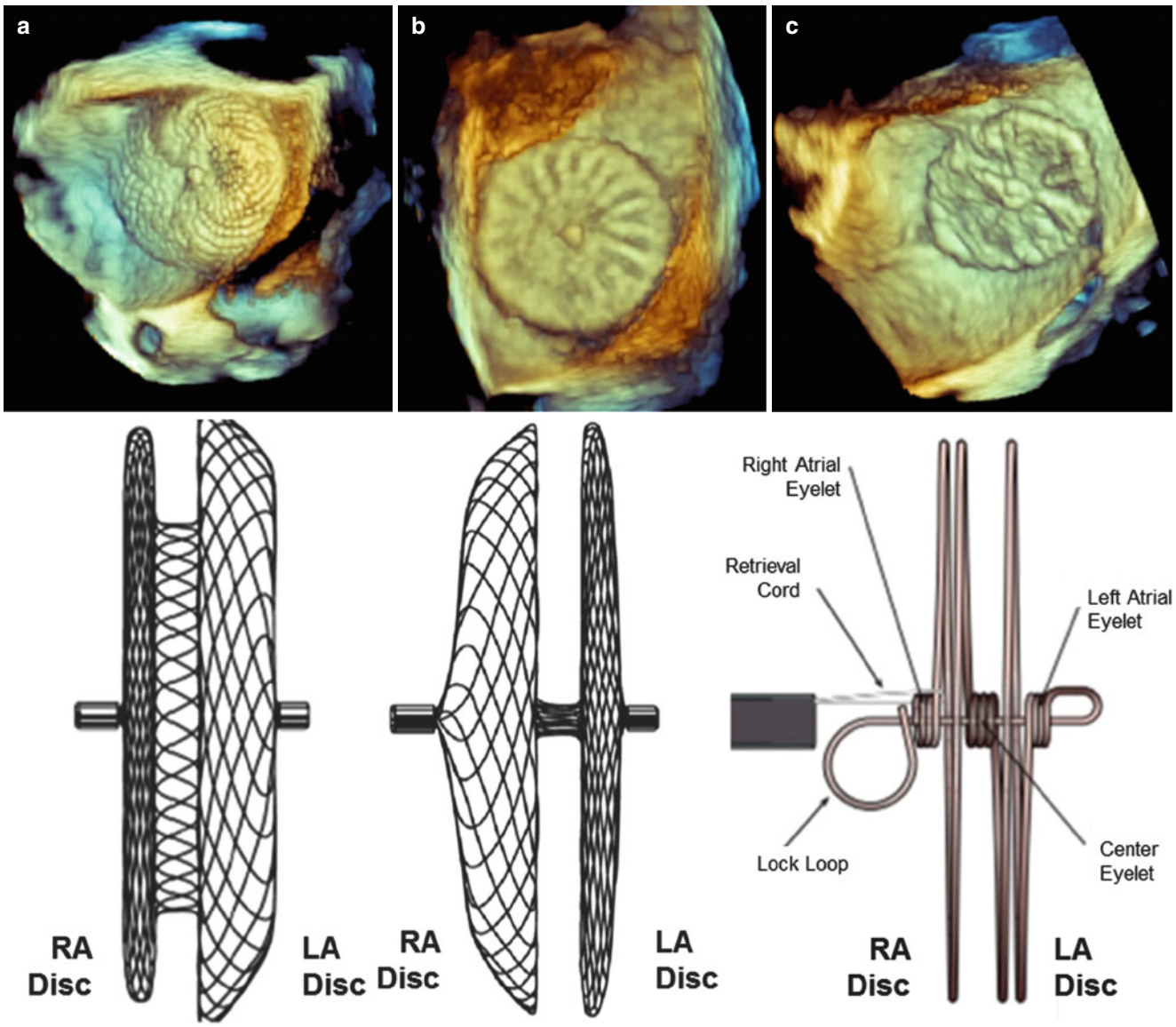

Fig. 5.6 Transcatheter devices available for ASD closure in the United States. Echocardiographic images (*top panel*) and diagrams (*bottom panel*) of the Amplatzer ASD Occluder (panel **a**), Amplatzer Multifenestrated Septal Occluder (Panel **b**), and Gore-Helex ASD Occluder (Panel **c**). *LA* left atrium, *RA* right atrium

Appropriate device selection is essential to minimize post-procedural complications after percutaneous ASD closure. Device embolization has been reported to occur after approximately 0.6 % of Amplatzer Septal Occluder deployments (Fig. 5.7) [17]. Risk factors for device embolization include device under-sizing, malposition during deployment, and inadequate ASD tissue rims. In general, tissue rims of at least 5 mm are necessary to ensure safe placement of the Amplatzer atrial septal occluder. This minimum dimension is determined by the size of the overhanging edge of the Amplatzer septal occluder's right atrial disk beyond its waist. When the Amplatzer multifenestrated atrial septal occluder is used, SVC and aortic rims should be greater than 9 mm. Measurement of ASD tissue rims with echocardiography is critical to facilitate appropriate device sizing and favorable procedural outcomes. Absence of the IVC rim is considered to be a contraindication to secundum ASD device closure.

Disc erosion into surrounding cardiac structures is another potentially devastating complication of percutaneous ASD closure. Disc erosion has been reported in 0.1 % of Amplatzer Septal Occluder implantations and can progress to perforation of the left atrial roof and/or aorta [17]. Absence of the aortic (anterior-superior) rim has been identified as a significant risk factor for Amplatzer septal occluder device erosion into surrounding

Fig. 5.5 Multi-plane reconstruction, grid and direct caliper measurements. Multi-plane reconstructions from 2D TEE orthogonal views can be used for measurements (Panel **a**). A rectangular grid superimposed on 3D TEE images provides semi-quantitative measurements (Panel **b**). Direct caliper measurements (Panel **c**) are preferred for accurate dimensions of structures visualized in the en face septal views

structures [18]. Oversized devices, contact by the edge of the device with the atrial wall, splaying of the device around the aortic root, or rotational and/or translational movement of the device relative to the motion of the heart are other important risk factors. Unlike the Amplatzer Septal Occluder, disc erosion has not been reported for the Gore-Helex septal occluder device.

Intra-procedural Echocardiography

Fluoroscopic and echocardiographic guidance are essential for proper device placement. Prior to beginning any planned percutaneous ASD repair, 2D-TEE should be performed to exclude intra-cardiac thrombus or other echocardiographic findings that might prohibit ASD closure. Once it has been determined to be safe to proceed, central venous access is obtained, typically through the femoral vein. A delivery catheter is advanced into the right atrium, across the ASD, and into the left atrium under echocardiographic guidance. Prior to delivery of a closure device, interventional operators may choose to confirm device sizing with inflation of a sizing balloon within the defect to determine the "stop-flow" diameter. Once the balloon has been placed within the defect under fluoroscopic guidance, color Doppler echocardiography should be used to demonstrate an absence of flow between the balloon and ASD margins. Transient ASD closure during inflation of a sizing balloon can also be used to evaluate the hemodynamic consequences of ASD closure. Closure should be aborted if hemodynamic instability or signs of acute pulmonary edema develop.

Once a final size determination has been made, a collapsed ASD closure device, attached to its delivery cable, is advanced through catheter. The left atrial disc is deployed first and positioned against the left atrial side of the ASD. Next, the right atrial disc is expanded, temporarily anchoring the device within the ASD. 2D and en face 3D TEE imaging of the septum is used to confirm proper placement of the left and right atrial disks (Fig. 5.8). 3D TEE images can greatly assist interventional cardiologists when repositioning devices to achieve optimal alignment. Once appropriately positioned, the closure device is released from the delivery cable and permanently deployed (Fig. 5.9). As an alternative to imaging with transesophageal echocardiography, intracardiac echocardiography can also be used to guide device placement during percutaneous ASD closure.

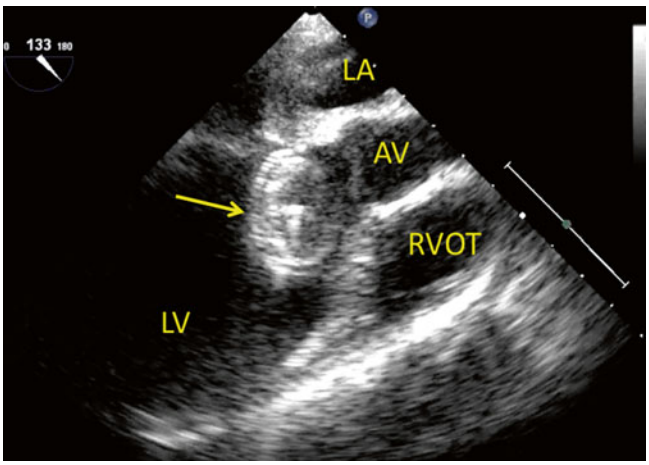

Fig. 5.7 Device embolization after Amplatzer Septal Occluder deployment. After deployment of an Amplatzer Septal Occluder, device embolization occurred. The septal occluder (*Arrow*) was noted to migrate to the left ventricular outflow tract. The device ultimately required surgical retrieval (See Video 5.5). *AV* aortic valve, *LA* left atrium, *LV* left ventricle, *RVOT* right ventricular outflow tract

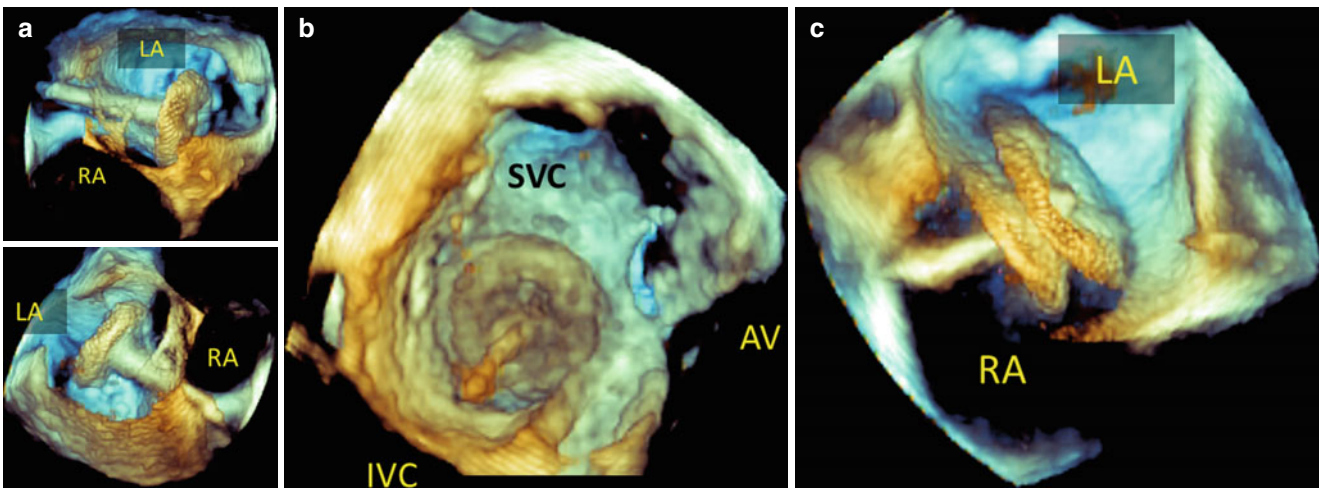

Fig. 5.8 En face 3D TEE images of the septum prior to device deployment. 3D TEE images can be used to confirm proper placement of the Amplatzer Septal Occluder. The left atrial disc is deployed first (Panel **a**), followed by the right atrial disc (Panel **b**). Left and right atrial discs are deployed in Panel (**c**). *AV* aortic valve, *IVC* inferior vena cava, *LA* left atrium, *RA* right atrium, *SVC* superior vena cava

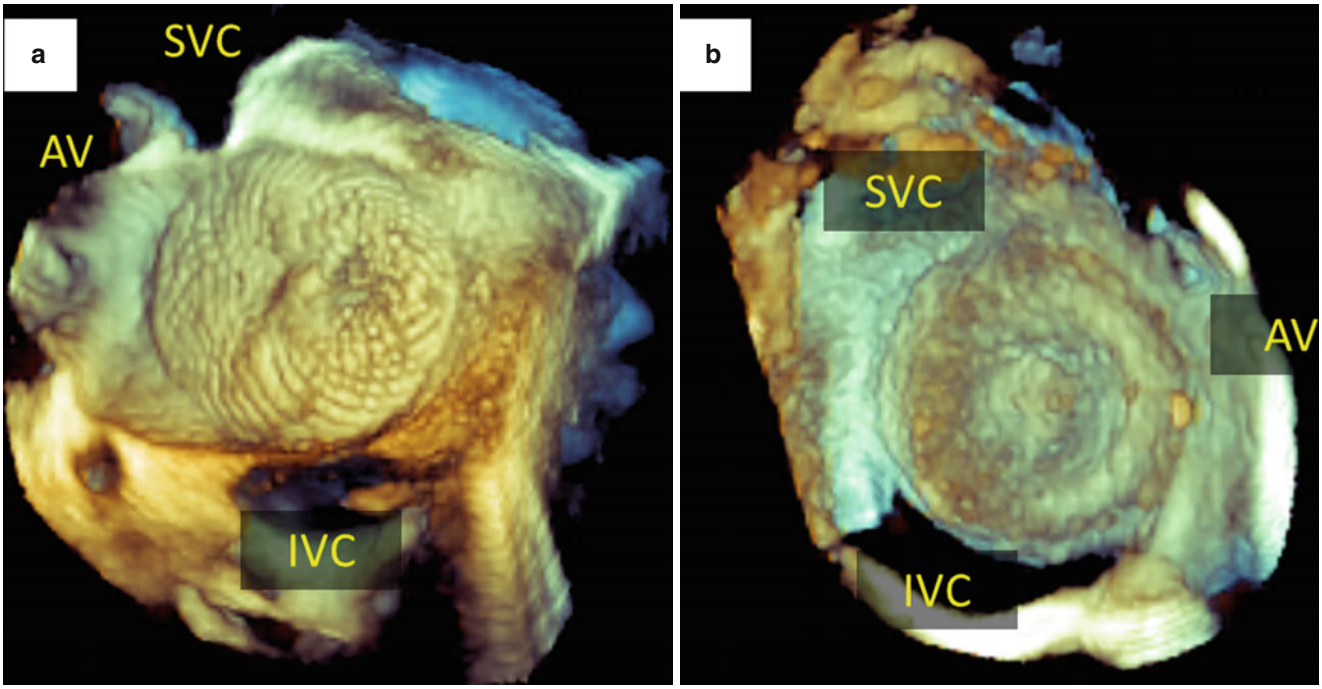

Fig. 5.9 3D TEE imaging after closure device deployment. Amplatzer Septal Occluder after deployment from the left atrial (Panel **a**) and right atrial (Panel **b**) perspectives. *AV* aortic valve, *IVC* inferior vena cava, *SVC* superior vena cava

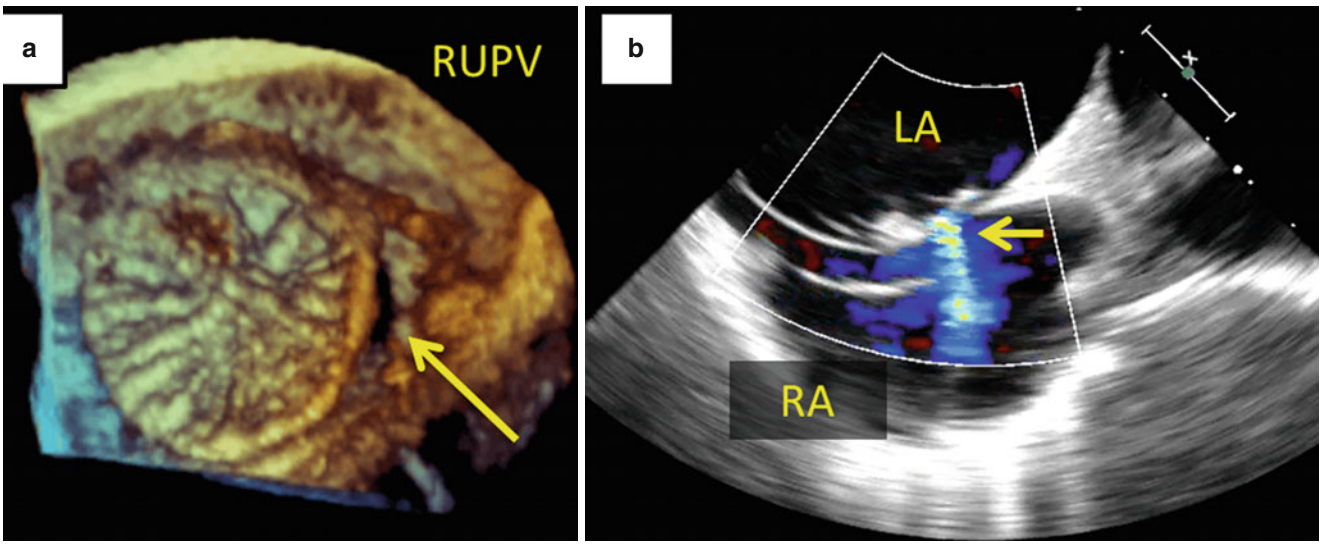

Fig. 5.10 Residual leak at the periphery of ASD closure device. A gap is visible between the Gore Helex Septal Occluder device and the ASD rim (Panel **a**). 2D TEE color Doppler imaging (Panel **b**) can be used to visualize the presence of residual leak (*Arrow*) (Video 5.6). *LA* left atrium, *RA* right atrium, *RUPV* right upper pulmonary vein

Echocardiography Following Percutaneous Closure

After device deployment, 2D and 3D TEE should be used to confirm appropriate device position and evaluate for complications such as perforation, pericardial effusion, or residual shunt. Color Doppler imaging should demonstrate complete absence of any flow at the periphery of the device that could suggest of a leak between the edges of the closure device and the ASD rim (Fig. 5.10). Small amounts of flow through the center of the device visualized on color Doppler are normal and typically resolve over time as endothelialization occurs. Routine follow up after closure should involve transthoracic echocardiography to ensure interval device migration, erosion, or other complications have not occurred.

References

1. van der Linde D, Konings EE, Slager MA, Witsenburg M, Helbing WA, Takkenberg JJ, et al. Birth prevalence of congenital heart disease worldwide: a systematic review and meta-analysis. J Am Coll Cardiol. 2011;58(21):2241–7. PubMed.
2. Meissner I, Whisnant JP, Khandheria BK, Spittell PC, O'Fallon WM, Pascoe RD, et al. Prevalence of potential risk factors for stroke assessed by transesophageal echocardiography and carotid ultrasonography: the SPARC study. Stroke prevention: assessment of risk in a community. Mayo Clin Proc. 1999;74(9):862–9. PubMed.
3. Hagen PT, Scholz DG, Edwards WD. Incidence and size of patent foramen ovale during the first 10 decades of life: an autopsy study of 965 normal hearts. Mayo Clin Proc. 1984;59(1):17–20. PubMed.
4. Geva T, Martins JD, Wald RM. Atrial septal defects. Lancet. 2014;383(9932):1921–32. PubMed.
5. Warnes CA, Williams RG, Bashore TM, Child JS, Connolly HM, Dearani JA, et al. ACC/AHA 2008 guidelines for the management of adults with congenital heart disease: a report of the American College of Cardiology/American Heart Association Task Force on Practice Guidelines (Writing Committee to Develop Guidelines on the Management of Adults With Congenital Heart Disease). Developed in Collaboration With the American Society of Echocardiography, Heart Rhythm Society, International Society for Adult Congenital Heart Disease, Society for Cardiovascular Angiography and Interventions, and Society of Thoracic Surgeons. J Am Coll Cardiol. 2008;52(23):e143–263. PubMed.
6. Baumgartner H, Bonhoeffer P, De Groot NM, de Haan F, Deanfield JE, Galie N, et al. ESC guidelines for the management of grown-up congenital heart disease (new version 2010). Eur Heart J. 2010;31(23):2915–57. PubMed.
7. Cohn LH. Fifty years of open-heart surgery. Circulation. 2003;107(17):2168–70. PubMed.
8. Lewis FJ, Taufic M. Closure of atrial septal defects with the aid of hypothermia; experimental accomplishments and the report of one successful case. Surgery. 1953;33(1):52–9. PubMed.
9. King TD, Thompson SL, Steiner C, Mills NL. Secundum atrial septal defect. Nonoperative closure during cardiac catheterization. JAMA. 1976;235(23):2506–9. PubMed.
10. Karamlou T, Diggs BS, Ungerleider RM, McCrindle BW, Welke KF. The rush to atrial septal defect closure: is the introduction of percutaneous closure driving utilization? Ann Thorac Surg. 2008;86(5):1584–90; discussion 90-1. PubMed.
11. Amin Z. Transcatheter closure of secundum atrial septal defects. Catheter Cardiovasc Interv. 2006;68(5):778–87. PubMed.
12. Mathewson JW, Bichell D, Rothman A, Ing FF. Absent posteroinferior and anterosuperior atrial septal defect rims: factors affecting nonsurgical closure of large secundum defects using the Amplatzer occluder. J Am Soc Echocardiogr Off Publ Am Soc Echocardiogr. 2004;17(1):62–9. PubMed.
13. Johri AM, Witzke C, Solis J, Palacios IF, Inglessis I, Picard MH, et al. Real-time three-dimensional transesophageal echocardiography in patients with secundum atrial septal defects: outcomes following transcatheter closure. J Am Soc Echocardiogr Off Publ Am Soc Echocardiogr. 2011;24(4):431–7. PubMed.
14. Roberson DA, Cui W, Patel D, Tsang W, Sugeng L, Weinert L, et al. Three-dimensional transesophageal echocardiography of atrial septal defect: a qualitative and quantitative anatomic study. J Am Soc Echocardiogr Off Publ Am Soc Echocardiogr. 2011;24(6):600–10. PubMed.
15. Taniguchi M, Akagi T, Watanabe N, Okamoto Y, Nakagawa K, Kijima Y, et al. Application of real-time three-dimensional transesophageal echocardiography using a matrix array probe for transcatheter closure of atrial septal defect. J Am Soc Echocardiogr Off Publ Am Soc Echocardiogr. 2009;22(10):1114–20. PubMed.
16. Saric M, Perk G, Purgess JR, Kronzon I. Imaging atrial septal defects by real-time three-dimensional transesophageal echocardiography: step-by-step approach. J Am Soc Echocardiogr Off Publ Am Soc Echocardiogr. 2010;23(11):1128–35. PubMed.
17. Moore J, Hegde S, El-Said H, Beekman 3rd R, Benson L, Bergersen L, et al. Transcatheter device closure of atrial septal defects: a safety review. JACC Cardiovasc Interv. 2013;6(5):433–42. PubMed.
18. Amin Z. Echocardiographic predictors of cardiac erosion after Amplatzer septal occluder placement. Catheter Cardiovasc Interv. 2014;83(1):84–92. PubMed.

Transcatheter Aortic Valve Replacement

6

Jonathan J. Passeri

Abstract

Symptomatic severe aortic stenosis portends a dismal prognosis without replacement of the aortic valve. For nearly half of a century, surgical aortic valve replacement (SAVR) was the mainstay of therapy. Transcatheter aortic valve replacement (TAVR) has more recently established itself as a highly-effective treatment for patients with symptomatic severe aortic stenosis. Currently indicated for patients who are at high or extreme risk for death or major morbidity with surgical aortic valve replacement, TAVR is likely to become a therapeutic option for intermediate and low surgical risk patients as well. Cardiac imaging plays a central role in achieving success with TAVR and is critical in pre-procedural evaluation, intra-procedural guidance, and post-procedural assessment.

Keywords

Transcatheter aortic valve replacement • Aortic stenosis • Aortic regurgitation • Echocardiography

Introduction

Aortic stenosis is the amongst the most common acquired valve diseases in industrialized nations. With the onset of symptoms, patients with severe aortic stenosis will develop progressive functional limitation, heart failure, and, ultimately, death unless the aortic valve is replaced. For decades, surgical aortic valve replacement was the mainstay of therapy for patients with symptomatic severe aortic stenosis. Transcatheter aortic valve replacement (TAVR) has become an increasingly utilized alternative for patients with symptomatic severe aortic stenosis who are high risk for death or major morbidity with surgery and, arguably, the standard of care for inoperable patients [1–4]. Ongoing studies of TAVR in intermediate surgical risk patients suggest that TAVR may become a therapeutic option for lower risk patients as well. The significant role of echocardiography for the pre-procedural, intraprocedural, and post-procedural evaluation of patients undergoing TAVR has been highlighted in consensus statements and clinical guidelines [5–7].

Background

Having a multidisciplinary team-based approach and high-quality cardiac imaging are included amongst those factors that a play major role in achieving success with TAVR. It is therefore not surprising that echocardiographers are an important part of the multidisciplinary team and should be

Electronic supplementary material The online version of this chapter (doi:10.1007/978-3-319-29428-5_6) contains supplementary material, which is available to authorized users.

J.J. Passeri, MD
Division of Cardiology, Department of Medicine, Corrigan Minehan Heart Center, Massachusetts General Hospital, 55 Fruit St, Yawkey Suite 5700, Boston, MA 02114, USA
e-mail: jpasseri@mgh.harvard.edu

M.H. Picard et al. (eds.), *Intraprocedural Imaging of Cardiovascular Interventions*, DOI 10.1007/978-3-319-29428-5_6

involved in every step of the process, including pre-procedural evaluation and therapeutic decision-making, intraprocedural guidance, and post-implantation assessment. The echocardiographer should be familiar with the pre-procedural screening requirements, the anatomy of the aortic valve complex as it pertains to TAVR, the structure of the available transcatheter valves, the procedural steps involved in valve implantation, and the complications that may arise at each stage of the procedure.

Pre-implantation Echocardiographic Assessment

While this chapter focuses upon imaging that is directly relevant to the successful performance of the TAVR procedure, it is worth noting the role of echocardiography in patient evaluation before the decision to perform TAVR is even made. Echocardiography remains the primary modality for establishing the diagnosis and determining the severity of aortic stenosis. Accurate assessment of the hemodynamic significance of aortic stenosis, determining ventricular size and function, estimation of pulmonary arterial systolic pressure, and identifying significant concomitant structural or other valve disease is of paramount importance for appropriate patient selection for TAVR and achieving optimal outcomes. Issues such as low-flow, low-gradient aortic stenosis, moderate or severe mitral regurgitation, or pulmonary hypertension, all of which are commonly identified by echocardiography, have been reported to be associated with increased mortality following TAVR. Thus, the pre-procedural assessment of patients being considered for TAVR begins with high-quality comprehensive transthoracic echocardiography performed and interpreted in accordance with the American Society of Echocardiography guidelines [7, 8].

Transesophageal echocardiography (TEE) is typically used for intraprocedural imaging. Before THV deployment, a comprehensive TEE is recommended for the morphologic and functional assessment of the cardiac chambers, all four heart valves, exclusion of intracardiac thrombus, assessment for pericardial effusion, and evaluation of the thoracic aorta [9]. There are several key points that are specific to TAVR and require particular emphasis.

Aortic Valve Complex

The aortic valve complex includes the left ventricular outflow tract (LVOT), the aortic annulus, the aortic valve cusps, the sinuses of Valsalva, and the sinotubular junction. Measurement of the aortic annulus and characterization of the aortic valve complex are important in selection of and determining the appropriate size of the transcatheter heart valve (THV) as well as for anticipating and avoiding complications, such as paravalvular regurgitation, aortic root rupture, or coronary artery occlusion [10–14].

Aortic Annulus

The most important measurement currently used for THV sizing is that of the virtual aortic annular plane, more commonly referred to as the "aortic annulus". This plane intersects the level of the lowest attachment site, or hinge points, of the three aortic cusps. Between these hinge points and the scalloped aortic cusps is the fibrous tissue of the interleaflet trigones [10]. The annular shape is dynamic throughout the cardiac cycle, being more elliptical (i.e., more oval) in diastole and less elliptical (i.e., more round) in systole [15]. Measurement of the aortic annulus for THV sizing is conventionally performed during mid systole. Historically, a two-dimensional measurement of the aortic annulus in the long-axis (sagittal) plane was used for determining THV size. Although this measurement proved to be adequate in the majority of cases, this measurement is difficult to accurately perform and has important limitations [14]. With a tricuspid aortic valve, a long-axis imaging window that visualizes two hinge-points, one on either side of the LVOT, does not bisect the annulus. Measurement of this hinge-point to hinge-point dimension therefore underestimates the true diameter of the annulus in the sagittal plane. The correct long-axis view that bisects the aortic annulus with a given hinge-point on one side does not visualize a hinge-point on the other side, but rather a region of fibrous tissue in the interleaflet trigone. With this imaging view, it is difficult to ensure that measurement of the diameter is being made at the level of the virtual aortic annular plane since only one hinge-point is in view and there is no anatomic landmark for the virtual annular plane within the interleaflet trigone (Fig. 6.1). The measurement is therefore made by assuming the annular plane is perpendicular to the long axis of the aorta. Lastly, the aortic annulus is frequently asymmetric and elliptical in shape. The larger annular diameter often lies in the coronal plane and the smaller annular diameter in the sagittal plane (Fig. 6.2) [16–18]. The more oval the shape of the annulus, the greater the likelihood that the sagittal diameter will underestimate the size of THV required. The two-dimensional long-axis measurement is no longer used for determining the size of THV and has been replaced by more robust measurements made using three-dimensional imaging. However, these imaging caveats of the aortic annulus remain relevant for optimizing the LVOT diameter measurement that is routinely used in the continuity equation for calculating the aortic valve area.

Aortic annular diameters, annular area, and perimeter measurements by cardiac-gated multislice computed tomography (MSCT) have been shown to improve the accuracy of THV sizing and MSCT has become the standard

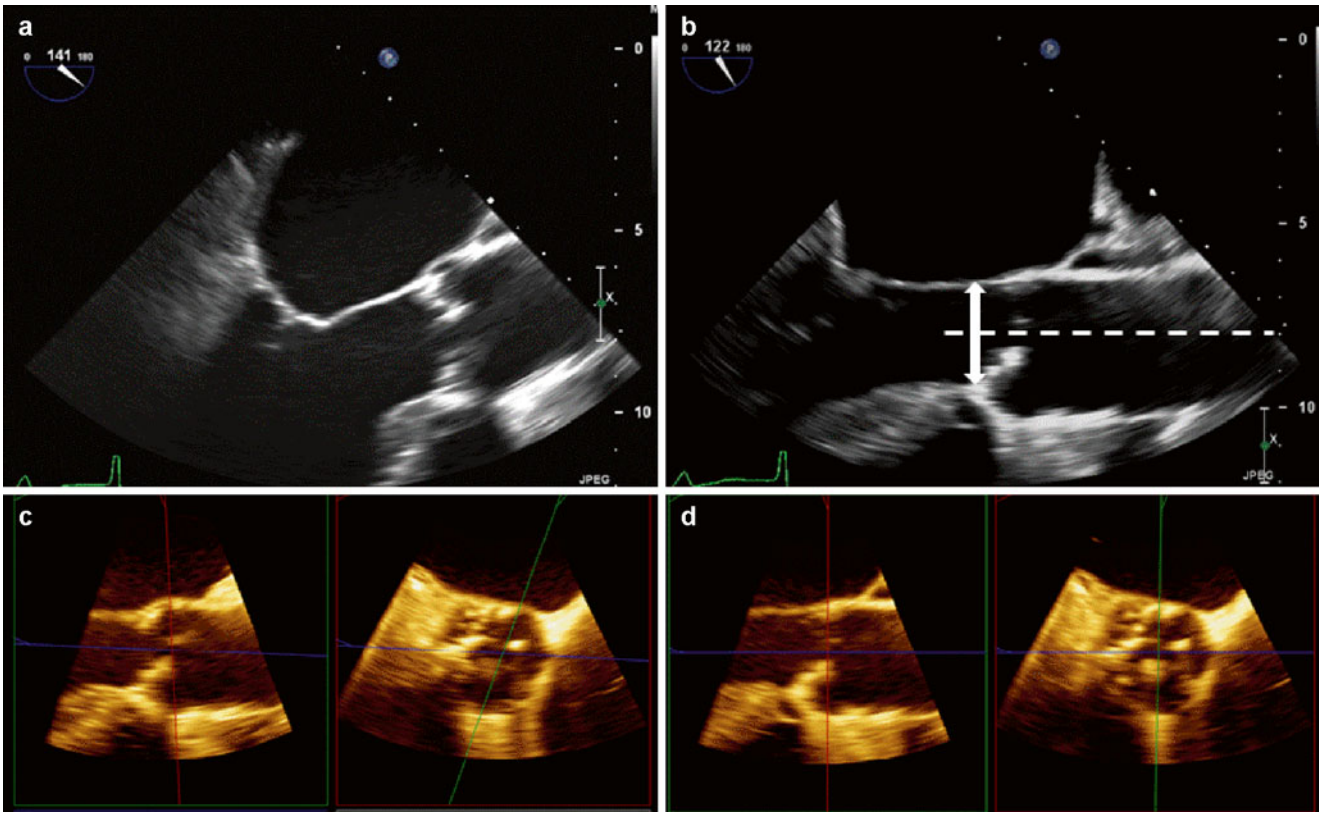

Fig. 6.1 Correct alignment of the long-axis view for measurement of the aortic annulus. In this two-dimensional long-axis view of the aortic annulus, the hinge points of the right and non-coronary aortic cusps are in view (**a**). Using three-dimensional transesophageal echocardiography (3D-TEE), multiplanar reconstruction reveals that this long-axis view of the aortic annulus does not bisect the largest sagittal dimension of the aortic annulus (**c**). In the correct alignment of the long-axis view for measuring the largest annular dimension, the hinge-point of the right coronary aortic cusp is visualized anteriorly and the fibrous interleaflet trigone between the left and non-coronary leaflets is visualized posteriorly (**b**, **d**). The plane of the virtual aortic annulus (*white double arrow*) is measured at the level of the hinge point of the right coronary cusp and perpendicular to the long-axis of the aorta (*white dotted line*)

imaging modality to measure the aortic annulus [15–21]. MSCT can provide reproducible measurements of annular geometry and characterization and quantification of calcium burden. However, this imaging method does have several limitations. Calcium appears approximately four times larger on CT than its actual size (i.e., "blooming artifact") and a high calcium burden diminishes the accuracy of annular measurements made by MSCT. Renal impairment and the need for intravenous contrast is a common issue for MSCT protocols and can be a significant problem for patients being considered for TAVR. Smoothing algorithms are required to avoid overestimation of the perimeter measurement in the short axis view. Gating and motion artifacts, resulting from irregular heart rhythms and respiratory motion during image acquisition, reduce the accuracy of this method. MSCT has inferior temporal resolution as compared to echocardiography. Ensuring that annular measurements are made during the optimal "phase" of the cardiac cycle can be challenging and require correct timing of the contrast bolus and, preferably, regularity of the cardiac cycle lengths. There are typically limited opportunities to obtain the optimal image of the aortic annulus during most MSCT protocols. Finally, exposure to ionizing radiation may become more of an issue as younger patients are considered for TAVR.

Multiple studies have demonstrated that three-dimensional transesophageal echocardiography (3D TEE) can accurately measure the diameters, area, and perimeter of the aortic annulus and that measurements made by 3D TEE are highly reproducible and compare favorably to MSCT [22–29]. Advantages of 3D TEE over MSCT include superior temporal resolution, the avoidance of ionizing radiation and intravenous contrast, and the opportunity to easily acquire three dimensional images of the aortic valve complex over multiple cardiac cycles and from different acoustic imaging planes. Furthermore, aortic valve complex can usually be imaged by matrix array transducers within a real-time three-dimensional volume that is acquired without the need for ECG-gating while MSCT generates a composite image of several cardiac cycles. 3D TEE therefore avoids gating artifacts and the annulus can easily be analyzed in multiple cardiac cycles. There are therefore numerous opportunities to select the optimal imaging window and cardiac cycle(s) for analysis and/or the results can be averaged. Nonetheless, the physics of ultrasound are unchangeable and consequently

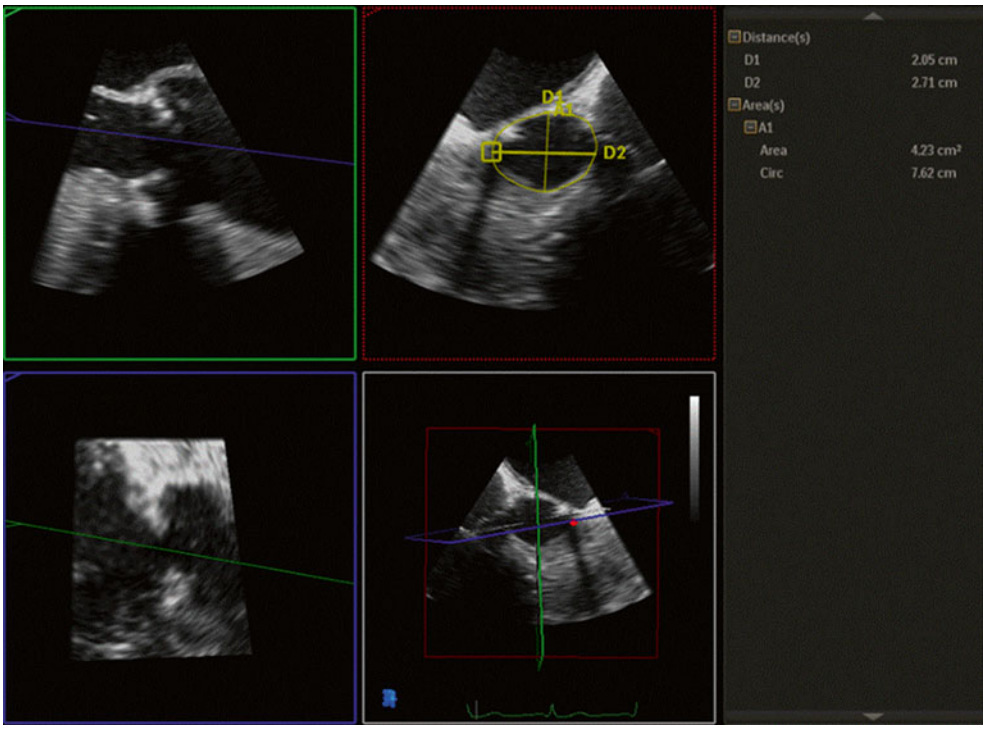

Fig. 6.2 The elliptical shape of the aortic annulus. A short-axis view of the aortic annulus is visualized using multiplanar reconstruction of a three-dimensional volume of the aortic valve complex (*red box*). In this example, the aortic annulus has an oval shape. The coronal dimension (D2) is larger than the sagittal dimension (D1). If the sagittal dimension alone were used, a 23 mm second generation balloon-expandable THV or a 26 mm self-expanding THV would be selected. However, the mean annular diameter (average of D1 and D2), area, and circumference all suggest that a 26 mm balloon-expandable valve or a 29 mm self-expanding valve should be used

3D TEE does have important limitations including acoustic shadowing from calcium, ultrasound artifacts, and lateral resolution that is inferior to that of axial resolution. Optimal assessment of the aortic valve complex for TAVR by either MSCT or 3D TEE requires a high level of expertise and experience. Both modalities are highly accurate for measuring the aortic annulus and characterizing the aortic valve complex. Each modality has inherent advantages and limitations. Rather than exclusively relying upon a single imaging modality, expertise in and integration of information from multiple imaging modalities is likely to yield the best outcomes in decision making regarding TAVR.

A matrix-array TEE transducer is used to acquire 3D volume data sets of the aortic valve complex from which the annulus can be measured. There are some key points to emphasize in acquiring a high-quality data set. First, I recommend using a zoomed or magnified "live" three-dimensional acquisition of the region of interest. The aortic valve complex is sufficiently small that the relevant structures can be fully encompassed within a volume that maintains an acceptable frame rate without the need for gated acquisition, thus avoiding the associated gating artifact. Second, the imaging view should be optimized to minimize acoustic shadowing resulting from calcium. In the standard mid-esophageal long-axis view of the aortic root, calcium along the posterior aspect of the valve complex may cast an acoustic shadow that obscures the anterior aspect of the annulus. By gradually advancing and anteflexing the transesophageal transducer, one can usually obtain an off-angle view of the aortic root complex in which the aortic annulus is no longer in line with the area of acoustic dropout (Fig. 6.3). Lastly, it is advisable to obtain multiple 3D data sets from different views and angulations to maximize the likelihood of optimal visualization of the aortic annulus.

Two different methods for measurement of the aortic annulus from the 3D data set have been described. The most common method utilizes standard multiplanar cropping to align a short-axis (transverse) imaging plane with that of the virtual annular plane, thus allowing one to directly planimeter the annulus and measure the major and minor diameters [30]. Ensuring the plane is appropriately aligned with the hinge-point of all three cusps requires a methodical approach. Increasing the slice thickness can sometimes help to achieve better definition of the annular border. An alternative method for measuring the annulus is indirect planimetry using vendor-specific software that was originally designed for the mitral valve. Validation of this method has been described with no significant differences in area and perimeter measurements compared to MSCT [22]. Both methods achieve highly accurate measurements of

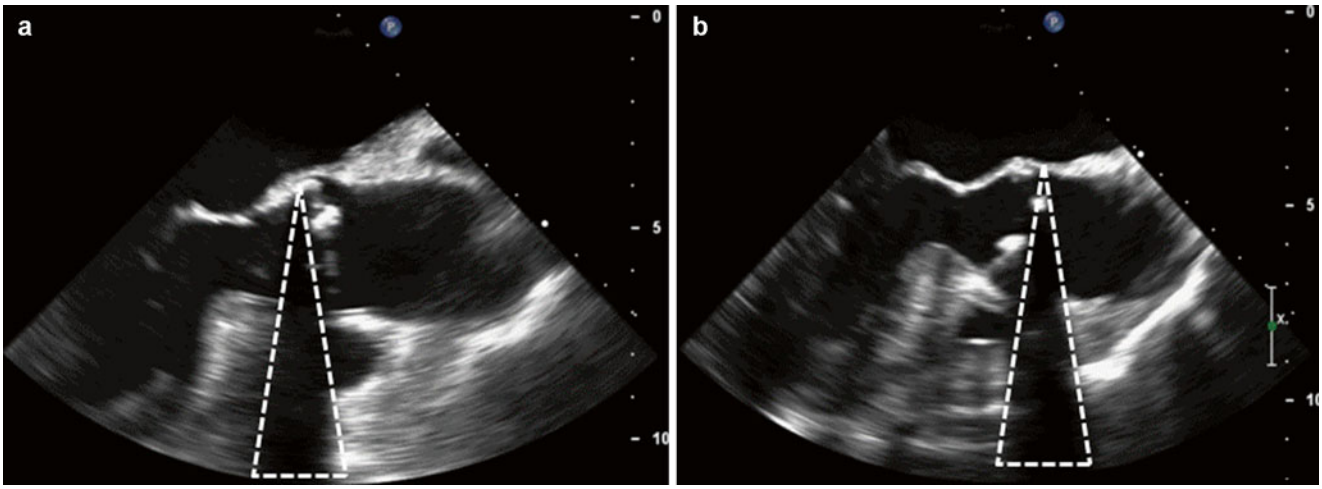

Fig. 6.3 Calcification causing acoustic shadowing. Calcium on the posterior aortic annulus casts an acoustic shadow (*dashed triangle*) that obscures the anterior aspect of the aortic annulus (**a**). By advancing and flexing the transducer, the anterior aspect of the aortic annulus is no longer obscured by the acoustic shadow (**b**)

the aortic annulus, but practice is necessary to develop proficiency with either technique (Fig. 6.4).

Left Ventricular Outflow Tract

The anatomy and features of the left ventricular outflow tract (LVOT) are important to the successful performance of TAVR. Prominent basal septal hypertrophy may increase the difficultly of accurate positioning and implantation of the THV by confounding coaxial alignment of the guidewire and/or THV or by resulting in superior displacement of the THV during deployment. Conversely, a markedly thin membranous septum, particularly with dystrophic calcification, may increase the risk of iatrogenic ventricular septal defect [31] (Fig. 6.5). Calcification within the LVOT is also a predictor of paravalvular aortic regurgitation following TAVR [32–34] and annular rupture [11].

Aortic Valve Anatomy and Morphology

The morphology of the aortic valve, symmetry of valve opening, length of the left coronary leaflet relative to the origin of the left main coronary artery, and extent and distribution of calcium can all impact procedural success. The degree of calcification has been associated with positioning and paravalvular regurgitation [33–35]. Bulky leaflet calcification also increases the risk of ostial coronary occlusion, disruption of the annulus or aortic root, aortic wall hematoma, and aortic dissection [11, 36, 37]. Numerous case reports have raised concerns about complications resulting from THV implantation in bicuspid aortic valves [38–40]. Some retrospective analyses of TAVR in patients with congenitally bicuspid aortic valves have suggested an increased rate of procedural mortality and higher incidence of paravalvular regurgitation as compared to trileaflet aortic valve patients [41].

Aortic Root

Successful deployment of a THV in the aortic position requires a comprehensive evaluation of the aortic root. The diameter of the sinuses of Valsalva, the diameter of the sinotubular junction, and the position of the coronary ostia may influence the size of the THV selected and decisions about position of valve placement. The currently available THV each have sizing recommendations derived from MSCT regarding the diameter of the sinuses of Valsalva and sinotubular junction. These measurements can be readily made with TEE as well. Occlusion of a coronary ostium is an infrequent but potentially catastrophic complication of TAVR. The location of the coronary ostia is of primary importance since having a low-lying coronary artery (<10 mm) is a risk factor for coronary occlusion [13]. 3D TEE allows for rapid and accurate measurement of the distance from the annulus to left main coronary ostium. Comparisons of 3D TEE and MSCT show a high agreement for measurement of the left coronary height above the aortic annulus (Fig. 6.6) [18].

Intraprocedural Echocardiographic Guidance

Ventricular pacing is used to decrease the forward stroke volume and limit cardiac motion during balloon aortic valvuloplasty and THV deployment. As such, a temporary

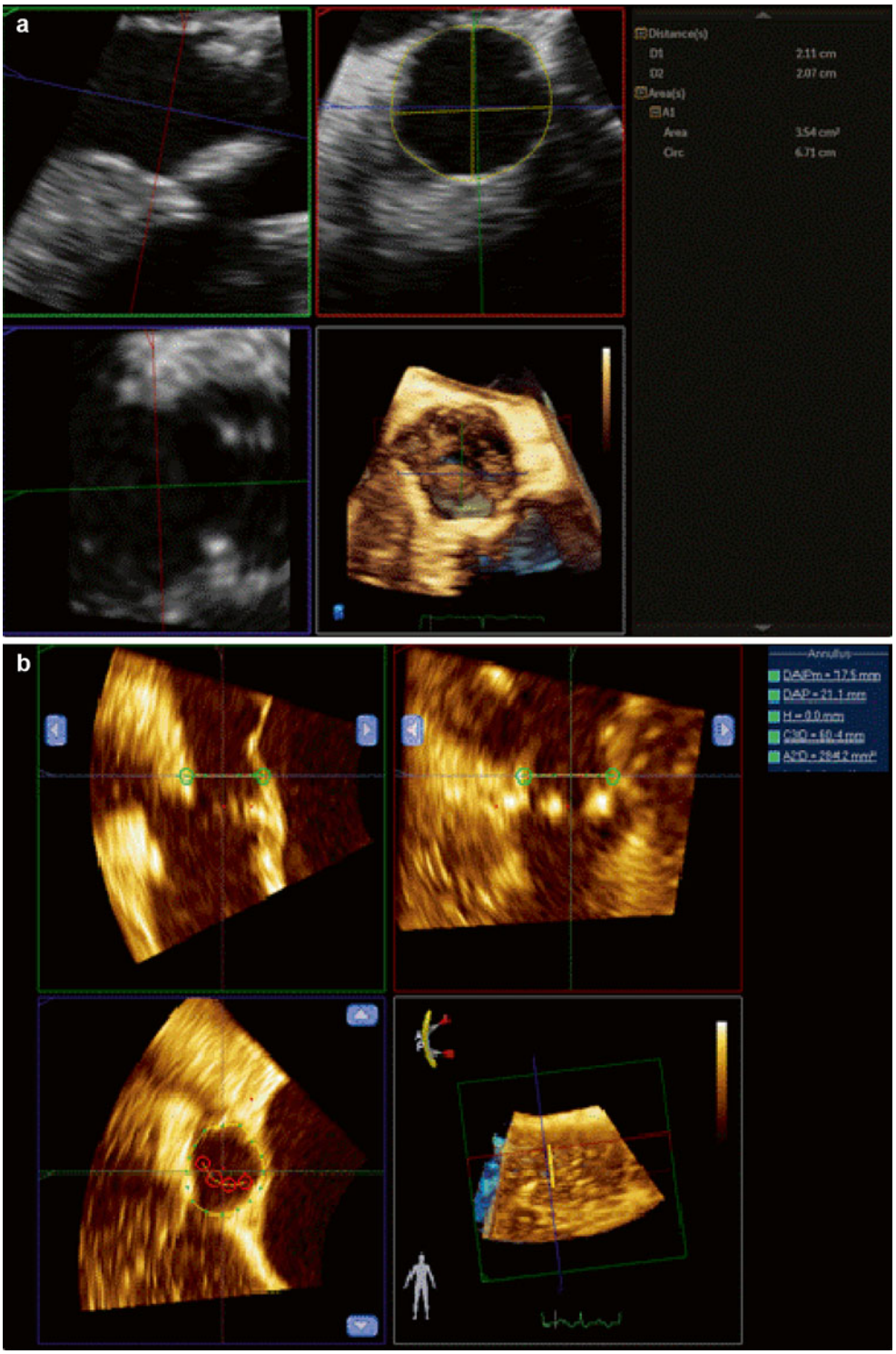

Fig. 6.4 Direct and indirect planimetry of the aortic annulus. Using multiplanar reconstruction of 3-dimensional volumes, a systolic short-axis view of the virtual annular plane (*red box*) is identified using orthogonal long-axis views for alignment. The area and circumference of the aortic annulus can be measured using direct planimerty (**a**). Alternatively, the indirect planimetry method for measuring the short-axis view of the annulus is performed using vendor-specific software and marking points along the aortic annular plane in a sequence of orthogonal long-axis views (**b**)

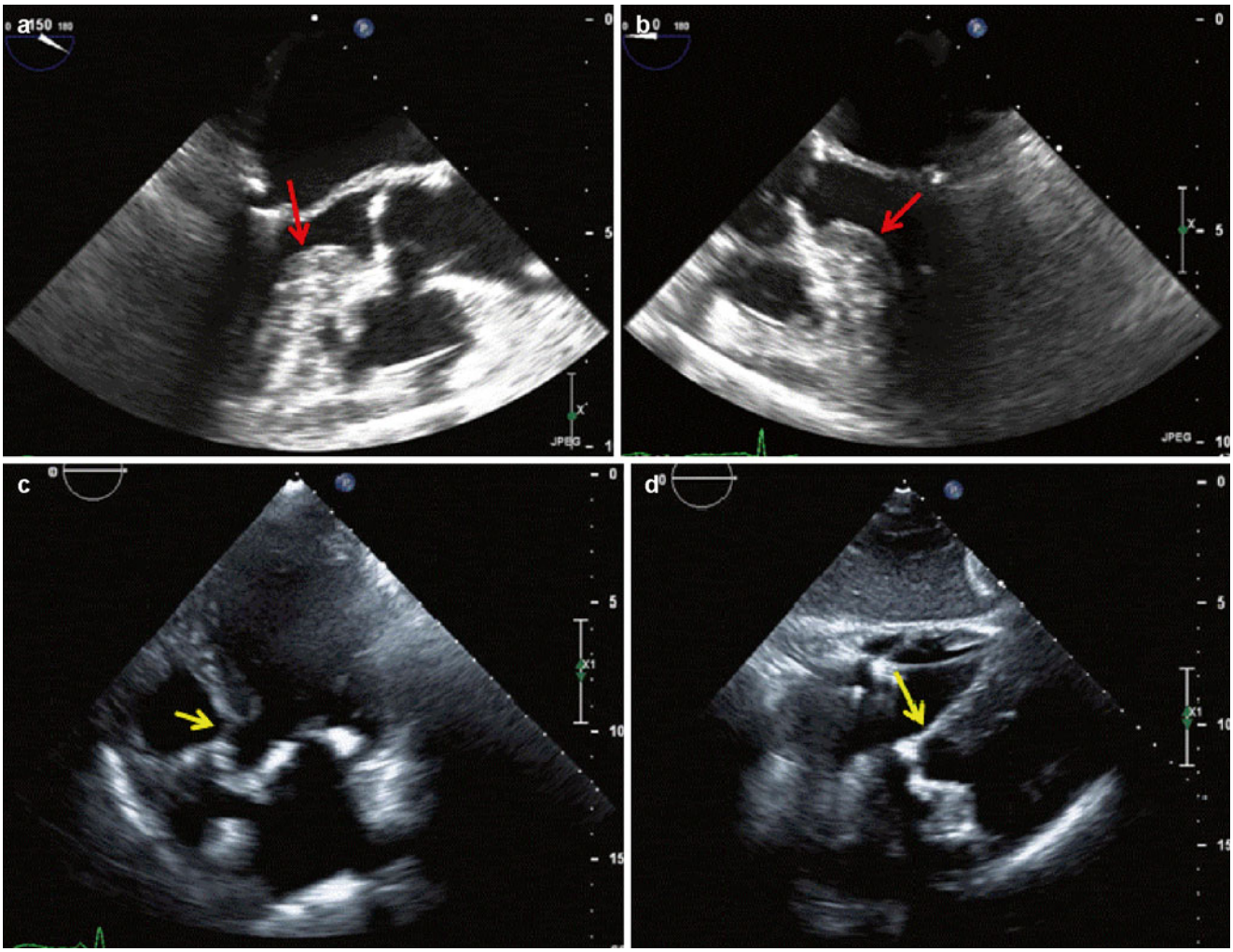

Fig. 6.5 Assessment of the left ventricular outflow tract. Upper septal hypertrophy (*red arrows*) is identified in the four-chamber and long-axis transesophageal views (**a**, **b**). A prominent thin portion of membranous septum is visualized (*yellow arrows*) in the apical (**c**) and subcostal (**d**) transthoracic windows. Particularly when dystrophic calcium is also present, this anatomy may increase the risk for development of an iatrogenic ventricular septal defection after implantation of a transcatheter heart valve

pacing wire is placed within the right ventricle at the outset of the procedure. Occasionally the position of the pacing wire must be confirmed with TEE. Following any wire placement into the heart, perforation and accumulation of a pericardial effusion should be excluded. A pigtail catheter in the aortic root and aortography are typically used throughout the procedure to assist in alignment and positioning of the THV. Placement of the pigtail catheter is usually within the right coronary cusp for deployment of a balloon-expandable THV, whereas the pigtail catheter is placed in the non-coronary cusp is during implantation of a self-expanding valve. Determining the position of the pigtail catheter within the aortic root is easily and quickly done with TEE (Fig. 6.7). Confirming the correct pigtail position with TEE rather than aortography can reduce the amount of contrast used during the procedure, which is of particular benefit for patients with renal insufficiency.

Most TAVR procedures require the aortic valve to be crossed retrograde with a stiff wire. The position of the wire within the left ventricle is easily visualized and assessed by echocardiography. Entanglement of the wire within the mitral apparatus may affect the stability or position of the balloon or THV and may cause mitral regurgitation. Both 2D and 3D imaging can be useful and provide complimentary information in assessing wire and/or catheter position in the left ventricle (Fig. 6.8). The transapical approach for TAVR requires additional imaging. Imaging of the left ventricular apex can ensure optimal location of the apical puncture site. A cannulation site in the anterior apex allows for appropriate alignment of the THV and avoids the mitral apparatus. Echocardiographic imaging of the apex while the cardiac surgeon externally pushes on the left ventricle at the proposed cannulation site is useful in ensuring the entry site is optimal. Continuous echocardiographic imaging during

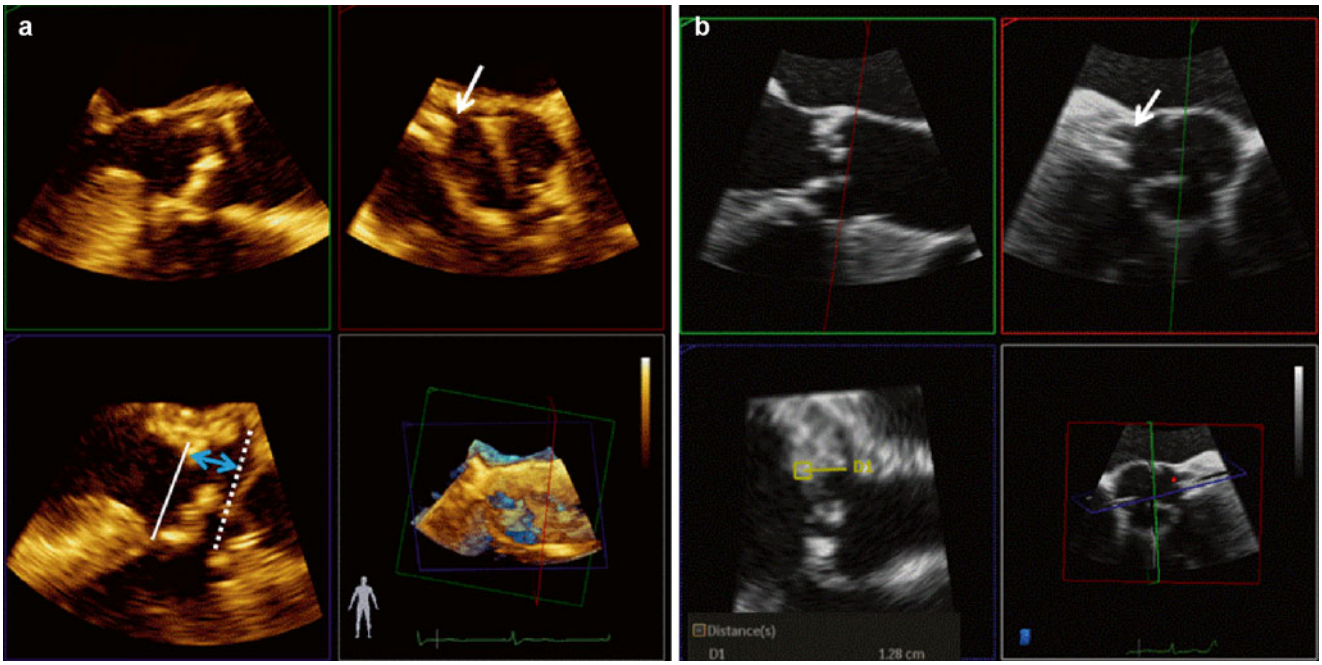

Fig. 6.6 Measurement of the left main coronary height. Measurement of the distance from aortic annulus to the ostium of the left coronary artery is shown using multiplanar reconstruction of a three-dimensional TEE volume. The left main is identified in the short axis view (**a** and **b**, *white arrows*). In the orthogonal long-axis view, the level of the annulus (**a**, *white solid line*) and level of the left main coronary artery (**a**, *white dotted line*) are displayed and the distance between them is measured (**a**, *blue double arrow*)

needle insertion, advancement of the guidewire, and insertion of the apical delivery sheath should be performed to ensure appropriate positioning and exclude interference with the mitral apparatus (Fig. 6.9).

Balloon aortic valvuloplasty (BAV) is often performed before implantation of the THV to increase cusp excursion, ensure an adequate cardiac output during the procedure, and make crossing the native aortic valve with and positioning of the unexpanded THV less difficult. Echocardiographic imaging during and following BAV is important to assess the functional results of the dilation and assess for possible complications. Imaging during the BAV is done with either the mid-esophageal long-axis view alone or, preferably, using simultaneous multiplane imaging to visual both the long-axis and short-axis views of the aortic valve (Fig. 6.10). During BAV and the portion of THV deployment that is performed with rapid pacing, it is useful to set the loop acquisition to time capture rather than number of beats. I recommend a 10 s loop to acquire the entire inflation and deflation of the balloon. Imaging during BAV can provide additional useful information regarding confirmation of annular sizing and prediction of calcium displacement and the likelihood of coronary obstruction by a calcified left coronary cusp during THV deployment [30, 42, 43]. Echocardiographic imaging following BAV is useful to detect complications, such as tamponade, severe aortic regurgitation, or aortic root disruption.

Balloon-Expandable Transcatheter Heart Valves

Three generations of balloon-expandable transcatheter heart valves SAPIEN, SAPIEN XT, and SAPIEN 3 (Edwards Lifesciences, Irvine, California) have been used in clinical trials and received FDA approval for the treatment of aortic stenosis. The newest of these valves, SAPIEN 3, has a cobalt chromium stent frame with wide strut angles and a polyethylene terephthalate skirt that extend around the outside of the lower row of cells to minimize paravalvular regurgitation [44, 45]. The prosthetic leaflets are constructed from treated bovine pericardium.

Precise positioning of a balloon expandable THV prior to deployment is critically important. Fluoroscopy remains the primary modality for positioning [35]. When used correctly, however, TEE can be an extremely useful adjunctive imaging modality to guide THV positioning and may improve the likelihood of correct positioning and/or reduce the amount of contrast that is required. The crimped stent of the THV can almost always be well differentiated from the balloon, which is less acoustically dense (Fig. 6.11). Reducing the overall gain may be useful in this differentiation. The ideal pre-deployment position depends on several factors. First, the motion of the valve during deployment and valve shortening characteristics depend on the generation of THV and delivery system. With the first generation of balloon-expandable

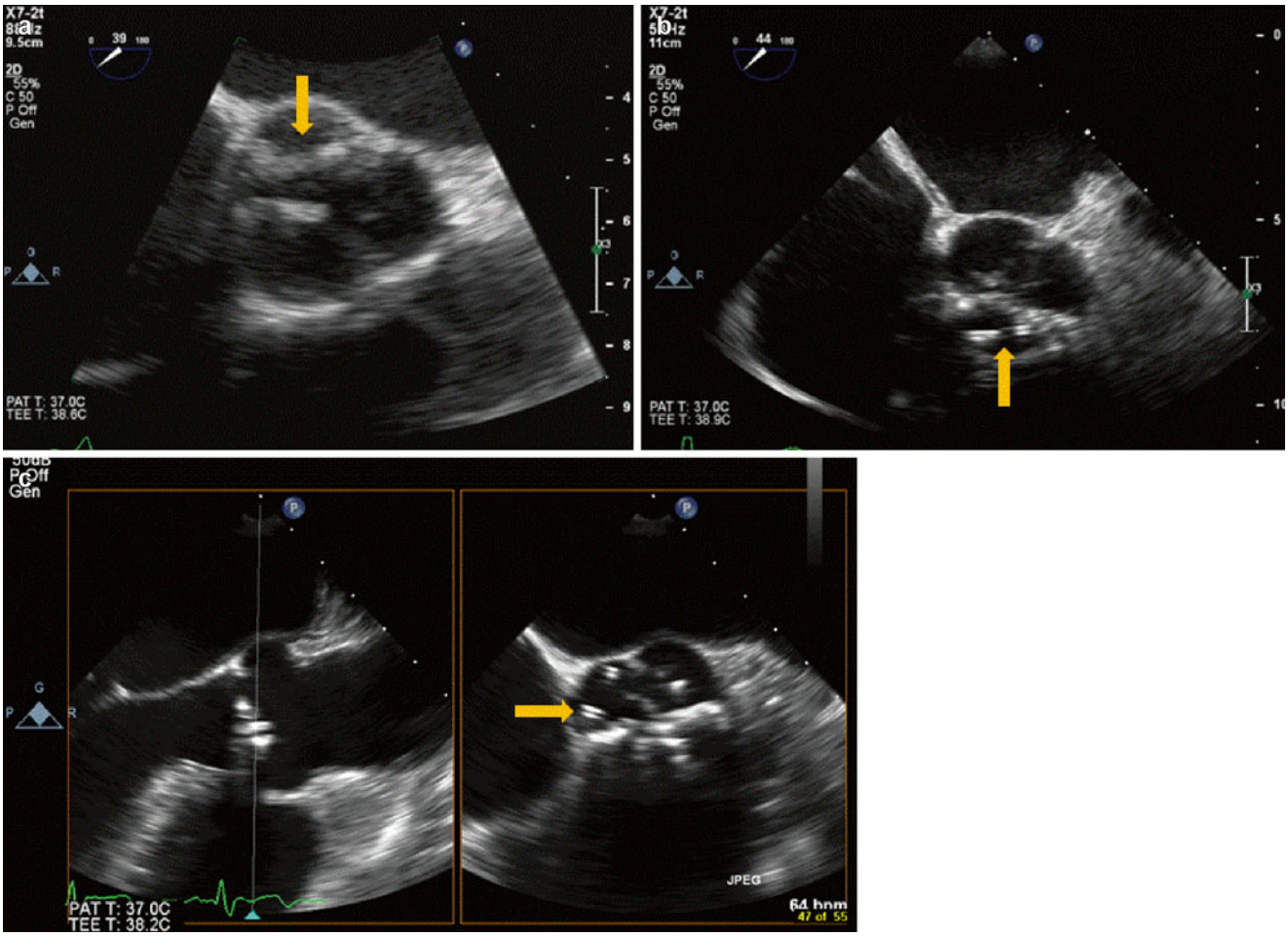

Fig. 6.7 Pigtail catheter in the aortic root. Short-axis view of the aortic valve demonstrating a pigtail catheter (*arrows*) in the non-coronary aortic cusp (**a**). Short-axis view of the aortic valve demonstrating a pigtail catheter in the right-coronary aortic cusp (**b**). A pigtail catheter in the non-coronary cusp is shown using simultaneous biplane imaging prior to implantation of a self-expanding transcatheter heart valve (**c**)

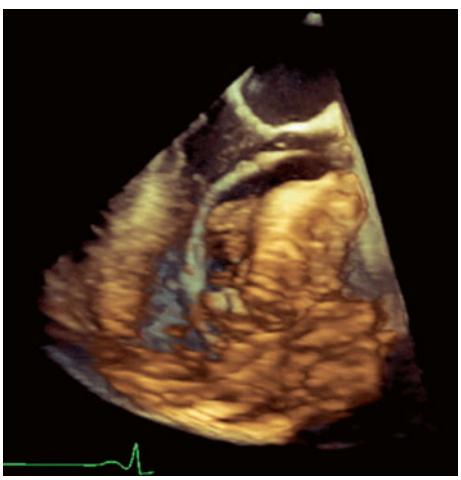

Fig. 6.8 Pigtail catheter within the left ventricle. In this live three-dimensional TEE image, a pigtail catheter is shown within the left ventricle. The catheter appears well positioned and does not interfere with the mitral apparatus

THV and earliest delivery systems, there was frequently upward (aortic) movement of the entire valve during balloon inflation. With the currently available third generation balloon-expandable THV, there is far greater stability during deployment. The crimped valve is longer than the fully expanded valve and, thus, there is valve shortening during balloon inflation and expansion of the stent. With all three generations of balloon-expandable THVs, there is asymmetric motion of the valve during deployment with greater motion of the inflow (ventricular) edge of the stent [35]. In other words, valve shortening occurs predominantly from the ventricular side. This asymmetric shortening is most extreme with the third generation of balloon-expandable THV in which the outflow or aortic edge of the stent barely moves during deployment while nearly the entire valve shortening during inflation occurs from the ventricular side. Understanding the normal shortening characteristics of the THV and the ideal final position of the prosthesis is essential in determining the correct pre-deployment position of the

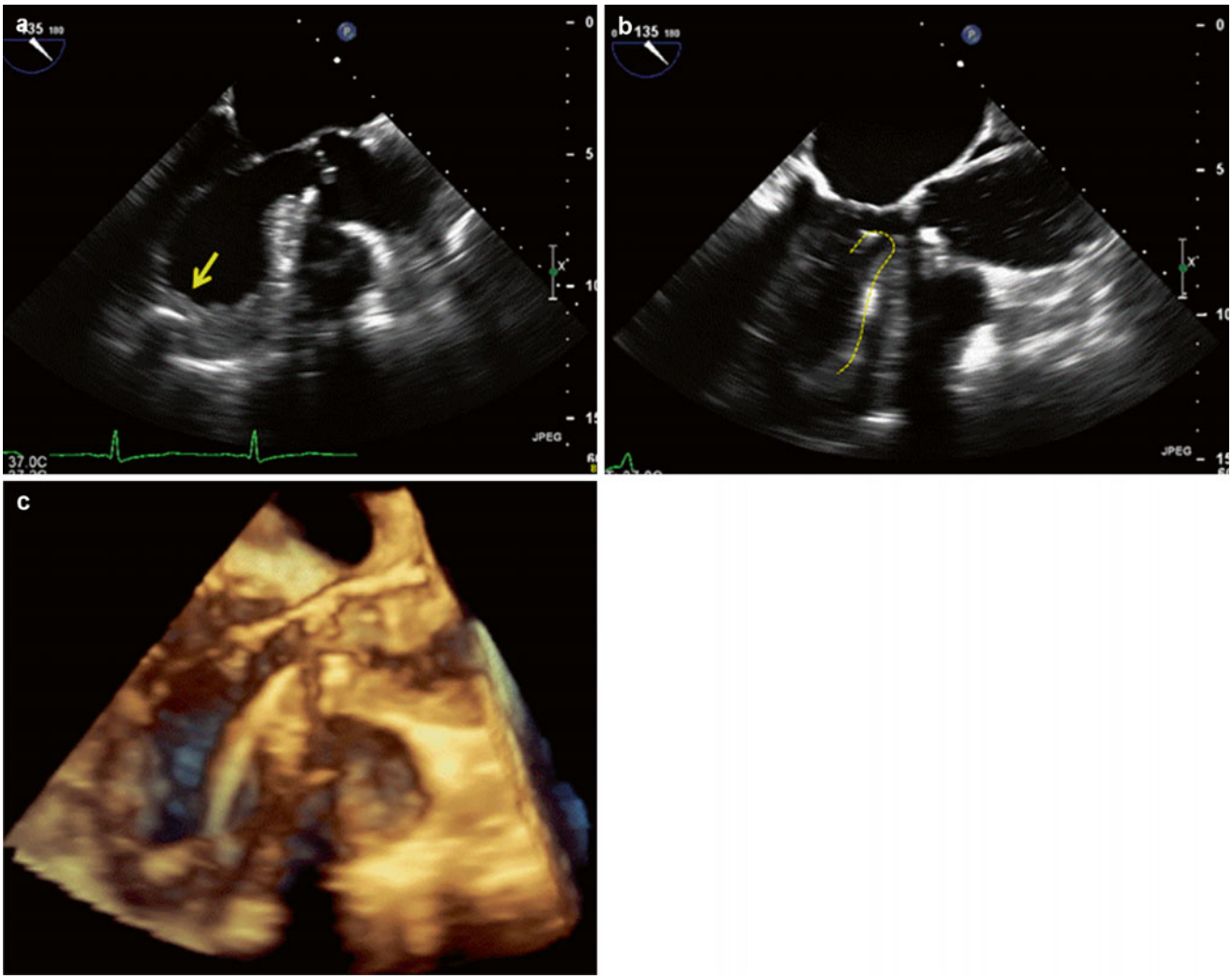

Fig. 6.9 Imaging of the transapical approach for TAVR. In this view, the optimal position for apical cannulation is identified by visualizing the finger of the surgeon palpating the apex of the left ventricle at the intended puncture site (*yellow arrow*, **a**). The J wire (identified by the *yellow dotted line*) is visualized within the left ventricle as the surgeon advances it to cross the aortic valve (**b**). This three dimensional view shows the course of the wire within the left ventricle from the apical cannulation site to crossing the aortic valve and demonstrating that the wire is free from the mitral apparatus (**c**)

stent. With the third generation of balloon-expandable THV, the majority (roughly three-fourths) of the stent is on the aortic side of the annulus when in the ideal final position. Because shortening occurs almost exclusively from the ventricular side, the ideal pre-deployment position is with approximately equal portions of the crimped stent on the ventricular and aortic sides of the annulus (the so called "50/50" position). Pre-deployment positioning of the crimped stent should primarily focus on the aortic edge, since this edge of the stent remains essentially stable during deployment. The stent should cover the native aortic leaflets but remain below the sinotubular junction (Fig. 6.12).

Prior to deployment, the crimped THV is frequently not in the center point of the annulus in all planes. The stent will therefore not contact the annulus on all sides simultaneously. It is important to anticipate the location of first annular contact as this often impacts the final position of the THV. Furthermore, the THV is rarely precisely perpendicular to the plane of the aortic annulus. The final position of the stent may be asymmetric relative to the aortic annulus, in which the distance from the annulus to the inflow and outflow edges of the stent differ along the circumference of the stent. In other words, the stent may be slightly canted relative to the plane of the annulus. Accounting for the angle of the stent relative to the plane of the annulus can also be useful in determining the optimal pre-deployment position of the THV (Fig. 6.13). I would emphasize that developing proficiency at positioning by TEE requires practice.

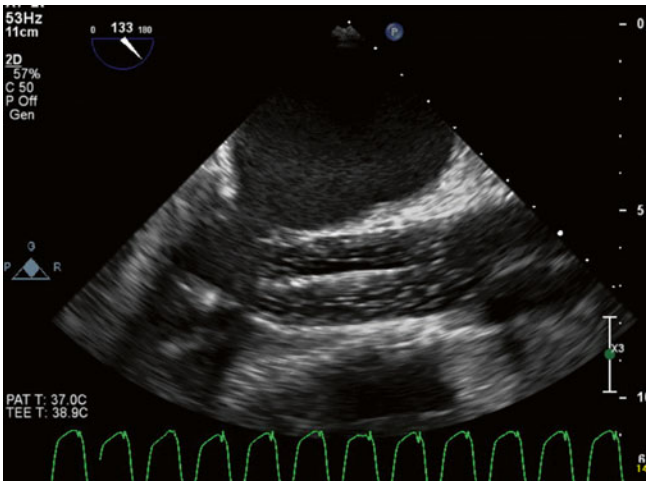

Fig. 6.10 Balloon-aortic valvuloplasty. In this long-axis view, the inflated balloon is visualized during balloon aortic valvulplasty. The size of the inflated balloon relative to the aortic annulus can be useful in selecting the appropriate size of transcatheter heart valve under some circumstances

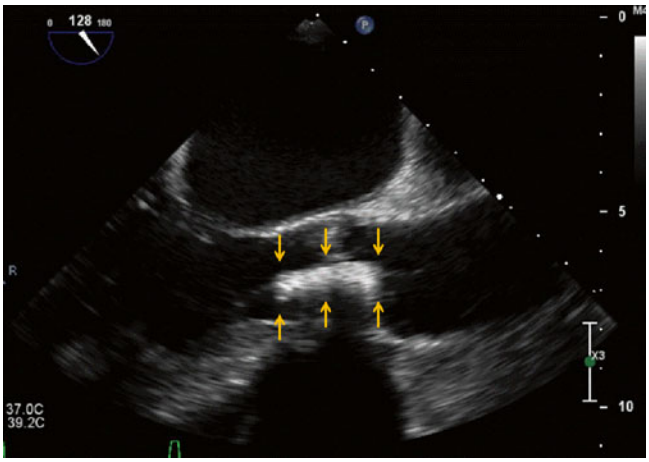

Fig. 6.11 Crimped transcatheter heart valve. In this long-axis view, reducing the overall gain allows for the crimped stent (*arrows*) of the balloon-expandable THV to be well differentiated from the less acoustically dense balloon

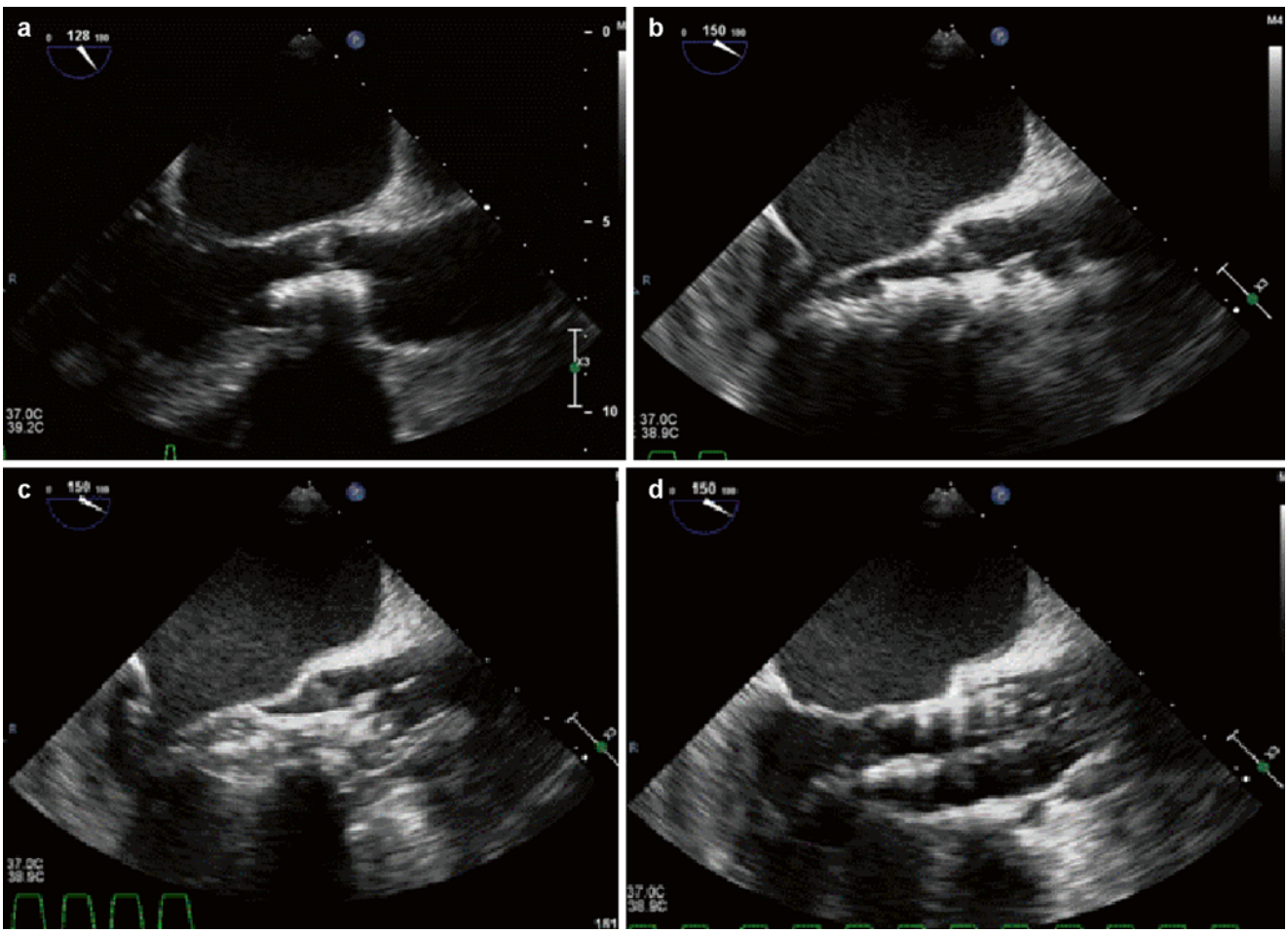

Fig. 6.12 Deployment of a balloon-expandable THV. The crimped stent is visualized prior to balloon inflation (**a**). Early, mid, and full inflation of the balloon and stent during deployment of the THV are shown (**b–d**). This long axis view shows the final position of the THV following deflation and removal of the deployment balloon (**e**)

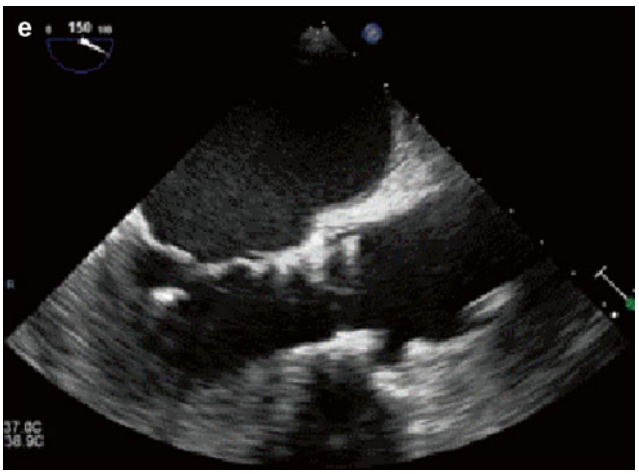

Fig. 6.12 (continued)

Self-Expanding Transcatheter Heart Valves

Two generations of self-expanding transcatheter heart valves, CoreValve Revalving System and EVOLUT-R (Medtronic, Minneapolis, Minnesota), have received FDA approval. Both of these are porcine pericardial valves mounted within a nitinol frame with a fabric skirt affixed to the inside of the stent. The stent frame has three distinct zones, each with different radial and hoop strengths, in order to allow proper orientation, anchoring, and placement of the valve. These self-expanding transcatheter valves are partially repositionable.

Fluoroscopy is the primary modality for positioning and deployment of a self-expanding THV. The use of TEE imaging as an adjunct to fluoroscopy is reasonable, may aid in improving procedural results, and provide a more rapid diagnosis of complications [46]. Deployment of the

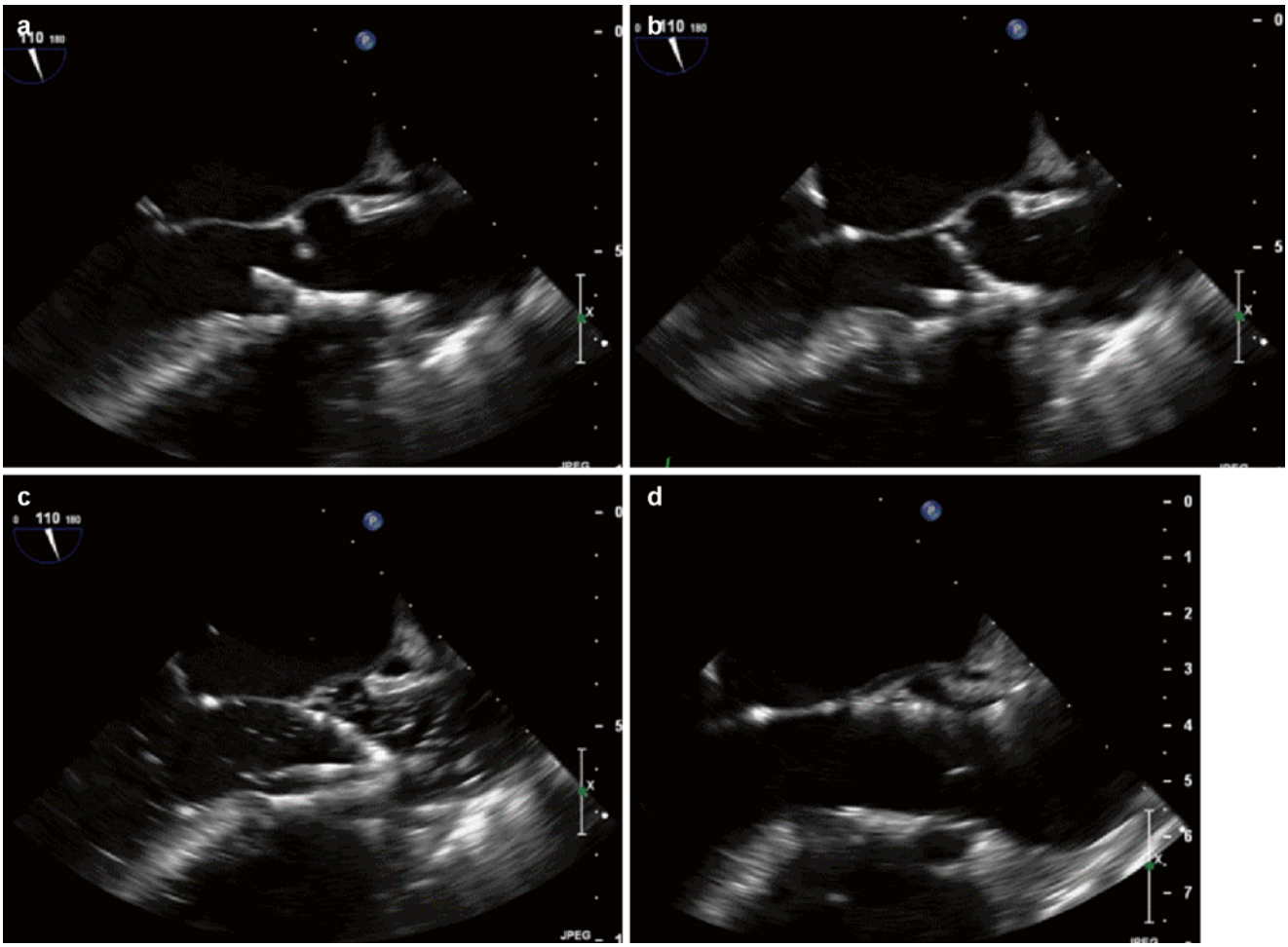

Fig. 6.13 Deployment of a self-expanding THV. As the THV is unsheathed, the distal portion of the stent begins to "flower" open (**a**) and then expands to make annular contact (**b**). The prosthetic valve begins to function when approximately two-thirds of the stent is unsheathed (**c**). In this image, the final position of the THV after being completely unsheathed is shown (**d**)

self-expanding THV is much slower and more controlled than that of a balloon-expandable valve. The sheathed self-expanding valves are typically not coaxial with the aorta prior to deployment. As the valve is deployed, the valve will begin to reorient to become more parallel with the long axis of the aorta by pivoting on the first point (usually the posterior edge) of annular contact. It is difficult to discern the exact starting position of the fully sheathed self-expanding valve by TEE, but relatively simple to determine the position of the valve once the inflow edge is unsheathed and the stent begins to "flower" open. The ideal final position is with the inflow (ventricular) edge of the stent approximately 4 mm below the annular plane for the first generation of self-expanding THV and approximately 3 mm below the annular plane for the second generation self-expanding valve. The imaging planes on TEE and fluoroscopy are very different. With experience, integrating the information from both modalities may allow for optimal positioning with less contrast required.

Post-Deployment Assessment

Following THV deployment, echocardiography provides rapid and accurate assessment of valve position and function.

Assessing Transcatheter Valve Function

Echocardiographic imaging can rapidly assess the final THV position, stent shape, and leaflet motion. Stent position is best determined in the long-axis view. Color Doppler is used to determine the presence and severity of valvular and paravlavular regurgitation. Multiple short-axis views and multiplane imaging are required to fully assess final stent shape and the presence, severity, and location of valvular and paravalvular regurgitation [9, 47]. Continuous and pulsed wave Doppler from the deep gastric views are used to determine transvalvular gradients and for calculation of the effective orifice area of the prosthesis by the continuity equation. Color and continuous wave Doppler of the aortic prosthesis from the deep gastric view can also provide additive information regarding the severity of aortic regurgitation (Figs. 6.14 and 6.15).

Paravalvular Regurgitation

The presence of significant paravalvular regurgitation following TAVR has been associated with increased mortality [12, 48–55]. Through advancements in transcatheter valve technology and improvements in the use of 3D imaging for sizing, the incidence of significant paravalvular regurgitation is lower with the current generation of valves [44, 45]. Nonetheless, detecting the presence, location, and determining the severity of paravalvular regurgitation remains key following THV deployment. Color Doppler imaging from both the long-axis and short-axis views should be performed immediately following THV deployment. The current generation of balloon-expandable transcatheter valve is constructed with a skirt on the inflow edge of the stent, and positioned on the ventricular side of the annulus, to reduce paravalvular regurgitation. When imaging in the short-axis view above the annulus, flow between the outer aspect of the stent and the aortic root or annulus that is caught by the skirt and does not enter the left ventricle can be visualized and potentially mistaken for paravalvular regurgitation that requires further treatment. It is therefore important to visualize the LVOT immediately adjacent to the stent to confirm that jets enter the left ventricle. Some paravalvular regurgitant jets, particularly those located anteriorly, can be acoustically shadowed in the mid-esophageal view and may be better visualized in the deep gastric view (Fig. 6.16).

Repeated assessment of paravalvular regurgitation should be done for several minutes following valve deployment. In some instances, there is hypotension immediately following the rapid pacing period of valve deployment and color Doppler interrogation during that time may underestimate the degree of regurgitation. As the blood pressure recovers, the degree of regurgitation may become more evident. Echocardiographers should take note of the hemodynamic condition of the patient during imaging. Conversely, small leaks may spontaneously resolve or the degree of paravalvular regurgitation may decrease over 10–15 min following valve deployment [56]. Self-expanding valves continue to expand as the nitinol warms up to body temperature and, consequently, many small paravalvular regurgitant jets regress.

Integration of multiple parameters and imaging obtained from multiple windows is critical in assessing paravalvular regurgitation. Still, determining the severity of paravalvular regurgitation quantitatively remains challenging. As the experience with TAVR continues to grow, it is likely that additional investigations will lead to refined methods of assessing paravalvular regurgitation. It is important to determine not only the severity, but the mechanism of paravalvular regurgitation. Final stent position, undersizing of the THV relative to the native aortic annulus, or bulky calcification may all contribute to paravalvular regurgitation following THV deployment [12]. Defining the mechanism may

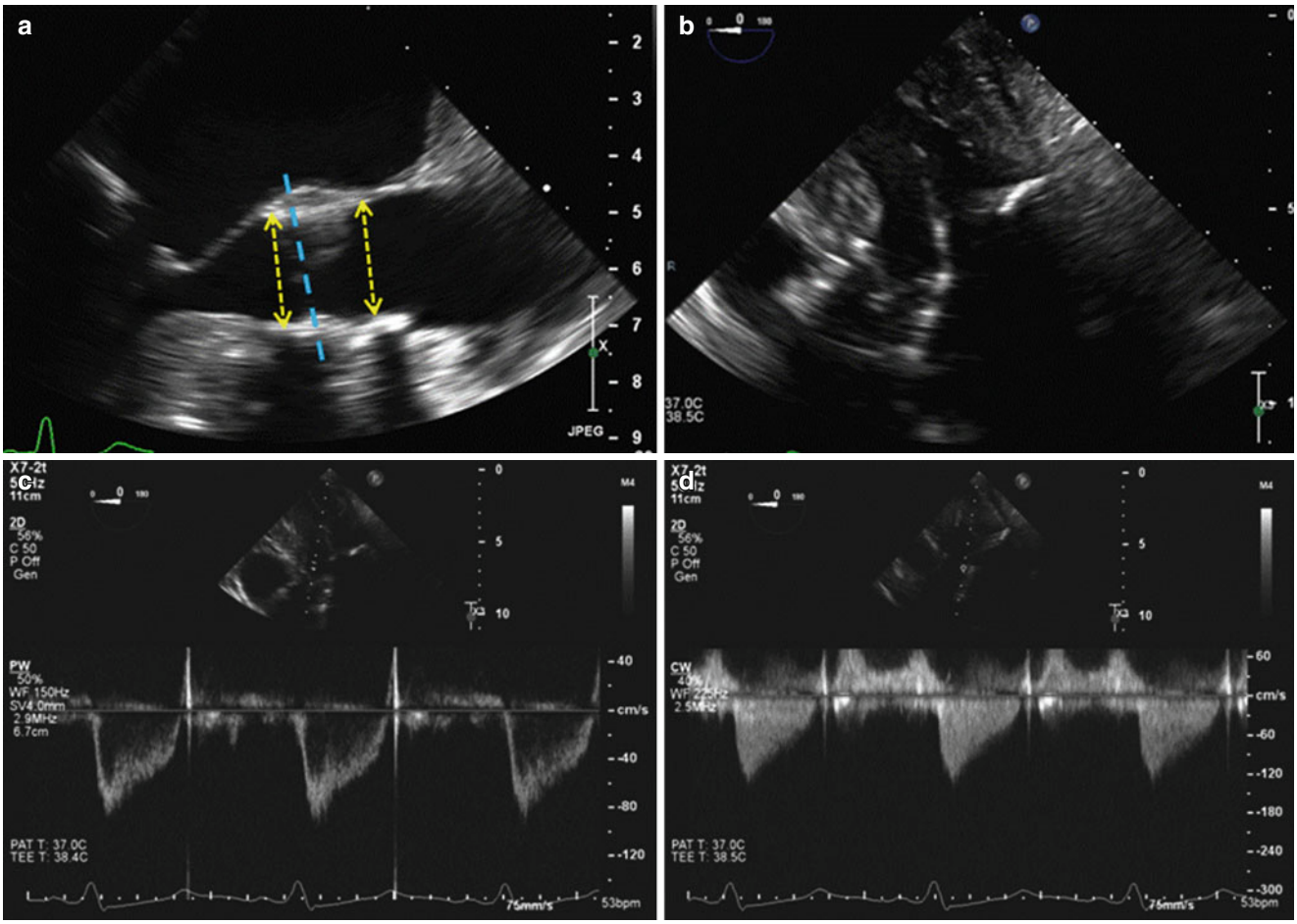

Fig. 6.14 Assessment of transcatheter heart valve position and function post-deployment. The position of the THV (*yellow double arrows*) relative to the plane of the native aortic annulus (*blue dashed line*) is visualized in the long axis view (**a**). The valve is visualized in the deep gastric view (**b**), which allows alignment for pulse-wave Doppler of the LVOT (**c**) and continuous wave Doppler across the valve (**d**) to be obtained for determining the trans valvular gradient and calculation of effective orifice area

influence procedural decision-making about the need for post-dilation, implantation of a second valve, or continued surveillance.

Complications

Perhaps the most critical role of echocardiography in TAVR is for the immediate detection and assessment of complications during the procedure. There are numerous potential mechanical complications that may occur with TAVR. Some of the major mechanical complications with illustrative case examples will be highlighted in this chapter. Additionally, echocardiography can provide valuable information during hemodynamic compromise beyond that of identification of mechanical complications. For example, TEE imaging can be used to assess underfilling of the left ventricle during major vascular bleeding or to confirm the position of the venous cannula in the right heart in a patient being emergently placed on cardiopulmonary bypass. The echocardiographer should be knowledgeable about, continuously monitor, and communicate the relevant information of specific interest to the anesthesiologist, interventional cardiologist, and cardiac surgeon during a complication.

Aortic Complications

Aortic dissection may occur as the result of direct trauma from the balloon, wires, catheters, or valve itself. Conversely, it may the consequence of displacement of jagged-edge, bulky calcium during the procedure. Aortic dissection may be immediately apparent or may become evident over time (Fig. 6.17). The extent of the dissection and potential involvement of the sinuses of Valsalva, coronary arteries, or head and neck vessels are critical for determining the best course of action. Microperforations of the intima and portion of the media can result in intramural

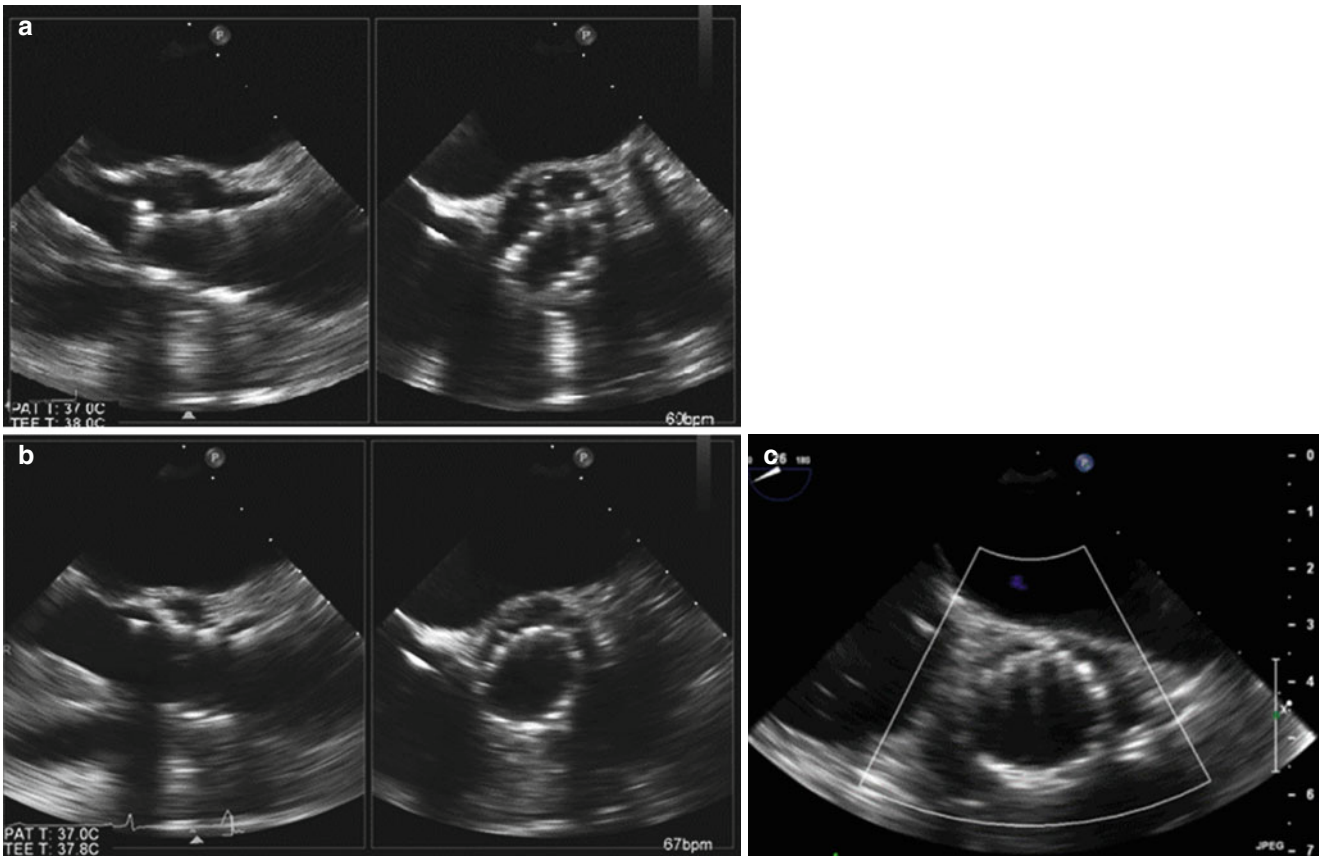

Fig. 6.15 Assessment of stent shape following implantation. In this example, expansion of a self-expanding THV is impeded by bulky calcium resulting in an oval shape of the stent and a large gap between the stent and native aortic annulus (**a**). Following balloon post-dilation, there is improvement in stent expansion and the shape of the stent is more circular (**b**). However, a gap remains between the stent and native annulus. Following a second post-dilation with a larger balloon, the stent is now fully expanded and circular in shape (**c**)

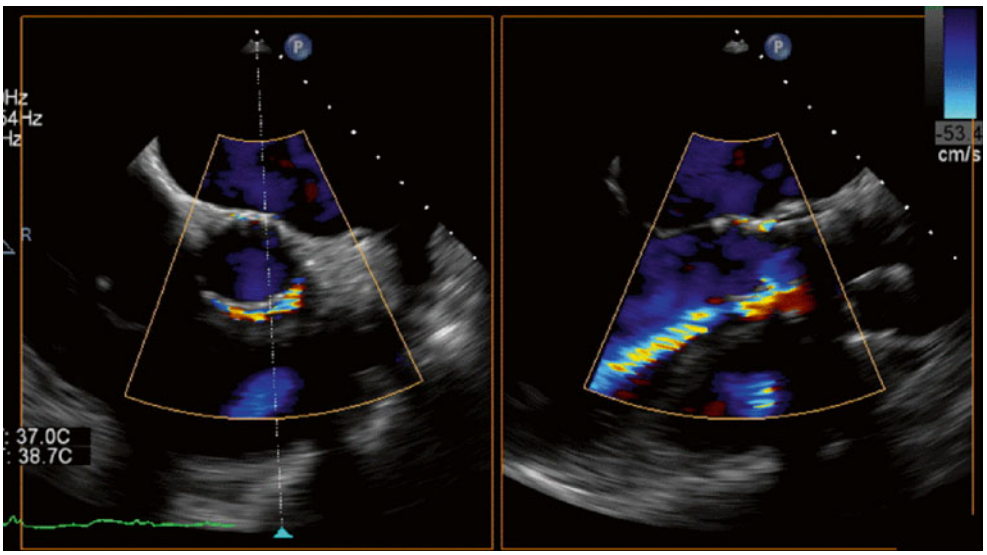

Fig. 6.16 Paravalvular regurgitation following TAVR. Simultaneous biplane imaging demonstrates severe paravalvular regurgitation after implantation of a self-expanding transcatheter heart valve. The full extent of the paravalvular leak is nearly 50 % of the circumference of the prosthetic valve (*short-axis view*, *left panel*). There is a visible gap between the stent and the anterior aspect of the native aortic annulus though which there is severe paravlavular regurgitation (*long-axis view*, *right panel*). A smaller paravalvular leak is visualized at the posterior aspect of the annulus

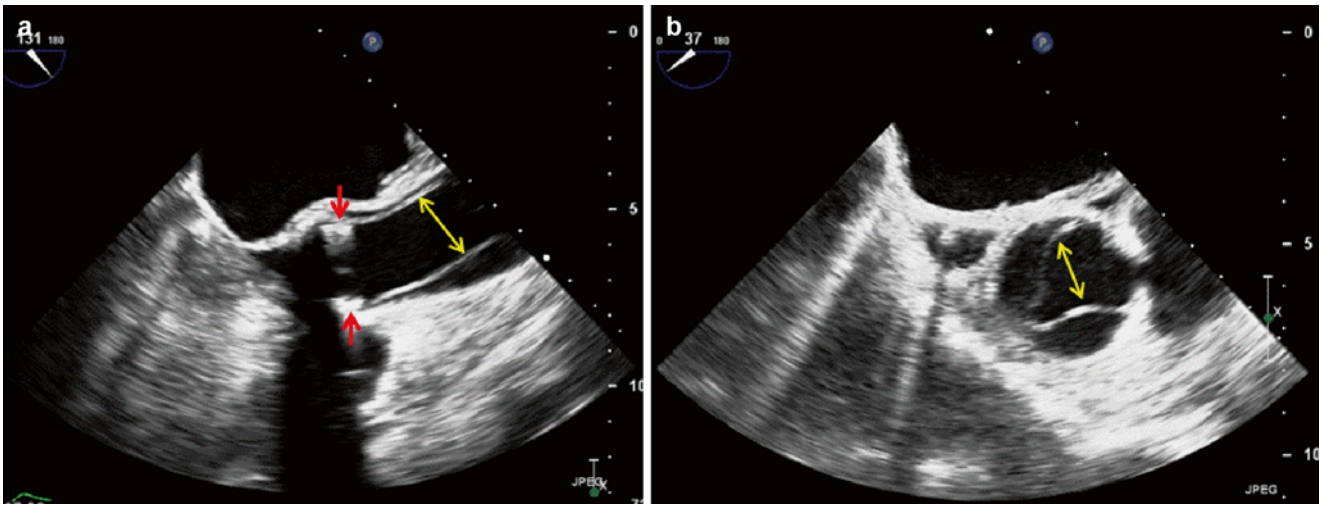

Fig. 6.17 Aortic dissection following TAVR. In the long-axis view, the outflow edge of the stent is marked by the red arrows (**a**). The flap of a spiral dissection of the ascending aorta is visualized in the long (**a**) and short (**b**) axis views (*yellow double arrows*)

hematomas while perforation through all three layers of the aortic wall can cause periaortic hematoma [36]. If recognized early, these conditions can sometimes be managed conservatively. In some instances, however, hematomas can compromise a coronary artery or progress to a more significant mechanical complication (Fig. 6.18). Annular rupture is a rare, but catastrophic, complication of TAVR. More extensive subannular calcification, oversizing of the prosthesis by more than 20 % of the annular area, and balloon post-dilation have all been implicated as risk factors for annular rupture (Fig. 6.19) [11].

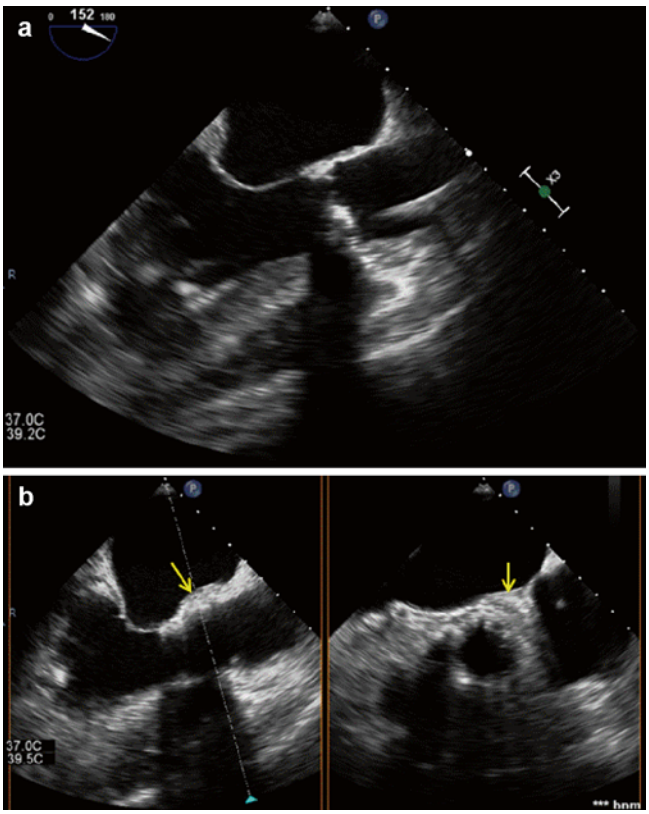

Fig. 6.18 Intramural hematoma following TAVR. Prior to valve implantation, the wall of the aortic root appears thin and normal (**a**). Following implantation of a balloon-expandable transcatheter heart valve, simultaneous biplane imaging reveals the development of an intramural hematoma of the wall of the non-coronary sinus of Valsalva (**b**)

Coronary Artery Obstruction

Obstruction of the ostium of a coronary artery is primarily related to displacement of a calcified native aortic valve leaflet following THV deployment (Fig. 6.20). Coronary occlusion with TAVR is thankfully rare with an overall incidence of <1 % [13]. When coronary obstruction occurs, it is most common with the left main coronary artery (83.3 % of cases) and can frequently be successfully treated with percutaneous coronary intervention. The identified and suggested risk factors for coronary obstruction include female sex, no prior bypass surgery, a narrow aortic root with shallow sinuses of Valsalva, low-lying (<10 mm) coronary height, and bulky calcification of the native left coronary aortic valve leaflet.

Aortic Regurgitation

Significant aortic regurgitation following TAVR may be valvular or paravalvular and distinguishing between these is crucial for deciding the appropriate treatment. Valvular aortic regurgitation may be seen immediate following deployment as a consequence of the stiff wire impeding closure of a prosthetic leaflet. Repositioning or removal of the wire alleviates this situation. Valvular regurgitation that

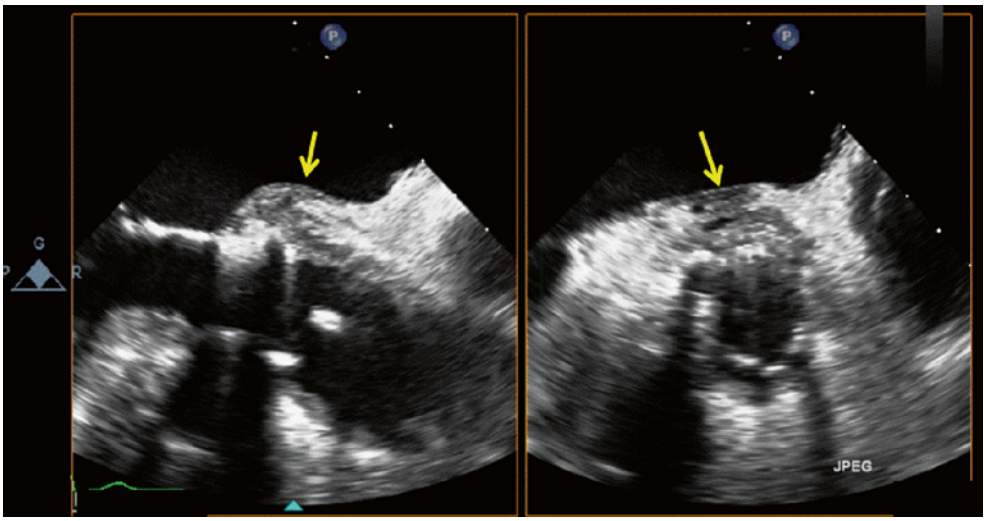

Fig. 6.19 Aortic root rupture following TAVR. Simultaneous biplane imaging demonstrates a periaortic hematoma (*yellow arrows*), resulting from aortic root rupture, following implantation of a balloon expandable valve

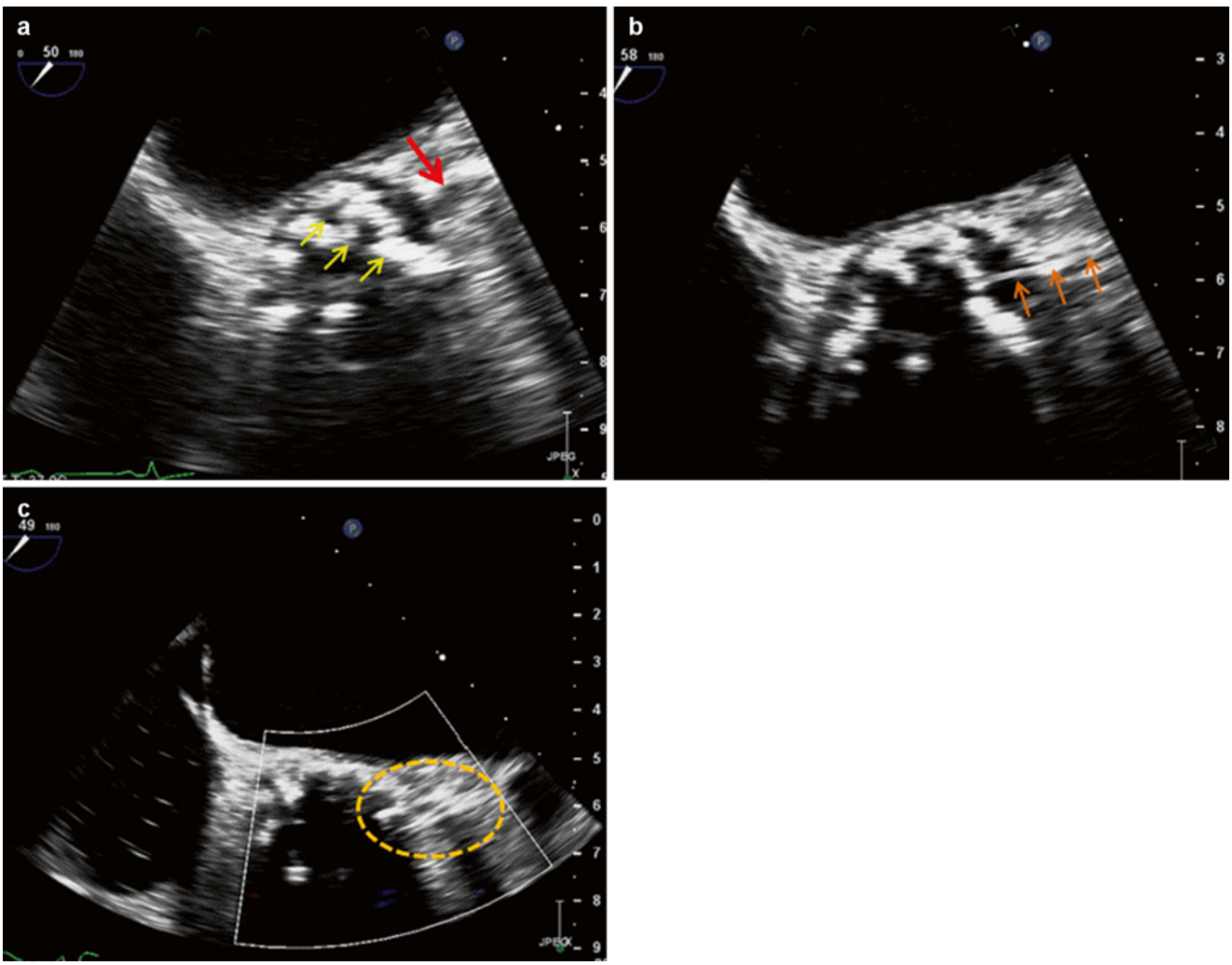

Fig. 6.20 Left coronary obstruction. Bulky calcification (*yellow arrows*) is noted on the left coronary leaflet in close proximity to the ostium of the left main (*red arrow*) coronary artery (**a**). Because of the high-risk anatomy for coronary obstruction, a guide wire (*orange arrows*) was placed in the left coronary artery prior to valve implantation (**b**). Following TAVR, the left main coronary artery was obstructed by bulky calcium on the left coronary leaflet necessitated emergent placement of a coronary stent (*orange dotted oval*) in the left main of the aortic valve following implantation of a balloon-expandable THV (**c**)

is not related to the stiff wire may result from protruding calcium or a native aortic valve leaflet that overhangs the transcatheter valve stent frame and impinges upon normal prosthetic leaflet motion. Alternatively, distortion of the stent frame may prevent normal closure and coaptation of the prosthetic leaflets. Placement of a second THV within the first valve (i.e., valve-in-valve implantation) is usually required under these latter circumstances [57] (Fig. 6.21).

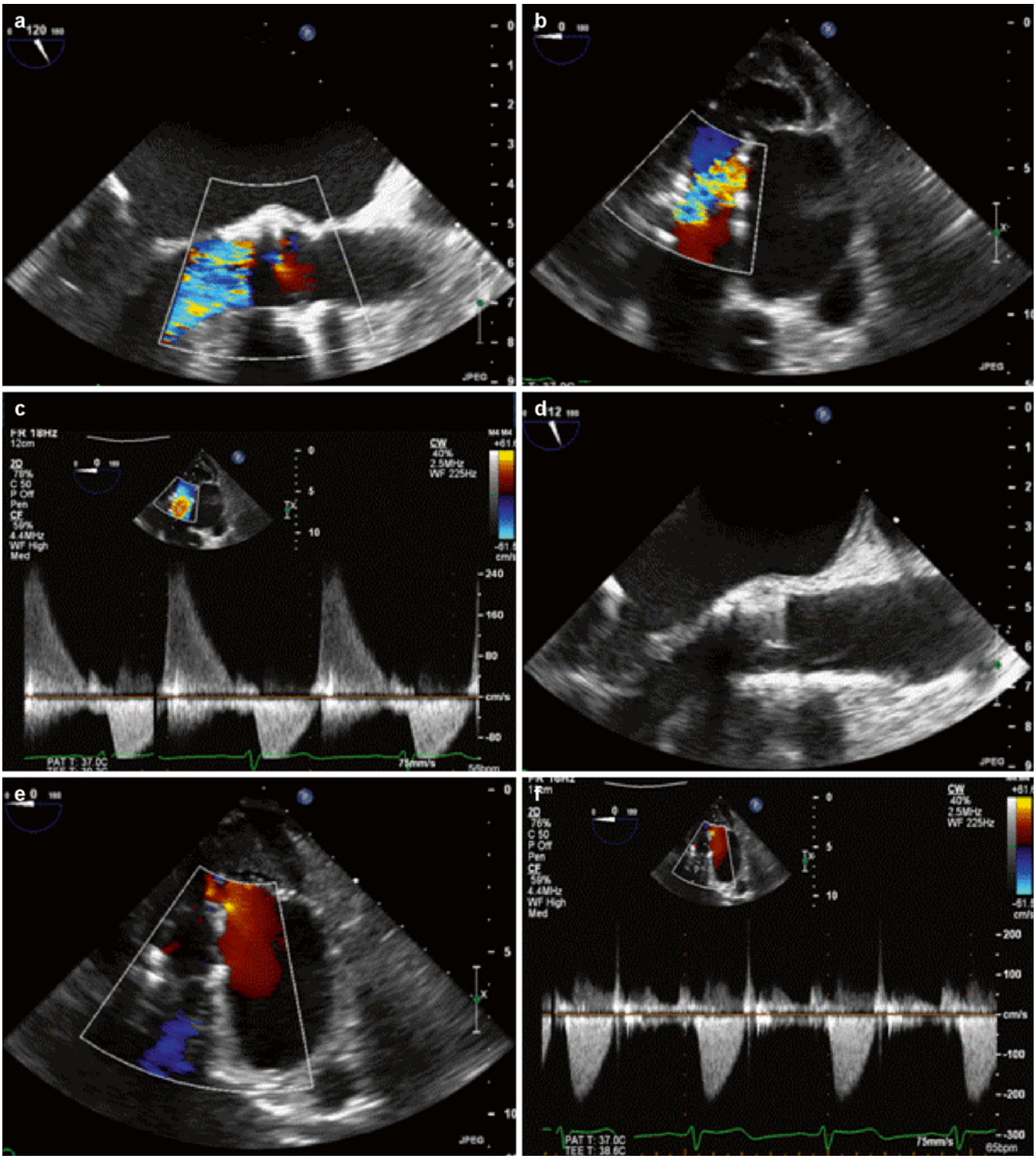

Fig. 6.21 Severe aortic regurgitation following implantation of a balloon-expandable THV. Following implantation of a balloon expandable THV, there is prosthetic leaflet dysfunction resulting in severe valvular aortic regurgitation detected by color (**a**, **b**) and continuous wave (**c**) Doppler. A second THV was immediately placed within this first valve (**d**), resulting in resolution of the aortic regurgitation (**e**, **f**)

Table 6.1 Prosthetic aortic valve regurgitation

	Mild	Moderate	Severe
Semi-quantitative parameters			
Diastolic flow reversal in the descending aorta – PW Doppler	Absent of brief early diastolic	Intermediate	Prominent, holodiastolic
Circumferential extent of prosthetic valve paravalvaular regurgitation (%)	<10 %	10–29 %	≥30 %
Quantitative parameters			
Regurgitant volume (mL/beat)	<30 mL	30–59 mL	≥60 mL
Regurgitant fraction (%)	<30 %	30–49 %	≥50 %
EROA (cm^2)	<0.10 cm^2	0.10–0.29 cm^2	≥0.30 cm^2

Adapted from Kappetein et al. [62]

Paravalvular regurgitation (PAR) has already been discussed, but it is worthy of reiterating some key points. Undersizing the THV relative to the aortic annulus, severity of aortic calcification, and implantation depth have all been identified as risk factors for the occurrence of PAR [17, 26, 32, 34, 49, 58–61]. Determining the severity, etiology, and recommending the appropriate intraprocedural treatment of PAR is one the primary focuses of post-implantation imaging. Yet these are amongst the most challenging issues we are faced with in the field. The applicability of traditional PAR grading schemes is highly debatable for TAVR. The grading recommendations in the most recent Valve Academic Research Consortium (VARC-2) consensus document are an improvement over the ASE guidelines, at least specifically related to TAVR (Table 6.1) [62]. However, comparison of echocardiography to cardiac magnetic resonance imaging (CMR) confirm the limitations of standard echocardiographic parameters for the accurate assessment of PAR severity [63–65]. Better imaging assessment, such as with 3D echocardiography [66], and refined parameters for the echocardiographic assessment of PAR are needed.

Cardiac Perforation and Tamponade

Any of the wires or catheters that enter the left ventricle may cause perforation. The temporary pacing wire may perforate the right ventricle and this may go undetected until the wire is removed. Perforation can usually be readily identifying by accumulation of blood into the pericardial space associated with tamponade physiology and hemodynamic collapse (Fig. 6.22). Many patients undergoing TAVR have hypertrophied left ventricles with a small intracavitary chamber size and, consequently, can develop significant hemodynamic compromise from even a small, acute accumulation of pericardial blood. Rapid identification and prompt action is critical for a successful outcome.

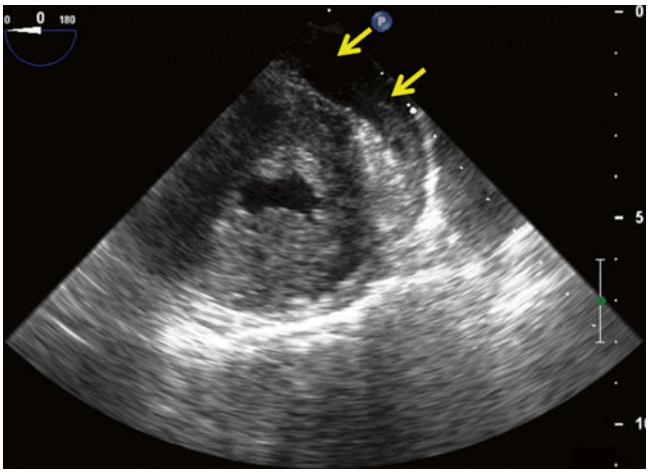

Fig. 6.22 Cardiac tamponade during TAVR. In this case, the patient developed acute hemodynamic compromise during the procedure. A pericardial effusion (*yellow arrows*) and small, compressed left ventricle are consistent with acute pericardial tamponade. Perforation of the lateral left ventricular wall was identified and surgically repaired in this patient

Perforation of the septum may occur adjacent to the stent, resulting in a membranous ventricular septal defect (Fig. 6.23) [67–70]. A muscular ventricular septal defect may occur as a result of perforation from the stiff wire or, rarely, direct cannulation from a transapical approach [71, 72].

Mitral Regurgitation

Reversible changes in the severity of mitral regurgitation may occur during TAVR due to wire entanglement in the mitral apparatus or acute ventricular dilation due to severe left ventricular dysfunction or severe aortic regurgitation. Mechanical complications, such as leaflet perforation or chordal rupture resulting in a flail mitral leaflet, may result in acute severe mitral regurgitation (Fig. 6.24). Detecting changes in and identifying the mechanism of mitral regurgitation is imperative.

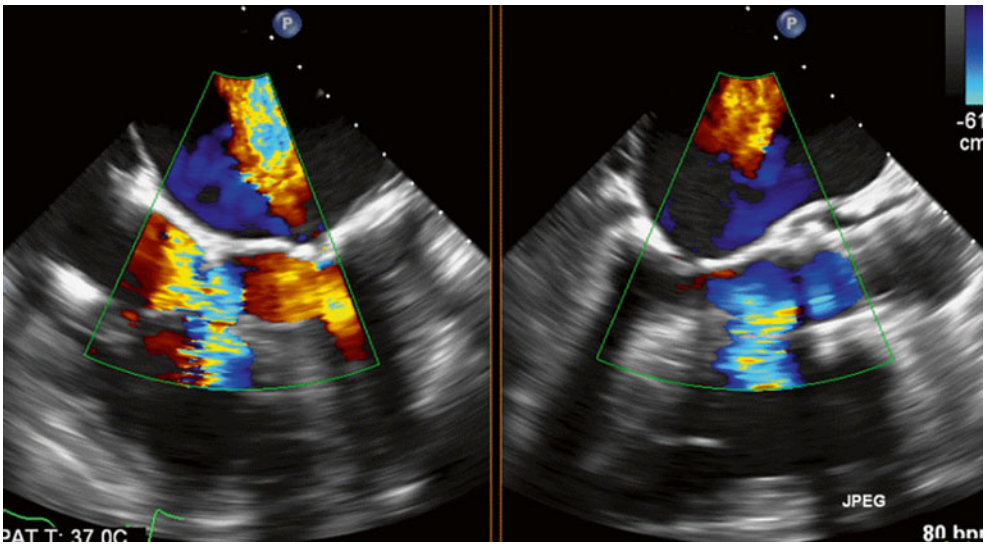

Fig. 6.23 Ventricular septal defect following implantation of a self-expanding transcatheter heart valve. Simultaneous biplane imaging with color Doppler demonstrates a large, iatrogenic, membranous ventricular septal defect following implantation of a self-expanding valve

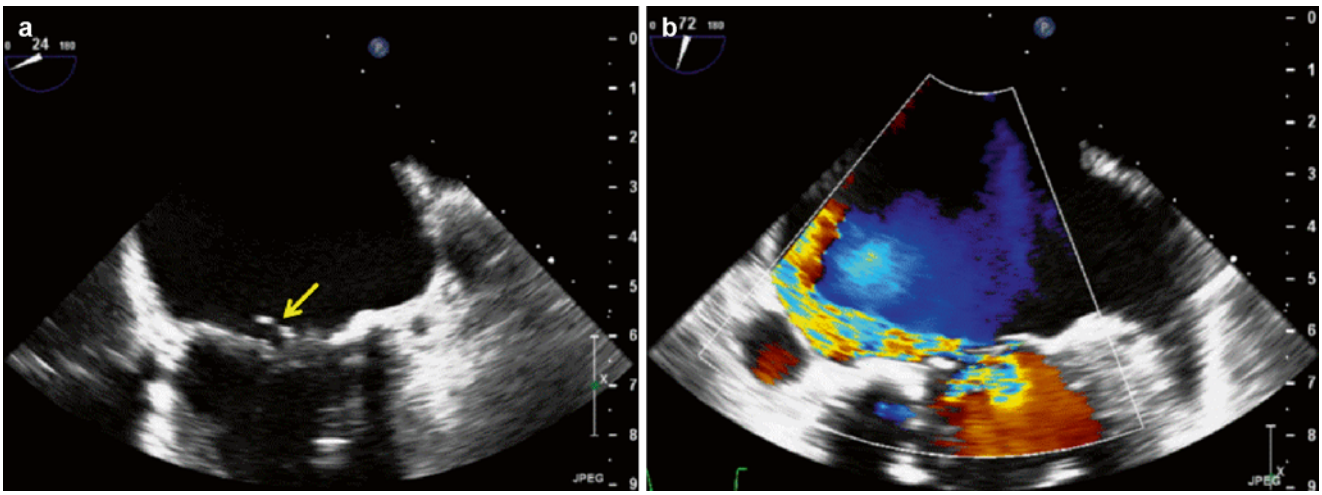

Fig. 6.24 Severe mitral regurgitation complicating TAVR. In this patient, advancement of the transapical delivery sheath resulted in ruptured chordae, a flail mitral leaflet (**a**), and severe mitral regurgitation (**b**)

Malpositioning of the Transcatheter Heart Valve

Embolization of the prosthesis into the aorta may occur if the pre-deployment position is too high or if there is unexpected motion of the valve during deployment. Conversely, embolization of the valve into the left ventricle may occur if the initial position of the valve is too low (Fig. 6.25). Ventricular embolization typically requires open surgical retrieval of the prosthesis [73]. Fortunately, malpositioning and aortic or ventricular embolization of the valve are rare. Advancements made with newer generations of THVs and delivery systems further reduce the likelihood of these complications.

Future Perspectives

Minimalist Approach

Several centers have begun performing TAVR with monitored conscious sedation (CS) rather than general anesthesia (GA), most of which do not use TEE for intraprocedural imaging when done with CS [74–78]. Some use transthoracic or intracardiac echocardiography [79–81], while others use fluoroscopy alone [75]. There continues to be considerable controversy regarding these strategies. Advocates of the so-called "minimalist approach" point to data that suggests TAVR without TEE can be done with

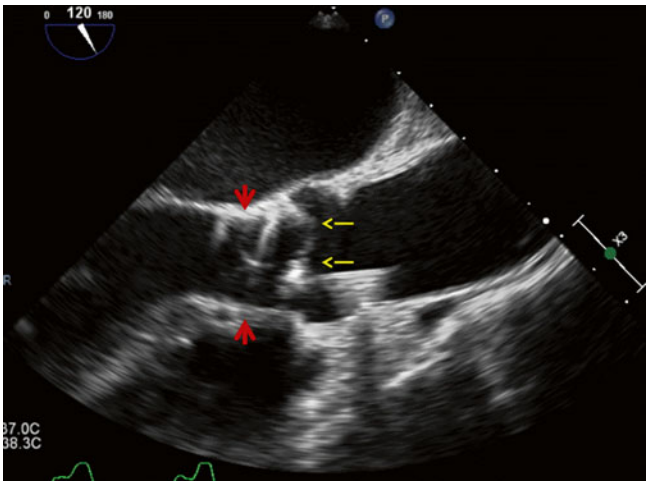

Fig. 6.25 Malpositioning of a transcatheter heart valve. In this long-axis view, it is evident that the balloon expandable THV was incorrectly placed too far on the ventricular aspect of the aortic annulus. The native aortic leaflets are seen to overhang the outflow edge of the stent

similar safety and outcomes as compared to GA with TEE. In fact, there is no data that performing TAVR is actually safer when performed without rather than with intraprocedural TEE. Conversely, there are several lines of data that suggests that TAVR is safer when performed with intraprocedural TEE. Data from the FRANCE II registry noted that patients who underwent TAVR with conscious sedation and local anesthesia had a higher incidence of post-procedural aortic regurgitation compared to GA patients, which was potentially related to the lower use of intraprocedural TEE with CS [82]. One study of TAVR in intermediate risk patients using a minimalist approach reported a 30-day mortality rate that was actually higher than observed in the higher risk patient population of the PARTNER (Placement of Aortic Transcatheter Valves Trial) Trial [48, 74]. Data from the European Society of Cardiology's TransCatheter Valve Treatment (TCVT) registry reported a higher immediate procedural success rate and a lower rate of periprocedural complications, such as cardiac tamponade, in patients undergoing TAVR with GA and TEE as compared to CS in which TEE was rarely used [83]. There was more acute kidney injury in the CS patients. Furthermore, there was a trend towards lower in hospital mortality in GA patients in spite of the fact that these patients had significantly higher Logistic-EuroSCORE at baseline. Finally, the use of intraprocedural TEE was found to be an independent protective factor against overall and late mortality in the Brazilian TAVI registry [84]. As the debate about the optimal intraprocedural imaging strategy for TAVR continues, it is important to be mindful that when TAVR becomes more widely used in lower risk patients, the bar for procedural safety should be set even higher and not lower.

Fusion Imaging

Technology that allows for the co-registration of the data from echocardiography onto the fluoroscopic image is now available [85–87]. This fusion imaging holds great potential for a number of structural heart interventions. Positioning of a THV with fusion imaging might reduce the amount of contrast used, fluoroscopic time required, or rate of malpositioning with TAVR. This technology is still under development and further improvements and study are necessary.

References

1. Leon MB, Smith CR, Mack M, et al. Transcatheter aortic-valve implantation for aortic stenosis in patients who cannot undergo surgery. N Engl J Med. 2010;363:1597–607.
2. Smith CR, Leon MB, Mack MJ, et al. Transcatheter versus surgical aortic-valve replacement in high-risk patients. N Engl J Med. 2011;364:2187–98.
3. Adams DH, Popma JJ, Reardon MJ, et al. Transcatheter aortic-valve replacement with a self-expanding prosthesis. N Engl J Med. 2014;370:1790–8.
4. Popma JJ, Adams DH, Reardon MJ, et al. Transcatheter aortic valve replacement using a self-expanding bioprosthesis in patients with severe aortic stenosis at extreme risk for surgery. J Am Coll Cardiol. 2014;63:1972–81.
5. Holmes Jr DR, Mack MJ, Kaul S, et al. ACCF/AATS/SCAI/STS expert consensus document on transcatheter aortic valve replacement. J Am Coll Cardiol. 2012;59:1200–54.
6. Nishimura RA, Otto CM, Bonow RO, et al. AHA/ACC guideline for the management of patients with valvular heart disease: executive summary: a report of the American College of Cardiology/American Heart Association Task Force on Practice Guidelines. J Am Coll Cardiol. 2014;63:2438–88.
7. Baumgartner H, Hung J, Bermejo J, et al. Echocardiographic assessment of valve stenosis: EAE/ASE recommendations for clinical practice. J Am Soc Echocardiogr. 2009;22:1–23; quiz 101–2.
8. Zoghbi WA, Enriquez-Sarano M, Foster E, et al. Recommendations for evaluation of the severity of native valvular regurgitation with two-dimensional and Doppler echocardiography. J Am Soc Echocardiogr. 2003;16:777–802.
9. Hahn RT, Abraham T, Adams MS, et al. Guidelines for performing a comprehensive transesophageal echocardiographic examination: recommendations from the American Society of Echocardiography and the Society of Cardiovascular Anesthesiologists. J Am Soc Echocardiogr. 2013;26:921–64.
10. Piazza N, de Jaegere P, Schultz C, Becker AE, Serruys PW, Anderson RH. Anatomy of the aortic valvar complex and its implications for transcatheter implantation of the aortic valve. Circ Cardiovasc Interv. 2008;1:74–81.
11. Barbanti M, Yang TH, Rodes Cabau J, et al. Anatomical and procedural features associated with aortic root rupture during balloon-expandable transcatheter aortic valve replacement. Circulation. 2013;128:244–53.
12. Athappan G, Patvardhan E, Tuzcu EM, et al. Incidence, predictors, and outcomes of aortic regurgitation after transcatheter aortic valve replacement: meta-analysis and systematic review of literature. J Am Coll Cardiol. 2013;61:1585–95.

13. Ribeiro HB, Nombela-Franco L, Urena M, et al. Coronary obstruction following transcatheter aortic valve implantation: a systematic review. JACC Cardiovasc Interv. 2013;6:452–61.
14. Detaint D, Lepage L, Himbert D, et al. Determinants of significant paravalvular regurgitation after transcatheter aortic valve: implantation impact of device and annulus discongruence. JACC Cardiovasc Interv. 2009;2:821–7.
15. Hamdan A, Guetta V, Konen E, et al. Deformation dynamics and mechanical properties of the aortic annulus by 4-dimensional computed tomography: insights into the functional anatomy of the aortic valve complex and implications for transcatheter aortic valve therapy. J Am Coll Cardiol. 2012;59:119–27.
16. Tzikas A, Schultz CJ, Piazza N, et al. Assessment of the aortic annulus by multislice computed tomography, contrast aortography, and trans-thoracic echocardiography in patients referred for transcatheter aortic valve implantation. Catheter Cardiovasc Interv. 2011;77:868–75.
17. Koos R, Altiok E, Mahnken AH, et al. Evaluation of aortic root for definition of prosthesis size by magnetic resonance imaging and cardiac computed tomography: implications for transcatheter aortic valve implantation. Int J Cardiol. 2012;158:353–8.
18. Altiok E, Koos R, Schroder J, et al. Comparison of two-dimensional and three-dimensional imaging techniques for measurement of aortic annulus diameters before transcatheter aortic valve implantation. Heart. 2011;97:1578–84.
19. Willson AB, Webb JG, Labounty TM, et al. 3-dimensional aortic annular assessment by multidetector computed tomography predicts moderate or severe paravalvular regurgitation after transcatheter aortic valve replacement: a multicenter retrospective analysis. J Am Coll Cardiol. 2012;59:1287–94.
20. Jilaihawi H, Kashif M, Fontana G, et al. Cross-sectional computed tomographic assessment improves accuracy of aortic annular sizing for transcatheter aortic valve replacement and reduces the incidence of paravalvular aortic regurgitation. J Am Coll Cardiol. 2012;59:1275–86.
21. Gurvitch R, Webb JG, Yuan R, et al. Aortic annulus diameter determination by multidetector computed tomography: reproducibility, applicability, and implications for transcatheter aortic valve implantation. JACC Cardiovasc Interv. 2011;4:1235–45.
22. Hahn RT, Khalique O, Williams MR, et al. Predicting paravalvular regurgitation following transcatheter valve replacement: utility of a novel method for three-dimensional echocardiographic measurements of the aortic annulus. J Am Soc Echocardiogr. 2013;26:1043–52.
23. Janosi RA, Kahlert P, Plicht B, et al. Measurement of the aortic annulus size by real-time three-dimensional transesophageal echocardiography. Minim Invasive Ther Allied Technol. 2011;20:85–94.
24. Santos N, de Agustin JA, Almeria C, et al. Prosthesis/annulus discongruence assessed by three-dimensional transoesophageal echocardiography: a predictor of significant paravalvular aortic regurgitation after transcatheter aortic valve implantation. Eur Heart J Cardiovasc Imaging. 2012;13:931–7.
25. Tsang W, Bateman MG, Weinert L, et al. Accuracy of aortic annular measurements obtained from three-dimensional echocardiography, CT and MRI: human in vitro and in vivo studies. Heart. 2012;98:1146–52.
26. Gripari P, Ewe SH, Fusini L, et al. Intraoperative 2D and 3D transoesophageal echocardiographic predictors of aortic regurgitation after transcatheter aortic valve implantation. Heart. 2012;98:1229–36.
27. Smith LA, Dworakowski R, Bhan A, et al. Real-time three-dimensional transesophageal echocardiography adds value to transcatheter aortic valve implantation. J Am Soc Echocardiogr. 2013;26:359–69.
28. Jilaihawi H, Doctor N, Kashif M, et al. Aortic annular sizing for transcatheter aortic valve replacement using cross-sectional 3-dimensional transesophageal echocardiography. J Am Coll Cardiol. 2013;61:908–16.
29. Khalique OK, Kodali SK, Paradis JM, et al. Aortic annular sizing using a novel 3-dimensional echocardiographic method: use and comparison with cardiac computed tomography. Circ Cardiovasc Imaging. 2014;7:155–63.
30. Kasel AM, Cassese S, Bleiziffer S, et al. Standardized imaging for aortic annular sizing: implications for transcatheter valve selection. JACC Cardiovasc Imaging. 2013;6:249–62.
31. Masson JB, Kovac J, Schuler G, et al. Transcatheter aortic valve implantation: review of the nature, management, and avoidance of procedural complications. JACC Cardiovasc Interv. 2009;2:811–20.
32. Ewe SH, Ng AC, Schuijf JD, et al. Location and severity of aortic valve calcium and implications for aortic regurgitation after transcatheter aortic valve implantation. Am J Cardiol. 2011;108:1470–7.
33. Khalique OK, Hahn RT, Gada H, et al. Quantity and location of aortic valve complex calcification predicts severity and location of paravalvular regurgitation and frequency of post-dilation after balloon-expandable transcatheter aortic valve replacement. JACC Cardiovasc Interv. 2014;7:885–94.
34. Azzalini L, Ghoshhajra BB, Elmariah S, et al. The aortic valve calcium nodule score (AVCNS) independently predicts paravalvular regurgitation after transcatheter aortic valve replacement (TAVR). J Cardiovasc Comput Tomogr. 2014;8:131–40.
35. Dvir D, Lavi I, Eltchaninoff H, et al. Multicenter evaluation of Edwards SAPIEN positioning during transcatheter aortic valve implantation with correlates for device movement during final deployment. JACC Cardiovasc Interv. 2012;5:563–70.
36. Genereux P, Reiss GR, Kodali SK, Williams MR, Hahn RT. Periaortic hematoma after transcatheter aortic valve replacement: description of a new complication. Catheter Cardiovasc Interv. 2012;79:766–76.
37. Leber AW, Kasel M, Ischinger T, et al. Aortic valve calcium score as a predictor for outcome after TAVI using the CoreValve revalving system. Int J Cardiol. 2013;166:652–7.
38. Wijesinghe N, Ye J, Rodes-Cabau J, et al. Transcatheter aortic valve implantation in patients with bicuspid aortic valve stenosis. JACC Cardiovasc Interv. 2010;3:1122–5.
39. Ferrari E, Locca D, Sulzer C, et al. Successful transapical aortic valve implantation in a congenital bicuspid aortic valve. Ann Thorac Surg. 2010;90:630–2.
40. Chiam PT, Chao VT, Tan SY, et al. Percutaneous transcatheter heart valve implantation in a bicuspid aortic valve. JACC Cardiovasc Interv. 2010;3:559–61.
41. Mylotte D, Lefevre T, Sondergaard L, et al. Transcatheter aortic valve replacement in bicuspid aortic valve disease. J Am Coll Cardiol. 2014;64:2330–9.
42. Babaliaros VC, Liff D, Chen EP, et al. Can balloon aortic valvuloplasty help determine appropriate transcatheter aortic valve size? JACC Cardiovasc Interv. 2008;1:580–6.
43. Patsalis PC, Al-Rashid F, Neumann T, et al. Preparatory balloon aortic valvuloplasty during transcatheter aortic valve implantation for improved valve sizing. JACC Cardiovasc Interv. 2013;6:965–71.
44. Amat-Santos IJ, Dahou A, Webb J, et al. Comparison of hemodynamic performance of the balloon-expandable SAPIEN 3 versus SAPIEN XT transcatheter valve. Am J Cardiol. 2014;114:1075–82.
45. Webb J, Gerosa G, Lefevre T, et al. Multicenter evaluation of a next-generation balloon-expandable transcatheter aortic valve. J Am Coll Cardiol. 2014;64:2235–43.
46. Klein AA, Skubas NJ, Ender J. Controversies and complications in the perioperative management of transcatheter aortic valve replacement. Anesth Analg. 2014;119:784–98.
47. Zoghbi WA, Chambers JB, Dumesnil JG, et al. Recommendations for evaluation of prosthetic valves with echocardiography and doppler ultrasound: a report from the American Society of Echocardiography's Guidelines and Standards Committee and

the Task Force on Prosthetic Valves, developed in conjunction with the American College of Cardiology Cardiovascular Imaging Committee, Cardiac Imaging Committee of the American Heart Association, the European Association of Echocardiography, a registered branch of the European Society of Cardiology, the Japanese Society of Echocardiography and the Canadian Society of Echocardiography, endorsed by the American College of Cardiology Foundation, American Heart Association, European Association of Echocardiography, a registered branch of the European Society of Cardiology, the Japanese Society of Echocardiography, and Canadian Society of Echocardiography. J Am Soc Echocardiogr. 2009;22:975–1014; quiz 1082–4.
48. Kodali SK, Williams MR, Smith CR, et al. Two-year outcomes after transcatheter or surgical aortic-valve replacement. N Engl J Med. 2012;366:1686–95.
49. Unbehaun A, Pasic M, Dreysse S, et al. Transapical aortic valve implantation: incidence and predictors of paravalvular leakage and transvalvular regurgitation in a series of 358 patients. J Am Coll Cardiol. 2012;59:211–21.
50. Abdel-Wahab M, Zahn R, Horack M, et al. Aortic regurgitation after transcatheter aortic valve implantation: incidence and early outcome. Results from the German transcatheter aortic valve interventions registry. Heart. 2011;97:899–906.
51. Tamburino C, Capodanno D, Ramondo A, et al. Incidence and predictors of early and late mortality after transcatheter aortic valve implantation in 663 patients with severe aortic stenosis. Circulation. 2011;123:299–308.
52. Moat NE, Ludman P, de Belder MA, et al. Long-term outcomes after transcatheter aortic valve implantation in high-risk patients with severe aortic stenosis: the U.K. TAVI (United Kingdom Transcatheter Aortic Valve Implantation) registry. J Am Coll Cardiol. 2011;58:2130–8.
53. Gotzmann M, Korten M, Bojara W, et al. Long-term outcome of patients with moderate and severe prosthetic aortic valve regurgitation after transcatheter aortic valve implantation. Am J Cardiol. 2012;110:1500–6.
54. Sinning JM, Hammerstingl C, Vasa-Nicotera M, et al. Aortic regurgitation index defines severity of peri-prosthetic regurgitation and predicts outcome in patients after transcatheter aortic valve implantation. J Am Coll Cardiol. 2012;59:1134–41.
55. Hayashida K, Morice MC, Chevalier B, et al. Sex-related differences in clinical presentation and outcome of transcatheter aortic valve implantation for severe aortic stenosis. J Am Coll Cardiol. 2012;59:566–71.
56. Daneault B, Koss E, Hahn RT, et al. Efficacy and safety of post-dilatation to reduce paravalvular regurgitation during balloon-expandable transcatheter aortic valve replacement. Circ Cardiovasc Interv. 2013;6:85–91.
57. Makkar RR, Jilaihawi H, Chakravarty T, et al. Determinants and outcomes of acute transcatheter valve-in-valve therapy or embolization: a study of multiple valve implants in the U.S. PARTNER trial (placement of AoRTic TraNscathetER valve trial Edwards SAPIEN transcatheter heart valve). J Am Coll Cardiol. 2013;62: 418–30.
58. Nombela-Franco L, Rodes-Cabau J, DeLarochelliere R, et al. Predictive factors, efficacy, and safety of balloon post-dilation after transcatheter aortic valve implantation with a balloon-expandable valve. JACC Cardiovasc Interv. 2012;5:499–512.
59. Schultz C, Rossi A, van Mieghem N, et al. Aortic annulus dimensions and leaflet calcification from contrast MSCT predict the need for balloon post-dilatation after TAVI with the Medtronic CoreValve prosthesis. EuroIntervention. 2011;7:564–72.
60. Marwan M, Achenbach S, Ensminger SM, et al. CT predictors of post-procedural aortic regurgitation in patients referred for transcatheter aortic valve implantation: an analysis of 105 patients. Int J Cardiovasc Imaging. 2013;29:1191–8.
61. John D, Buellesfeld L, Yuecel S, et al. Correlation of device landing zone calcification and acute procedural success in patients undergoing transcatheter aortic valve implantations with the self-expanding CoreValve prosthesis. JACC Cardiovasc Interv. 2010;3:233–43.
62. Kappetein AP, Head SJ, Genereux P, et al. Updated standardized endpoint definitions for transcatheter aortic valve implantation: the Valve Academic Research Consortium-2 consensus document. J Am Coll Cardiol. 2012;60:1438–54.
63. Cawley PJ, Hamilton-Craig C, Owens DS, et al. Prospective comparison of valve regurgitation quantitation by cardiac magnetic resonance imaging and transthoracic echocardiography. Circ Cardiovasc Imaging. 2013;6:48–57.
64. Abdel-Wahab M, Mehilli J, Frerker C, et al. Comparison of balloon-expandable vs self-expandable valves in patients undergoing transcatheter aortic valve replacement: the CHOICE randomized clinical trial. JAMA. 2014;311:1503–14.
65. Ribeiro HB, Le Ven F, Larose E, et al. Cardiac magnetic resonance versus transthoracic echocardiography for the assessment and quantification of aortic regurgitation in patients undergoing transcatheter aortic valve implantation. Heart. 2014;100:1924–32.
66. Altiok E, Frick M, Meyer CG, et al. Comparison of two- and three-dimensional transthoracic echocardiography to cardiac magnetic resonance imaging for assessment of paravalvular regurgitation after transcatheter aortic valve implantation. Am J Cardiol. 2014;113:1859–66.
67. Patel Y, Vassileva C, Mishkel G. Rare complication of ventricular septal defect in three patients following transcatheter aortic valve replacement. Catheter Cardiovasc Interv. 2014;83:497–501.
68. Tzikas A, Schultz C, Piazza N, van Geuns RJ, Serruys PW, de Jaegere PP. Perforation of the membranous interventricular septum after transcatheter aortic valve implantation. Circ Cardiovasc Interv. 2009;2:582–3.
69. Gerckens U, Latsios G, Pizzulli L. Percutaneous treatment of a post-TAVI ventricular septal defect: a successful combined procedure for an unusual complication. Catheter Cardiovasc Interv. 2013;81:E274–7.
70. Aminian A, Lalmand J, Dolatabadi D. Late contained aortic root rupture and ventricular septal defect after transcatheter aortic valve implantation. Catheter Cardiovasc Interv. 2013;81:E72–5.
71. Al-Attar N, Ghodbane W, Himbert D, et al. Unexpected complications of transapical aortic valve implantation. Ann Thorac Surg. 2009;88:90–4.
72. Massabuau P, Dumonteil N, Berthoumieu P, et al. Left-to-right interventricular shunt as a late complication of transapical aortic valve implantation. JACC Cardiovasc Interv. 2011;4:710–2.
73. Eggebrecht H, Schmermund A, Kahlert P, Erbel R, Voigtlander T, Mehta RH. Emergent cardiac surgery during transcatheter aortic valve implantation (TAVI): a weighted meta-analysis of 9,251 patients from 46 studies. EuroIntervention. 2013;8:1072–80.
74. Greif M, Lange P, Nabauer M, et al. Transcutaneous aortic valve replacement with the Edwards SAPIEN XT and Medtronic CoreValve prosthesis under fluoroscopic guidance and local anaesthesia only. Heart. 2014;100:691–5.
75. Durand E, Borz B, Godin M, et al. Transfemoral aortic valve replacement with the Edwards SAPIEN and Edwards SAPIEN XT prosthesis using exclusively local anesthesia and fluoroscopic guidance: feasibility and 30-day outcomes. JACC Cardiovasc Interv. 2012;5:461–7.
76. Motloch LJ, Rottlaender D, Reda S, et al. Local versus general anesthesia for transfemoral aortic valve implantation. Clin Res Cardiol. 2012;101:45–53.
77. Yamamoto M, Meguro K, Mouillet G, et al. Effect of local anesthetic management with conscious sedation in patients undergoing transcatheter aortic valve implantation. Am J Cardiol. 2013;111:94–9.
78. Babaliaros V, Devireddy C, Lerakis S, et al. Comparison of transfemoral transcatheter aortic valve replacement performed in the

catheterization laboratory (minimalist approach) versus hybrid operating room (standard approach): outcomes and cost analysis. JACC Cardiovasc Interv. 2014;7:898–904.
79. Bartel T, Bonaros N, Muller L, et al. Intracardiac echocardiography: a new guiding tool for transcatheter aortic valve replacement. J Am Soc Echocardiogr. 2011;24:966–75.
80. Ussia GP, Barbanti M, Sarkar K, et al. Accuracy of intracardiac echocardiography for aortic root assessment in patients undergoing transcatheter aortic valve implantation. Am Heart J. 2012;163:684–9.
81. Bartel T, Bonaros N, Edlinger M, et al. Intracardiac echo and reduced radiocontrast requirements during TAVR. JACC Cardiovasc Imaging. 2014;7:319–20.
82. Oguri A, Yamamoto M, Mouillet G, et al. Clinical outcomes and safety of transfemoral aortic valve implantation under general versus local anesthesia: subanalysis of the French Aortic National CoreValve and Edwards 2 registry. Circ Cardiovasc Interv. 2014;7:602–10.
83. Dall'Ara G, Eltchaninoff H, Moat N, et al. Local and general anaesthesia do not influence outcome of transfemoral aortic valve implantation. Int J Cardiol. 2014;177:448–54.
84. De Brito Jr FS, Carvalho LA, Sarmento-Leite R, et al. Outcomes and predictors of mortality after transcatheter aortic valve implantation: results of the Brazilian registry. Catheter Cardiovasc Interv. 2015;85:E153–62.
85. Gao G, Penney G, Ma Y, et al. Registration of 3D trans-esophageal echocardiography to X-ray fluoroscopy using image-based probe tracking. Med Image Anal. 2012;16:38–49.
86. Lang P, Seslija P, Chu MW, et al. US-fluoroscopy registration for transcatheter aortic valve implantation. IEEE Trans Biomed Eng. 2012;59:1444–53.
87. Mountney P, Ionasec R, Kaizer M, et al. Ultrasound and fluoroscopic images fusion by autonomous ultrasound probe detection. Med Image Comput Comput Assist Interv. 2012; 15:544–51.

Transcatheter Closure of Paravalvular Regurgitation: Case-Based Learning

7

Rebecca T. Hahn

Abstract

Current class IIa indications for percutaneous interventions for closure of paravalvular leaks includes patients with prosthetic heart valves and intractable hemolysis or NYHA class III/IV HF who are at high risk for surgery and have anatomic features suitable for catheter-based therapy when performed in centers with expertise in the procedure. Recent reports show high procedural success, defined typically as ≤1+ residual regurgitation. Improvement in heart failure symptoms is usually limited to patients with no or mild residual regurgitation following closure. Patients with hemolytic anemia however, often fail to improve despite successful closure with persistent or worsening hemolysis reported in up to 33 % of patients and new-onset hemolysis in 10 %. Transesophageal imaging is key to pre-procedural planning and involves a determination of: (a) the number and location of defects; (b) the shape and exact size of each defect; (c) the distance and orientation of the defect to the sewing ring or prosthesis. Intra-procedural imaging is essential for guidance of wire/catheter placement and an assessment of complications such as cardiac perforation, prosthetic valve dysfunction or device embolization.

Keywords

Transcatheter • Paravalvular regurgitation • Prosthetic valve

Introduction and Review

Paravalvular regurgitation occurs in 2–10 % of aortic prosthetic valves and 7–17 % of mitral prosthetic valves [1]. Whereas most of these patients are asymptomatic, 1–3 % of patients may present with heart failure, hemolysis or both. According to the AHA/ACC Valvular Heart Disease guidelines, the class I indication for surgical intervention includes operable patients with mechanical heart valves with intractable hemolysis or heart failure due to severe prosthetic or paraprosthetic regurgitation (level of evidence B) [2]. Class IIa indications for operation include operable patients with severe symptomatic or asymptomatic bioprosthetic regurgitation (level of evidence C) with the caveat that blood cultures should be draw to exclude infectious endocarditis.

In symptomatic patients with severe paravalvular regurgitation the risk of adverse outcome with repeat surgery is up to 16 % [3, 4] increasing with each re-operation [4]. A number of studies have shown that percutaneous closure of paravalvular regurgitation is not only possible using a number of different devices [5–9], but successful in treating both heart failure and hemolysis [10–13]. Thus percutaneous repair is an attractive alternative to repeat valve replacement given the high procedural success rate [10, 11]. Thus the current class IIa indication for percutaneous intervention includes patients with prosthetic heart valves and intractable hemolysis or NYHA class III/IV HF who are at high risk for surgery and have anatomic features suitable for catheter-based therapy when performed in centers with expertise in the procedure (Level of Evidence B).

R.T. Hahn, MD, FACC, FASE
Medicine, Division of Cardiology, The New York Presbyterian Hospital/Columbia University Medical Center,
177 Fort Washington Avenue, New York, NY 10032, USA
e-mail: rth2@columbia.edu

M.H. Picard et al. (eds.), *Intraprocedural Imaging of Cardiovascular Interventions*, DOI 10.1007/978-3-319-29428-5_7

Early studies reported variable success rates [14] however recent reports show high procedural success, defined typically as ≤1+ residual regurgitation. Ruiz et al. reported procedural success of 86 % with complication rate of 13 % [11]. Sorajja et al. reported success of 89 % with complication rate of ~9 % [12]. Procedural success may be influenced by the prosthetic valve location. Ruiz et al. reported a higher success rate with para-mitral regurgitation (89 %) versus para-aortic regurgitation (73 %) [11]. This may be related to the difference in imaging the three-dimensional prosthetic annulus; frequent acoustic shadowing of at least part of the aortic annulus [15] may limit the accurate assessment of defect anatomy and location as well as intra-procedural guidance. Complications of the procedure are not trivial. Sorajja et al. [10] reported a 30-day complication rate of 8.7 % (sudden and unexplained death, 1.7 %; stroke, 2.6 %; emergency surgery, 0.9 %; bleeding, 5.2 %). The 3-year estimate for survival free of all-cause mortality was only 64.3 % and did not significantly differ for patients with no (69.9 %) mild (62.4 %), or moderate or severe (58.1 %) residual regurgitation.

Clinical success is determined by the procedural success and the presenting symptom. Improvement in heart failure symptoms is typically limited to patients with no or mild residual regurgitation following closure [12]. Patients with hemolytic anemia however, often fail to improve despite successful closure. Hein et al. [16] observed that 33 % of patients requiring transfusions had worsening hemolysis after the procedure, and there was newly developed hemolysis in 10 % of all patients. Persistent or worsening hemolysis may be due to the typical off-label use of devices used to close these leaks which are woven from a larger-caliber nitinol mesh which fail to conform to the irregular shapes of the paravalvular defects. Small, high velocity jets can typically be seen between and through the nitinol mesh resulting in persistent hemolysis. More recently the Amplatzer vascular plug (AVP II and IV) devices have been used which have a smaller profile and conform to the shape of the defect allowing them to fit into the small, irregular paravalvular defects resulting in reduced para-device leak. Similar to surgical intervention for hemolysis [15] patients with persistent hemolytic anemia after attempted paravalvular closure, determined by level of lactate dehydrogenase (given the oversensitivity of haptoglobin), predicts poor survival and need for cardiac surgery [17].

Percutaneous repair is contraindicated in patients with active endocarditis or significant dehiscence involving more than one-fourth to one-third of the valve ring [18]. Significant dehiscence is echocardiographically suggested by excessive rocking motion of the mitral prosthesis relative to the annulus [19]. For the aortic prosthesis, motion discordant with the motion of the adjacent aortic root and native annulus usually indicates significant (40–90 % of the annular circumference) dehiscence [20].

Case-Based Approach to Paravalvular Regurgitation Closure

Case 1 A 60 year old male with history of tissue AVR for bacterial endocarditis in 2001 now presents with severe bioprosthetic AR. The transesophageal echocardiogram is shown in Fig. 7.1. The retrograde approach was used to position an AVP II device (Fig. 7.2, panel A) with nearly complete resolution of the paravalvular jet (Fig. 7.2, panel B).

Case 2 87 year old female transferred from an outside hospital with NYHA IV SOB, and a history of a bioprosthetic MVR for infective endocarditis. She had a history of recurrent endocarditis treated medically as well as hypertension, atrial fibrillation, stroke, chronic obstructive pulmonary disease requiring steroids. The transesophageal echocardiogram is shown in Fig. 7.3. The paravalvular regurgitant lesion is well-imaged at 5 o'clock (panel A). An Agilis catheter was introduced via an antegrade, trans-sepal approach (panel B) with initial placement of an AVP 4 device (panel C). Fig. 7.3, panel D shows is a higher magnification of the device, now 90° turned from panel C for better imaging. This device was malpositioned and removed, with final position (Fig. 7.4, panel A) and color Doppler (panel B) showing with nearly complete resolution of the paravalvular jet.

Approach

Periaortic leaks can typically be approached via a retrograde aortic approach. Transcatheter closure of mitral paravalvular regurgitation can be approached from a retrograde or antegrade approach. Frequently this is decided by the number, location and shape of the defects. The retrograde method can be performed from a femoral arterial approach (and thus across the aortic valve into the ventricle or retro-aortic) or a direct transapical approach; the latter may be ideal for patients requiring multiple devices since multiple wires can be introduced simultaneously through the apex either by direct puncture or with a small surgical apical window. For some operators, the approach to a mitral paravalvular defect can be more systematically determined by the location of the defect: the trans-septal-antegrade technique for leaks located between 6 o'clock and 9 o'clock; the retro-aortic technique for leaks located between 10 and 2 o'clock; the transapical approach for the majority of mitral paravalvular leaks, especially if located between 10 and 6 o'clock. The transapical approach for mitral paravalvular leak closure has been shown to reduce procedural and fluoroscopy time [21].

The antegrade method requires a trans-septal puncture and three-dimensional transesophageal guidance may be

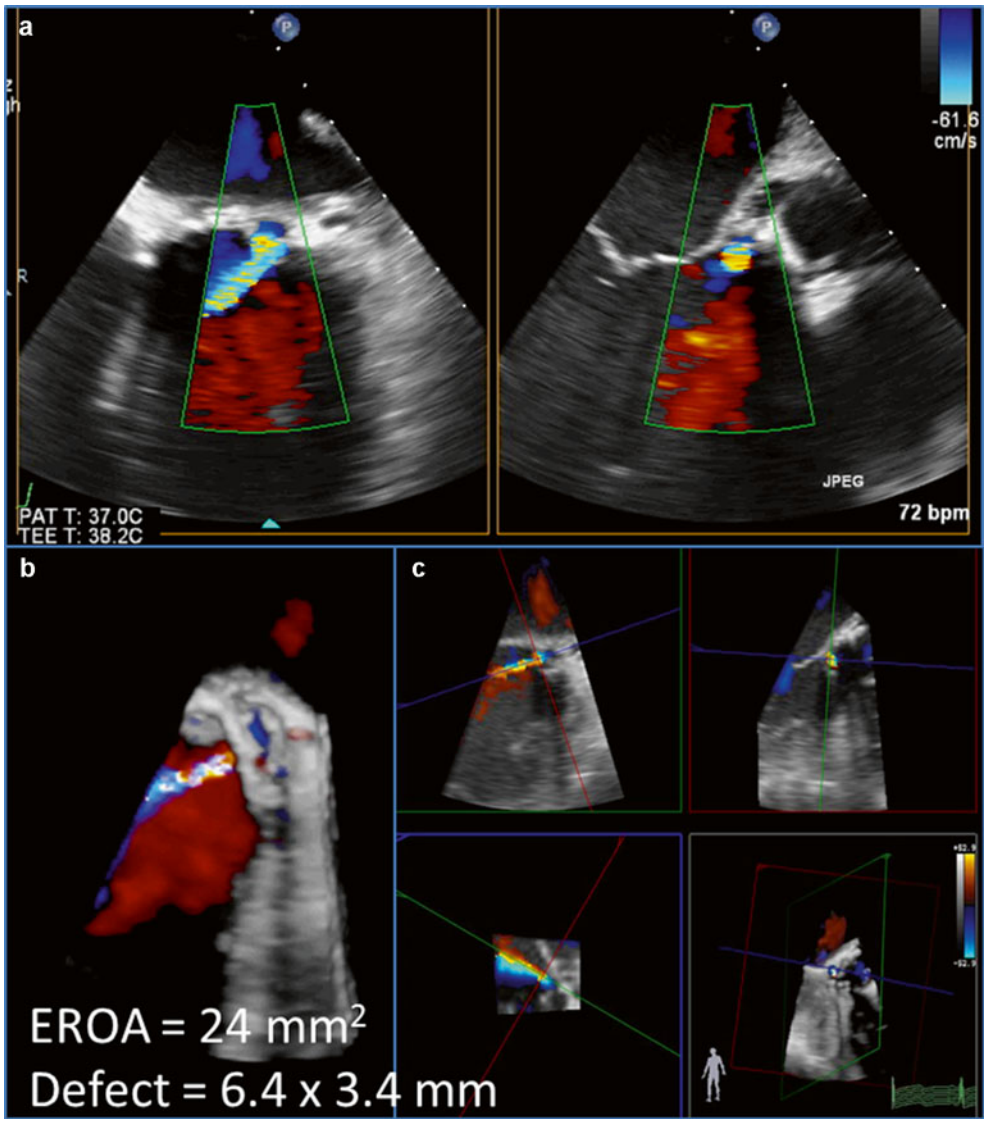

Fig. 7.1 Transesophageal echocardiogram showing in panel (**a**), the simultaneous multiplane color Doppler images show the posterolateral paravalvular regurgitant jet. Panel (**b**) is the three-dimensional color Doppler imaging of the paravalvular regurgitant jet with panel (**c**) showing the multi-planar reconstruction of the jet dimensions (6.4 × 3.4 mm) and area (24 mm^2)

helpful in identifying the optimal location for the puncture. For lateral jets, standard trans-septal puncture position may be used since once across the septum, the catheters are directly toward the lateral sewing ring. For medial defects, a higher and more posterior trans-septal puncture may be required for optimal catheter positioning although steerable guide catheter (i.e. Agilis) have make the antegrade approach highly feasible for any para-mitral paravalvular defect.

Procedural Imaging

Standard transesophageal imaging views for the aortic and mitral valves should be used throughout the pre-interventional imaging and procedural guidance [22]. Much of the pre-procedural assessment of paravalvular leaks are performed by three-dimensional imaging [23]. The surgical or anatomic view of the mitral valve is suggested by the American Society of Echocardiography guidelines places the aortic valve anterior (or at 12 o'clock) with the left atrial appendage identifying the lateral sewing ring (9 o'clock), and the interatrial septum the medial sewing ring (3 o'clock). Maintaining this anatomic view for pre-procedural and intra-procedural imaging will improve the communication between imager and interventionalists.

Echocardiographic imaging for aortic prostheses is less than ideal. Because of acoustic shadowing of the anterior sewing ring, off-axis imaging (deep esophageal or transgastric views) may be necessary; occasionally transthoracic imaging may be better than transesophageal imaging. Defects in the posterior sewing ring are easily imaged on transesophageal echocardiography. Alternatively intracardiac echocardiography can be used, but the experience with this imaging modality during paravalvular leak closure is more limited. Three dimensional orientation of the valve, places the left sinus of Valsalva anterior and to the right with the right sinus of Valsalva directly posterior (6 o'clock).

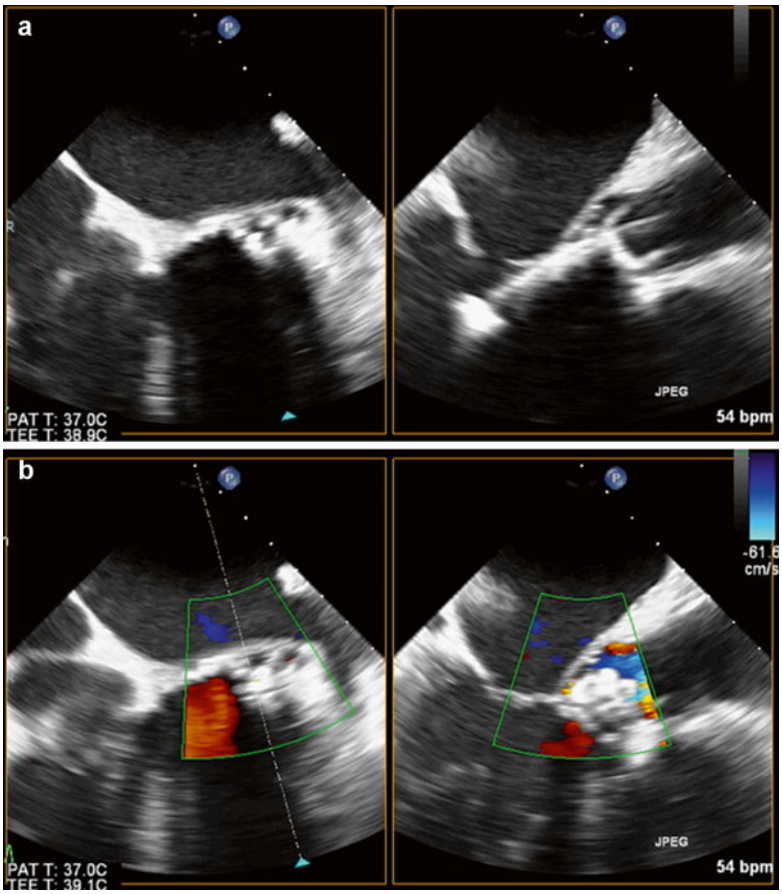

Fig. 7.2 Transesophageal echocardiogram showing the simultaneous multiplane image of the AVP II device being positioned (panel **a**) and resolution of the posterolateral paravalvular regurgitant jet (panel **b**)

Pre-procedural planning for transcatheter closure of paravalvular regurgitation requires a determination of: (a) the number and location of defects; (b) the shape and exact size of the each defect; (c) the distance and orientation of the defect to the sewing ring or prosthesis. This assessment requires extensive two-dimensional and well as three-dimensional transesophageal imaging [11, 17, 24]. The shape and size of the defect determines the choice of device. Long, crescent shaped leaks often require multiple closure devices. Para-aortic leaks tend to be smaller than para-mitral leaks and simultaneous or sequential closure devices are infrequently necessary.

The location of the defect may influence the success of the procedure. Anterolateral para-mitral defects close to the left atrial appendage frequently have a serpiginous superior-to-inferior orientation because of massive left atrial dilation, with the inferior (or left ventricular origin) of the defect located closer to the valve prosthesis. This orientation of the defect may result in tilting of the device after deployment that may not be identified when the device is still attached to the deployment catheter. Once deployed the device may seat 90° to the annular plane, obstructing normal leaflet motion of tilting-disk valve (Fig. 7.5) [18]. This complication may be recognized on fluoroscopy as well. Obstruction or impingement of bioprosthetic leaflets may be more difficult to recognize, but echocardiographic evidence of sudden valvular regurgitation or an increased transvalvular gradient are important clues to this complication. Once deployed in a suboptimal position (or if embolized), removal of the device can be accomplished with a snare or a long, flexible bioptome, thus avoiding the need for open retrieval.

Other procedure-related complications include stroke, hemothorax, device embolization and complications associated with trans-septal puncture. Coronary artery obstruction may occur when para-aortic defects are treated, because devices may protrude over the ostia of the coronary arteries. Theoretically, occlusion of the circumflex artery may occur with posterior mitral prosthetic valve devices. Following device deployment, a full assessment of prosthetic valve function should be performed. This includes (but is not limited to): two- and three-dimensional imaging of the prosthesis to assess function, continuous wave Doppler across the prosthetic orifice for assessment of peak/mean gradients, two- and three-dimensional color Doppler assessment of residual paravalvular regurgitation, effect of device placement on flow in the pulmonary veins as well as pulmonary artery pressures, and residual trans-septal defect.

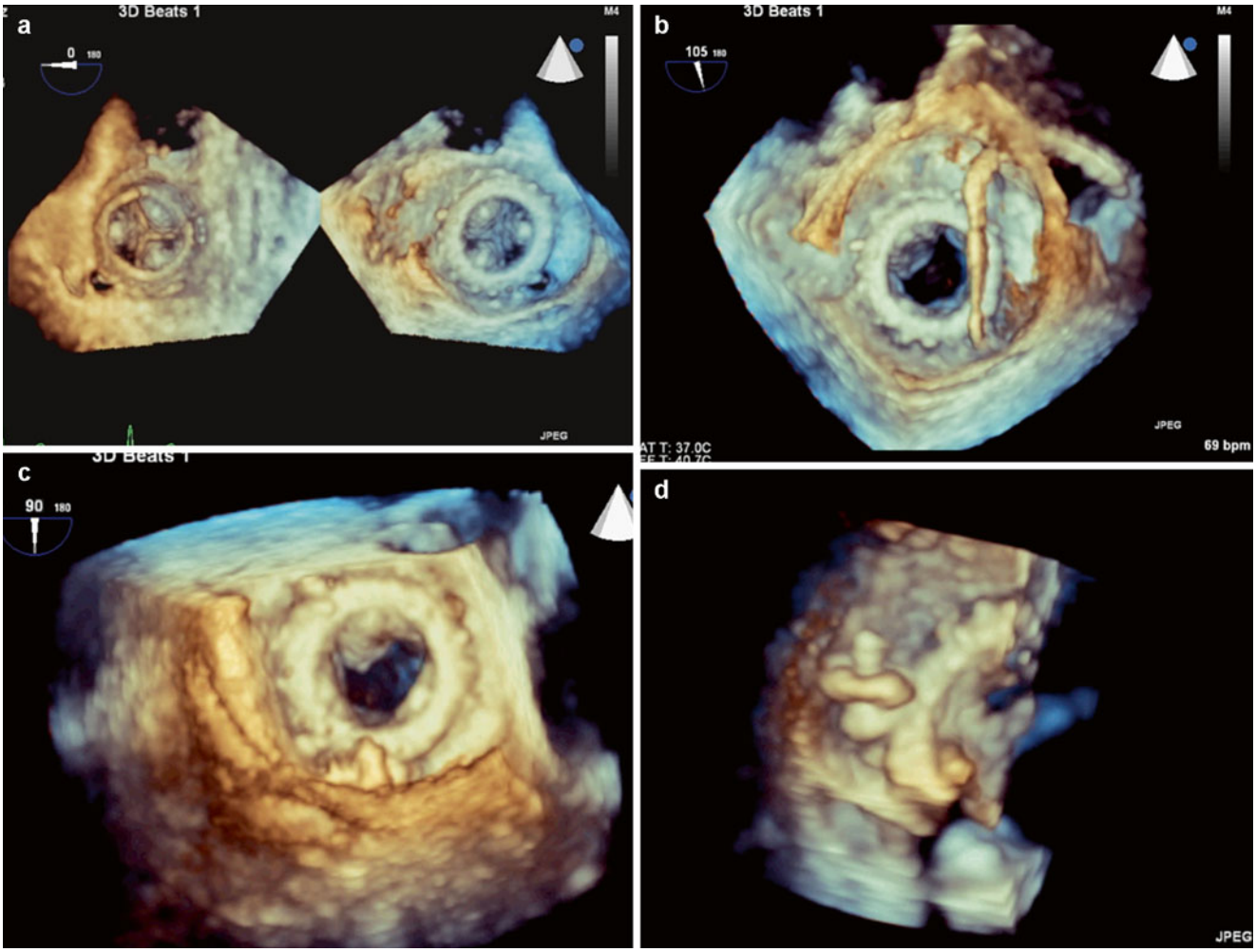

Fig. 7.3 The paravalvular regurgitant lesion is well-imaged at 5 o'clock (panel **a**). An Agilis catheter was introduced via an antegrade, trans-sepal approach (panel **b**) with initial placement of an AVP 4 device (panel **c**). Panel (**d**) shows is a higher magnification of the device, now 90° turned from panel (**c**) for better imaging

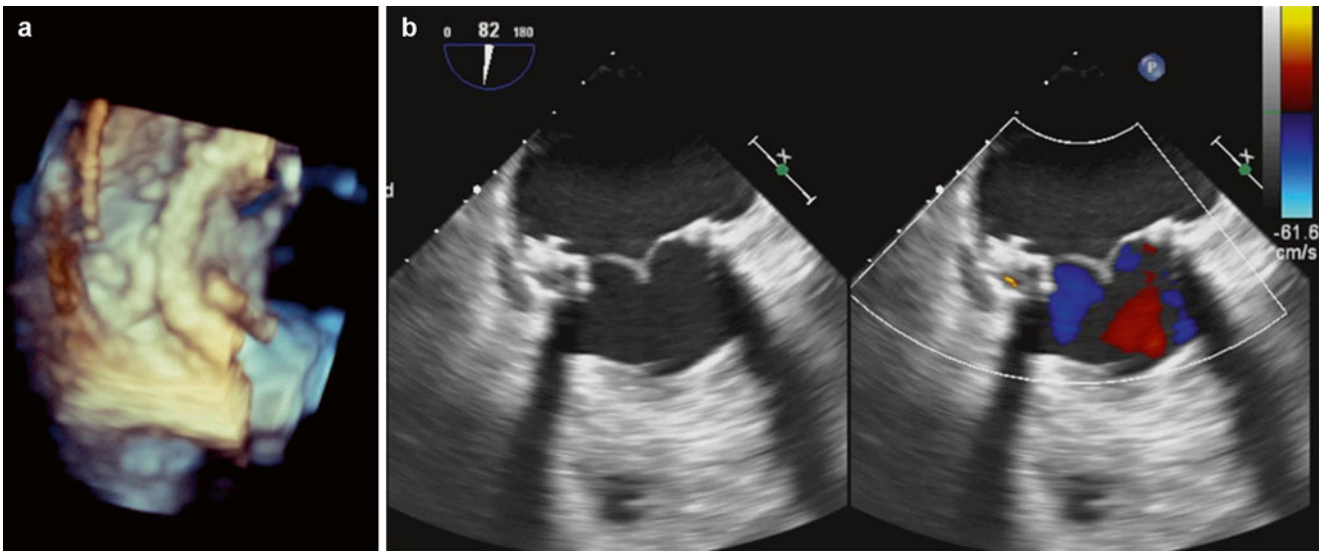

Fig. 7.4 Following re-positioning, the device now is seated against the sewing ring (panel **a**) and color Doppler (panel **b**) shows nearly complete resolution of the paravalvular jet

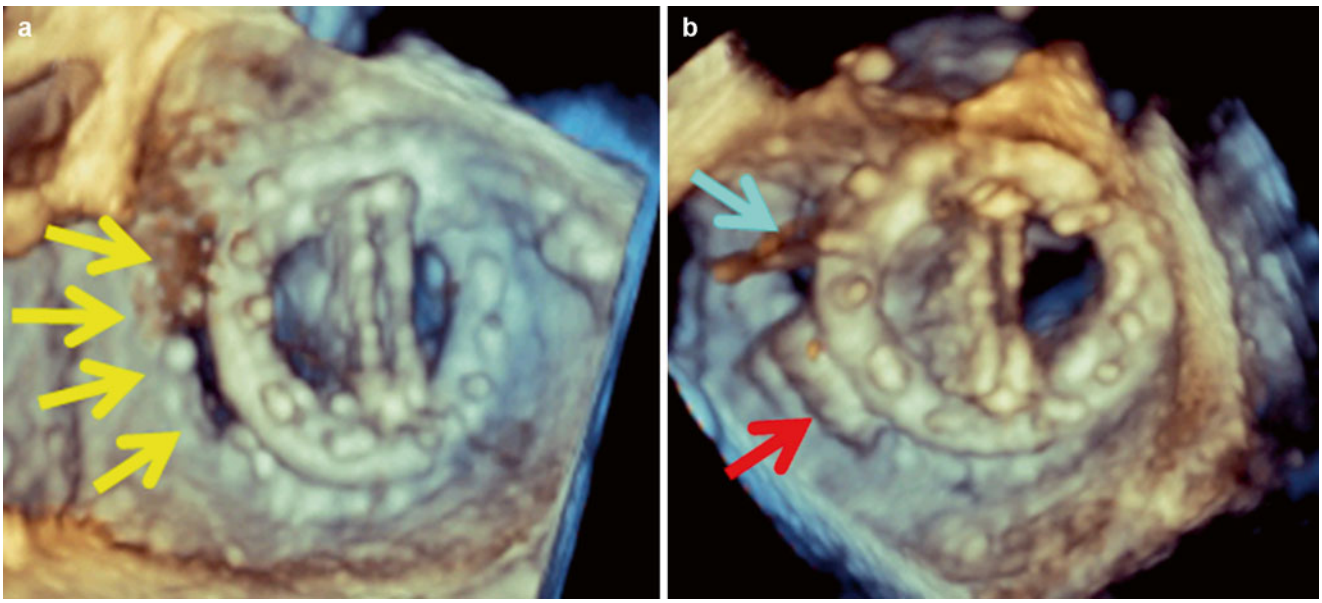

Fig. 7.5 A large anterolateral paravalvular defect is noted (panel **a**, *yellow arrows*) and the deployed AVP 4 closure device turned 90° on release (panel **b**, *red arrow*) resulting in occlusion of the lateral mechanical disc. A snare was positioned (*blue arrow*) to remove the device

References

1. Taramasso M, Maisano F, Latib A, Denti P, Guidotti A, Sticchi A, et al. Conventional surgery and transcatheter closure via surgical transapical approach for paravalvular leak repair in high-risk patients: results from a single-centre experience. Eur Heart J Cardiovasc Imaging. 2014;15(10):1161–7.
2. Nishimura RA, Otto CM, Bonow RO, Carabello BA, Erwin 3rd JP, Guyton RA, et al. 2014 AHA/ACC guideline for the management of patients with valvular heart disease: executive summary: a report of the American College of Cardiology/American Heart Association Task Force on Practice Guidelines. J Am Coll Cardiol. 2014;63(22):2438–88.
3. Hammermeister K, Sethi GK, Henderson WG, Grover FL, Oprian C, Rahimtoola SH. Outcomes 15 years after valve replacement with a mechanical versus a bioprosthetic valve: final report of the Veterans Affairs randomized trial. J Am Coll Cardiol. 2000;36(4):1152–8.
4. Echevarria JR, Bernal JM, Rabasa JM, Morales D, Revilla Y, Revuelta JM. Reoperation for bioprosthetic valve dysfunction. A decade of clinical experience. Eur J Cardiothorac Surg Off J Eur Assoc Cardiothorac Surg. 1991;5(10):523–6. discussion 7.
5. Hourihan M, Perry SB, Mandell VS, Keane JF, Rome JJ, Bittl JA, et al. Transcatheter umbrella closure of valvular and paravalvular leaks. J Am Coll Cardiol. 1992;20(6):1371–7.
6. Moore JD, Lashus AG, Prieto LR, Drummond-Webb J, Latson LA. Transcatheter coil occlusion of perivalvular mitral leaks associated with severe hemolysis. Catheter Cardiovasc Interv Off J Soc Card Angiography Interv. 2000;49(1):64–7.
7. Eisenhauer AC, Piemonte TC, Watson PS. Closure of prosthetic paravalvular mitral regurgitation with the Gianturco-Grifka vascular occlusion device. Catheter Cardiovasc Interv Off J Soc Card Angiography Interv. 2001;54(2):234–8.
8. Webb JG, Pate GE, Munt BI. Percutaneous closure of an aortic prosthetic paravalvular leak with an Amplatzer duct occluder. Catheter Cardiovasc Interv. 2005;65(1):69–72.
9. Nietlispach F, Johnson M, Moss RR, Wijesinghe N, Gurvitch R, Tay EL, et al. Transcatheter closure of paravalvular defects using a purpose-specific occluder. JACC Cardiovasc Interv. 2010;3(7):759–65.
10. Sorajja P, Cabalka AK, Hagler DJ, Rihal CS. Percutaneous repair of paravalvular prosthetic regurgitation: acute and 30-day outcomes in 115 patients. Circ Cardiovasc Interv. 2011;4(4):314–21.
11. Ruiz CE, Jelnin V, Kronzon I, Dudiy Y, Del Valle-Fernandez R, Einhorn BN, et al. Clinical outcomes in patients undergoing percutaneous closure of periprosthetic paravalvular leaks. J Am Coll Cardiol. 2011;58(21):2210–7.
12. Sorajja P, Cabalka AK, Hagler DJ, Rihal CS. Long-term follow-up of percutaneous repair of paravalvular prosthetic regurgitation. J Am Coll Cardiol. 2011;58(21):2218–24.
13. Moscucci M, Deeb GM, Bach D, Eagle KA, Williams DM. Coil embolization of a periprosthetic mitral valve leak associated with severe hemolytic anemia. Circulation. 2001;104(16):E85–6.
14. Pate GE, Al Zubaidi A, Chandavimol M, Thompson CR, Munt BI, Webb JG. Percutaneous closure of prosthetic paravalvular leaks: case series and review. Catheter Cardiovasc Interv Off J Soc Card Angiography Interv. 2006;68(4):528–33.
15. Zoghbi WA, Chambers JB, Dumesnil JG, Foster E, Gottdiener JS, Grayburn PA, et al. Recommendations for evaluation of prosthetic valves with echocardiography and doppler ultrasound: a report From the American Society of Echocardiography's Guidelines and Standards Committee and the Task Force on Prosthetic Valves, developed in conjunction with the American College of Cardiology Cardiovascular Imaging Committee, Cardiac Imaging Committee of the American Heart Association, the European Association of Echocardiography, a registered branch of the European Society of Cardiology, the Japanese Society of Echocardiography and the Canadian Society of Echocardiography, endorsed by the American College of Cardiology Foundation, American Heart Association, European Association of Echocardiography, a registered branch of the European Society of Cardiology, the Japanese Society of Echocardiography, and Canadian Society of Echocardiography. J Am Soc Echocardiogr. 2009;22(9):975–1014. quiz 82–4.
16. Hein R, Wunderlich N, Robertson G, Wilson N, Sievert H. Catheter closure of paravalvular leak. EuroIntervention J EuroPCR Collab Work Group Interv Cardiol Eur Soc Cardiol. 2006;2(3):318–25.

17. Kim MS, Casserly IP, Garcia JA, Klein AJ, Salcedo EE, Carroll JD. Percutaneous transcatheter closure of prosthetic mitral paravalvular leaks: are we there yet? JACC Cardiovasc Interv. 2009;2(2):81–90.
18. Rihal CS, Sorajja P, Booker JD, Hagler DJ, Cabalka AK. Principles of percutaneous paravalvular leak closure. JACC Cardiovasc Interv. 2012;5(2):121–30.
19. Hahn RT. Mitral prosthetic valve assessment by echocardiographic guidelines. Cardiol Clin. 2013;31(2):287–309.
20. Effron MK, Popp RL. Two-dimensional echocardiographic assessment of bioprosthetic valve dysfunction and infective endocarditis. J Am Coll Cardiol. 1983;2(4):597–606.
21. Jelnin V, Dudiy Y, Einhorn BN, Kronzon I, Cohen HA, Ruiz CE. Clinical experience with percutaneous left ventricular transapical access for interventions in structural heart defects a safe access and secure exit. JACC Cardiovasc Interv. 2011;4(8):868–74.
22. Hahn RT, Abraham T, Adams MS, Bruce CJ, Glas KE, Lang RM, et al. Guidelines for performing a comprehensive transesophageal echocardiographic examination: recommendations from the American society of echocardiography and the society of cardiovascular anesthesiologists. J Am Soc Echocardiogr. 2013;26(9):921–64.
23. Lang RM, Badano LP, Tsang W, Adams DH, Agricola E, Buck T, et al. EAE/ASE Recommendations for image acquisition and display using three-dimensional echocardiography. J Am Soc Echocardiogr. 2012;25(1):3–46.
24. Zamorano JL, Badano LP, Bruce C, Chan KL, Goncalves A, Hahn RT, et al. EAE/ASE recommendations for the use of echocardiography in new transcatheter interventions for valvular heart disease. J Am Soc Echocardiogr. 2011;24(9):937–65.

Transcatheter Treatment of Mitral Regurgitation

8

Jacob P. Dal-Bianco

Abstract

Transcatheter mitral valve (MV) repair with the MitraClip safely reduces mitral regurgitation (MR) in patients who are not appropriate for MV surgery. The procedural success of transcatheter MV repair is highly dependent on advanced Echo imaging and team communication. This chapter discusses the basic mechanisms of MR, MitraClip specific MV Echo screening criteria, and offers a detailed, step-by-step approach explaining optimal MitraClip procedure Echo guidance.

Keywords

Mitral regurgitation • Mitral valve • MitraClip • TMVR • Transcatheter • Percutaneous • Repair • Degenerative • Functional • Mitral valve prolapse • Flail

By translating the surgical mitral valve (MV) Alfieri edge-to-edge stitch repair technique [1] to a percutaneous/transcatheter approach [2, 3], the MitraClip (Abbott, Menlo Park, CA) allows for a transcatheter/percutaneous and thus minimally invasive reduction in primary (degenerative) mitral regurgitation (DMR) and secondary (functional/ischemic) MR (FMR) [4–13].

The MitraClip is a 15 mm long, cobalt chromium, two-armed device with gripper arms in the device center that can be independently opened and closed against a set of larger and movable outer arms (Fig. 8.1). This design allows grasping and permanent apposition of sections of the anterior and posterior MV leaflets (MitraClip arm width: 5 mm). Guided by intraprocedural transesophageal echocardiography (TEE) the MitraClip is delivered to the MV from the femoral vein by crossing the interatrial septum with a 24French (8 mm) steerable guide and delivery catheter system (Fig. 8.1). Once the MitraClip is at the desired MV location, the device mechanism allows grasping both MV leaflets repeatedly until MR appears optimally reduced, upon which the device can be detached and permanently deployed.

The MitraClip procedure is safe and hemodynamically well tolerated, but the acute procedural success, the amount and durability of MR reduction, and the increased need for repeat surgical/procedural MR intervention make the MitraClip significantly inferior to MV surgery [4–9]. Successful MitraClip therapy however leads to an immediate improvement in (1) cardiac output and LV loading conditions [14], (2) subsequent favorable left ventricular (LV), mitral annulus (MA) and LA remodeling, and (3) improvement of heart failure (HF) symptoms with a reduction in HF hospitalizations – even when MR remains moderate [5, 6, 8, 11]. Fibrous tissue overgrowth on the MitraClip forms a rigid anterior to posterior MV leaflet bridge overtime [15] that appears to stabilize the anterior – posterior MA dimensions, which probably helps to maintain MR reduction overtime [4, 6]. Importantly however, this fibrous tissue response does not preclude later MV repair if needed [16]. This chapter focuses on the Echo guidance of the MitraClip procedure, and a detailed discussion on the safety and clinical outcomes of the MitraClip therapy can be found elsewhere [17].

Financial Disclosure Nothing to disclose.

J.P. Dal-Bianco, MD, FACC, FASE
Division of Cardiology, Department of Medicine,
Massachusetts General Hospital, Harvard Medical School,
55 Fruit Street, Yawkeyc 5B, Boston, MA 02114, USA
e-mail: jdalbianco@partners.org

M.H. Picard et al. (eds.), *Intraprocedural Imaging of Cardiovascular Interventions*, DOI 10.1007/978-3-319-29428-5_8

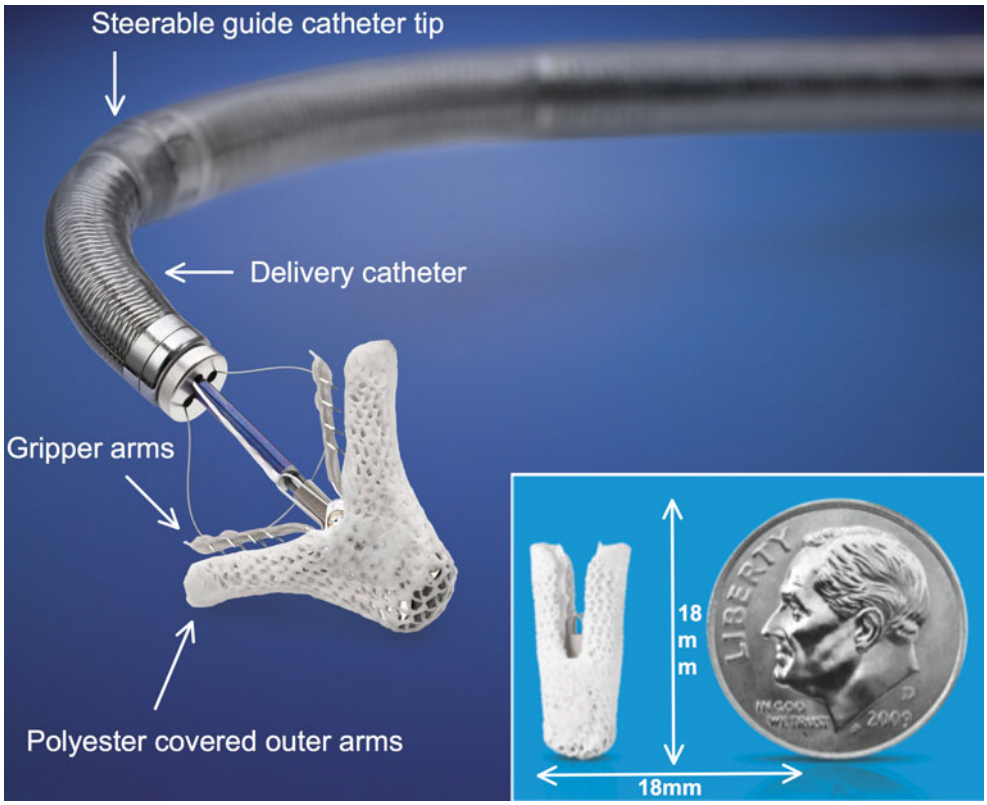

Fig. 8.1 The MitraClip is mounted at the tip of it's delivery catheter, which is advanced into the left atrium via a steerable guide catheter. The MitraClip has a pair of movable polyester covered arms with spiked gripper arms in the device center that can be independently opened and closed. The device length is 15 mm, the arm width is 5 mm, and the device span when fully opened is 20 mm (*inset*, closed MitraClip compared to a US 10 cent coin). The MitraClip can be opened by more than 180°, and completely closed (*inset*) and detached from its delivery catheter once successfully attached to the mitral valve leaflets (*inset*) (Images provided and adapted from Abbott, Menlo Park, CA)

MitraClip Echocardiography Screening

Transthoracic echocardiography (TTE) and three-dimensional (3D) TEE imaging are key to determine MR severity and the predominant mechanism (DMR vs FMR), the anatomic and hemodynamic state of MR-related cardiac remodeling, other significant CV disease and MV "clipability". The very different DMR and FMR mechanisms and leaflet pathology dictate specific Echo MitraClip anatomy screening criteria, as DMR is characterized by excess leaflet motion (e.g. MV leaflet prolapse/flail; Fig. 8.2a–c) and FMR by restricted MV leaflet motion and closure in the setting of LV dilatation and dysfunction (Fig. 8.2d–f) [18].

The most established MitraClip Echo eligibility criteria are based on the inclusion and exclusion criteria from the EVEREST trials (Table 8.1) [4, 5]. With the now worldwide growing MitraClip experience most anatomic criteria have proven less "absolute" – with the major caveat that this development is driven by high volume and thus very experienced MitraClip centers [19, 20]. Nevertheless, extensive MV leaflet calcifications in the grasping area (Fig. 8.3a, b), very immobile/mobile or thick leaflets (Fig. 8.3c) and leaflet clefts (Fig. 8.3d, e) will likely remain unclipable with the current generation MitraClip device.

A critical MitraClip Echo measurement that is used to prevent post-clip mitral stenosis (MS) hemodynamics (Fig. 8.3f) is diastolic MV opening area (MVA) (Fig. 8.4). One MitraClip approximately halves MVA [21, 22], and the currently recommended and established diastolic MVA to prevent MS is 4.0 cm^2 or more. This minimum MVA is usually available in DMR (Fig. 8.4c), but can be a limiting factor in FMR (Fig. 8.4a, b, d). Nevertheless, MitraClips have also been placed with reasonable outcomes in MVA smaller than 4 cm^2 [19].

MitraClip Procedure TEE Guidance

The MitraClip procedure is performed under general anesthesia in the cardiac catheterization lab, and procedure outcomes are critically dependent on advanced 3D-TEE imaging and optimal communication and teamwork between interventional cardiology/surgery and the echocardiographer. MitraClip procedure failure rates for DMR have been reported to be as high as 26 % when compared to FMR, although DMR outcomes have improved significantly with increasing procedural and patient selection experience [4, 5, 20, 23]. A key to this improvement has been the recognition of a need to adapt procedural techniques to account for the differing MR mechanisms and MV leaflet pathologies. The recommended central leaflet (A2/P2) MitraClip placement is motivated by the lack of local chordal leaflet insertions in this region, which minimizes chordal – MitraClip

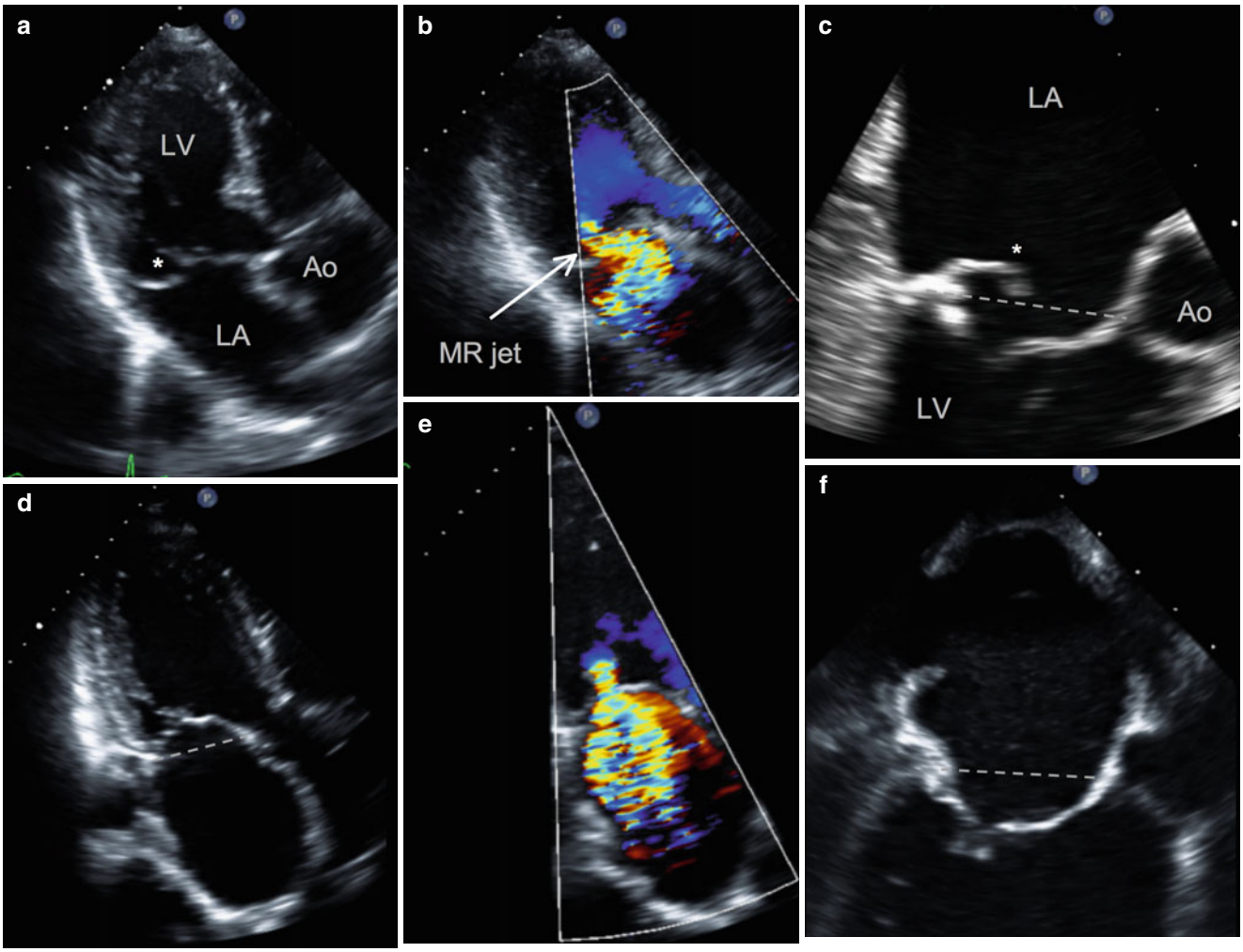

Fig. 8.2 Echo characteristics of degenerative MR (DMR, **a**–**c**) and functional MR (FMR, **d**–**f**). DMR is characterized by impaired mitral valve (MV) coaptation due to excessive leaflet motion in the setting of leaflet prolapse or flail. Panel (**a**) shows a transthoracic echo (TTE) 3-chamber view with the *asterisk* indicating a partially flail posterior leaflet, also shown by transesophageal echo (TEE) with the posterior leaflet breaking the mitral annulus plane towards the left atrium (**c**, *dashed line*). Panel (**b**) shows eccentric, anterior directed mitral regurgitation (*MR*), which is typical for posterior leaflet prolapse or flail. FMR on the other hand is characterized by restricted MV closure motion due to apical leaflet tethering in the setting of left ventricular (*LV*) dilatation or dysfunction (**d**–**f**). These FMR geometric changes result in MV leaflet tip coaptation displaced towards the LV apex as shown by TTE (**d**, *dashed line*) and TEE (**f**, *dashed line*). Once apical MV displacement starts to impair leaflet coaptation, FMR develops with a usually centrally directed jet (**e**). *Ao* aorta, *LA* left atrium, *LV* left ventricle, *MR* mitral regurgitation

Table 8.1 Anatomic MitraClip Echo Criteria

EVEREST trial inclusion criteria [4, 5]
The primary mitral regurgitant jet is noncommissural. If a secondary jet exists, it must be considered clinically insignificant
Mitral valve opening area ≥4.0 cm^2
Minimal calcification in the grasping area
No leaflet cleft in the grasping area
Sufficient leaflet mobility, thickness and length (>10 mm)
DMR: Leaflet flail width <15 mm; Leaflet flail gap <10 mm
FMR: MV coaptation depth <11 mm; MV leaflet tip coaptation length ≥2 mm
Expanded criteria (MitraClip implantation rate 96%) [19]
Mitral valve opening area >2.0 cm^2
Flail width ≤25 mm and flail gap ≤20 mm

entanglement [24, 25]. However, with evolving procedural strategies more lateral (A1/P1) and medial (A3/P3) MR has been treated successfully [26, 27]. The same applies to more extensive MV pathologies including extensive leaflet flails due to chordal or even papillary muscle ruptures [28, 29].

Left Atrium and Left Atrial Appendage Sweep

Prior to interatrial septum (IAS) puncture the LA and left atrial appendage (LAA) should be carefully evaluated for thrombus to minimize the risk of embolization during LA/LAA wire and catheter manipulation. If there is clear evidence for thrombus, then the procedure should be aborted.

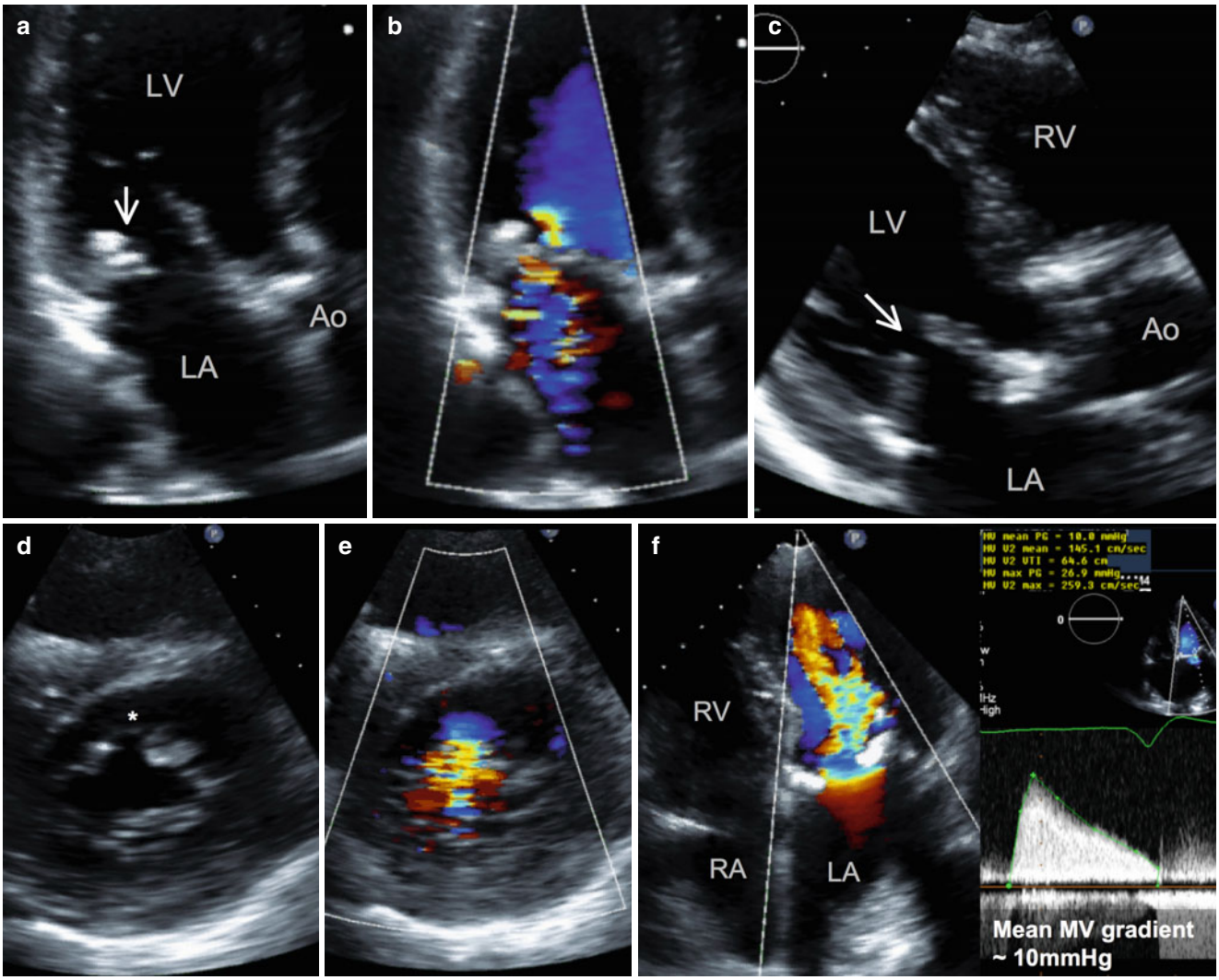

Fig. 8.3 Challenging/unsuitable mitral valve (MV) anatomies. (**a**, **b**) Excessive posterior mitral annulus calcification with a very short and calcified posterior leaflet (**a**, *arrow*), which will prevent/limit a secure MitraClip leaflet grasp. (**c**) Very thick MV leaflets (**c**, *arrow*) can be difficult to grasp by the MitraClip, and may prevent complete closure of the MitraClip. (**d**, **e**) Anterior MV leaflet cleft in a parasternal short axis view (**d**, *asterisk*) with significant MR (**e**). The lack of anterior leaflet tissue prevents MitraClip therapy. (**f**) There is baseline calcific mitral stenosis physiology with a mean MV inflow gradient of 10 mmHg due to close to circumferential mitral annulus calcification. *Ao* aorta, *LA* left atrium, *LV* left ventricle, *MR* mitral regurgitation, *RA* right atrium, *RV* right ventricle

Interatrial Septum Puncture

An optimal IAS puncture location reduces the amount of steerable guide catheter and MitraClip manipulation required to advance the MitraClip into its desired location. The aim of 3D TEE guidance is to help redirecting the Mullins sheath and puncture needle into a central, slighty posterior location (~ Fossa ovalis) about 3.5–4 cm superior to MV leaflet coaptation (Fig. 8.5). Advancing the needle/guidewire through a persistent foramen ovale should be avoided if possible. The Mullins sheath and puncture needle positions can be identified by Echo artifact and IAS tenting towards the LA (Fig. 8.5a–c, arrows, asterisk). The anterior – posterior IAS location can usually be well visualized at a 35–45° transducer angle (Fig. 8.5a) and the superior – inferior IAS location in a bicaval view (Fig. 8.5b). The IAS puncture site to MV leaflet coaptation distance can be visualized at 0° and by flexing the TEE probe with the goal to have both IAS tenting and MV leaflet coaptation in view (Fig. 8.5c). By extrapolating the anticipated intra-LA guidewire path one can approximately measure this distance (Fig. 8.5c, double headed arrows). Once the optimal IAS puncture site has been confirmed in the above views the IAS is punctured and a guidewire advanced into the LA (Fig. 8.5d, arrows).

Guidewire and Steerable Guide Catheter Positioning

The guidewire is then carefully advanced into the left upper pulmonary vein (LUPV) as a safe "parking" location (Fig. 8.6a, b, arrows). Multiple sweeping TEE views/angles

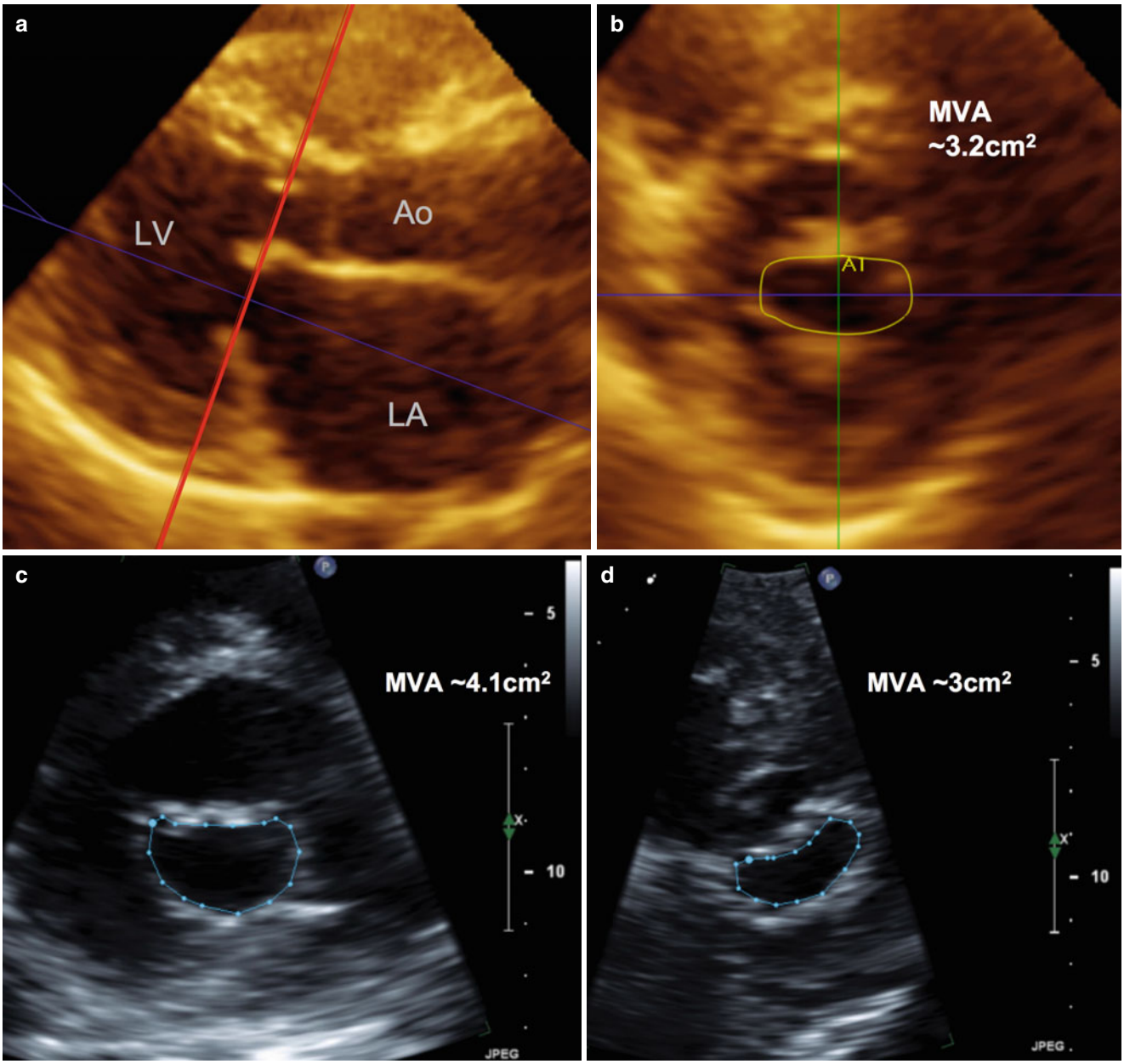

Fig. 8.4 Mitral valve diastolic opening area (*MVA*) assessment. The *upper* panels (**a**, **b**) are derived by cropping a 3D transthoracic echo (TTE) parasternal full volume image into parasternal long axis (**a**) and short axis views (**b**). The advantage of 3D MVA assessment is that it allows to select an optimal plane through the anterior and posterior leaflet tips (**a**, *red line*) at an optimal diastolic time-point. The corresponding short axis view (**b**) allows to measure MVA precisely if image quality is sufficient. The *lower* panels (**c**, **d**) show MVA assessment in 2D TTE short axis views, which – if care was taken to acquire the images at the level of the MV tips – also allows to make reliable measurements. MVA is usually sufficient in degenerative MR (**c**), but can be a limiting factor in functional MR (**a**, **b**, **d**). *Ao* aorta, *LA* left atrium, *LV* left ventricle, *MVA* Mitral valve area

may be required to visualize the wire and its tip to safely guide it into the LUPV, which can usually be visualized in a 60–90° angle view. The LAA should be avoided due to risk of perforation and acute tamponade. Once the guidewire is securely positioned in the LUPV (Fig. 8.6a, b, arrows) the IAS puncture site is pre-dilated (Fig. 8.6c, arrow), and the IAS slowly crossed with the steerable guide catheter tip. This should always be done under direct TEE visualization since the catheter tip may be rotated and/or "jump" with risk for LA wall perforation and acute tamponade. The steerable guide catheter tip can be recognized by its characteristic appearance (Fig. 8.6d, e, arrows) and oftentimes by exiting microbubbles. A safe steerable guide catheter tip LA position is considered to be ~2–3 cm into the LA when measured from the IAS, without contact with any intra-LA structures (Fig. 8.6d, e, arrows).

MitraClip Positioning: Left Atrium

Mounted on the delivery catheter (Fig. 8.1), the MitraClip device is then carefully advanced into the LA via the steerable guide catheter. This procedure step should always be done

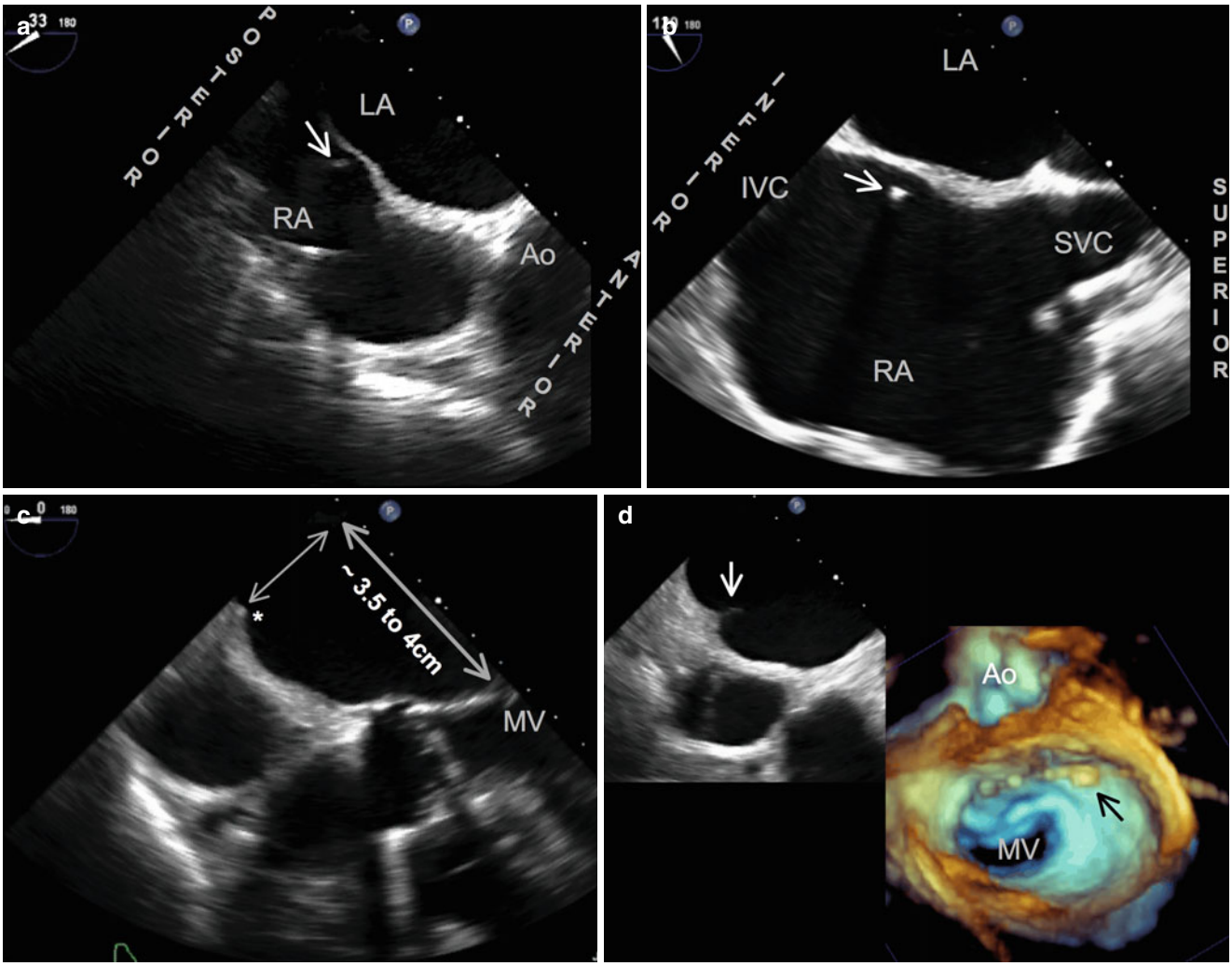

Fig. 8.5 Transesophageal echo (TEE) guidance of optimal interatrial septum (IAS) puncture is a very important step in the MitraClip procedure since it determines the location of the steerable guide catheter tip, which is the starting point for any MitraClip manipulation. A 30–45° TEE view (**a**) allows to visualize the right atrium, IAS, left atrium (*LA*) and aorta, and thus helps to guide anterior – posterior IAS puncture (**a**, *arrow*: needle artifact). Care should be taken to puncture the IAS centrally to posterior, and to avoid the aorta. The bicaval TTE view (**b**) visualizes the inferior and superior vena cavae, and thus superior – inferior IAS puncture location (**b**, *arrow*: needle artifact). The echocardiographer may need to switch briskly between both TEE views multiple times since e.g. anterior – posterior Mullins sheath manipulation may lead to unnoticed changes in the superior – inferior IAS location. Depending on individual cardiac anatomy both TEE views can be simultaneously depicted. Once the desired IAS puncture site has been determined advancing the needle will result in IAS tenting towards the LA (**c**, *asterisk*). Subsequently the TEE imaging aim is to visualize the IAS tenting and MV coaptation locations (usually at 0°) to perpendicular measure their distances from each other (**c**, *thick double headed arrow*). If the distance is ~3.5–4 cm then the IAS is punctured and a guidewire advanced into the LA (**d**, *white and black arrows*). A distance too close or too far away from the MV may make MitraClip positioning and deployment very difficult or impossible due the technical limits of the steerable guide and delivery catheters. *Ao* aorta, *LA* left atrium, *LV* left ventricle, *IVC* inferior vena cava, *MV* mitral valve, *RA* right atrium, *SVC* superior vena cava

under direct TEE visualization since once the MitraClip exits the steerable guide catheter, it may initially point towards a LA wall with risk of perforation and acute tamponade (Fig. 8.7a, arrow). The MitraClip is TEE guided into the LUPV (Fig. 8.7b, arrow) and then, with care to avoid the coumadin ridge (Fig. 8.7c, d, asterisks), is pulled back and oriented towards the MV (Fig. 8.7c, d, arrows; Fig. 8.8a–c, arrows). Under real-time 3D TEE imaging, visualizing the MV from the LA perspective, the MitraClip is then positioned into a central LA position with its tip pointing towards the MV (Fig. 8.8d). Next the MitraClip arms are opened to 180° (Fig. 8.8e) and the device is rotated (if necessary) to a perpendicular arm orientation relative to the MV coaptation line. Based on the leaflet malcoaptation/main MR location and clipping strategy chosen to reduce MR, the same real time 3D TEE view allows the guidance of lateral to medial MitraClip positioning based on its anticipated projected path towards the MV, which is determined by catheter orientation.

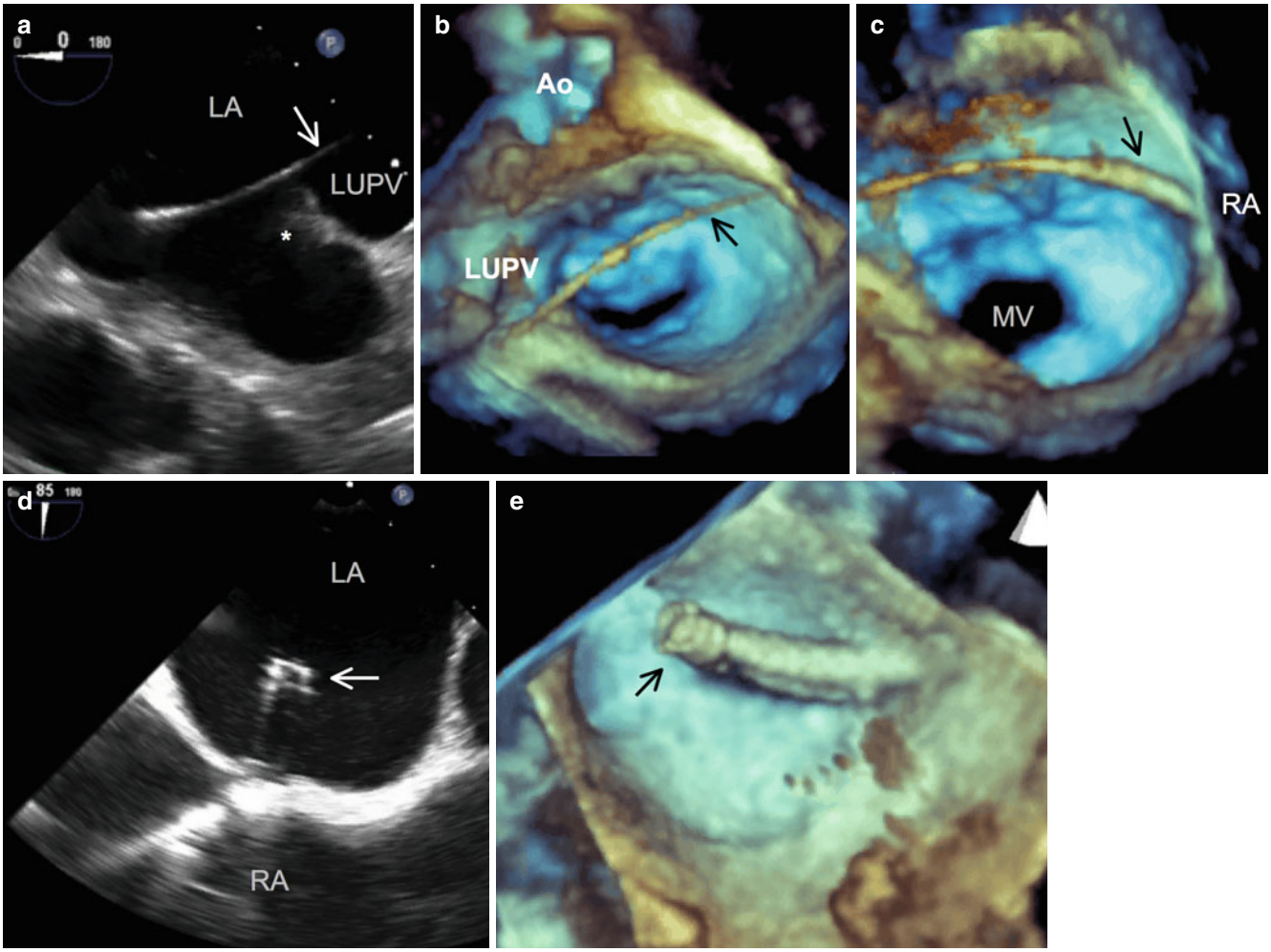

Fig, 8.6 Following interatrial septal (IAS) puncture and under constant TEE visualization, the guidewire (**a**, *arrow*) is then carefully manipulated over the coumadin ridge (**a**, *asterisk*) into the left upper pulmonary vein (*LUPV*, **a**). Real-time 3D TEE imaging from the left atrium (*LA*) perspective allows visualization of the guidewire (**b**, *arrow*) as it crosses the LA. After the IAS puncture site has been pre-dilatated (**c**, *arrow*) the steerable guide catheter is advanced into the LA. Its characteristic tip can be appreciated in 2D (**d**, *arrow*) and 3D TEE (**e**, *arrow*), and should be followed by constant TEE visualization to prevent LA wall injury. *Ao* aorta, *LA* left atrium, *LUPV* left upper pulmonary vein, *MV* mitral valve, *RA* right atrium

Optimal MitraClip arm orientation and positioning is important because once the MitraClip is advanced through the MV into the subvaluvlar MV apparatus any major arm re-orientation or lateral – medial repositioning, especially if the MitraClip targets are not the central A2/P2 scallops, can result in chordal entanglement.

MitraClip Positioning: Mitral Valve Orifice/Left Ventricle

Once the desired MitraClip arm orientation and position have been achieved, the opened MitraClip is advanced towards the MV orifice under TEE guidance. After the MitraClip enters the MV orifice and LV, a bicommissural 60–90° TEE view in combination with simultaneous orthogonal imaging allows optimal visualization of the MitraClip's superior – inferior, medial – lateral (bicommissural view) and anterior – posterior (LV outflow tract view, ~120°) positions. Figure 8.9 explains this 3D TEE approach with bicommissural views in the left panels (Fig. 8.9a, c) and the corresponding orthogonal LV outflow tract planes in the right panels (Fig. 8.9b, d). These are determined in this case by the selected imaging plane through the MitraClip (Fig. 8.9a, c, red lines). Figure 8.9a, b show the MitraClip procedure in DMR and Fig. 8.9c, d in FMR. Note the difference in systolic MV leaflet position relative to the opened MitraClip arms (Fig. 8.9b partially flail posterior leaflet versus bileaflet MV tenting in Fig. 8.9d. The simultaneous orthogonal 3D TEE imaging approach also enables verification that the MitraClip arm orientation – once within the LV – is maintained since the arms are not visible in the bicommissural view (Fig. 8.9a, c), but well visualized in the orthogonal planes (Fig. 8.9b, d). Another approach to verify

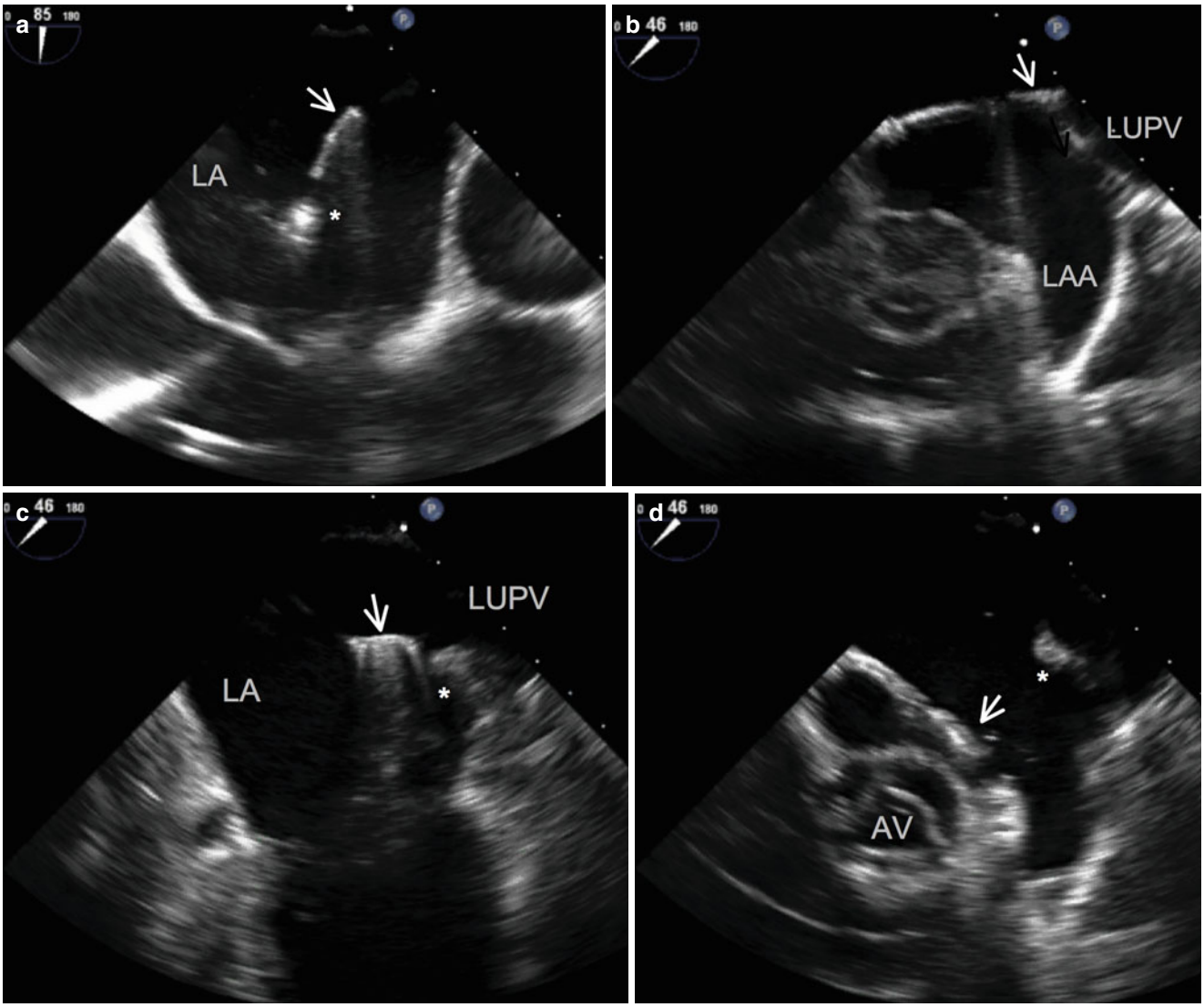

Fig. 8.7 Once the steerable guide catheter is securely positioned, the delivery catheter with the MitraClip at its tip is advanced into the left atrium (*LA*). Advancing the delivery system may lead to steerable guide catheter tip repositioning, and thus its position should be monitored by TEE. Once the MitraClip (**a**, *arrow*) exits the steerable guide catheter tip (**a**, *asterisk*), the TEE imaging focus is to always keep the MitraClip in view and to safely guide it into the left upper pulmonary vein (*LUPV*, **b**, *arrow*). Once in the LUPV and always guided by TEE, the steerable guide and delivery catheters are then manipulated to redirect the MitraClip past the coumadin ridge (**c**, **d**, *asterisks*). *AV* aortic valve, *LA* left atrium, *LAA* left atrial appendage, *LUPV* left upper pulmonary vein

intra-LV MitraClip arm orientation is the real-time 3D-TEE view with gains reduced to visualize the MitraClip below the level of the MV leaflets (Fig. 8.9e, arrow).

MitraClip Leaflet Grasping and Deployment

Once optimal MitraClip position (guided by the MV leaflet malcoaptation/main MR location/procedural strategy) has been confirmed by TEE (Fig. 8.10a, b), the open MitraClip is slowly pulled back towards the LA with the aim to catch and grasp the anterior and posterior leaflet tips (Fig. 8.10c, d). This process can be more challenging in DMR than FMR (Fig. 8.9a–d), and is dependent on the extent and mobility of the MV leaflets and the procedural experience of the MitraClip team. Once TEE imaging confirms that both MV leaflets tips have reduced mobility and appear "wedged" into the MitraClip, the gripper arms are lowered against the outer arms to grasp and secure the leaflets (Fig. 8.10d, arrow) and then the device slowly closed (Fig. 8.10f, arrow). Grabbing enough leaflet tissue is very important for the quality and durability of the grasp, and to reduce the risk of short and long term partial or complete MitraClip detachment. When in doubt, repeated leaflet grasping attempts should be made as outlined above. A leaflet grasp "stress test" can be performed by increasing LV afterload with vasopressors for a

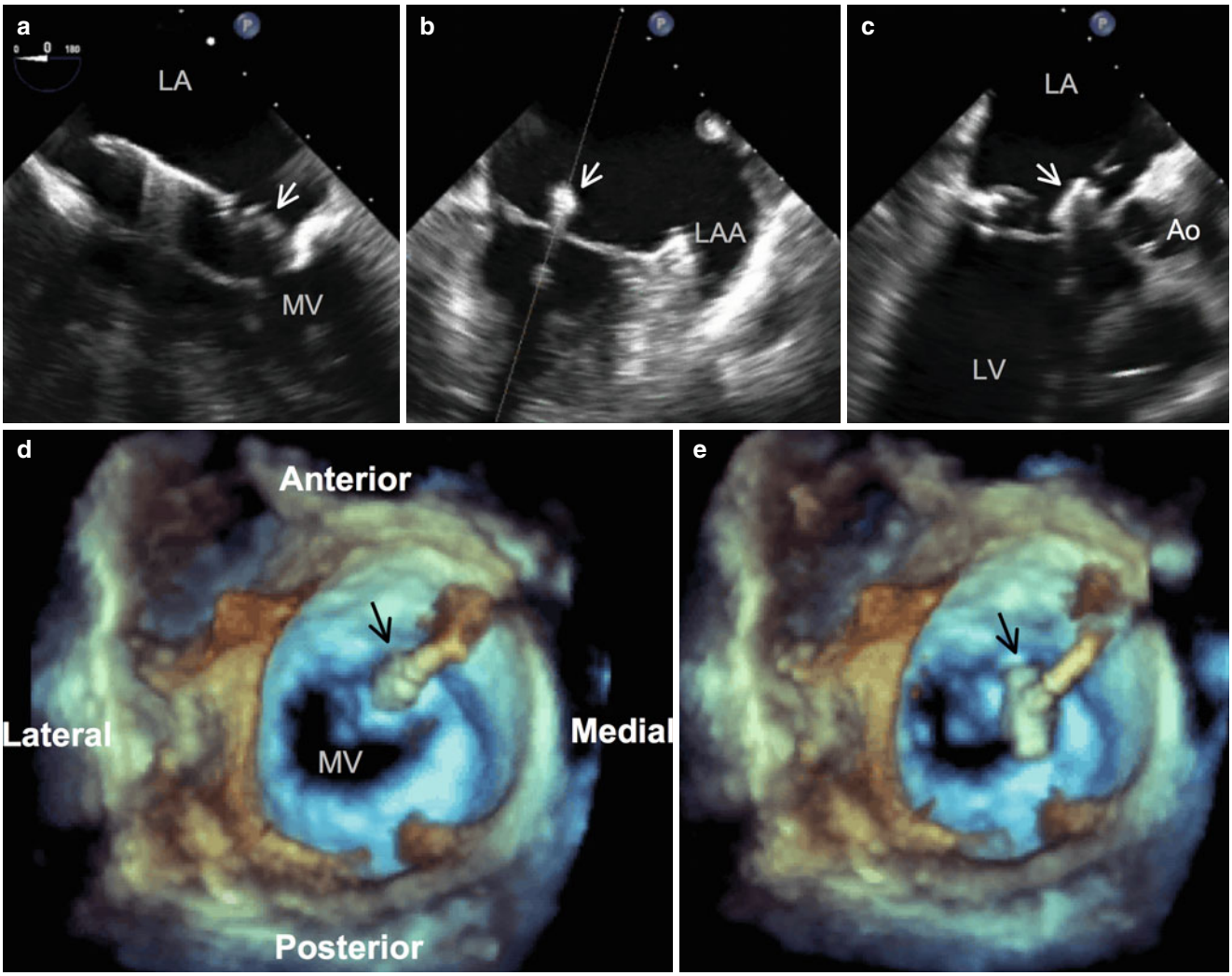

Fig. 8.8 The MitraClip is redirected towards the mitral valve (**a**–**c**, *arrows*). Real-time 3D-TEE of the MV from the LA perspective allows optimal visualization of the MitraClip in the left atrium (**d**, *arrow*) and to verify its open arm orientation (**e**, *arrow*). A common start is to orient the MitraClip arms perpendicular to the presumed mitral valve (*MV*) coaptation line at the mitral regurgitation target area; clock or counter clockwise MitraClip rotation can be easily guided in this 3D-TEE view. *Ao* aorta, *LA* left atrium, *LAA* left atrial appendage, *LUPV* left upper pulmonary vein, *LV* left ventricle, *MV* mitral valve

short duration. A good MitraClip grasp results in much reduced local anterior and posterior leaflet motion (Fig. 8.10f), and the formation of a stable double orifice MV (Fig. 8.11a). Color Doppler imaging allows for the rapid visualization of MR reduction, and the location of remaining MR (Fig. 8.11b). Other echo evidence for reduced MR severity is a change in PV inflow pattern indicating reduced LA filling pressures (Fig. 8.11c). Once there is convincing evidence for significant MR reduction in the setting of a sufficient leaflet grasp, the LA to LV inflow gradients through both the lateral and medial neo-MV orifices are measured with Echo Doppler (Fig. 8.11d, e). An averaged gradient ≥5 mmHg should probably be avoided [22], but is unlikely in the setting of one MitraClip if the starting MVA was sufficient, and the MR reduction significant (trans-MV gradient is flow dependent). Over the long-term, the post-MitraClip gradients usually remain stable [6]. If clip position by imaging and hemodynamics by Doppler are satisfactory, the MitraClip can be deployed and permanently detached from the delivery catheter (Figs. 8.1 and 8.11a, asterisk) and the catheter carefully pulled out of the LA under TEE guidance.

Additional MitraClip Deployment

The total number of MitraClips deployed is motivated by optimal MR reduction and limited by creating MS hemodynamics. Other factors that may prompt consideration of placing additional MitraClips in order to reduce "wear and tear" of leaflets or device erosion, even if MR appears optimally

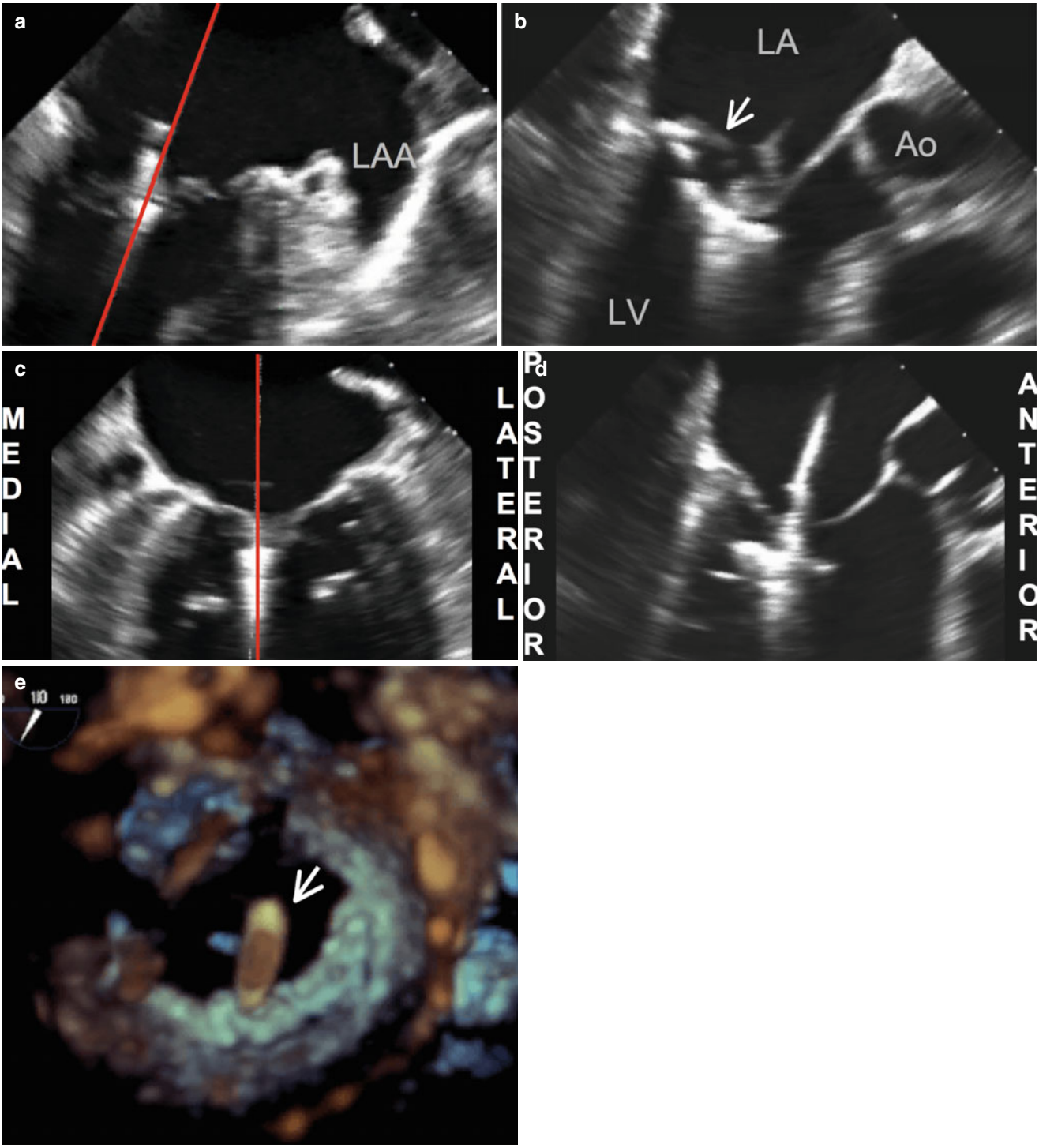

Fig. 8.9 Guidance of MitraClip positioning and deployment can be greatly facilitated by using standardized simultaneous TEE imaging with a bicommissural reference view (**a**, **c**) and an orthogonal LV outflow tract view (**b**, **d**) determined by the chosen plane (**a**, **c**, *red lines*). This TEE imaging approach allows to effectively and rapidly assess main mitral regurgitation pathology and MitraClip position in relationship to the mitral valve (MV) lateral (A1/P1), central (A2/P2) and medial (A3/P3) scallops. Panels (**a**, **b**) show a patient with degenerative MR (DMR) and panels (**c**, **d**) a patient with functional MR (FMR). Note the difference of the systolic MV leaflet positions with a partial flail posterior leaflet (P2) in DMR (**b**, *arrow*) versus bileaflet MV tethering in FMR (**d**). The leaflet grasping process can be easier in FMR, since the tethered leaflet configuration dovetails with the open MitraClip arms (**d**). Besides simultaneous multiplane TEE 2D imaging, a real time 3D TEE view from the left atrium with much reduced gains can be very helpful to determine MitraClip arm orientation once the MitraClip is positioned in the left ventricle (**e**, *arrow*). *Ao* aorta, *LA* left atrium, *LAA* left atrial appendage, *LV* left ventricle

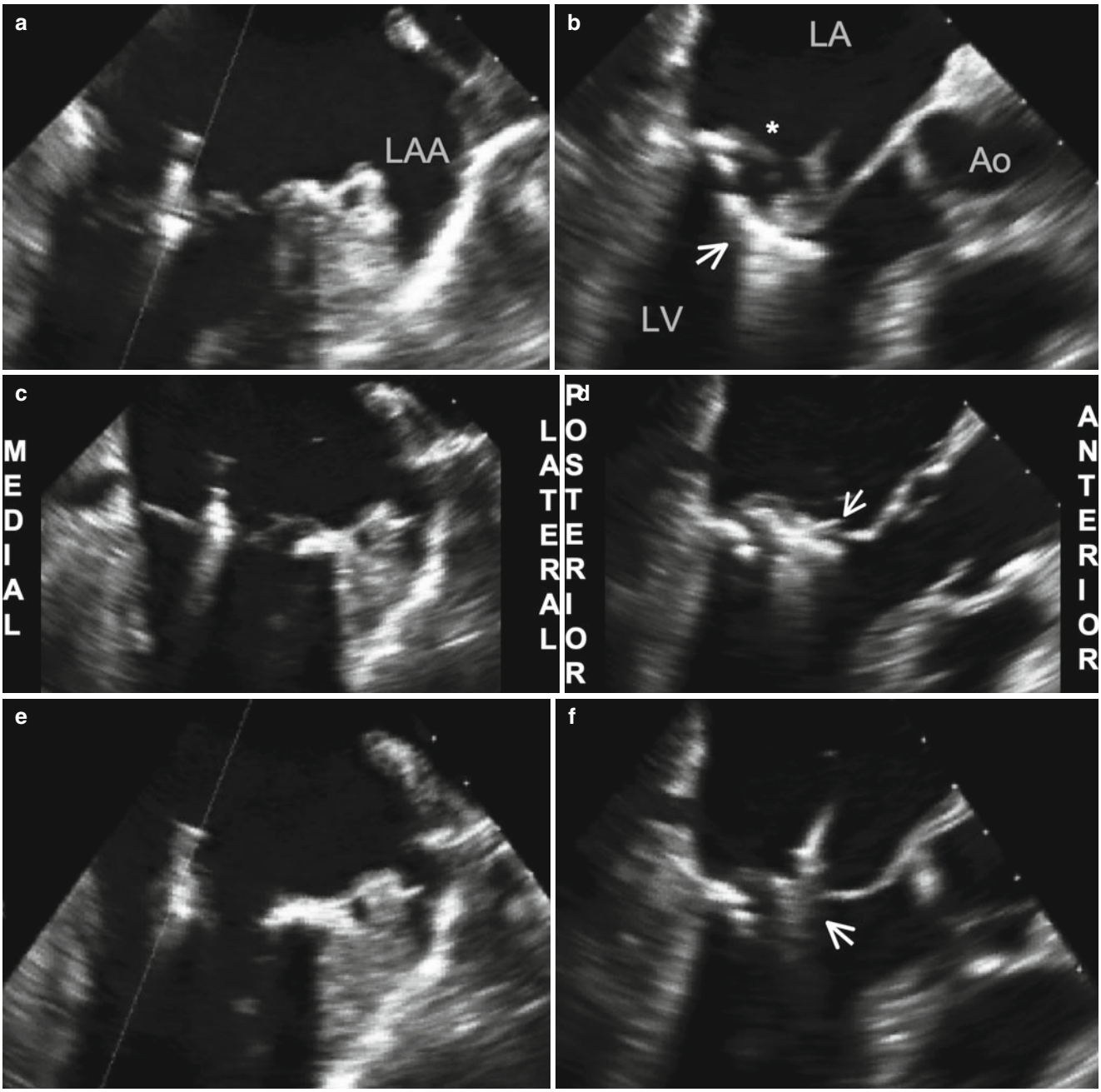

Fig. 8.10 Simultaneous multi-plane TEE imaging guidance of MitraClip positioning and deployment in degenerative mitral regurgitation. The opened MitraClip is advanced into the left ventricle (LV), and maintained correct device arm alignment/orientation can be verified by minimal MitraClip visualization in the bicommissural view (**a**), and maximum device arm span in the orthogonal LV outflow tract view (**b**). The MitraClip arms (**b**, *arrow*) are aligned to grasp the central portions of the anterior (A2) and flail posterior (P2) leaflet (**b**, *asterisk*). The MitraClip delivery catheter is then slowly pulled back towards the LA with the aim to grasp/catch the moving leaflets, which when caught show reduced/arrested leaflet tip motion (**d**). Following, the gripper arms (**d**, *arrow*) are closed against the outer arms to "sandwich" the leaflets, the leaflet grasp confirmed and the MitraClip slowly closed (**f**, *arrow*). *Ao* aorta, *LA* left atrium, *LAA* left atrial appendage, *LV* left ventricle

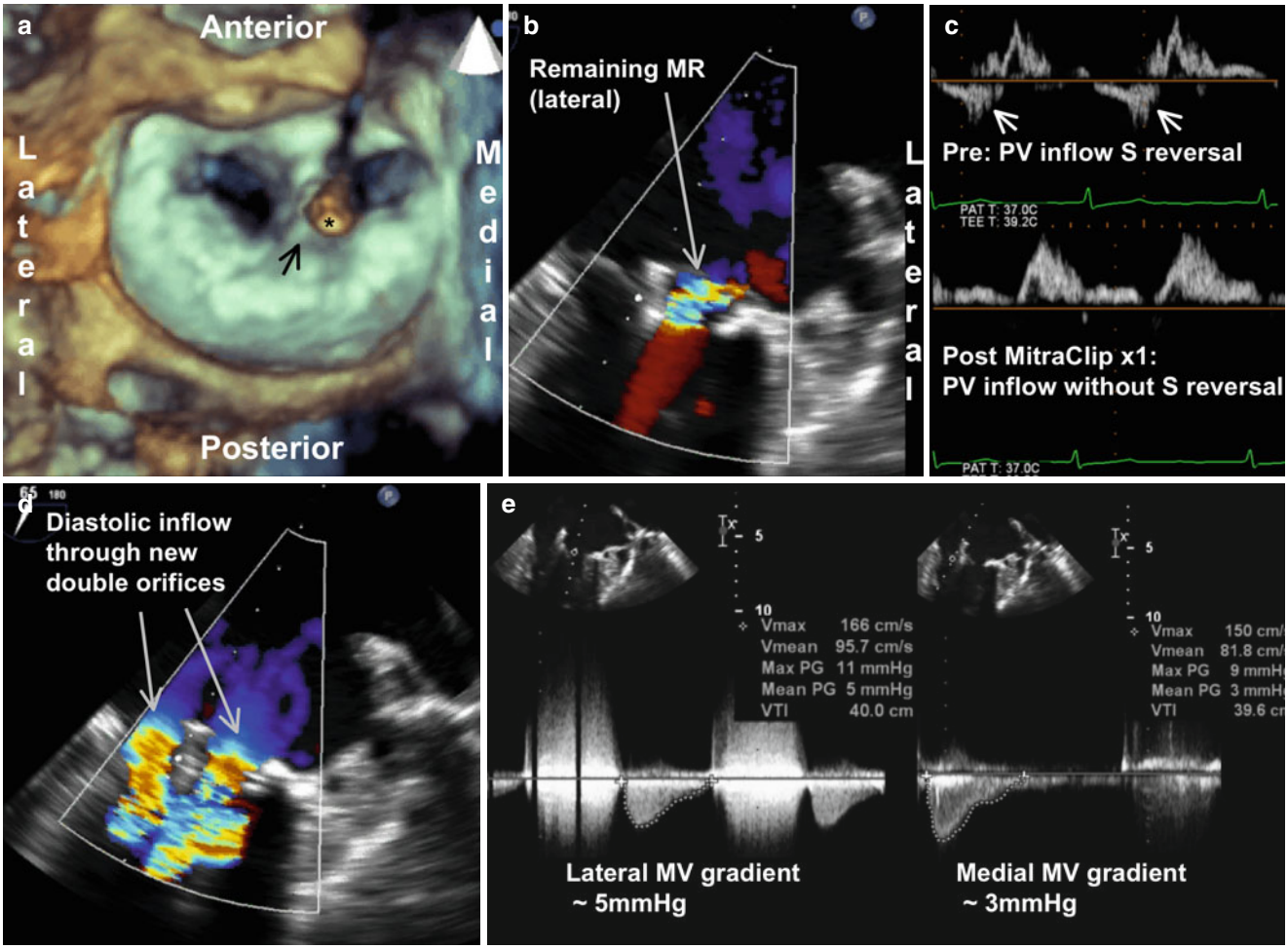

Fig. 8.11 A real-time 3D TEE view confirms the creation of a double orifice mitral valve (**a**) with the MitraClip forming a central anterior – posterior leaflet bridge (**a**, *arrow*). With the MitraClip still attached to its delivery catheter (**a**, *asterisk*) remaining mitral regurgitation (MR) is assessed in a bicommissural TEE view with color Doppler (**b**). Overall reduction of MR can be supported by a change in pulmonary vein inflow from pre to post MitraClip deployment (**c**). Diastolic mitral valve inflow is visualized in the same view (**d**) and Doppler is used to measure the medial and lateral MV neo-orifice gradients (**e**). Once the decision is made to permanently deploy the MitraClip, the delivery system is removed (under TEE guidance) and above color Doppler and Doppler assessments repeated. *MR* mitral regurgitation, *PV* pulmonary vein

treated, can be the echocardiographic leaflet tissue appearance, MitraClip device mobility and stability relative to the MV, and associated leaflet mobility next to the MitraClip. This applies especially to DMR MVs which can have a wide spectrum of leaflet anatomy and tissue characteristics ranging from thin ("Fibroelastic deficiency"/FED [30, 31]) to thick myxomatous leaflets ("Barlow's disease" [32]). The EVEREST MitraClip trials appear to have included both of these leaflet pathologies equally. In clinical practice – at least in the US – there is likely to be a therapy shift toward FED MVs since the current FDA approved DMR MitraClip indication is limited to prohibitive surgical risk patients, who are usually older patients and thus more likely to have FED. In more recent DMR MitraClip studies including older and higher risk patients there now appears an increasing trend for the use of two MitraClips [7, 8, 23], which may be prompted by experience and concerns for MitraClip gripping quality, fibrous tissue response and overall durability of MitraClip repair in DMR. FMR leaflets, on the other hand, are usually thick and fibrotic and restricted in motion and thus less likely to "wear & tear" overtime [33], even in the setting of one MitraClip.

If the decision is made to place an additional MitraClip, a new delivery system (Fig. 8.1) is advanced through the steerable guide catheter into the LA and the MitraClip positioning steps are repeated as above. Bicommissural and simultaneous orthogonal plane TEE imaging with both color Doppler (Fig. 8.12a, b) and 2D (Fig. 8.12c, d) modalities will help to establish the MR location and MV anatomy. In this patient there was remaining significant lateral MR

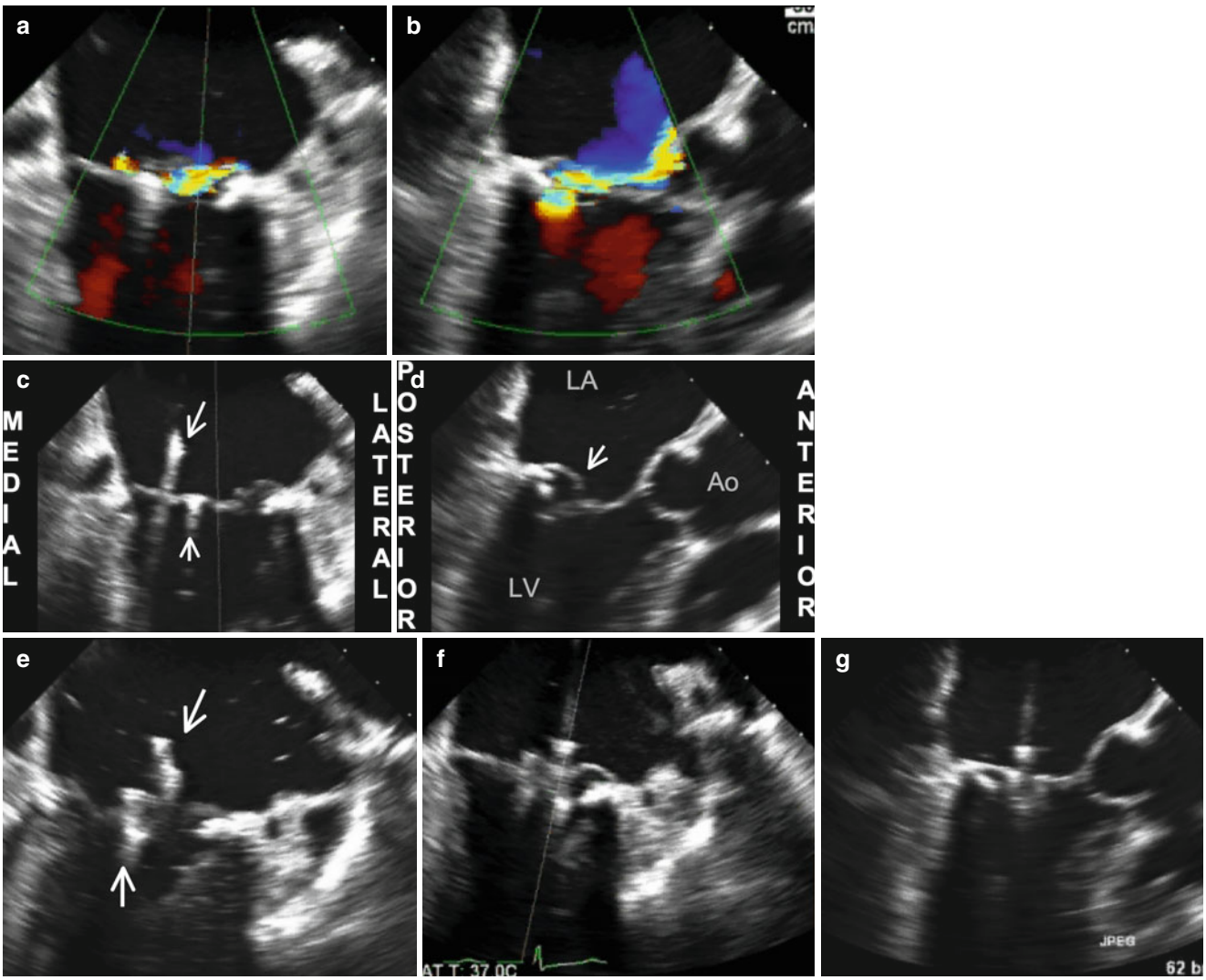

Fig. 8.12 Remaining significant mitral regurgitation (MR) after initial MitraClip deployment (**a**, **b**) can be treated with another MitraClip if there are no concerns creating mitral stenosis hemodynamics. An additional MitraClip (**c**, *long arrow*) is – after open device arm orientation has been optimized as outlined previously– carefully navigated towards the mitral valve (MV) target area in its closed configuration (**d**), avoiding direct contact with the prior placed MitraClip (**c**, *short arrow*; **e**, *arrows*). The MV leaflets are then grasped as outlined previously (**f**) and the MitraClip closed (**g**). *Ao* aorta, *LA* left atrium, *LV* left ventricle

(Fig. 8.12a) due to a partially flail (lateral) posterior leaflet (Fig. 8.12d, arrow). After confirming open MitraClip arm orientation by 3D-TEE, the MitraClip is re-closed before it is carefully advanced towards the MV (Fig. 8.12c, longer arrow) with the aim to avoid direct contact with the prior deployed MitraClip (Fig. 8.12c, shorter arrow, e). Once the second MitraClip has been advanced into the LV below the level of the MV its arms are opened and the device pulled back to grasp the leaflets (Fig. 8.12f, g). Simultaneous orthogonal 2D and real-time 3D-TEE imaging (Fig. 8.9e) can be very helpful to assess and carefully adjust intra-LV MitraClip arm orientation. Once a sufficient MV leaflet grasp has been confirmed the MitraClip arms are closed, and remaining MR visualized by color Doppler (Fig. 8.13a, b). As previously mentioned, the PV inflow Doppler pattern provides supporting information regarding MR reduction (Fig. 8.13c). If there is convincing evidence for optimal MR reduction in the setting of a sufficient leaflet grasp, the MV gradients through the neo-MV orifices are re-measured (Fig. 8.13d). If deemed acceptable, the MitraClip is deployed (Fig. 8.13e) and the catheter system carefully removed. At completion, the post-procedure atrial septal defect and absence or presence of pericardial effusion are documented.

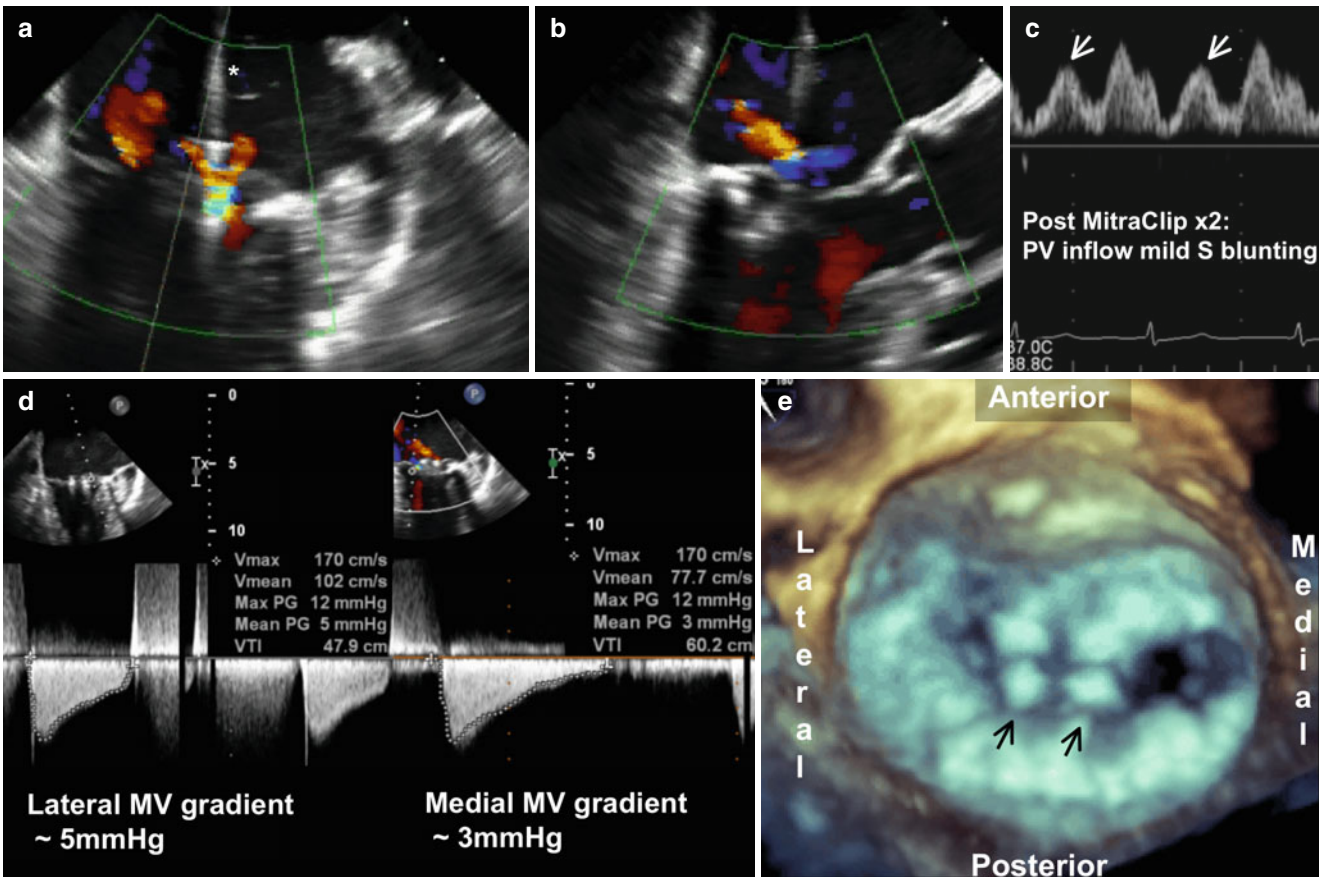

Fig. 8.13 With the MitraClip still attached to its delivery catheter (**a**, *asterisk*), remaining mitral regurgitation (MR) is assessed with color Doppler (**b**), and improvement of MR confirmed by a change in pulmonary vein inflow (**c**). Final diastolic mitral valve inflow gradients through the medial and lateral neo-orifices are assessed (**d**), and if acceptable the MitraClip deployed. Panel (**e**) shows a real-time 3D TEE LA view with 2 central MitraClips (*arrows*). *MR* mitral regurgitation, *PV* pulmonary vein

Summary/Conclusions

Transcatheter MV repair with the MitraClip safely reduces MR, but its success strongly depends on echo imaging to optimally guide patient selection and the actual MitraClip procedure. An understanding of cardiac anatomy and advanced skills in 2D and 3D TEE imaging are critical. Lastly the ability to communicate the echo findings to the interventional/surgical team in a clear and consistent manner is important.

References

1. Fucci C, Sandrelli L, Pardini A, Torracca L, Ferrari M, Alfieri O. Improved results with mitral valve repair using new surgical techniques. Eur J Cardiothorac Surg. 1995;9(11):621–6; discuss 626–7.
2. St Goar FG, Fann JI, Komtebedde J, Foster E, Oz MC, Fogarty TJ, Feldman T, Block PC. Endovascular edge-to-edge mitral valve repair: short-term results in a porcine model. Circulation. 2003;108(16):1990–3.
3. Fann JI, St Goar FG, Komtebedde J, Oz MC, Block PC, Foster E, Butany J, Feldman T, Burdon TA. Beating heart catheter-based edge-to-edge mitral valve procedure in a porcine model: efficacy and healing response. Circulation. 2004;110(8):988–93.
4. Feldman T, Kar S, Rinaldi M, Fail P, Hermiller J, Smalling R, Whitlow PL, Gray W, Low R, Herrmann HC, Lim S, Foster E, Glower D. Percutaneous mitral repair with the MitraClip system: safety and midterm durability in the initial EVEREST (Endovascular Valve Edge-to-Edge REpair Study) cohort. J Am Coll Cardiol. 2009;54(8):686–94.
5. Feldman T, Foster E, Glower DD, Kar S, Rinaldi MJ, Fail PS, Smalling RW, Siegel R, Rose GA, Engeron E, Loghin C, Trento A, Skipper ER, Fudge T, Letsou GV, Massaro JM, Mauri L. Percutaneous repair or surgery for mitral regurgitation. N Engl J Med. 2011;364(15):1395–406.
6. Mauri L, Foster E, Glower DD, Apruzzese P, Massaro JM, Herrmann HC, Hermiller J, Gray W, Wang A, Pedersen WR, Bajwa T, Lasala J, Low R, Grayburn P, Feldman T. 4-year results of a randomized controlled trial of percutaneous repair versus surgery for mitral regurgitation. J Am Coll Cardiol. 2013;62(4):317–28.
7. Reichenspurner H, Schillinger W, Baldus S, Hausleiter J, Butter C, Schaefer U, Pedrazzini G, Maisano F. Clinical outcomes through 12 months in patients with degenerative mitral regurgitation treated with the MitraClip(R) device in the ACCESS-EUrope Phase I trial. Eur J Cardiothorac Surg. 2013;44(4):e280–8.
8. Lim DS, Reynolds MR, Feldman T, Kar S, Herrmann HC, Wang A, Whitlow PL, Gray WA, Grayburn P, Mack MJ, Glower DD. Improved

functional status and quality of life in prohibitive surgical risk patients with degenerative mitral regurgitation after transcatheter mitral valve repair. J Am Coll Cardiol. 2014;64(2):182–92.
9. Feldman T, Foster E, Qureshi M, Whisenant B, Williams J, Glower D, Mauri L. TCT-788 The EVEREST II Randomized Controlled Trial (RCT): three year outcomes. J Am Coll Cardiol. 2012. 60(17_S):B229.
10. Whitlow PL, Feldman T, Pedersen WR, Lim DS, Kipperman R, Smalling R, Bajwa T, Herrmann HC, Lasala J, Maddux JT, Tuzcu M, Kapadia S, Trento A, Siegel RJ, Foster E, Glower D, Mauri L, Kar S. Acute and 12-month results with catheter-based mitral valve leaflet repair: the EVEREST II (Endovascular Valve Edge-to-Edge Repair) High Risk Study. J Am Coll Cardiol. 2012;59(2):130–9.
11. Grayburn PA, Foster E, Sangli C, Weissman NJ, Massaro J, Glower DG, Feldman T, Mauri L. Relationship between the magnitude of reduction in mitral regurgitation severity and left ventricular and left atrial reverse remodeling after MitraClip therapy. Circulation. 2013;128(15):1667–74.
12. Maisano F, Franzen O, Baldus S, Schafer U, Hausleiter J, Butter C, Ussia GP, Sievert H, Richardt G, Widder JD, Moccetti T, Schillinger W. Percutaneous mitral valve interventions in the real world: early and 1-year results from the ACCESS-EU, a prospective, multicenter, nonrandomized post-approval study of the MitraClip therapy in Europe. J Am Coll Cardiol. 2013;62(12):1052–61.
13. Baldus S, Schillinger W, Franzen O, Bekeredjian R, Sievert H, Schofer J, Kuck KH, Konorza T, Mollmann H, Hehrlein C, Ouarrak T, Senges J, Meinertz T. MitraClip therapy in daily clinical practice: initial results from the German transcatheter mitral valve interventions (TRAMI) registry. Eur J Heart Fail. 2012;14(9):1050–5.
14. Siegel RJ, Biner S, Rafique AM, Rinaldi M, Lim S, Fail P, Hermiller J, Smalling R, Whitlow PL, Herrmann HC, Foster E, Feldman T, Glower D, Kar S. The acute hemodynamic effects of MitraClip therapy. J Am Coll Cardiol. 2011;57(16):1658–65.
15. Ladich E, Michaels MB, Jones RM, McDermott E, Coleman L, Komtebedde J, Glower D, Argenziano M, Feldman T, Nakano M, Virmani R. Pathological healing response of explanted MitraClip devices. Circulation. 2011;123(13):1418–27.
16. Argenziano M, Skipper E, Heimansohn D, Letsou GV, Woo YJ, Kron I, Alexander J, Cleveland J, Kong B, Davidson M, Vassiliades T, Krieger K, Sako E, Tibi P, Galloway A, Foster E, Feldman T, Glower D. Surgical revision after percutaneous mitral repair with the MitraClip device. Ann Thorac Surg. 2010;89(1):72–80; discussion p 80.
17. Beigel R, Wunderlich NC, Kar S, Siegel RJ. The evolution of percutaneous mitral valve repair therapy: lessons learned and implications for patient selection. J Am Coll Cardiol. 2014;64(24):2688–700.
18. Levine RA, Schwammenthal E. Ischemic mitral regurgitation on the threshold of a solution: from paradoxes to unifying concepts. Circulation. 2005;112(5):745–58.
19. Franzen O, Baldus S, Rudolph V, Meyer S, Knap M, Koschyk D, Treede H, Barmeyer A, Schofer J, Costard-Jackle A, Schluter M, Reichenspurner H, Meinertz T. Acute outcomes of MitraClip therapy for mitral regurgitation in high-surgical-risk patients: emphasis on adverse valve morphology and severe left ventricular dysfunction. Eur Heart J. 2010;31(11):1373–81.
20. Lubos E, Schluter M, Vettorazzi E, Goldmann B, Lubs D, Schirmer J, Treede H, Reichenspurner H, Blankenberg S, Baldus S, Rudolph V. MitraClip therapy in surgical high-risk patients: identification of echocardiographic variables affecting acute procedural outcome. JACC Cardiovasc Interv. 2014;7(4):394–402.
21. Herrmann HC, Kar S, Siegel R, Fail P, Loghin C, Lim S, Hahn R, Rogers JH, Bommer WJ, Wang A, Berke A, Lerakis S, Kramer P, Wong SC, Foster E, Glower D, Feldman T. Effect of percutaneous mitral repair with the MitraClip device on mitral valve area and gradient. EuroIntervention. 2009;4(4):437–42.
22. Biaggi P, Felix C, Gruner C, Herzog BA, Hohlfeld S, Gaemperli O, Stahli BE, Paul M, Held L, Tanner FC, Grunenfelder J, Corti R, Bettex D. Assessment of mitral valve area during percutaneous mitral valve repair using the MitraClip system: comparison of different echocardiographic methods. Circ Cardiovasc Imaging. 2013;6(6):1032–40.
23. Taramasso M, Maisano F, Denti P, Latib A, La Canna G, Colombo A, Alfieri O. Percutaneous edge-to-edge repair in high-risk and elderly patients with degenerative mitral regurgitation: midterm outcomes in a single-center experience. J Thorac Cardiovasc Surg. 2014;148(6):2743–50.
24. Lam JH, Ranganathan N, Wigle ED, Silver MD. Morphology of the human mitral valve. I. Chordae tendineae: a new classification. Circulation. 1970;41(3):449–58.
25. Millington-Sanders C, Meir A, Lawrence L, Stolinski C. Structure of chordae tendineae in the left ventricle of the human heart. J Anat. 1998;192(Pt 4):573–81.
26. Estevez-Loureiro R, Franzen O, Winter R, Sondergaard L, Jacobsen P, Cheung G, Moat N, Ihlemann N, Ghione M, Price S, Duncan A, Streit Rosenberg T, Barker S, Di Mario C, Settergren M. Echocardiographic and clinical outcomes of central versus noncentral percutaneous edge-to-edge repair of degenerative mitral regurgitation. J Am Coll Cardiol. 2013;62(25):2370–7.
27. Rogers JH, Franzen O. Percutaneous edge-to-edge MitraClip therapy in the management of mitral regurgitation. Eur Heart J. 2011;32(19):2350–7.
28. Couture P, Cloutier-Gill LA, Ducharme A, Bonan R, Asgar AW. MitraClip intervention as rescue therapy in cardiogenic shock: one-year follow-up. Can J Cardiol. 2014;30(9):1108 e15–6.
29. Bilge M, Alemdar R, Yasar AS. Successful percutaneous mitral valve repair with the MitraClip system of acute mitral regurgitation due to papillary muscle rupture as complication of acute myocardial infarction. Catheter Cardiovasc Interv. 2014;83(1):E137–40.
30. Carpentier A, Guerinon J, Deloche A, Fabiani JN, Relland M. In: Kalmanson D, editor. The mitral valve-a pluridisciplinary approach. Acton: Publishing Sciences Group; 1976.
31. Fornes P, Heudes D, Fuzellier JF, Tixier D, Bruneval P, Carpentier A. Correlation between clinical and histologic patterns of degenerative mitral valve insufficiency: a histomorphometric study of 130 excised segments. Cardiovasc Pathol. 1999;8(2):81–92.
32. Rabkin E, Aikawa M, Stone JR, Fukumoto Y, Libby P, Schoen FJ. Activated interstitial myofibroblasts express catabolic enzymes and mediate matrix remodeling in myxomatous heart valves. Circulation. 2001;104(21):2525–32.
33. Dal-Bianco JP, Aikawa E, Bischoff J, Guerrero JL, Handschumacher MD, Sullivan S, Johnson B, Titus JS, Iwamoto Y, Wylie-Sears J, Levine RA, Carpentier A. Active adaptation of the tethered mitral valve: insights into a compensatory mechanism for functional mitral regurgitation. Circulation. 2009;120(4):334–42.

Catheter-Based Left Atrial Appendage Closure

9

Matthew J. Price, Michael R. Smith, and David S. Rubenson

Abstract

Atrial fibrillation (AF) is the most common sustained arrhythmia and is associated with an increased risk of stroke and systemic embolism. While anticoagulation reduces the risk of thromboembolism in AF, safe and consistent long-term treatment can be challenging with oral anticoagulation regimens. The left atrial appendage (LAA) is thought to be the major source of thromboembolism in AF. Novel, mechanical catheter-based strategies have been developed to exclude communication between the LAA and the left atrium in order to reduce the risk of thromboembolism in AF without the need for long-term OAC. Transesophageal echocardiography (TEE) imaging plays a critical role in transcatheter closure of the LAA. This chapter provides details on the multiple roles of TEE in LAA closure ranging from baseline evaluation (to establish eligibility and correct size of device) to procedural guidance (including transseptal puncture) to later follow up.

Keywords

Left atrial appendage • Left atrial thrombus • Atrial fibrillation • Left atrial appendage closure • Transseptal puncture

Introduction

Atrial fibrillation (AF) is the most common sustained arrhythmia and is associated with an increased risk of stroke and systemic embolism. Oral anticoagulation (OAC) with warfarin or the non-vitamin-K antagonists dabigatran, apixaban, rivoraxaban, and edoxaban significantly reduces this risk. However, OAC is underutilized, and safe and consistent long-term treatment can be challenging with both warfarin and the non-vitamin-K antagonists. The left atrial appendage (LAA) is thought to be the major source of thromboembolism in AF. Therefore, catheter-based strategies have been developed to occlude or ligate the LAA in order to reduce the risk of thromboembolism without the need for long-term OAC. Two approaches have been studied or are currently available in the United States. The WATCHMAN LAA occluder (Boston Scientific, Natwick, MA) consists of a self-expanding nitinol frame and perforated polyethylene terephthalate membrane cap that is delivered via a transeptal approach. It has been evaluated in two randomized clinical trials [1, 2]; the Food and Drug Administration (FDA) has recently approved this device for

M.J. Price, MD (✉)
Cardiac Catheterization Laboratory,
Scripps Clinic, Scripps Green Hospital,
10666 North Torrey Pines Road, Maildrop S1056,
La Jolla, CA 92037, USA

Scripps Translational Science Institute, La Jolla, CA USA

Division of Cardiovascular Diseases, Scripps Clinic,
La Jolla, CA USA
e-mail: price.matthew@scrippshealth.org

M.R. Smith, MD
Division of Cardiovascular Diseases, Scripps Clinic,
La Jolla, CA USA

D.S. Rubenson, MD
Division of Cardiovascular Diseases, Scripps Clinic,
La Jolla, CA USA

Cardiac Non-Invasive Laboratory, Scripps Green Hospital,
La Jolla, CA USA

M.H. Picard et al. (eds.), *Intraprocedural Imaging of Cardiovascular Interventions*, DOI 10.1007/978-3-319-29428-5_9

patients who are deemed suitable candidates for warfarin but have an appropriate rationale to seek a non-pharmacologic alternative to warfarin. The Lariat device (SentreHeart, Redwood City, California) enables the percutaneous ligation of the LAA through the delivery of a surgical suture via a combined transseptal and sub-xiphoid approach [3]. The device is 510K-cleared by the FDA for the approximation of soft-tissue, and it has been applied clinically to LAA closure. Trans-esophageal echocardiography (TEE) imaging plays a critical role in the work-up, procedural guidance, and follow-up for both treatment approaches. Herein, we review the use of TEE in the setting of transcatheter LAA closure.

Baseline TEE Evaluation Prior to LAA Closure

A thorough pre-procedural TEE evaluation prior to LAA closure is required for appropriate patient selection. Specific items to evaluate include the presence of potential thromboembolism sources in addition to the LAA, whether LAA thrombus is present, and whether the LAA anatomy is suitable for device closure.

Alternative Sources of Thromboembolism

The primary rationale for LAA closure is to reduce the risk of thromboembolism without the need for long-term OAC. The procedure should not be performed if OAC may be clinically indicated for reasons other than potential LAA thrombus. Therefore, the presence of mobile aortic atheroma, papillary fibroelastoma, ventricular thrombus, or other source of cardioembolism beside the LAA must be excluded. If a large patent foramen ovale or atrial septal defect is present in a patient with a prior stroke, these may be percutaneously closed post-procedure if the clinician feels that the defect poses a long-term risk for paradoxical embolism.

LAA Thrombus

The presence or suspicion of LAA thrombus should warrant deferral of transcatheter LAA closure, and, if possible, the patient should be treated with OAC until the thrombus resolves on repeat imaging. A practical "rule-of-thumb" is to defer intervention if the echocardiographic appearance of the LAA would be sufficient to preclude electrical cardioversion.

Anatomic Eligibility

Anatomic criteria for Lariat transcatheter LAA ligation are derived for the most part from computed tomography: appendages with diameter >40 mm, presence of lobes behind the pulmonary artery, or a posteriorly-oriented appendage should generally be avoided [4]. In the case of LAA closure with the WATCHMAN occluder, TEE provides critical information regarding LAA shape, lobar anatomy, and dimensions that assist in the selection of the appropriate device size. Further details regarding LAA assessment for WATCHMAN implantation are noted below.

Procedural Guidance with TEE: Transseptal Puncture

Transcatheter LAA occlusion and ligation both require access to the left atrium via a transseptal puncture. Although transseptal puncture can be safely achieved with fluoroscopic guidance alone, TEE allows for the accurate positioning of the puncture for successful LAA closure and also provides visual cues that allow the operator to avoid complications. The echocardiographer plays a critical role in achieving safe and optimal transseptal crossing by identifying the tip of the transseptal system and orienting the operator accordingly. Two views of the interatrial septum are key for echocardiographic guidance, and can be obtained with either TEE or intracardiac echocardiography (ICE): the short axis view, identified by the aortic valve in cross-section, defines the anterior-posterior plane, while the long axis view, identified by visualization of the superior and inferior venae cavae, defines the superior-inferior plane. Biplane imaging with TEE is particularly helpful, as it clearly indicates both the anterior-posterior and superior-inferior orientation of the transseptal needle through simultaneous imaging of the short axis and bicaval views. The aorta is an anterior structure, and therefore tenting of the inter-atrial septum close to the aorta in the short axis view can be rectified by clockwise rotation of the transseptal sheath/dilator/needle system, while tenting directed too far posteriorly toward the left atrial free wall can be corrected with counterclockwise rotation (Fig. 9.1). For the WATCHMAN procedure, the transseptal puncture should be located posterior and inferiorly to allow for a co-axial approach of the delivery sheath toward the LAA (which is an anterior and superior structure) (Fig. 9.2). A posterior-inferior location is also helpful for transcatheter ligation with the Lariat, although a puncture site within the mid-septum is generally sufficient. The transseptal needle should never be advanced if tenting is not clearly seen on echocardiography. Once the septum is crossed and the operator advances a wire into the left atrium, the echocardiographer should confirm that the wire is appropriately placed within the pulmonary vein and not within the LAA (which could result in perforation).

Echocardiographic Guidance: Lariat Procedure and Follow-Up

The Lariat procedure combines a transseptal and transpericardial approach. In addition to directing transseptal puncture, echocardiography plays a central role in procedural guidance and clinical follow-up.

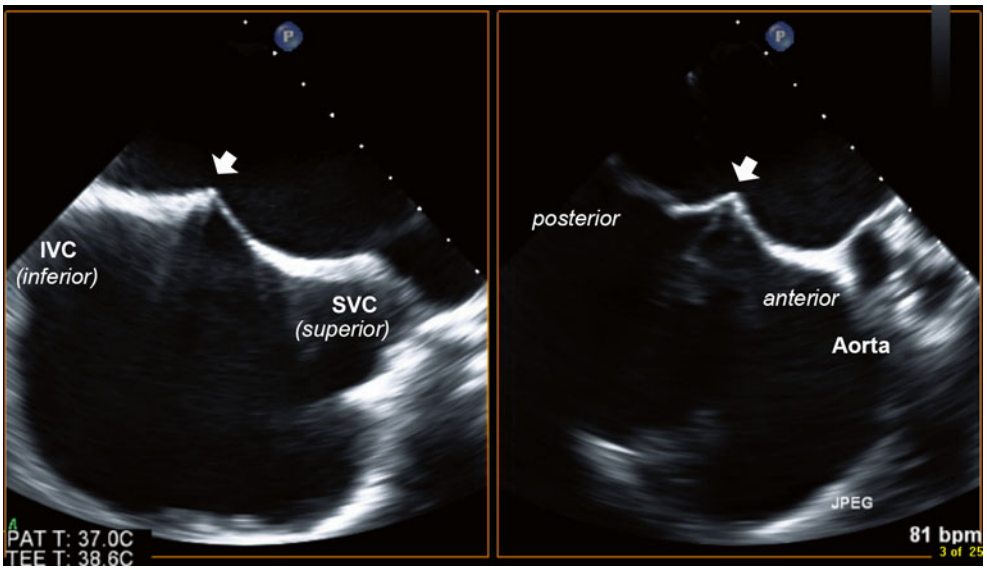

Fig. 9.1 TEE guidance of transseptal puncture. The exact location of the transseptal puncture along the interatrial septum can be visualized by simultaneous imaging of the bicaval and aortic short axis planes using a three-dimensional probe. Clockwise rotation of the transseptal system will direct the system more posteriorly, away from the aorta (visualized in the aortic short axis plane), while withdrawal of the system will bring the puncture inferior (visualized in the bicaval plane). For left atrial appendage (LAA) occlusion or ligation, a posterior-inferior puncture is advantageous as it allows for a coaxial approach for equipment to be introduced into the LAA. In this particular case, the transseptal dilator is tenting the mid-portion of the interatrial septum. *Arrows*: tenting of interatrial septum by the transseptal sheath dilator

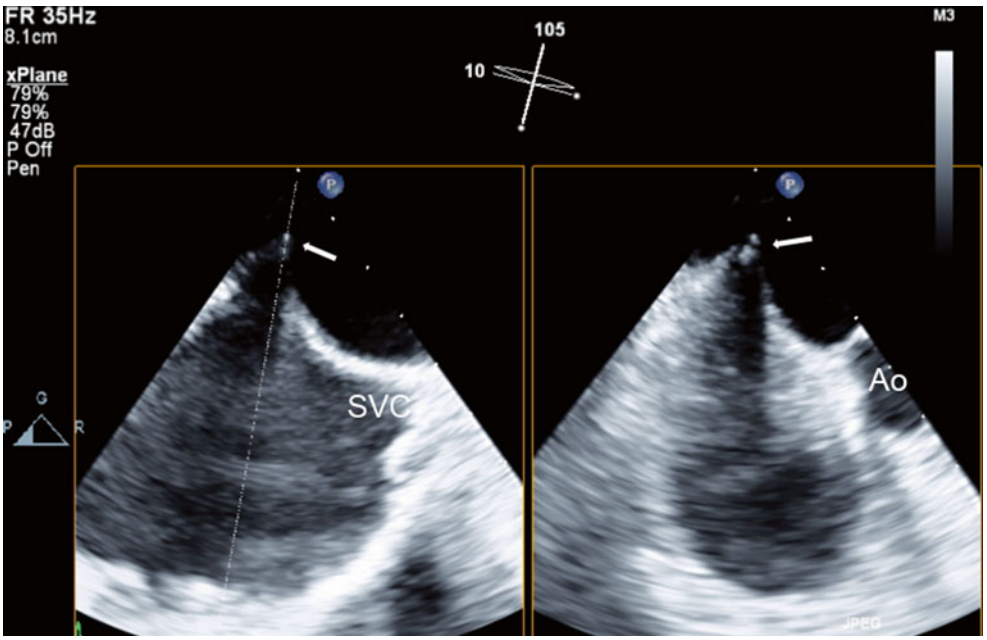

Fig. 9.2 Optimal transseptal location for WATCHMAN left atrial appendage occlusion. In this particular case, the tenting of the septum is inferior (on the opposite end of the interatrial septum from the superior vena cava) and posterior (opposite to the aortic valve). This allows for the device delivery sheath to approach the left atrial appendage in a coaxial fashion, as the appendage is located in the anterior and superior portion of the left atrium. *Ao* aorta, *SVC* superior vena cava; *arrow* tenting of interatrial septum by transseptal needle

Procedural Guidance for the Lariat

Pericardial access and sheath placement. Dry pericardial access is generally performed under fluoroscopic guidance. However, echocardiographic imaging can help confirm that the guidewire advanced through the introducer needle is within the pericardial space, rather than inside the right ventricle or the anterior mediastinum. As the sheath is advanced over the wire into the pericardium, the right ventricle should be imaged; if there is compression of the right ventricle, the operators should consider pericardial puncture at an alternative site.

Advancement of endo-wire into anterior lobe of the LAA. The Lariat snare is advanced to the LAA over a rail formed by the connection between a magnet-tipped wire within the anterior lobe of the LAA (the endo-wire, delivered through the transeptal sheath) and a complementary magnet-tipped wire introduced through the pericardial sheath (the epi-wire). If the endo-wire is not within the anterior lobe, but rather is in a posterior position, Lariat LAA ligation will be challenging and will likely be unsuccessful. The echocardiographer may assist the operator by confirming the anterior position of the endo-wire by examining the course of the wire within the LAA (Fig. 9.3).

Position of the LAA os. TEE plays an important role in co-registering the anatomic LAA os so that the LAA can be snared by the Lariat device at the proper site. The operator advances a balloon catheter over the Endo-wire into the LAA and inflates the balloon with dilute contrast. The echocardiographer guides the operator to place the balloon at the mouth of the LAA, and the balloon position can be seen by fluoroscopy (Fig. 9.3). This provides a fluoroscopic marker for the position where the operator should close the Lariat snare over the LAA.

Confirmation of complete closure. Complete LAA closure should be confirmed after snaring of the LAA and prior to suture release. Residual lobes due to partial ligation" or residual flow must be excluded.

Monitor for complications. Pericardial effusions are not uncommon with the Lariat procedure [5], and the presence of a new or growing effusion should be actively monitored. Potential etiologies of peri-procedural pericardial effusions include transseptal puncture, pericardial access, left atrial perforation with the magnetic-tipped wires, and LAA tearing or evulsion (Fig. 9.4).

Echocardiographic Follow-Up After Lariat LAA Ligation

Serial TEE follow-up after Lariat LAA ligation should be performed at approximately 6 weeks and 3 months post-procedure. Late leaks, pericardial effusions, and stump thrombus have been reported (Fig. 9.5) [5, 6]. TEE can be used to guide successful transcatheter closure of post-lariat leaks (Fig. 9.6) [7].

Echocardiographic Guidance: WATCHMAN Procedure and Follow-Up

Assessment for Anatomic Eligibility and Selection of Device Size

LAA occluder device implantation requires a thorough assessment of the LAA in multiple views. The LAA is imaged at 0, 45, 90, and 135°. In each plane, the diameter of the LAA mouth is measured, defined as the distance just below the left circumflex artery at the level of the mitral annulus to approximately 2 cm below the tip of the ridge of the left upper pulmonary vein; alternatively, the distance can be measured from the mitral valve annulus across to the left upper pulmonary venous ridge perpendicular to the planned axis of the delivery sheath. The length (or depth) of the LAA is measured from the center of this line to the tip of the primary lobe (Fig. 9.7). The WATCHMAN device is available in five sizes, ranging from 21 to 33 mm in diameter; the length is approximately equal to the width. The device manufacturer recommends over-sizing the device by 8–20 %, and therefore, the WATCHMAN may be used to occlude LAAs between approximately 17 and 30 mm in diameter, as long as there is sufficient depth. An initial "working" device size is selected based upon the largest measured diameter of the LAA ostium, incorporating the necessary oversizing, as long as there is sufficient depth to accommodate it. This selection may be modified once the delivery sheath is introduced into the LAA, which may clarify the maximal implantation depth. Particular appendage shapes, such as "chicken wing" anatomy, may represent a challenge for device placement because of the broad width but shallow depth of the initial portion of the LAA before the first bend. There are initial case reports describing the use of 3D printing based on CT datasets to create a model of the LAA in advance of the procedure in cases where the pre-procedural TEE suggests complex or potentially unsuitable [.8]. Such 3D models could allow optimization of the sizing of devices outside of the body before deployment in the heart.

Procedural Guidance

Introduction of delivery sheath into the LAA. As noted above, TEE is required to establish the appropriate inferior and posterior puncture site at the inter-atrial septum. The next step of the procedure is to introduce the 14 French delivery sheath into the left upper pulmonary vein over a stiff 0.35 in. wire and then into the LAA over a diagnostic pigtail catheter. Echocardiography can aid in the safety of this maneuver by confirming that the stiff wire is in the pulmonary vein (rather than the thin-walled and friable LAA) and to aid the operator in manipulating the pigtail catheter anteriorly from the pulmonary vein into the LAA. The delivery sheath is then advanced over the pigtail deeply into the LAA. TEE imaging can assist the operator in establishing a coaxial position within the LAA and defining whether the sheath is within the anterior or posterior lobe (Fig. 9.8).

Evaluating adequacy of device implantation. The operator and echocardiographer can use the acronym "PASS" as

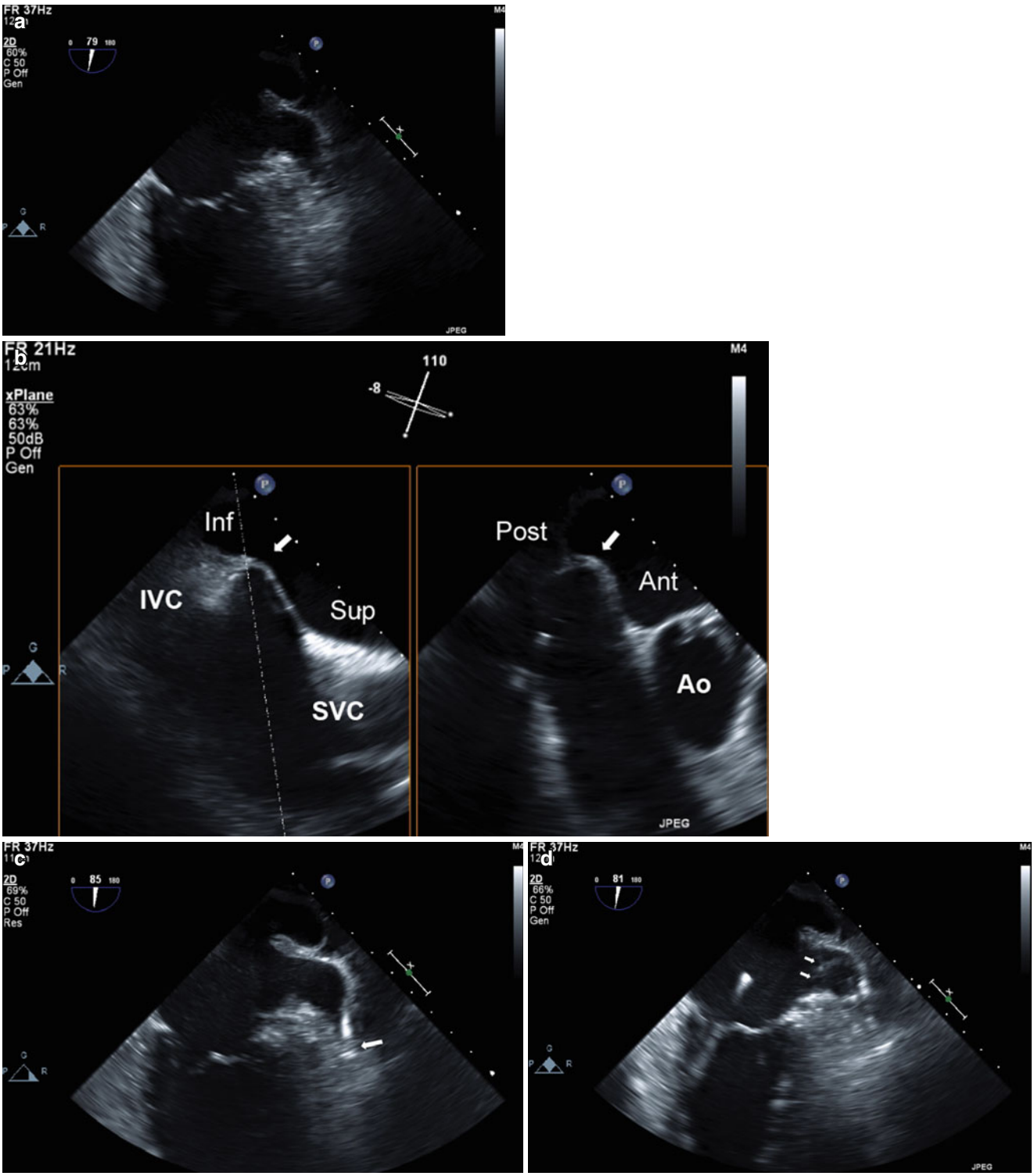

Fig. 9.3 Case of LAA ligation with the Lariat device. An 82 year-old male with atrial fibrillation and high risk for thromboembolism ($CHA_2DS_2VASc=4$) and high risk for bleeding on oral anticoagulation underwent transcatheter LAA ligation with the Lariat. (**a**) Baseline TEE showing the LAA. (**b**) TEE guidance of transseptal puncture. An inferior and posterior puncture site is confirmed using a TEE in the biplanar view (*arrows*, tenting of septum). (**c**) Placement of the magnet-tipped wire through the transseptal sheath into the LAA is confirmed by TEE (*arrow*, wire tip). (**d**) A compliant balloon filled with dilute contrast is inflated within the mouth of the LAA to identify this anatomic location on fluoroscopy (*double arrow*, balloon). (**e**) Final images demonstrating complete closure of the LAA after Lariat deployment (*asterisk*, sealed LAA). *Ao* Aorta, *Ant* anterior, *Inf* inferior, *IVC* inferior vena cava, *Sup* superior, *SVC* superior vena cava

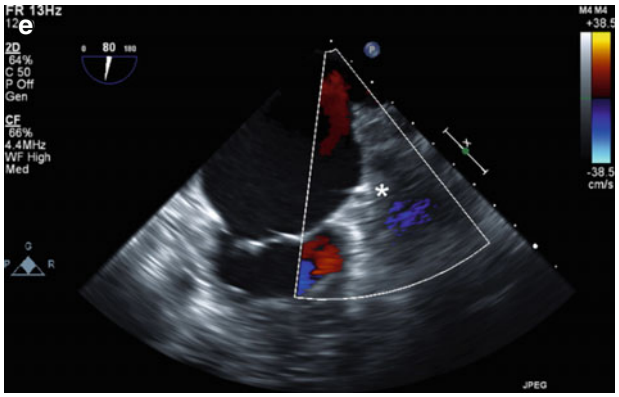

Fig. 9.3 (continued)

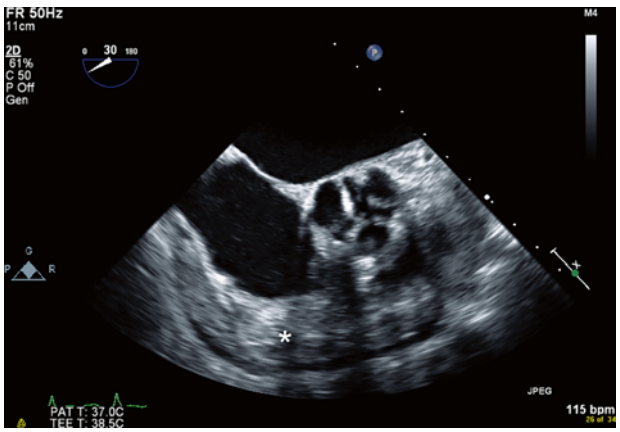

Fig. 9.4 Intraprocedural pericardial effusion during transcatheter LAA ligation with the Lariat. In this case, a pericardial effusion formed soon after pericardial access, and the effusion was persistent despite prolonged autotransfusion. Hemodynamic stability could not be maintained, and the patient went urgently to cardiac surgery, where the pericardial clot (*asterisk*) was evacuated, revealing a needle perforation at the apex of the right ventricle that was easily repaired

a final checklist to assess device implantation and confirm that the device may be safely released from the delivery cable. P stands for *position* on TEE and fluoroscopy; A for anchor, assessed by a "tug-test", in which the LAA and the device should move in unison on TEE when the operator gently tugs on the delivery cable; S for *sealed* on TEE and fluoroscopy, the former assessed by color Doppler; and S for *size*, where on TEE, the shoulder-to-shoulder length of the device should be 8–20 % less than the nominal device size (Fig. 9.9).

Follow-up. In the randomized trials of the WATCHMAN device, routine TEE follow-up was performed at 6 weeks. At this time, a careful assessment is performed for peri-device flow. If peri-device flow was <5 mm in diameter, warfarin was discontinued and aspirin and clopidogrel prescribed for 5 more months followed by indefinite aspirin monotherapy. Some degree of peri-device flow into the LAA (usually <3 mm in maximum width) is not uncommon after WATCHMAN implantation. In the WATCHMAN Left Atrial Appendage System for Embolic Protection in Patients with Atrial Fibrillation (PROTECT-AF) trial, some flow around the device was detected by TEE in 41 % and 32 % of patients at 6 weeks and 1 year post-procedure, respectively. In a post-hoc analysis, there was no association between clinical events and the presence of peri-device flow, irrespective of size and whether or not warfarin was continued [9].

Future Directions

Although TEE is the primary imaging modality to evaluate the LAA and to guide transcatheter ligation and occlusion, there are several challenges to its practical use. First,

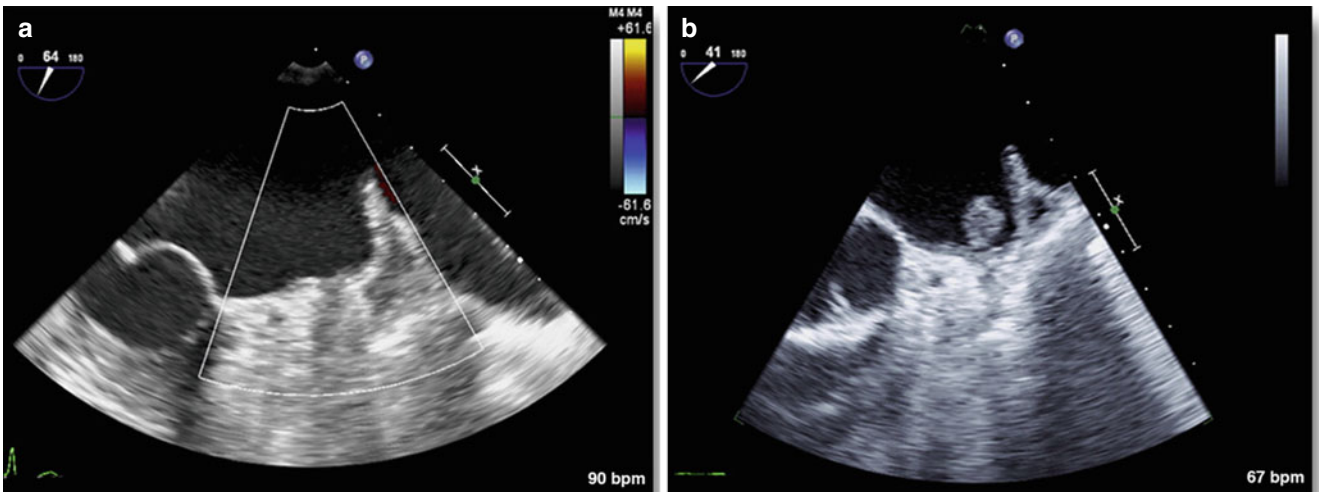

Fig. 9.5 Case of left atrial thrombus after Lariat LAA ligation. A 63 year-old male with paroxysmal atrial fibrillation, prior systemic embolism, and at high risk for bleeding on oral anticoagulation due to cirrhosis and esophageal varices underwent transcatheter LAA ligation with the Lariat. Anticoagulant therapy was discontinued post-procedure. (**a**) Intraprocedural TEE shows complete closure of the LAA with no evidence of residual leak. (**b**) At 3 months post-procedure, follow-up TEE demonstrates a new mobile thrombus at the site of the LAA stump, attached to the left atrial wall. Despite his bleeding risk, the patient was started on warfarin and remained asymptomatic with no neurologic sequelae. Repeat TEE 2 months later showed complete resolution of thrombus. This case, and other reports, suggests that a short course of anticoagulation therapy and routine surveillance TEE after the Lariat ligation should be strongly considered (Adapted from Gray and Rubenson [6])

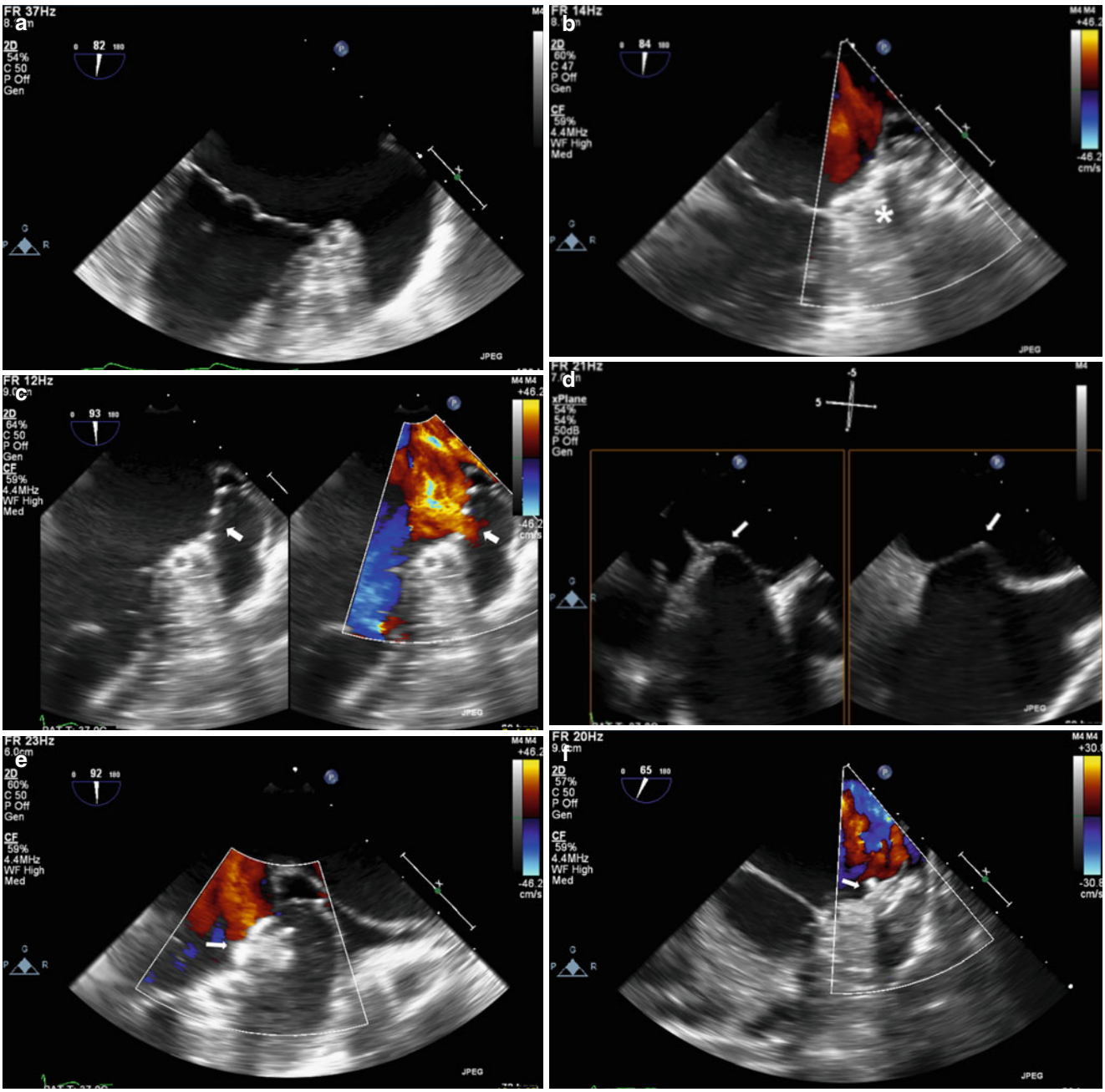

Fig. 9.6 Case of transcatheter closure of late leak after Lariat LAA ligation. A 68 year-old female with atrial fibrillation, prior stroke, CHA_2DS_2VASc score of 4, and high bleeding risk underwent transcatheter LAA ligation with the Lariat device. Despite complete closure at the end of the procedure, a late leak was identified at follow-up TEE; the leak was subsequently closed with an Amplatzer device. (**a**) TEE imaging of the LAA at baseline. (**b**) Transcatheter ligation with the LAA was successful and uncomplicated, with complete LAA closure at the end of the procedure (*asterisk*). (**c**) At 6-week TEE follow-up, a central leak is noted with apparent reconstitution of the LAA (*arrow*). The patient underwent transcatheter closure of the post-Lariat leak given her high risk of thromboembolism and bleeding. (**d**) Transseptal puncture guided by biplane TEE. The anterior-posterior plane (*short-axis view*) is seen on the left side of the panel, and the superior-inferior plane (*long-axis view*) is seen on the right side of the panel. Posterior and central tenting of the inter-atrial septum is observed (*arrows*). (**e**) No residual leak is noted after delivery of an Amplatzer Duct Occluder (ADO) II 6/4 mm. (*arrow*). (**f**) At 6 week TEE follow-up after leak closure, obliteration of the LAA is observed (*arrow*, ADOII device). *LAA* left atrial appendage, *TEE* transesophageal echocardiography

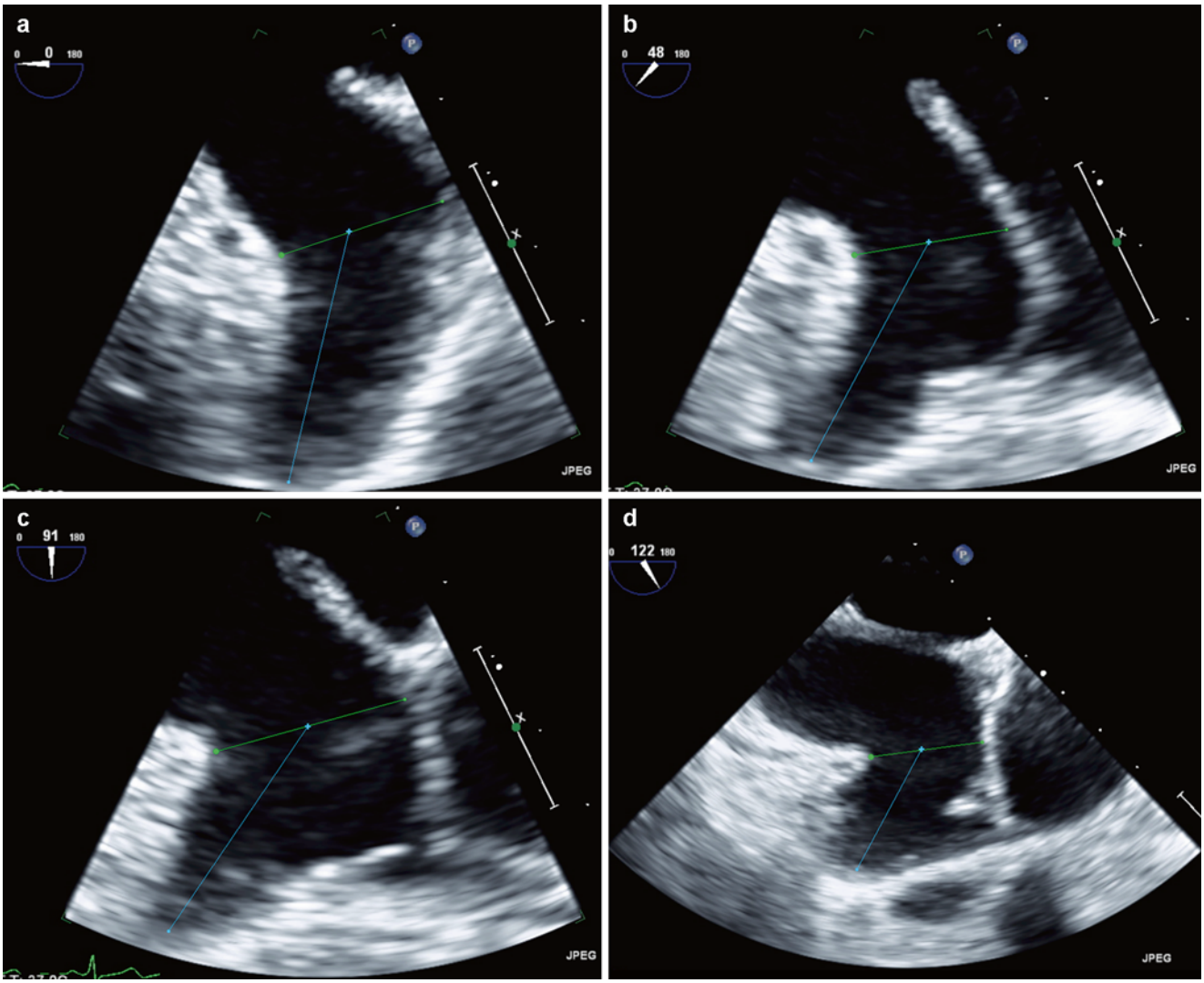

Fig. 9.7 Pre-procedural TEE assessment of the LAA for WATCHMAN occluder implantation. Prior to the procedure, TEE is performed to exclude the presence of LAA thrombus and to confirm LAA anatomy is feasible for occlusion. The diameter and depth of the LAA is measured at 0, 45, 90, and 135° (Panels **a**–**d** respectively). The diameter of the LAA is defined as the distance from a point just distal to the left circumflex artery to roughly 1–2 cm from tip of the left upper pulmonary vein limbus. An initial device size is selected to be approximately 10–20 % greater than the maximal width provided there is sufficient depth; the decision on device size may be adjusted after fluoroscopic landmarks are obtained once the delivery sheath is advanced deep within the LAA. In this particular case of a 75-year old female with paroxysmal atrial fibrillation being evaluated for a WATCHMAN occluder, the LAA has a modest anterior "chicken wing" morphology, which may increase procedural complexity but did not preclude procedural success (Adapted from Price [11])

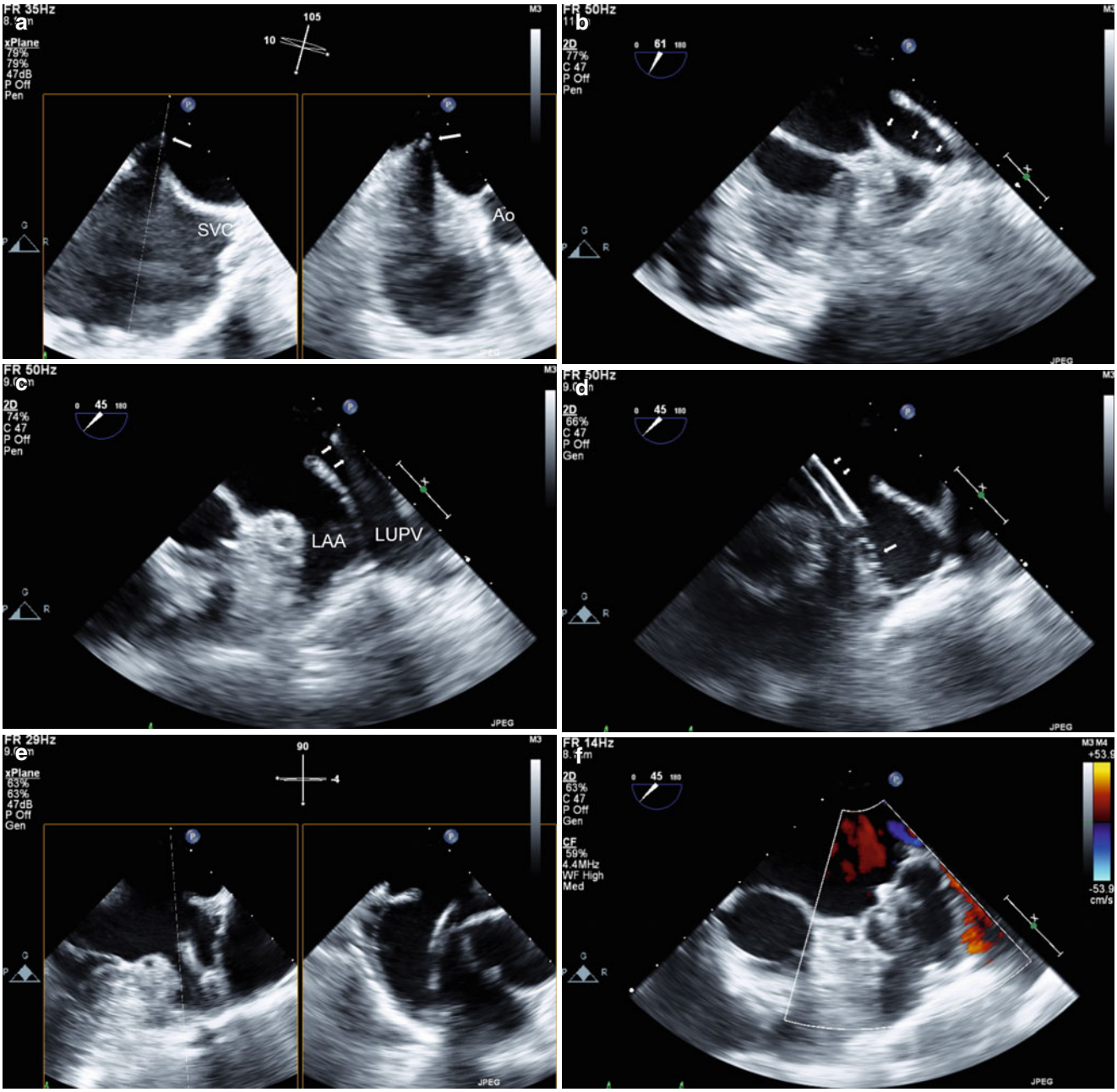

Fig. 9.8 LAA closure with the WATCHMAN occluder. A 75 year-old female with paroxysmal atrial fibrillation, CHA_2DS_2VASc score of 4, and need for chronic non-steroidal inflammatories underwent LAA occlusion with the WATCHMAN. Refer to Fig. 9.1 above for the baseline LAA images of this patient which were without evidence of thrombus, alternative sources of thromboembolism, and an estimated device size of 30 mm. (**a**) Posterior and inferior transseptal puncture is performed using TEE biplane guidance. *Arrow*, tenting of interatrial septum (**b**) While attempting to introduce a 0.35 in. wire into the left upper pulmonary vein through the transseptal sheath, the wire was inadvertently advanced into the LAA, which was quickly identified by TEE (*arrows*) and withdrawn. Manipulation of stiff wires in the LAA may cause perforation since the appendage is thin-walled and friable. (**c**) After withdrawal of the wire from the LAA and posterior (*clockwise*) rotation of the transseptal sheath, the wire is readvanced and the appropriate position of the wire within the left upper pulmonary vein is confirmed on TEE (*double arrows*). (**d**) The 14 French delivery sheath (*double arrow*) is advanced deeply into the LAA over the pigtail catheter (*single arrow*), which is then removed. (**e**) Biplane TEE demonstrates deep and coaxial position of the delivery catheter. (**f**) Final imaging after implantation and release of a 30 mm device, demonstrating good device position and no color flow into the LAA, consistent with complete occlusion. *Ao* Aorta, *LAA* left atrial appendage, *LUPV* left upper pulmonary vein, *SVC* superior vena cava

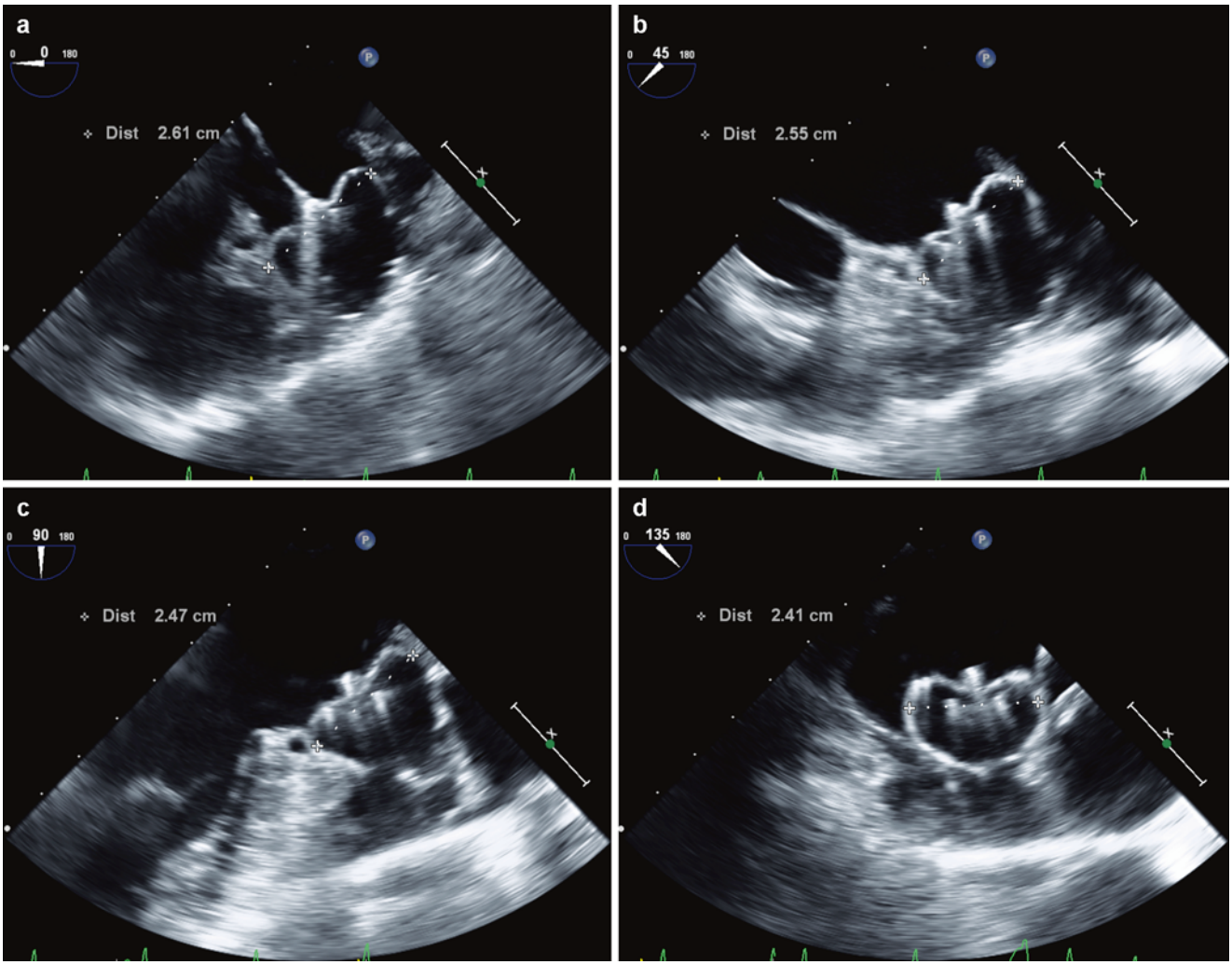

Fig. 9.9 TEE assessment after WATCHMAN occluder implantation. After deployment of a WATCHMAN 30 mm LAA occluder, the device is assessed at 0, 45, 90, and 135° (Panels **a–d**, respectively). Compression is determined by measuring the distance across the shoulders of the device. The device is released if compression and position are adequate, the LAA is sealed by color Doppler and left atrial angiography, and the device is well-anchored according to a "tug test". In this case, the device was approximately 13–20 % compressed, the device was well positioned, there was no color flow around the device into the LAA, and the LAA moved with the device as a unit when the delivery cable was tugged gently. Therefore, the device was released from the cable with successful LAA occlusion. Per protocol in the research studies, the patient was treated with warfarin and aspirin for 6 weeks, when a repeat TEE confirmed LAA closure without thrombus, and then the warfarin discontinued. The patient was treated with aspirin and clopidogrel for 6 more months, and then was continued on aspirin monotherapy (Adapted from Price [11])

patients generally require general anesthesia. Second, it requires an additional operator and complicates procedural scheduling. Finally, TEE is associated with a small yet finite clinical risk, such as esophageal tearing or laceration. ICE imaging may have several practical advantages compared with TEE. The use of ICE to guide transcatheter LAA closure has been reported [10], but experience is limited and optimal image acquisition may be difficult. As experience with the technology increases, the selected use of ICE guidance in appropriate patients may be advantageous.

Conclusions

Transcatheter LAA closure is a novel, mechanical approach to stroke prevention in atrial fibrillation. Ultrasound imaging, primarily by TEE, plays a critical role in patient evaluation, procedural guidance, and clinical follow-up. LAA closure is a truly multidisciplinary procedure, requiring substantial, real-time communication and interaction between the operator and the imager. Both the interventionalist and the structural imager must share fluency in the echocardiographic anatomy of the interatrial septum, pulmonary vein, and LAA in order to treat patients safely and successfully with this novel management strategy.

References

1. Holmes DR, Reddy VY, Turi ZG, Doshi SK, Sievert H, Buchbinder M, Mullin CM, Sick P. Percutaneous closure of the left atrial appendage versus warfarin therapy for prevention of stroke in patients with atrial fibrillation: a randomised non-inferiority trial. Lancet. 2009;374:534–42.
2. Holmes Jr DR, Kar S, Price MJ, Whisenant B, Sievert H, Doshi SK, Huber K, Reddy VY. Prospective randomized evaluation of the Watchman Left Atrial Appendage Closure device in patients with atrial fibrillation versus long-term warfarin therapy: the PREVAIL trial. J Am Coll Cardiol. 2014;64:1–12.
3. Lee RJ, Bartus K, Yakubov SJ. Catheter-based left atrial appendage (LAA) ligation for the prevention of embolic events arising from the LAA: initial experience in a canine model. Circ Cardiovasc Interv. 2010;3:224–9.
4. Bartus K, Han FT, Bednarek J, Myc J, Kapelak B, Sadowski J, Lelakowski J, Bartus S, Yakubov SJ, Lee RJ. Percutaneous left atrial appendage suture ligation using the LARIAT device in patients with atrial fibrillation: initial clinical experience. J Am Coll Cardiol. 2013;62:108–18.
5. Price MJ, Gibson DN, Yakubov SJ, Schultz JC, Di Biase L, Natale A, Burkhardt JD, Pershad A, Byrne TJ, Gidney B, Aragon JR, Goldstein J, Moulton K, Patel T, Knight B, Lin AC, Valderrabano M. Early safety and efficacy of percutaneous left atrial appendage suture ligation: results from the U.S. transcatheter LAA ligation consortium. J Am Coll Cardiol. 2014;64:565–72.
6. Gray J, Rubenson D. De-novo thrombus formation and latent ligation failure following LAA exclusion. JACC Cardiovasc Imaging. 2013;6:1218–9.
7. Mosley 2nd WJ, Smith MR, Price MJ. Percutaneous management of late leak after lariat transcatheter ligation of the left atrial appendage in patients with atrial fibrillation at high risk for stroke. Catheter Cardiovasc Interv. 2014;83:664–9.
8. Otton JM, Spina R, Sulas R, Subbah RN, Jacobs N, Muller DWM, Gunalingan. Left atrial appendage closure guided by personalized 3D-printed cardiac reconstruction. JACC Cardiovasc Interv. 2015;8:1004–6 (letter).
9. Viles-Gonzalez JF, Kar S, Douglas P, Dukkipati S, Feldman T, Horton R, Holmes D, Reddy VY. The clinical impact of incomplete left atrial appendage closure with the Watchman Device in patients with atrial fibrillation: a PROTECT AF (Percutaneous Closure of the Left Atrial Appendage Versus Warfarin Therapy for Prevention of Stroke in Patients With Atrial Fibrillation) substudy. J Am Coll Cardiol. 2012;59:923–9.
10. Berti S, Paradossi U, Meucci F, Trianni G, Tzikas A, Rezzaghi M, Stolkova M, Palmieri C, Mori F, Santoro G. Periprocedural intracardiac echocardiography for left atrial appendage closure: a dual-center experience. JACC Cardiovasc Interv. 2014;7:1036–44.
11. Price MJ. Left atrial appendage occlusion with the WATCHMAN for stroke prevention in atrial fibrillation. Rev Cardiovasc Med. 2014;15:142–51.

Percutaneous Ventricular Septal Defect Closure

10

Christina Chrysohoou, Ankit Parikh, and Stamatios Lerakis

Abstract

Ventricular Septal Defects (VSD) are common in early childhood but the prevalence in adulthood is low due to spontaneous closure. Echocardiography can assess the location and size of the VSD, the direction of the intra-cardiac shunt, the effect of the VSD on the cardiac chambers and other associated anomalies. Percutaneous closure of the VSD has become an alternative to surgery. The location of the VSD determines it's feasibility for device closure. Echocardiography guidance is critical for the safe and successful VSD closure as well for the follow up evaluations.

Keywords

Ventricular Septal Defect (VSD) • Percutaneous closure • Echocardiographic guidance • Kirklin VSD classification

A ventricular septal defect (VSD) is an abnormal communication in the ventricular septum between the left and right ventricles. VSDs can be either isolated or occur in combination with other cardiac defects. They are common congenital heart anomalies in early childhood, occurring in about 3–3.5 per 1,000 live born infants. In the adult population, due to the spontaneous closure of small defects, the prevalence is lower, occurring in about 0.3 per 1,000 persons. According to the location of the defect in the ventricular septum, VSDs can be classified as either membranous or muscular defects [1, 2]. They also can be categorized in terms of their size in relation to the aortic annular diameter. Small VSDs are those that measure ≤25 % of the aortic annular diameter, moderate ones are those that measure between 25 % and 75 % of the aortic annular diameter, and large VSDs measure ≥75 % of the aortic annular diameter. Small defects are usually restrictive, with a Qp:Qs ratio <1.4. In these cases, the pulmonary artery, left ventricle, and left atrium typically remain normal sized. Moderate defects can cause mild-to-moderate left ventricular, left atrial, and pulmonary artery enlargement with a Qp:Qs ratio ranging from 1.4 to 2.2. Large nonrestrictive VSDs with Qp:Qs ratios 2.2 can cause volume overload and dilation of the left-sided cavities and pulmonary artery. Many of these patients will develop pulmonary vascular disease leading to a reduction in left-to-right shunting or possible shunt reversal due to the occurrence of Eisenmenger physiology [3].

The initial echocardiographic evaluation of a patient with suspected or known VSD should include assessment of the location and size of the VSD, the direction and magnitude of intracardiac shunting, the size and function of the cardiac chambers, right and left ventricular outflow measurements, valvular morphology and function (including assessment for aortic valve prolapse), pulmonary artery pressures, and the presence of any other associated cardiac anomalies [4].

One of the most important observations is the anatomic location of the defect, as it defines the feasibility of device closure. The Kirklin classification describes the location of the VSD in relation to the ventricular septum when the defect is viewed from the right ventricle. A type I defect refers to a subarterial defect, which is located at the anterosuperior part of the ventricular septum; type I defects are seen in about

C. Chrysohoou, MD, PhD
Division of Cardiology, Emory University School of Medicine, Atlanta, GA, USA

Hippokration Hospital, University of Athens, Athens, Greece
e-mail: chrysohoou@usa.net

A. Parikh, MD
Department of Internal Medicine, Emory University School of Medicine, Atlanta, GA, USA
e-mail: ankit.parikh.md@gmail.com

S. Lerakis, MD, PhD (✉)
Division of Cardiology, Emory University School of Medicine, Atlanta, GA, USA
e-mail: stam-lerakis@emoryhealthcare.org

M.H. Picard et al. (eds.), *Intraprocedural Imaging of Cardiovascular Interventions*, DOI 10.1007/978-3-319-29428-5_10

5 % of cases in the United States. A type II defect refers to a perimembranous VSD that is located in the middle of the upper portion of the ventricular septum in close proximity to the aortic valve. Type II defects are present in 75 % of patients with a VSD; these are associated with a high incidence of spontaneous closure. A type III defect is a perimembranous VSD with inlet extension; it is present in the posterior portion of the ventricular septum in close proximity to the tricuspid valve, and it is present in about 5 % of patients. A type IV defect is a muscular VSD. It is present in 10–15 % of patients and is most commonly present at the apical septum. Muscular VSDs can be single or multiple; in the latter case they may be referred to as a "Swiss cheese" VSD due to their appearance.

First introduced by Lock and colleagues, transcatheter VSD closure has become an alternate approach to surgery [5]; early efforts involved the use of a Rashkind double-umbrella device. The use of Amplatzer devices designed for muscular and perimembranous VSDs have been associated with a 100 % success rate in one study with up to 12 months of post-procedural follow-up [4]. Important complications of device closure include device embolization, hypotension, bleeding, and conduction abnormalities. The reported rate for muscular VSD closure complications is 10.7 %. Perimembranous VSD closure is associated with even higher rates of complications, with considerable risk of damage to the aortic valve, tricuspid valve, and conduction system. Because of the high risk of complications, perimembranous VSD closure has been partially abandoned [6, 7]. In general, device closure carries a class IIb indication (level of evidence C). Device closure can be considered as a treatment option if the VSD is not close to the tricuspid and aortic valves and if it is associated with severe left-sided chamber enlargement or pulmonary hypertension [8].

Although transcatheter closure is an established method of treating selected congenital VSDs, there is less clinical experience regarding transcatheter closure of post-infarction VSDs. The procedure is considered difficult because the margins of the defect may have necrotic borders upon which the device may not anchor and the patients tend to be critically ill at the time of the procedure [9]. Even in successful cases, the mortality remains high due to advanced patient age, comorbidities, severity of coronary artery disease, hemodynamic instability, and procedural complications. In a recent clinical trial, the 30-day survival was 35 % and the long-term survival was 30 % [10, 11].

Percutaneous closure is typically performed under general anesthesia and echocardiographic guidance. Either a transthoracic (TTE) or transesophageal (TEE) approach can be used. Echocardiography will guide the proceduralist on the number and size defects, their location, and their position with respect to the valves and other nearby structures. In some cases the right internal jugular vein, femoral vein, and femoral artery are all accessed for the procedure. Right internal jugular access is especially helpful in patients with a mid, posterior, or apical VSD. For mid-muscular, posterior, or apical VSDs, a left ventricular angiogram is performed in the hepatoclavicular view (35° left anterior oblique [LAO]/35° cranial) to delineate the location, size, and number of VSDs; for anterior defects, the long axial oblique (60° LAO/15° cranial) view is used. Either a Judkins right coronary artery catheter or a Cobra catheter can be used to cross the VSD from the left ventricular side. Typically a right heart catheterization is also performed prior to crossing the VSD; once the VSD is crossed from the left ventricular side, a long guidewire can be used to traverse the lesion and a snare device in the right heart can be used to pull back the long guidewire, externalizing it with respect to the venous access site. This in effect creates an "arteriovenous (AV) loop" that serves as a stable rail from the venous circulation to the arterial circulation across which the device can be deployed. As the device is passed from the venous circulation into the right ventricle and across the VSD, both echocardiography and angiography can be used to verify device position, as well as the deployment of the device discs, the release and stability of the device, and the presence of any residual shunting.

The distance from the aortic valve leaflets is an important measurement that should be determined before the procedure, as the absence of tissue separating the aortic valve leaflets from the orifice can result in complications. In general, the defect should be at least 2 mm away from the aortic valve. Additionally the presence of accessory tissue around the defect must be verified, as the prosthesis must be attached to the muscular septum. Some defects have large amounts of surrounding accessory tissue, forming an aneurysm, which significantly reduces the size of the original orifice. These defects may be occluded with smaller devices, which are positioned inside the aneurysm sac and do not compromise tricuspid or aortic valve function. The presence of aortic valve prolapse, especially of the right coronary leaflet, can be seen in 2–7 % of VSDs, leading to aortic insufficiency. Although this may be a relative contraindication for a percutaneous procedure, there are cases of device implantation performed under these circumstances that have been carried out safely and effectively. Echocardiography should also define the presence of any associated defects, such as a subaortic membrane or a right ventricular muscle band; these may require a surgical approach. Lesions such as pulmonary or aortic valve stenosis, persistent ductus arteriosus, and aortic coarctation can also be treated percutaneously, depending on their anatomical features [12–14].

Muscular VSDs located in the trabecular and apical regions of the septum can also be treated percutaneously. Although there are fewer anatomical variations, the

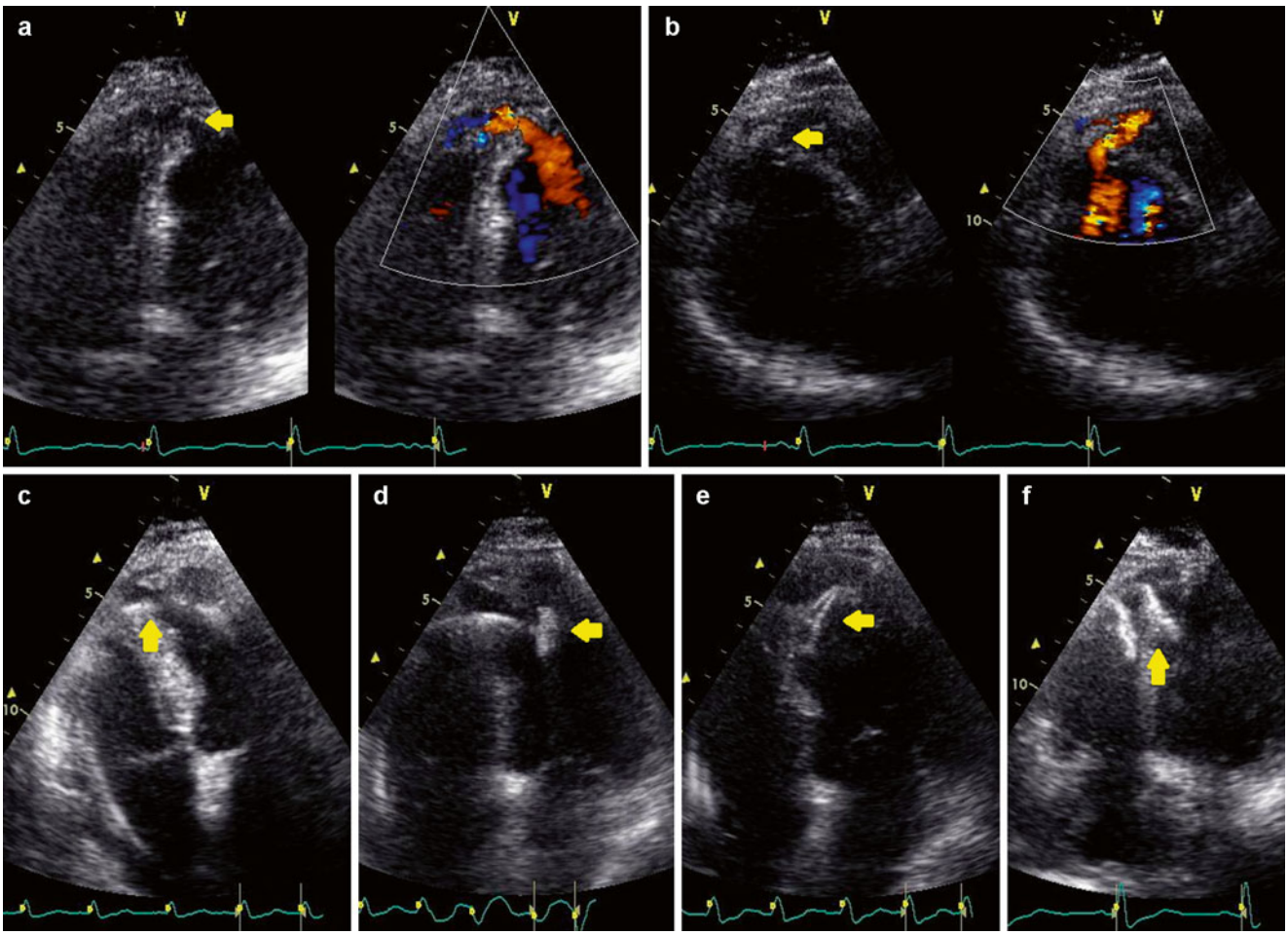

Fig. 10.1 Transthoracic echocardiographic imaging demonstrating percutaneous closure of a post-infarct apical muscular VSD. Panels (**a**, **b**) were obtained prior to the procedure, demonstrating the presence of VSD from apical four chamber (panel **a**) and off-axis parasternal long axis (panel **b**) views (*arrows*). The corresponding color Doppler images demonstrate flow across the VSD. Panel (**c**) demonstrates the course of the AV loop of guidewire (*arrow*), which is created when the long guidewire that had been passed through the VSD from the left ventriclular side is snared from the right ventricular side and externalized. Panel (**d**) demonstrates deployment of the left ventricular disc, which is subsequently pulled back until it abuts the ventricular septum (panel **e**). Finally, panel (**f**) shows deployment of the right ventricular disc and release of the device, which is well seated against the apical septum

presence of multiple orifices is common, particularly in the ventricular apex. When there is a single orifice, the Amplatzer device is the best choice, as it has small retention discs that occupy a small amount of space on the interventricular septum [15].

Recently, a hybrid approach for the management of very young patients (<6 months of age) with large muscular VSDs has been utilized. These patients are taken to the operating room for a thoracotomy to expose the heart. Through a right ventricular free wall puncture, a guidewire is introduced into the left ventricle through the VSD. A short sheath is then advanced over the guidewire allowing for device positioning. The procedure is performed under TEE monitoring. This innovative approach, in which the interventionalist, echocardiographer, and cardiac surgeon all work together, prevents the deleterious effects of extracorporeal circulation, and results in occlusion rates >90 %.

Echocardiography During Percutaneous VSD Closure

The procedure can be performed with TTE or TEE guidance. Although echocardiographic imaging is important for guiding the procedure, fluoroscopy and angiography are also utilized during the intervention [16–18]. If TEE is being used, intermediate transducer image planes between 0 and 180° can usually provide visualization of the VSD and device positioning. Similar to ASD closure, echocardiography is used for orifice measurement and device size choice, monitoring the guidewires, catheters, and sheaths as they are positioned inside the heart, and determining the location of the device discs before and after deployment. The echocardigrapher must also carefully evaluate the aortic and tricuspid valves, as well as evaluating the interventricular septum for the detection and grading of possible residual shunts.

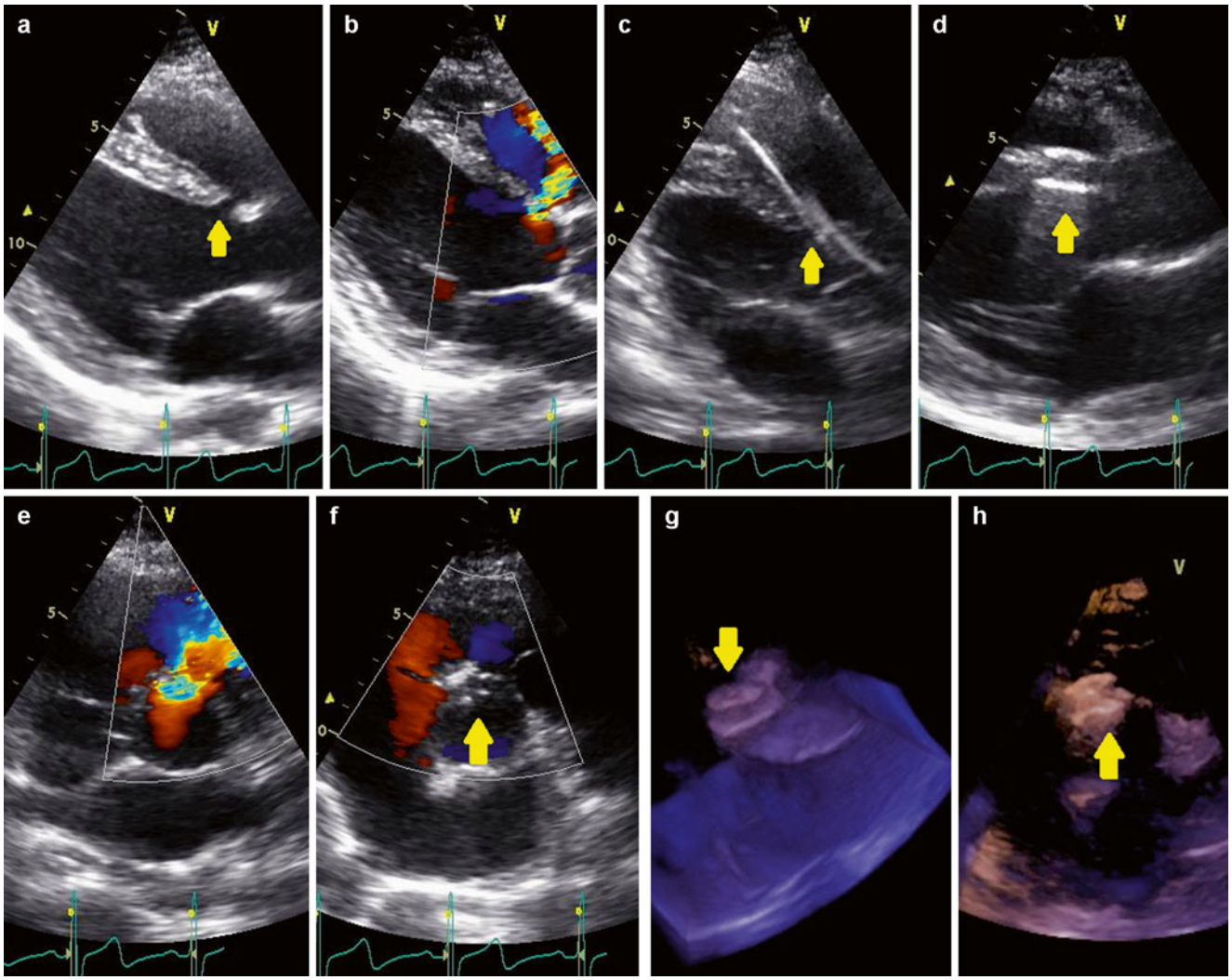

Fig. 10.2 Transthoracic echocardiographic imaging demonstrating percutaneous closure of a congenital perimembranous VSD. Panels (**a**, **b**, **e**) were obtained prior to the procedure, demonstrating the presence of VSD from parasternal long axis (panels **a**, **b**) and short axis (panel **e**) views. The color Doppler images in panels (**b** and **e**) demonstrate left to right flow across the VSD. Panel (**c**) demonstrates the AV loop of wire (*arrow*), passing from the aorta, into the left ventricle, across the VSD, and into the right ventricle. Panel (**d**) demonstrates in the parasternal long axis view the deployed device, which is well seated against the interventricular septum. Minimal residual device flow was visualized (panel **f**), with a substantial decrease noted between panel (**e**) (pre-procedure) and panel (**f**). Panels (**g**, **h**) show three-dimensional images of the deployed device (*arrows*)

Figures 10.1 and 10.2 demonstrate guidance of percutaneous closures of post-infarct and congenital VSDs, respectively, using TTE. Regardless of the approach used, the image quality is dependent on the experience of the echocardiographer as well as the patient's echocardiographic windows. If the patient is intubated, short periods of held ventilation may help stabilize the position of the heart in the chest to allow for better quality images. While standard imaging planes are certainly helpful, the echocardiographer should not be committed only to these and should try alternate planes and/or off-axis imaging as needed to obtain optimum visualization.

Follow-Up Echocardiography After Percutaneous VSD Closure

After percutaneous VSD closure is performed, patients are followed with serial clinical assessments and TTEs. Several parameters must be evaluated, including the left-sided cavity dimensions (which typically return to normal in the first year after closure), the positioning of the device, the presence and severity of any residual shunts, the evaluation and measurement of a possible gradient in the left ventricular outflow tract, and the function of the aortic and tricuspid valves.

References

1. Uebing A, Kaemmerer H. Ventricular septal defects. In: Gatzoulis M, Webb G, Daubeney P, editors. Diagnosis and management of adult congenital heart disease. 2nd edn. Philadelphia: Elsevier Saunders; 2011.
2. VanPraagh R, Geva T, Kreutzer J. Ventricular septal defects. How shall we describe, name and classify them? JACC. 1989;14: 1298–9.
3. Eisenmenger V. Z Klin Med. 1898;32(Suppl):1.
4. Knauth AL, Lock JE, Perry SB, McElhinney DB, Kimberlee G, Landzberg MJ, Rome JJ, Hellenbrand WE, Ruiz CE, Jenkins KJ. Transcatheter device closure of congenital and post operative residual ventricular septal defects. Circulation. 2004;110:501–7.
5. Lock JE, Block PC, McKay RG, et al. Transcatheter closure of ventricular septal defects. Circ. 1988;78:361–8.
6. Acar P, Abadir S, Aggoun Y. Transcatheter closure of perimembranous ventricular septal defects with Amplatzer occluder assessed by real-time three-dimensional echocardiography. Eur J Echocardiogr. 2007;8(2):110–5.
7. Acar P, Abdel-Massih T, Douste-Blazy MY, Dulac Y, Bonhoeffer P, Sidi D. Assessment of muscular ventricular septal defect closure by transcatheter or surgical approach: a three-dimensional echocardiographic study. Eur J Echocardiogr. 2002;3(3):185–9.
8. Arora R, Trehan V, Thakur AK, Mehta V, Sengupta PP, Nigam M. Transcatheter closure of congenital muscular ventricular septal defect. J Interv Cardiol. 2004;17(2):109–15.
9. Barb IT, Kwarteng CA, Block P, Morris DC, Lerakis S. Transesophageal echo to help percutaneous closure of ventricular septal defect post acute myocardial infarction. Acute Card Care. 2011;13:190–3.
10. Szkutnik M, Bialkowski J, Kusa J, et al. Postinfarction ventricular septal defect closure with Amplatzer occluders. Eur J Cardiothorac Surg. 2003;23(3):323–7.
11. Lopez-Sendon J, Gurfinkel EP, Lopez de Sa E, et al. Factors related to heart rupture in acute coronary syndromes in the Global Registry of Acute Coronary Events. Eur Heart J. 2010;31(12):1449–56.
12. Hijazi ZM, Hakim F, Al-Fadley F, Abdelhamid J, Cao Q. Transcatheter closure of single muscular ventricular septal defects using the Amplatzer muscular VSD occluder: initial results and technical considerations. Cathet Cardiovasc Interv. 2000;49: 167–72.
13. Holzer R, Latson L, Hijazi ZM. Device closure of membranous ventricular septal defects after prosthetic aortic valve replacement using the Amplatzer membranous ventricular septal defect occluder. Catheter Cardiovasc Interv. 2004;62(2):276–80.
14. Chessa M, Carminati M, Cao QL, Butera G, Giusti S, Bini RM, Hijazi ZM. Transcatheter closure of congenital and acquired muscular ventricular septal defects using the Amplatzer device. J Invasive Cardiol. 2002;14:322–7.
15. Pedra CA, Pedra SR, Esteves CA, et al. Percutaneous closure of perimembranous ventricular septal defects with the Amplatzer device: technical and morphological considerations. Catheter Cardiovasc Interv. 2004;61:403–10.
16. Pedra CA, Pedra SR, Esteves CA, Chamie F, Christiani LA, Fontes VF. Transcatheter closure of perimembranous ventricular septal defects. Expert Rev Cardiovasc Ther. 2004;2:253–64.
17. Bacha EA, Cao QL, Starr JP, Waight D, Ebeid MR, Hijazi ZM. Perventricular device closure of muscular ventricular septal defects on the beating heart: technique and results. J Thorac Cardiovasc Surg. 2003;126:1718–23.
18. Cao QL, Du ZD, Joseph A, et al. Immediate and six-month results of the profile of the Amplatzer septal occluder as assessed by transesophageal echocardiography. Am J Cardiol. 2001;88:754–9.

Echocardiographic Guidance for Catheter-Based Removal of Right-Sided Intracardiac Thrombus

11

Nino Mihatov and David M. Dudzinski

Abstract

Pulmonary embolus and clot-in-transit represent medical emergencies that, depending in part on hemodynamic compromise and imaging findings, may require invasive percutaneous therapies. Echocardiography provides immediate noninvasive bedside information to diagnose these conditions and risk stratify these patients. Percutaneous treatment modalities are then guided by real-time transesophageal echocardiography. Procedural echocardiographers must be knowledgeable of the differential diagnosis of intracardiac masses, familiar with use of three-dimensional imaging, and aware of relevant transesophageal echocardiographic anatomy that will help the interventionalist guide their therapeutic devices within the confines of the beating heart as well as confirm complete extraction of intracardiac masses.

Keywords

Pulmonary embolism • Clot-in-transit • Intracardiac thrombi • Right heart • Right ventricle transthoracic echocardiography • Transesophageal echocardiography • Suction thrombectomy

Introduction

Pulmonary embolism (PE), with an annual incidence estimated at ~7 per 10,000 individuals, is a major source of morbidity and mortality in developed countries [1]. Although mortality estimates vary, the in-hospital mortality rate has been previously reported as high as 50 % in patients with the most severe ("massive") PE [2]. Approximately 4 % of patients with PE have evidence of right-sided intracardiac thrombi or "clot-in-transit" (CIT); these patients are typically more severely ill and may merit more urgent and invasive therapies due to the inherently unstable nature of that thrombus [3, 4]. Diagnostic modalities and therapeutic approaches for PE and CIT vary based on the severity of illness and institutional experience. Echocardiography in particular conveniently and safely provides useful diagnostic information but more importantly serves as an adjunct in the management of CIT and PE, both to prognosticate and gauge the urgent need for invasive therapies, and then to provide real-time guidance for invasive percutaneous therapies.

Electronic supplementary material The online version of this chapter (doi:10.1007/978-3-319-29428-5_11) contains supplementary material, which is available to authorized users.

N. Mihatov, MD
Department of Medicine, Massachusetts General Hospital,
55 Fruit Street, Boston, MA 02114, USA
e-mail: nmihatov@partners.org

D.M. Dudzinski, MD, JD (✉)
Divisions of Cardiology, Echocardiography, and Critical Care,
Massachusetts General Hospital, 55 Fruit Street,
Boston, MA 02114, USA

Division of Pulmonary/Critical Care, and Cardiac Ultrasonography Laboratory, Massachusetts General Hospital, Boston, MA, USA
e-mail: ddudzinski@partners.org

Echocardiography in Diagnosis and Differential Diagnosis of Pulmonary Embolism and Clot-in-Transit

In the diagnosis of PE, multidetector computed tomography (CT) has the highest sensitivity for detection of emboli in the pulmonary artery tree. Echocardiography does not function

M.H. Picard et al. (eds.), *Intraprocedural Imaging of Cardiovascular Interventions*, DOI 10.1007/978-3-319-29428-5_11

in a primary diagnostic role in PE given its limited ability to image the distal pulmonary vasculature [5]. Transthoracic echocardiography (TTE) serves mainly to identify secondary changes in cardiac structure and function that represent manifestations of hemodynamically significant PE. In hemodynamically unstable patients in whom multidetector CT is either unavailable or not safely feasible (e.g. acute renal insufficiency, and/or critically ill patients who cannot travel to the CT scanner), the presence of right ventricular dysfunction on echocardiography can function in a diagnostic role [6].

In suspected cases of PE, echocardiography can demonstrate a free-floating intracardiac thrombus, or clot-in-transit. Overall, various types of CIT confer a higher mortality risk justifying empiric treatment for PE and consideration of thrombus removal. These CIT typically originate from distant deep veins, appearing as seemingly free-floating, highly mobile masses with "worm"-like or serpiginous shapes and relatively homogenous echotexture, and that continuously change shape throughout the cardiac cycle (Figs. 11.1, 11.2, 11.3, and 11.4). Imaging characteristics of any visualized intracardiac mass should always be considered to ensure that the finding is an acute thrombus, as opposed to a chronic thrombus, benign tumor or metastasis, foreign body, or vegetation. Tumors may be more heterogeneously shaped and have variegated echotexture; some tumors may appear homogenous with smooth borders but may be immobile (Fig. 11.5). In addition, catheter-associated thrombi may be encountered, and these may be variably shaped and highly mobile, or, if resulting from thrombus deposition on an area of atrial endocardial injury, may appear smoothed and immobile with a broad base of attachment to endocardium (Fig. 11.6).

Transesophageal echocardiography (TEE) may confirm the diagnosis of PE or CIT due to additional available views for visualization of the right heart, the main pulmonary artery, the right pulmonary artery, and the proximal portion

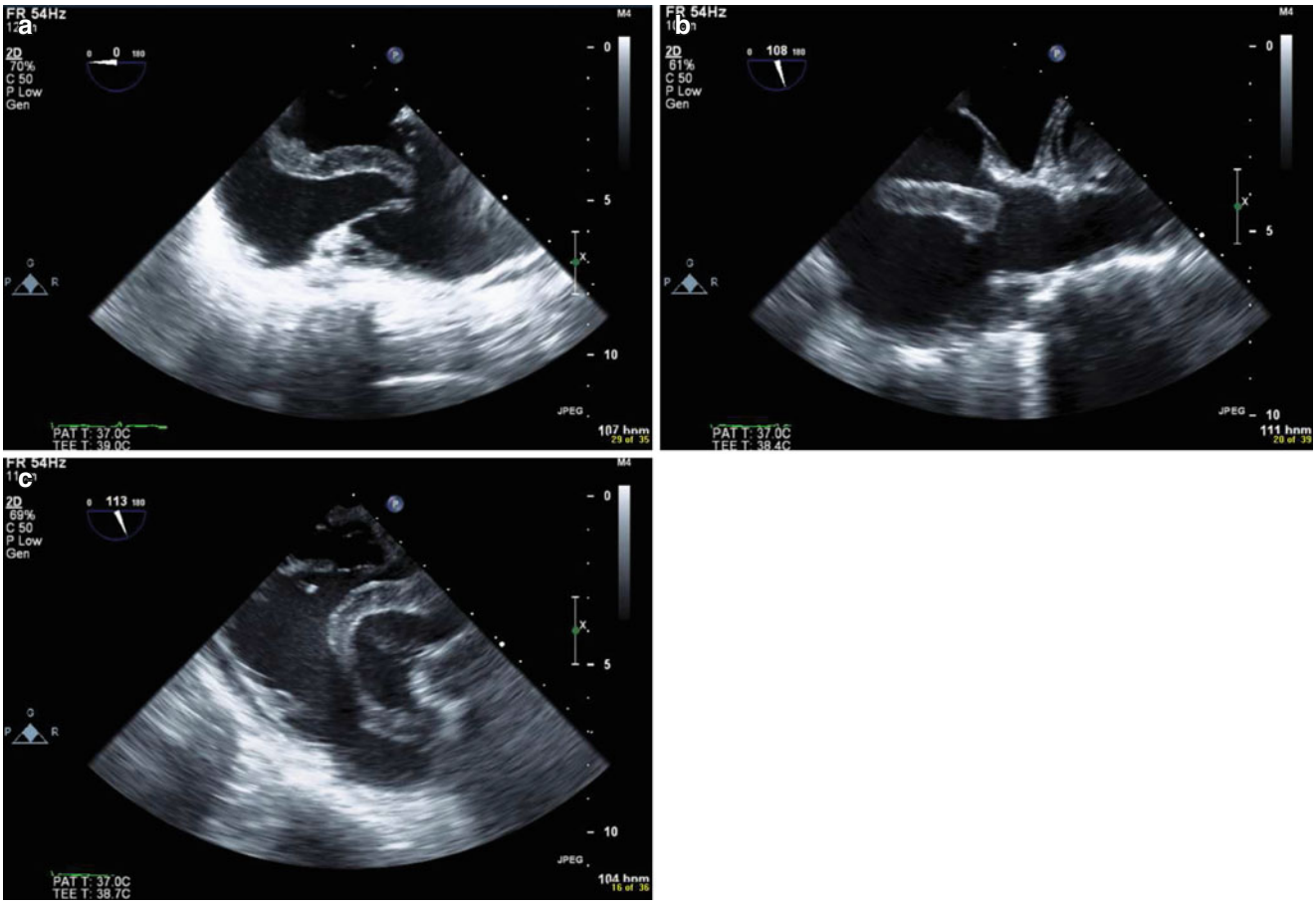

Fig. 11.1 Echocardiographic appearance of intracardiac venous thromboemboli. TEE images from a 76 year old woman with sickle cell trait and recent hospitalization who presented with dyspnea and presyncope, found to be hypoxemic and hypotensive, on whom imaging revealed bilateral main pulmonary emboli and mobile clot-in-transit in the right atrium. Panel (**a**) shows the mid-esophageal four chamber view rotated to focus on the right atrium and right ventricle; a smooth generally homogenously echotextured mass is seen in the right atrium with an overall shape that is reminiscent of a "cast" of a deep vein, and these characteristics suggest venous thromboembolism as likely etiology. Panel (**b**) shows the same finding in a bicaval view, showing no mass in the superior vena cava. Panel (**c**) shows a transgastric right ventricle inflow view, with the mass extending from the right atrium into the right ventricle

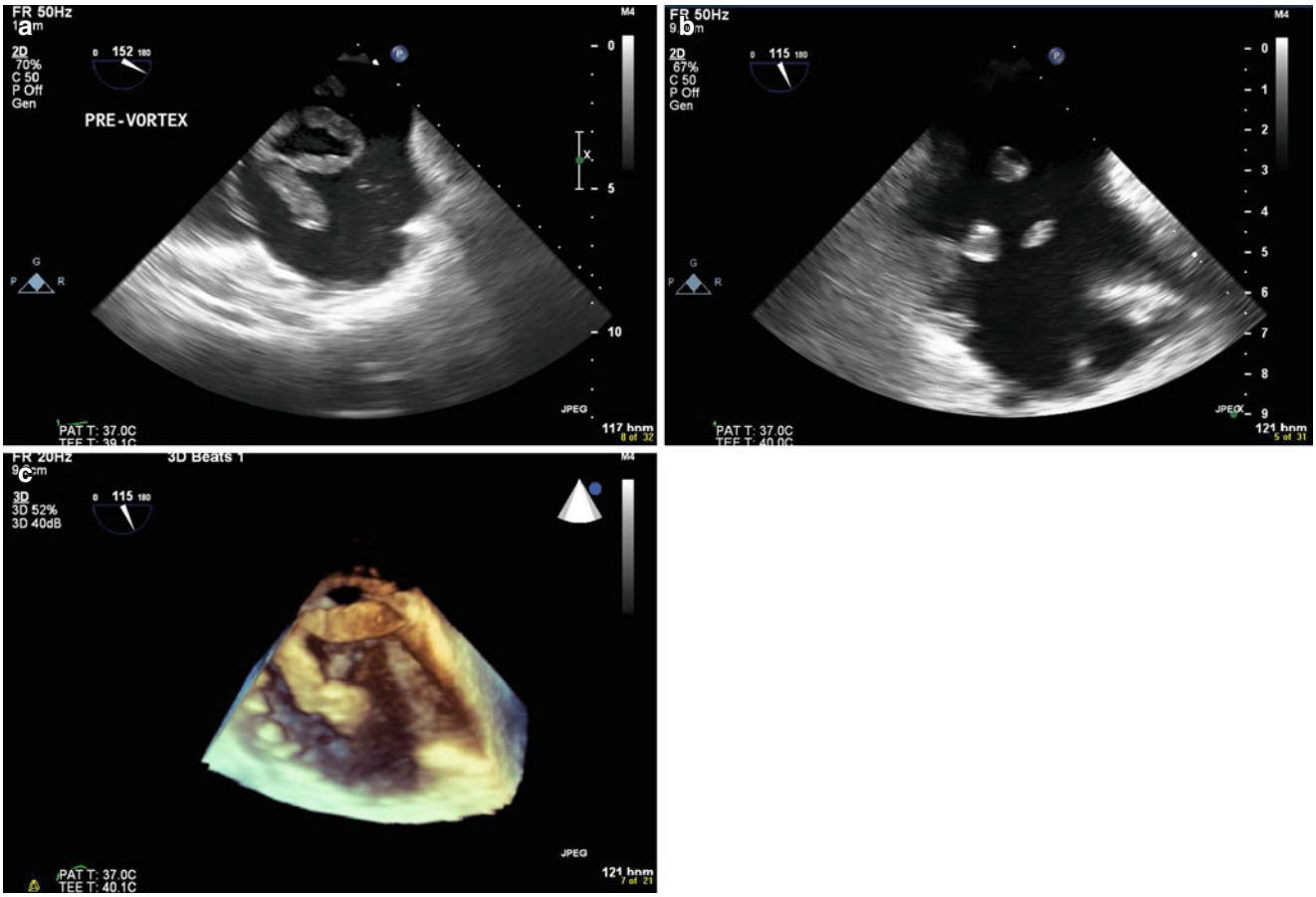

Fig. 11.2 Echocardiographic appearance of intracardiac venous thromboemboli. These TEE images show a clot-in-transit on a 66 year old male with no prior medical history who presented with 6 days of dyspnea and chest congestion, found to have bilateral segmental and subsegmental pulmonary emboli. Panel (**a**) taken from a modified bicaval view, shows the "worm"-like shape with homogenous echotexture suggestive of venous thromboembolism, now located in the right atrium (See associated Movie 11.1). Panel (**b**) shows how the worm-shape venous thromboembolism appears on two-dimensional imaging due to its movement with the cardiac cycle; the three masses seen are not independent but rather part of a contiguous, serpiginous mass. Panel (**c**) shows a three dimensional representation of the image from panel (**b**), confirming that there is a single, long, serpiginous venous thromboembolism (See associated Movie 11.2)

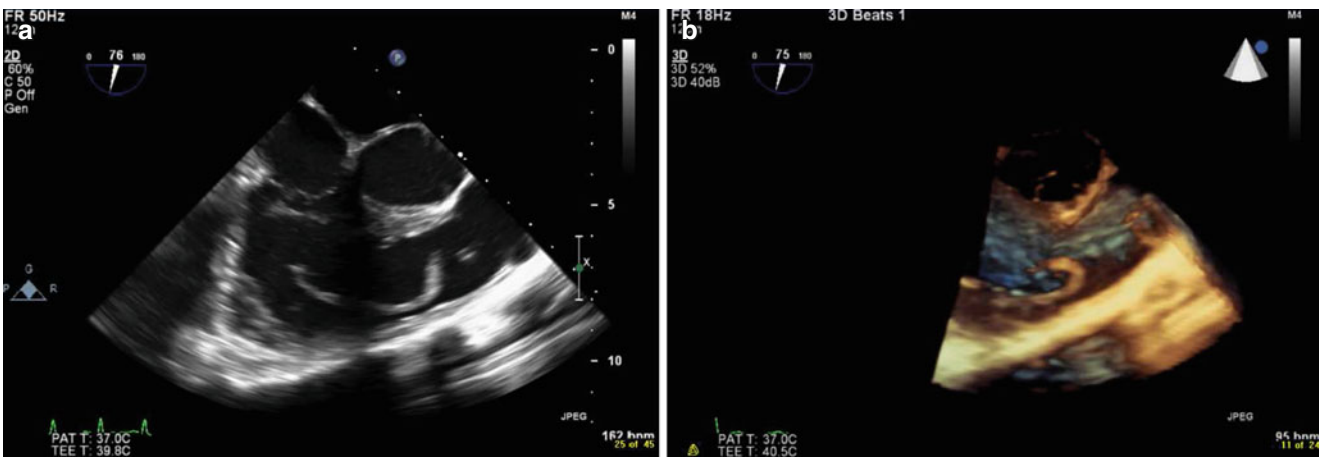

Fig. 11.3 Echocardiographic appearance of intracardiac venous thromboemboli. TEE images from a 24 year old male hospitalized for 2 weeks with abdominal compartment syndrome requiring three laparotomies after complications from a liver biopsy for evaluation of liver failure show a mobile thrombus in the right ventricle and proximal pulmonary artery. Panel (**a**) is a two dimensional view and panel (**b**) represents a three dimensional image (See associated Movie 11.3)

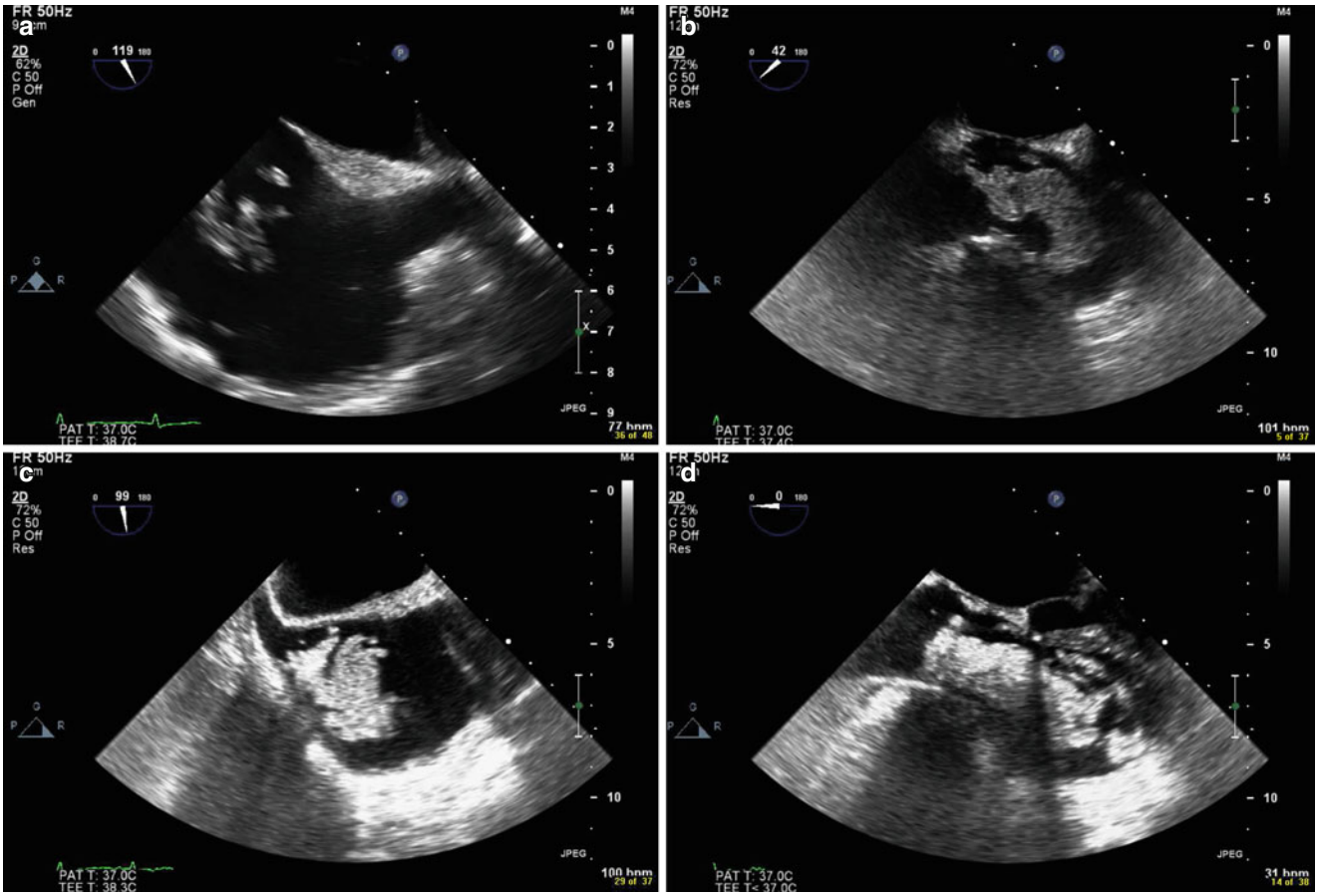

Fig. 11.4 Other echocardiographic and morphological manifestations of venous thromboemboli. These TEE images all show histopathologically confirmed venous thrombi (based on examination of percutaneously extracted specimens). Panel (**a**) shows a mass that lacks smooth borders and has some heterogenous echotexture. Panel (**b**) shows a mass with homogenous echotexture but again with irregular borders. Panels (**c**, **d**) show a mass of significant size that nearly obstructs the right heart, and with markedly irregular borders. Thus various echocardiographic features may be associated with venous thromboembolism

of the left pulmonary artery (Fig. 11.7) [7]. TEE has been utilized to identify large centrally located emboli with a reported sensitivity of 80 % and specificity as high as 100 % [8]. In patients being considered for surgical thrombectomy, localization of a PE by TEE can help ascertain the feasibility of surgical removal. In addition, with TEE the location of clot origin may be assessed (e.g. inferior or superior vena cava) and additional definition of the interaction of the intracardiac mass and right sided cardiac structures is available (Fig. 11.7).

Echocardiography in Risk Stratification of Pulmonary Embolism

Early risk stratification in suspected or confirmed cases of PE is essential to guideline-based concepts of therapeutic decision-making [9, 10]. Pulmonary emboli increase pulmonary vascular resistance and pulmonary artery (PA) pressure, which in turn increases right ventricular (RV) afterload, and manifesting as RV dilatation and systolic dysfunction. Due to fixed pericardial constraint, RV dilatation can impact the interventricular septum resulting in left ventricular under-filling, which causes decreased cardiac output and hemodynamic consequences. Hemodynamically unstable patients are classified to have "massive" or "high-risk" PE and may derive the most benefit from invasive therapies such as thrombolysis, surgery, or percutaneous embolectomy [9]. In hemodynamically stable patients, markers of RV dysfunction as demonstrated by echocardiography, CT, and elevated natriuretic peptide or troponin levels convey prognostic risk and are classified as "submassive" or "intermediate risk" PE, but may also merit consideration of advanced therapeutic options [9].

Although no single TTE measure best predicts severity of PE, findings including RV dilatation and RV hypokinesis independently predict 30-day mortality in hemodynamically stable patients [11, 12]. RV dilatation is indicated by relative RV:LV size in the apical four chamber view, and quantitatively by ratio of RV to LV end diastolic diameter>1. Regional RV

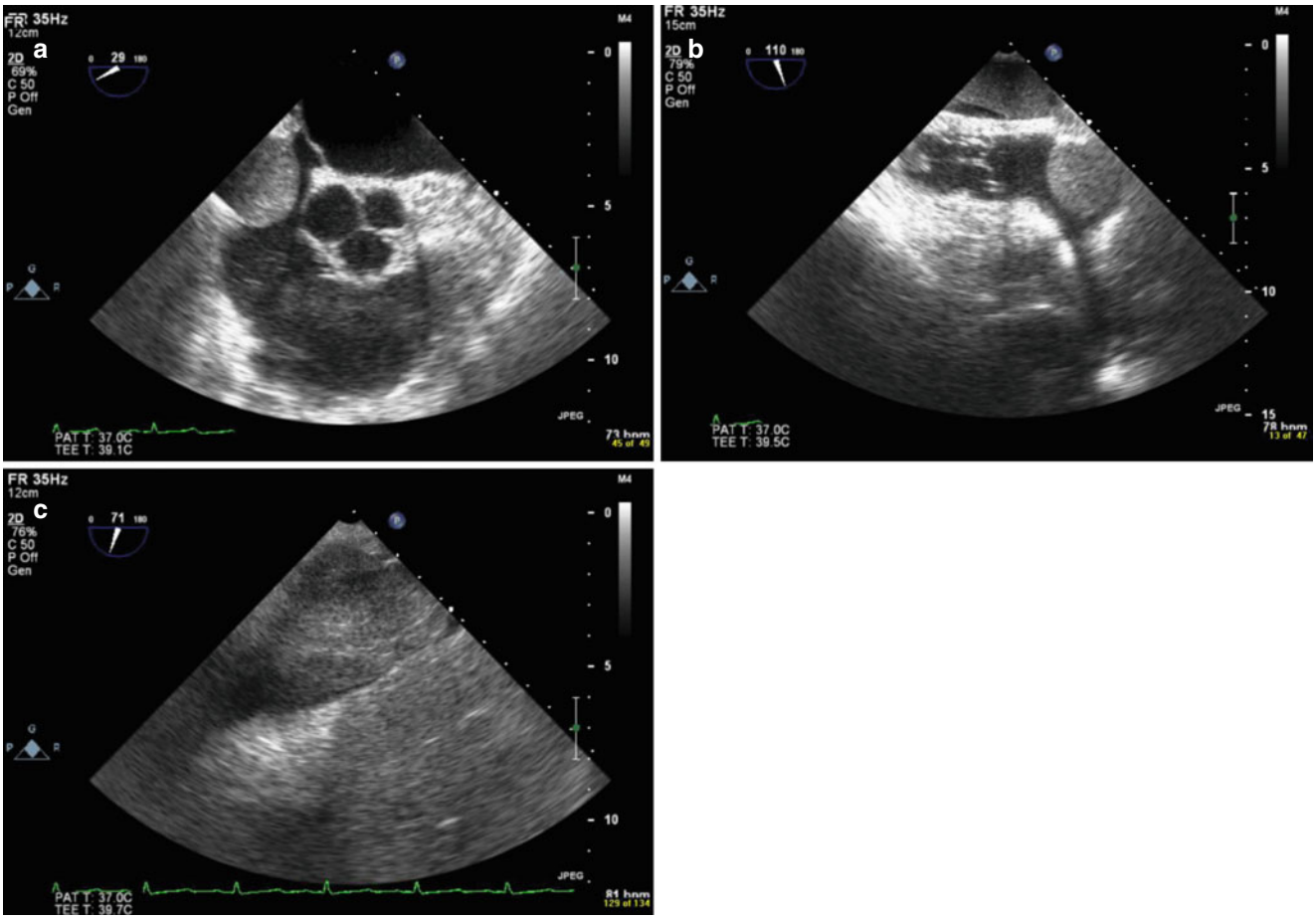

Fig. 11.5 Echocardiographic and morphological manifestations of a malignancy invading the right heart via the inferior vena cava. These TEE images show an adrenal cortical tumor obstructing the right atrium and inferior vena cava in a 66 year old male who presented with new onset edema and rapid respiratory failure. Echocardiography showed a mass in the right atrium, as depicted in the right ventricle inflow-outflow short-axis view in Panel (**a**). Panel (**b**) depicts the mass in the transgastric right ventricle inflow view as totally obstructing the inferior vena cava. Panel (**c**) shows a completely obstructed intrahepatic inferior vena cava

hypokinesis can be difficult to image given the RV contraction along its longitudinal axis. Surrogate measures of longitudinal function include tricuspid annular systolic plane excursion (TAPSE), which reflects translation of the RV basal myocardium, and its related parameter the systolic excursion velocity of the RV basal myocardium (S′), both of which correlate with MRI measures of RV global function in normal patients. Accurate assessment of RV dysfunction based on surrogate measures becomes confounded in PE because there may be regionality in the pattern of affected RV segments. For example, a particular pattern of regional RV dysfunction with apical sparing, commonly called "McConnell's sign", indicates acute cor pulmonale [13]. This pattern of RV dysfunction also makes the aforementioned surrogates of global RV function less accurate. Atrial and ventricular septal geometry, particularly bowing of the right side into the left side indicate consequences of right sided hypertension, with interventricular septum bowing an independent predictor of death related to PE [14]. Doppler techniques identify elevated pulmonary artery pressure by measuring the peak velocity of the tricuspid regurgitant jet. An important caveat is that RV failure can occur without significant elevations of PA pressure [15]. Increased right sided pressures may elevate the right atrial over left atrial pressures, resulting in shunt through an occult patent foramen ovale (PFO). PFO, in the setting of PE, portends an independent increase in mortality, and thus must be searched for on echocardiography in acute PE [16], including as part of the echocardiographic examination when TEE is performed during guidance of percutaneous interventions (Fig. 11.8).

In assessing suspected PE and planning intervention, consideration should be given to the acuity versus chronicity of the findings, as the latter may weigh against requiring acute invasive therapies. Unfortunately, many of the echocardiographic signatures of PE and CIT do not differ as regards chronicity, except possibly RV hypertrophy. However, in the absence of comparison echocardiograms

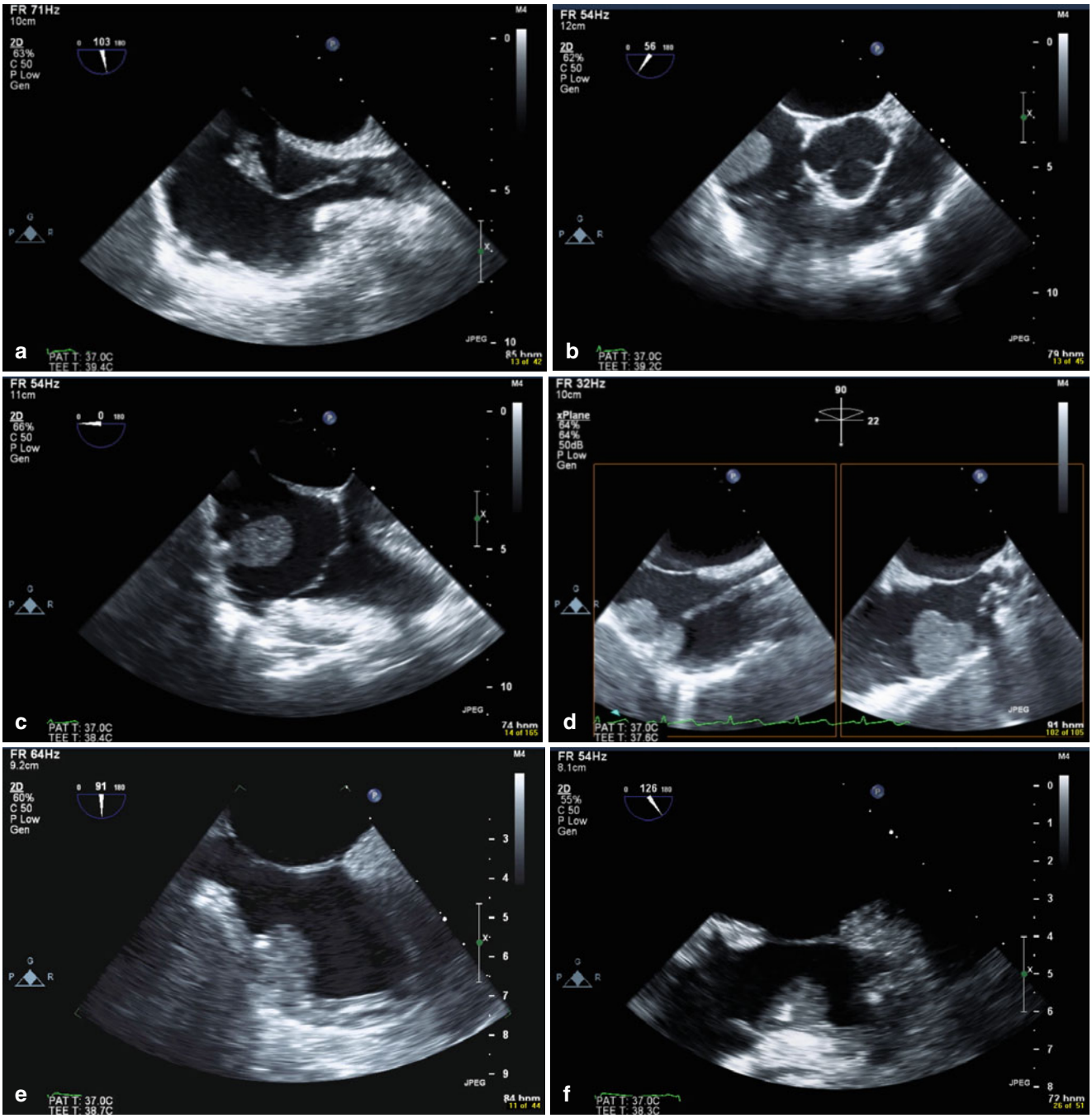

Fig. 11.6 Echocardiographic and morphological manifestations of catheter-associated venous thrombi in the right heart. Figure 11.6 depicts TEE appearance of histopathologically confirmed venous thrombi that are all catheter-associated. Panel (**a**) shows a mobile right atrial mass attached to the superior vena cava catheter tip (See associated Movie 11.4). (Panels **b**–**d**) show a mass of homogenous echotexture attached to the lateral right atrial wall just proximal to the tricuspid valve; the mass is relatively immobile with a broad base, and based on the geometry in panel (**d**) is likely related to catheter trauma and resultant thrombus-in-situ. Panels (**e**, **f**) show a similar finding in another patient who had a central catheter for leukemia chemotherapy; the mass also exhibits generally homogenous echotexture, but has an echodense spot which may indicate calcification and thus suggest chronicity

demonstrating progression of RV wall thickness, acuity is difficult to assess. Even hypertrophy, which may be a result of preexisting cardiac or lung disease, then needs to be cautiously interpreted with reference to absolute, population-based standards.

The presence of a free-floating heart thrombus or CIT portends higher risk for overall PE mortality. While relatively rare among acute PE patients, CIT has also been identified as an independent predictor of hemodynamic collapse and mortality in initially apparently stable patients with

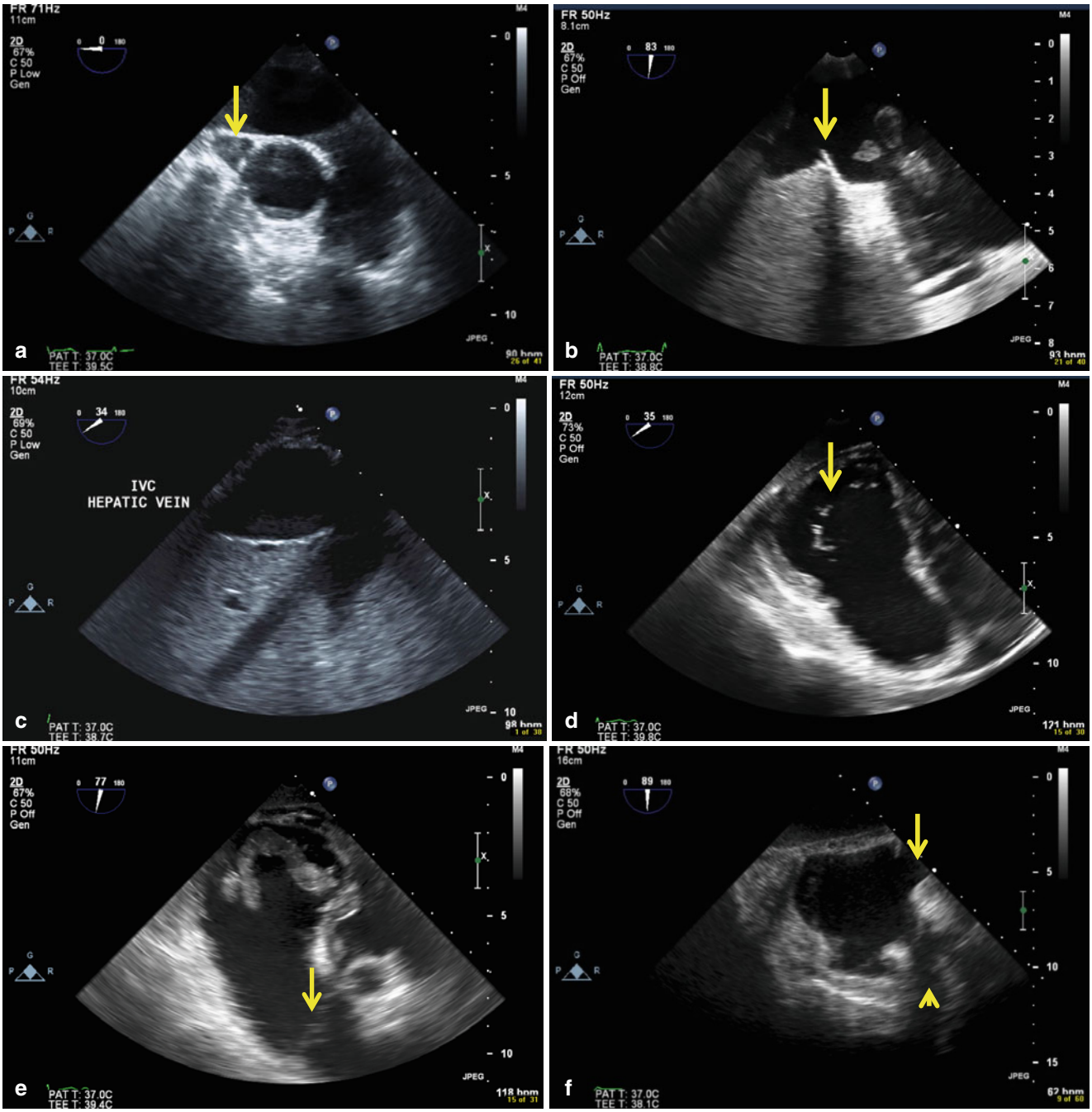

Fig. 11.7 Additional TEE views to evaluate the right heart. This figure depicts additional TEE views to evaluate the right heart and sources of intracardiac emboli. (Panel **a**) is an upper esophageal *short axis* view of the main and right pulmonary artery; the superior vena cava is also visible in cross section (*arrow*). Panel (**b**) is a mid-esophageal four chamber with the probe inserted more distally and rotated so as to track from the right atrium into the inferior vena cava; the Eustachian valve is visible (*arrow*) and this is a location where intracardiac masses migrating from the inferior vena cava into the right atrium may be caught or appear attached (See associated Movie 11.5). Panel (**c**) shows the results of further interrogation of the intra-hepatic inferior vena cava with hepatic vein branches. Panels (**d**–**f**) are transgastric views of the right heart; panels (**d**, **e**) represent right ventricle outflow views with the tricuspid valve en face (*arrow*) visible in (**d**) and the pulmonic valve visible in (**e**) (*arrow*). Panel (**f**) shows the right ventricle inflow/right atrium view with a focus on the inferior vena cava, superior vena cava (*arrowhead*), and right atrial appendage (*asterisk*)

PE. Data from the International Cooperative Pulmonary Embolism Registry (ICOPER) showed that for PE patients treated with heparin alone between January 1995 and November 1996, there was a threefold increase in 14 day mortality with CIT (23.5 %) versus those who did not have CIT (8.0 %) [3]. These patients presented with shorter duration of symptoms (2.2 versus 4.3 days), lower systolic blood pressure, and 50 % higher incidence of RV hypokinesis on

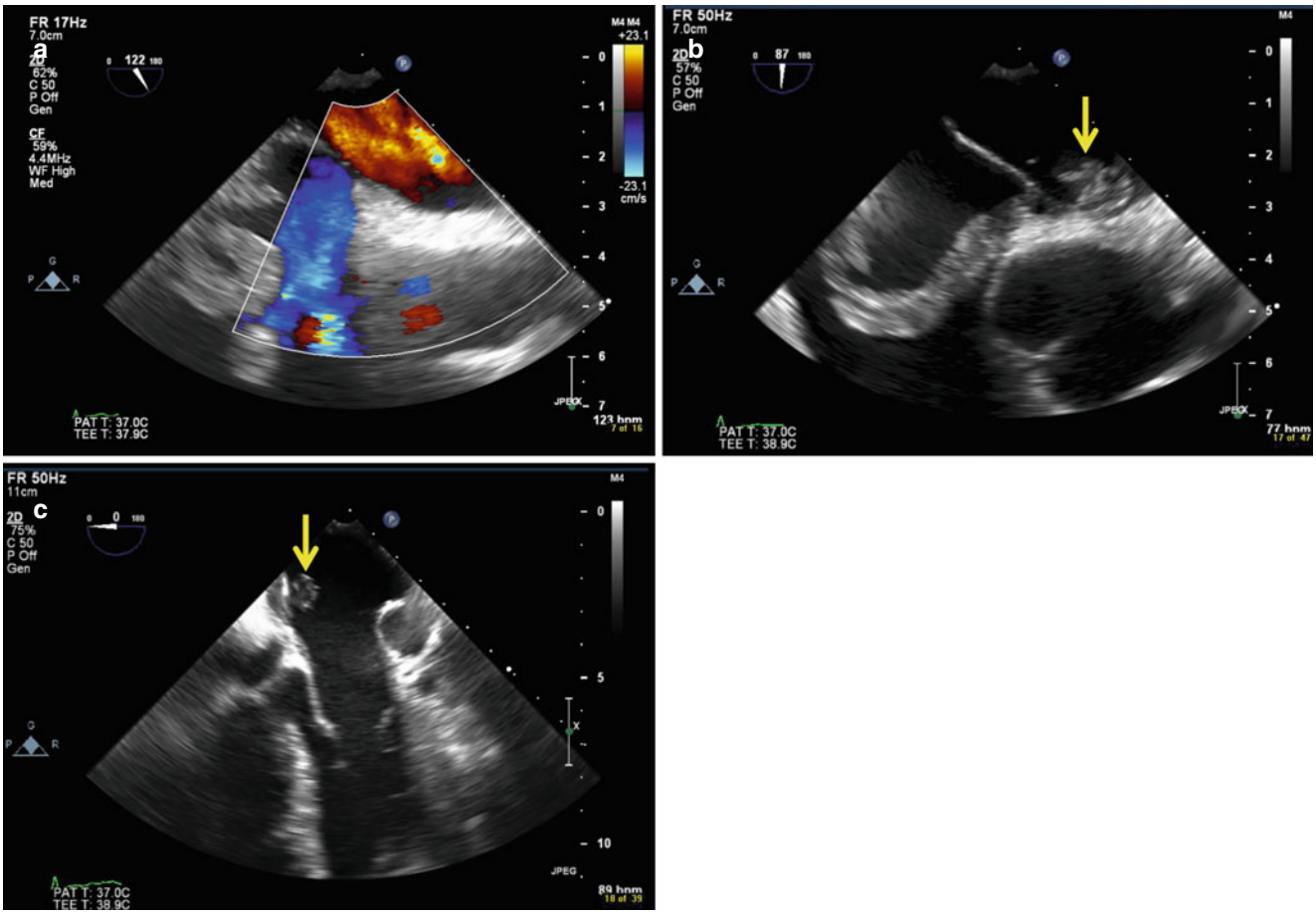

Fig. 11.8 TEE assessment for patent foramen ovale. Patent foramen ovale must be excluded when evaluating patients for percutaneous interventions in pulmonary emboli and clot-in-transit. This can be done with two-dimensional, color Doppler, and contrast enhanced techniques, from windows in the mid-esophageal short axis aortic valve view (depicting the interatrial septum in an anteroposterior orientation) and the bicaval view (depicting the interatrial septum in superoinferior orientation). Panel (**a**) shows a color Doppler picture from the bicaval view, excluding a color communication between the right atrium (where *blue* flows are located) and left atrium (where *red* flows are located) in this picture. Panel (**b**) shows a venous thrombus in the right atrium projecting through the foramen ovale resulting in a portion of the venous thrombus in the left atrium (*arrow*). Panel (**c**) shows that in the same patient in the mid-esophageal four chamber view, the left atrial portion of the thrombus that had embolized across the foramen ovale is visible along the interatrial septum (*arrow*)

echocardiography [3]. Although the overall prevalence of right heart thrombus in PE was low at 4 % in ICOPER, the prevalence has been cited as high as 18 % in hemodynamically unstable patients with PE [17]. This higher prevalence may be related to higher pulmonary artery pressures and decreased cardiac output with relative right heart stasis and consequent slower peripheral clot migration to the pulmonary vasculature. Accordingly, echocardiographic examinations performed earlier in the disease course may be more likely to identify the presence of right heart thrombi in hemodynamically unstable patients. Thus, the presence of CIT in suspected PE may correlate with the degree of hemodynamic compromise.

Echocardiography as an Adjunct in Acute Catheter-Based Management of Pulmonary Embolism and Intracardiac Thrombi

Guidelines review multiple options for management of PE and CIT depending on the severity of cardiopulmonary and hemodynamic insult, size and location of clot, patient comorbidities, and institutional expertise [9, 10]. Lower risk PE and those cases without CIT are generally managed with systemic anticoagulation without need for further intervention. Systemic fibrinolysis can be considered in submassive and massive PE patients [9, 10, 18], but the risks of bleeding, in particular intracerebral hemorrhage, has driven

development of alternative approaches for removal of intracardiac thrombi. Catheter-based intervention and surgical embolectomy are available to address those scenarios because they offer rapid debulking and removal of CIT. Multiple classes of catheter-based interventions are available, including thrombus fragmentation, suction thrombectomy, rheolytic thrombectomy, and rotational thrombectomy [profiled in 9], though often catheter-based therapies are paired with some intravenous thrombolytic (so called pharmacomechanical therapy). For such catheter directed therapies, clinical success rates defined as hemodynamic stabilization, resolution of hypoxemia, and improvement in hospital survival has been reported to exceed 86 % [19, 19A]. Additional techniques in the armamentarium for treatment of PE and CIT include surgical pulmonary embolectomy and ultrasound-assisted thrombolysis (USAT). Surgical pulmonary embolectomy is available as a therapy for patients with severe RV dysfunction [20, 21], for patients with PFO, for patients with contraindications to systemic fibrinolytic therapy, or for those undergoing percutaneous therapy when echocardiographic disappearance of the thrombus occurs [22]. USAT uses local 2.2 MHz ultrasound pulses to distort the clot's fibrin structure and expose plasminogen binding sites, and has been shown to improve echocardiographic measures of RV strain [23, 24].

No single therapeutic approach for CIT has been shown to be superior, and that in part is due to the difficulty in planning prospective, controlled comparative trials. Retrospective reviews of patients with right heart thrombi have suggested lower in hospital mortality when treated with surgical intervention (24 %) or thrombolysis (11 %) than anticoagulation alone (29 %) [25]. This may be because of the potential significant morbidity particularly of CIT and risk of urgent decompensation, especially for those patients who may not have the cardiopulmonary reserve required to withstand additional distal pulmonary emboli, and who thus may benefit from intervention to prevent the embolization of intracardiac thrombus into the pulmonary circulation [25].

At our institution there is aggregate expertise in using a large bore suction thrombectomy device (AngioVac, AngioDynamics, Latham, New York) [26]. This device is a reinforced cannula with a balloon supported expandable funnel-shaped tip (Fig. 11.9). It is designed for "*en bloc* removal of undesirable intravascular material" [26], including thrombus, tumor, or vegetation, while patient is on veno-venous extracorporeal bypass to return blood to the patient [27] (Figs. 11.10 and 11.11). In the initial Massachusetts General Hospital series of consecutive patients treated with this device, 73 % had intracardiac masses (some uses of the therapy were for caval thrombi or tumors), and complete evacuation was achieved in 73 %, with only 7 % conversion to surgical embolectomy, and 87 % survival to hospital discharge, and no report of cardiac perforations [26].

Real-time intraprocedural guidance of the suction thrombectomy cannula requires transesophageal echocardiography. The device can be introduced from either femoral vein or internal jugular vein, with access plan determined in part by the location of the target intravascular material. Percutaneous steering and manipulating the suction thrombectory device can be challenging, in part due to the large size and relative inflexibility of the catheter. While the device can relatively easily be introduced into the cava, expert interventionalists are needed to access the right atrium and maneuver the catheter across the tricuspid valve into the RV, with increasing difficulty encountered in traversing the pulmonic valve into the pulmonary artery and its branches (Fig. 11.9). In the Massachusetts General Hospital case series, technical success was lower when trying to address intravascular material in the pulmonary arterial tree [26]. In addition, because stiff guiding wires may be needed, risk of cardiac (particularly right atrial) perforation is a significant concern [26]. Accordingly, real-time visualization with transesophageal echocardiography is an essential part of the procedure. Mapping intracardiac masses and thrombi can be difficult given deformation and apparent changes in length and shape with cardiac contraction (e.g. Fig. 11.2). The echocardiographer should try to map continuously along any visualized mass, to identify proximal and distal ends, with three-dimensional techniques where possible, so as to accurately gauge overall length (Fig. 11.12); this exercise will help corroborate that the entire mass has been retrieved. During and after the extraction procedure, the echocardiographer must attempt to comprehensively image the relevant field, using slight gradations of transducer imaging plane angle, probe depth, and rotation, so as to ensure complete mass removal and exclude residual debris attached to cardiac walls or valvular structures (Fig. 11.13).

Percutaneous *en bloc* removal of intracardiac thrombi overall has been reported with varying degrees of success. Other case reports of TEE guided removal of a mobile right atrial thrombus with a basket retrieval device suggest technical success at thrombus extraction [28, 29]. Complete extraction was technically challenging with a limited ability to prevent distal clot fragmentation with basket manipulation. To minimize the risk of basket devices fragmenting thrombus, percutaneous catheter aspiration of intracardiac thrombi under TTE guidance has also been reported [30]. Percutaneous removal of intracardiac thrombi is further limited by an inability to appreciate fully the basket retrieving the entire thrombus by echocardiography. The technical challenges and

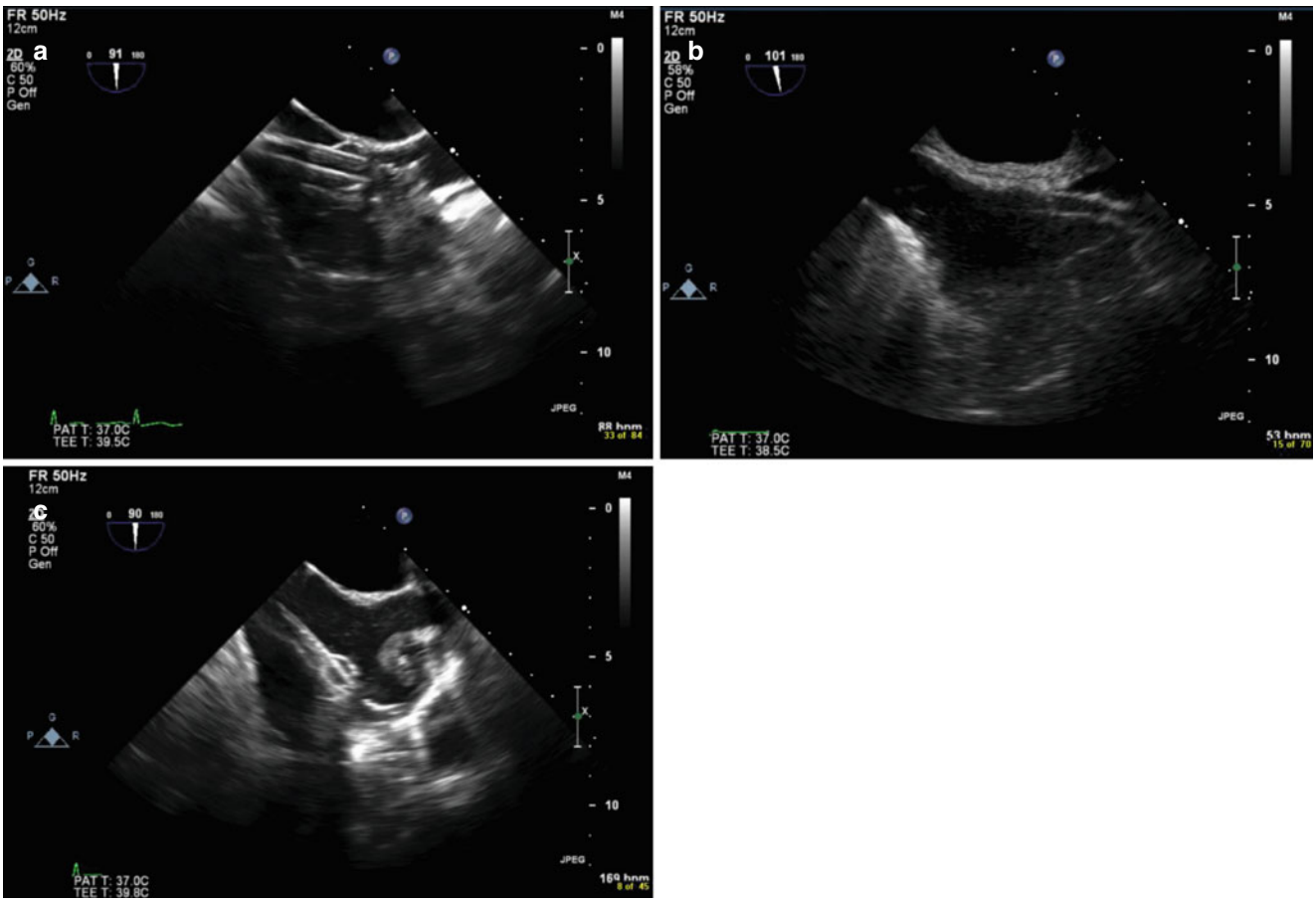

Fig. 11.9 TEE visualization and guidance of large bore suction thrombectomy device. These TEE images show the echocardiographic appearance of a large bore suction thrombectomy catheter (AngioVac). The device is visible as two parallel echodense lines with a balloon supporting a funnel shaped-tip (panel **a**). Panels (**b**, **c**) show the ability to maneuver the device from the right atrium into the superior vena cava (panel **b**, See associated Movie 11.6), and toward the right atrial appendage (panel **c**). The image in panel (**c**) is taken after aspiration of intracardiac debris, and note that the lumen of the catheter no longer appears to be echolucent. In both panels (**b**, **c**) the tricuspid valve is located at approximately 7 o'clock; given the reinforced nature of the cannula device, maneuvering this catheter across the tricuspid valve is challenging

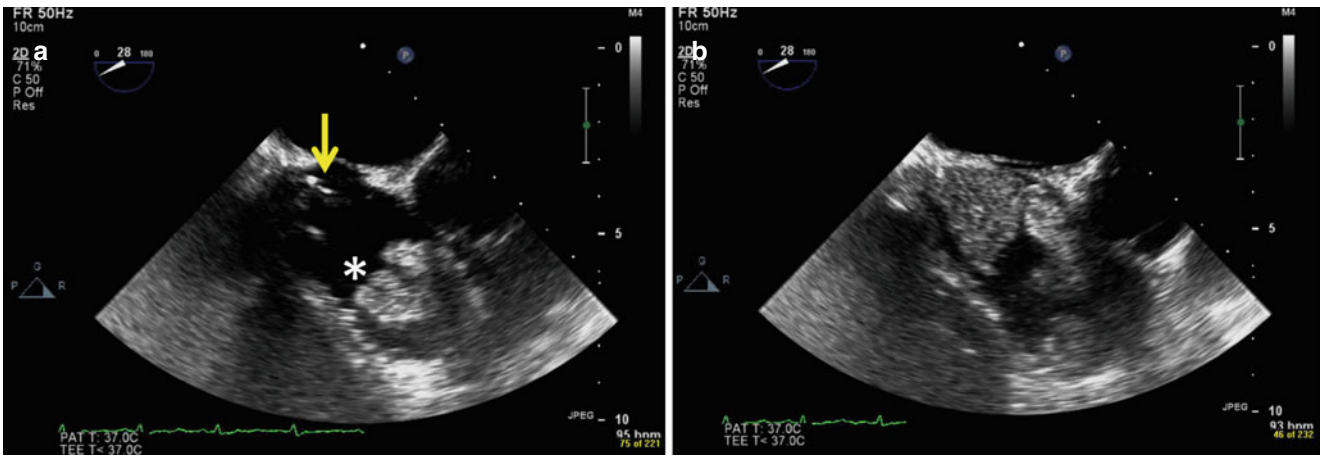

Fig. 11.10 Clot extraction via suction thrombectomy device. Panels (**a**, **b**), taken from mid-esophageal RV inflow views, represent the migration of intracardiac material with large bore suction thrombectomy over a time span of a few seconds. Panel **a**) shows the catheter (*arrow*) approaching the mass (*asterisk*); after suction is activated, the intracardiac mass moves into the suction catheter (See associated Movie 11.7)

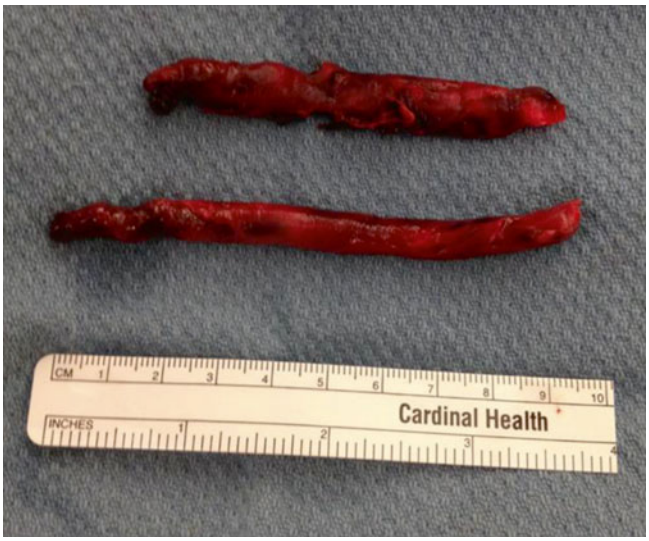

Fig. 11.11 Gross specimen of venous thrombus extraction via suction thrombectomy device. This is a photograph of a gross specimen of clot-in-transit retrieved en bloc from the right atrium (Reprinted with permission of John Wiley & Sons, from Donaldson et al. [27]

limited experience suggest percutaneous removal of intracardiac thrombi may be reserved for patients with contraindications to surgery or thrombolysis.

Echocardiography in Follow-Up of Pulmonary Embolism

Follow-up echocardiographic evaluation of patients after PE demonstrates normalization of RV dysfunction within 3 months in treatment responders [31]. Organized residual thromboemboli may however affect the pulmonary circulation and prevent complete RV recovery. The long-term sequelae of persistent RV dysfunction or elevated pulmonary artery pressures post treatment remains poorly defined in the absence of robust population and longitudinal studies. While routine follow-up echocardiography is not presently recommended, patients with a history of PE and clinical symptoms of dyspnea suggestive of pulmonary

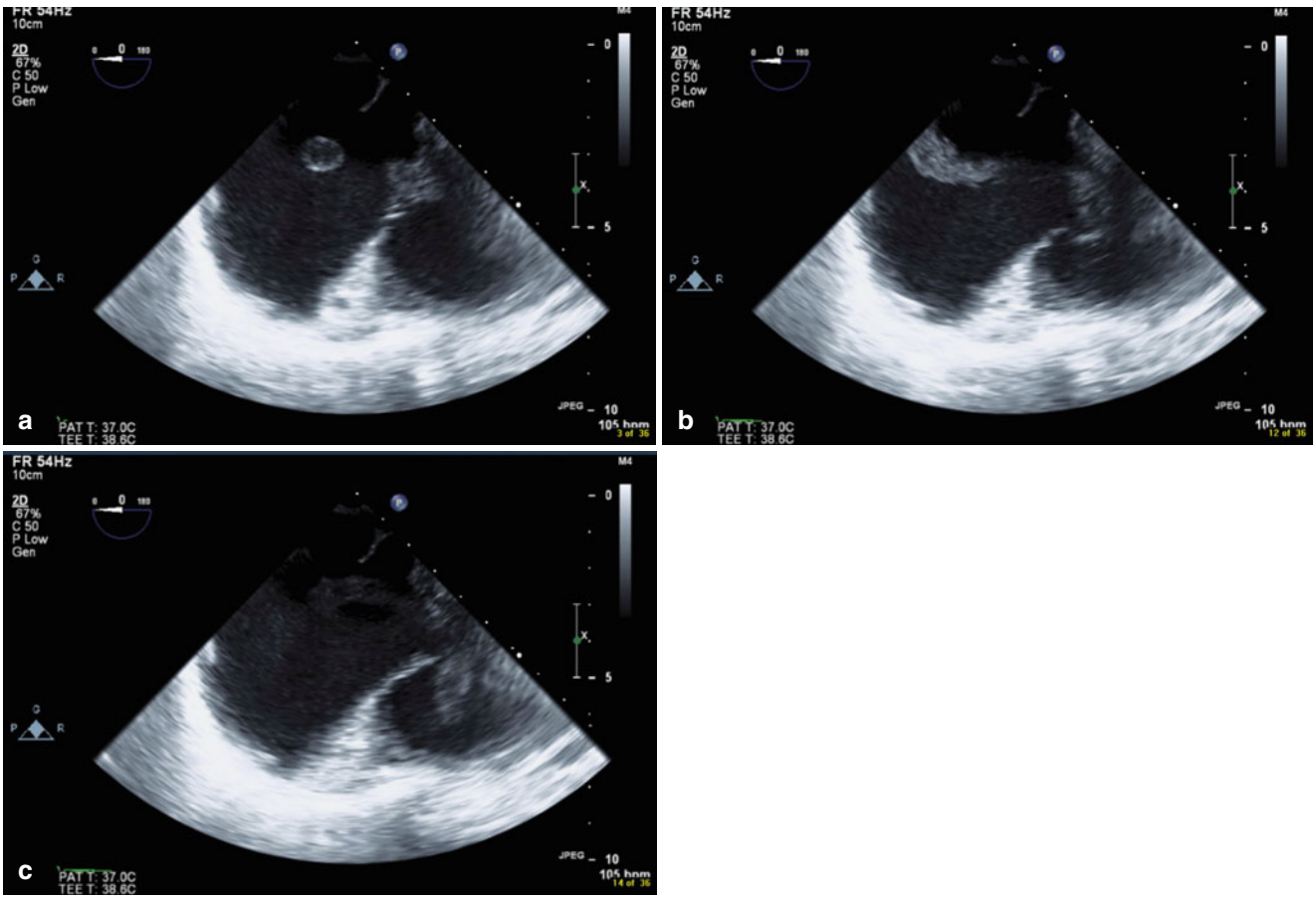

Fig. 11.12 Assessment of overall length of thromboembolic material. Akin to Fig. 11.2b, cardiac motion will render difficult a true ascertainment of the length of venous thromboemboli. Accurate determinations of the distal and proximal ends are useful to gauge overall length so that extraction can be deemed complete or incomplete. Panels (**a**–**c**) show representative right atrium-right ventricle mid-esophageal views that depict motion of the clot with the cardiac cycle; in panel (**a**) the mass appears to be "floating" in the right atrium, but the proximal end lies more superior in the right atrium (panel **b**) and the distal end has prolapsed across the tricuspid valve into the right ventricle (panel **c**)

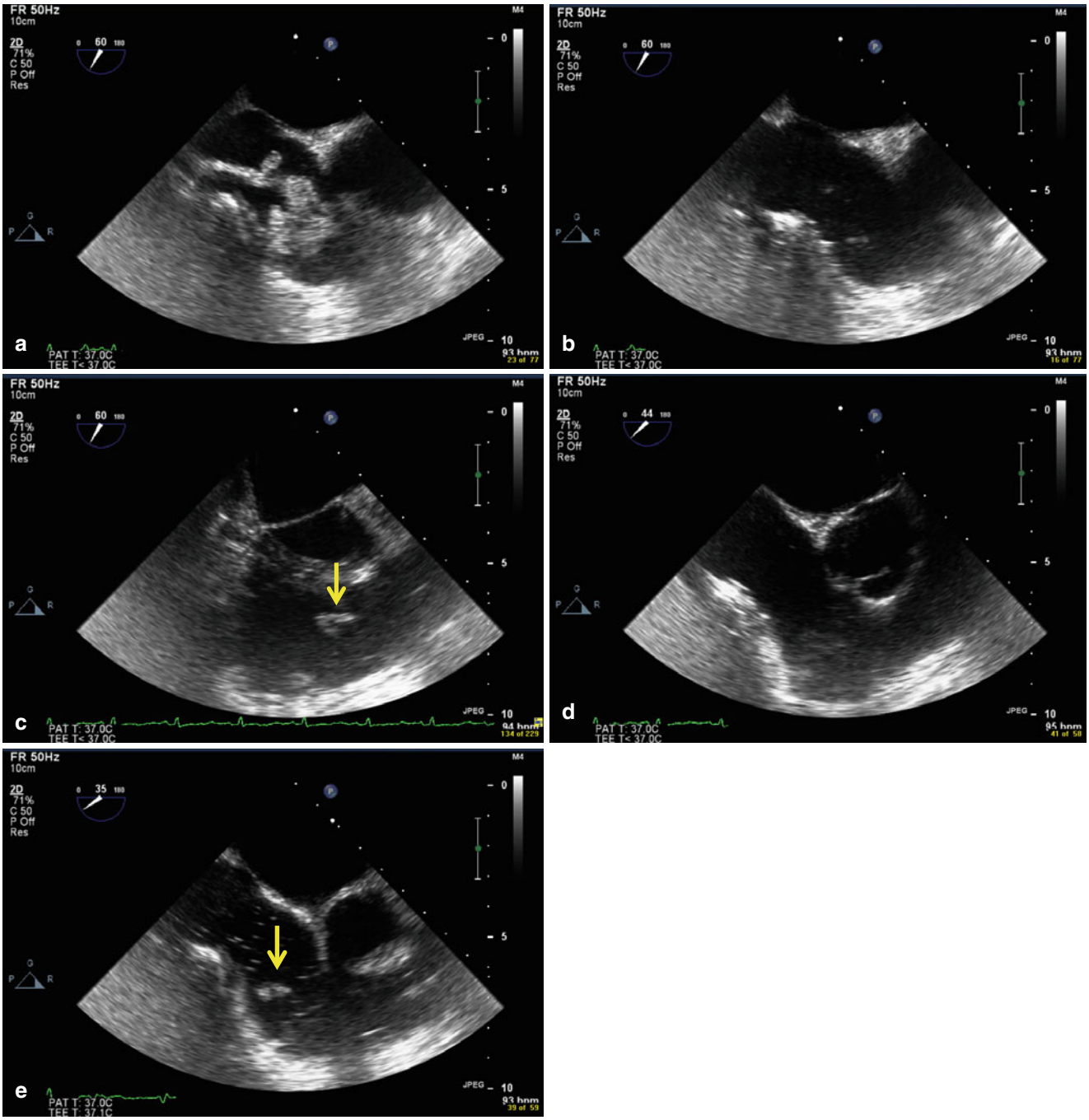

Fig. 11.13 Post-thrombectomy echocardiographic surveillance. These images show results suction thrombectomy of a clot-in-transit from a post-orthopaedic surgery female. Panel (**a**) a mid-esophageal right ventricle inflow view, shows the clot in the right atrium and right ventricle. Panel (**b**) taken in the same view and same omniplane angle, shows the result of what appears to be complete extraction of the mass after suction thrombectomy. Panel (**c**) also taken from the same view and same omniplane angle, shows that with slight rotation of the probe, an independently mobile echodensity (*arrow*) is visible and that is may be associated with the sub-tricuspid valve apparatus; see associated Movie 11.8. The echocardiographer must obtain comprehensive imaging during percutaneous guidance of clot-in-transit removal procedures, by using probe rotation, advancement/withdrawal, and omniplane angle changes in small discrete increments so as to not miss residual clot-in-transit or pieces of debris caught in trabeculations or valve chordae. Panel (**d**) shows the result of suction thrombectomy from the same patient in the mid-esophageal right ventricle inflow-outflow view. Panel (**e**) shows a similar window as panel (**d**) but note that with the slightly lower ominplane angle there is visualized a mobile echodense mass (*arrow*) on the atrial side of the tricuspid valve

hypertension merit close follow-up and reevaluation for new thromboembolism.

Conclusion

PE represents the third most common cause of death from cardiovascular disease after heart attack and stroke. Echocardiography provides immediate noninvasive bedside information to aid in diagnosis and risk stratification of PE and CIT. Transesophageal echocardiography also serves an invaluable role in real-time guidance of novel percutaneous therapies used in the management of submassive and massive PE and for CIT.

References

1. Silverstein MD, et al. Trends in the incidence of deep vein thrombosis and pulmonary embolism: a 25-year population-based study. Arch Intern Med. 1998;158(6):585–93.
2. Torbicki A, et al. Guidelines on the diagnosis and management of acute pulmonary embolism: the Task Force for the Diagnosis and Management of Acute Pulmonary Embolism of the European Society of Cardiology (ESC). Eur Heart J. 2008;29(18):2276–315.
3. Torbicki A, ICOPER Study Group, et al. Right heart thrombi in pulmonary embolism: results from the International Cooperative Pulmonary Embolism Registry. J Am Coll Cardiol. 2003;41(12):2245–51.
4. Kabrhel C, et al. Case records of the Massachusetts General Hospital. Case 29-2014. A 60-year-old woman with syncope. N Engl J Med. 2014;371(12):1143–50.
5. Douglas PS, et al. ACCF/ASE/AHA/ASNC/HFSA/HRS/SCAI/SCCM/SCCT/SCMR 2011 appropriate use criteria for echocardiography. J Am Soc Echocardiogr. 2011;24:229–67.
6. Agnelli G, Becattini C. Acute pulmonary embolism. N Engl J Med. 2010;363(3):266–74.
7. Pruszczyk P, et al. Transoesophageal echocardiography for definitive diagnosis of haemodynamically significant pulmonary embolism. Eur Heart J. 1995;16(4):534–8.
8. Hahn RT, et al. Guidelines for performing a comprehensive transesophageal echocardiographic examination: recommendations from the American Society of Echocardiography and the Society of Cardiovascular Anesthesiologists. J Am Soc Echocardiogr. 2013;26:921–64.
9. Jaff MR, et al. Management of massive and submassive pulmonary embolism, iliofemoral deep vein thrombosis, and chronic thromboembolic pulmonary hypertension A scientific statement From the American Heart Association. Circulation. 2011;123(16):1788–830.
10. Konstantinides S, et al. 2014 ESC guidelines on the diagnosis and management of acute pulmonary embolism: the Task Force for the Diagnosis and Management of Acute Pulmonary Embolism of the European Society of Cardiology (ESC). Eur Heart J. 2014;35(18):3033–80.
11. Kucher N, et al. Prognostic role of echocardiography among patients with acute pulmonary embolism and a systolic arterial pressure of 90 mm Hg or higher. Arch Intern Med. 2005;165(15):1777–81.
12. Sanchez O, et al. Prognostic value of right ventricular dysfunction in patients with haemodynamically stable pulmonary embolism: a systematic review. Eur Heart J. 2008;29(12):1569–77.
13. McConnell MV, et al. Regional right ventricular dysfunction detected by echocardiography in acute pulmonary embolism. Am J Cardiol. 1996;78(4):469–73.
14. Araoz PA, et al. Pulmonary embolism: prognostic CT findings. Radiology. 2007;242(3):889–97.
15. Jardin F, Dubourg O, Bourdarias JP. Echocardiographic pattern of acute cor pulmonale. Chest. 1997;111(1):209–17.
16. Konstantinides S, et al. Patent foramen ovale is an important predictor of adverse outcome in patients with major pulmonary embolism. Circulation. 1998;97(19):1946–51.
17. Casazza F, et al. Prevalence and prognostic significance of right-sided cardiac mobile thrombi in acute massive pulmonary embolism. Am J Cardiol. 1997;79(10):1433–5.
18. Meyer B, et al. Fibrinolysis for patients with intermediate-risk pulmonary embolism. N Engl J Med. 2014;370(15):1402–11.
19. Kuo WT, et al. Catheter-directed therapy for the treatment of massive pulmonary embolism: systematic review and meta-analysis of modern techniques. J Vasc Interv Radiol. 009;20(11):1431–40.

19A. Kuo WT, et al. Pulmonary Embolism Response to Fragmentation, Embolectomy, and Catheter Thrombolysis (PERFECT): initial results from a Prospective Multicenter Registry. Chest. 2015; 148(3):667–73.

20. Leacche M, et al. Modern surgical treatment of massive pulmonary embolism: results in 47 consecutive patients after rapid diagnosis and aggressive surgical approach. J Thorac Cardiovasc Surg. 2005;129(5):1018–23.
21. Goldhaber SZ. Surgical pulmonary embolectomy. Tex Heart Inst J. 2013;40(1):5–8.
22. Yoo YP, Kang KW. Successful embolectomy of a migrated thrombolytic free-floating massive thrombus resulting in a pulmonary thromboembolism. J Cardiovasc Ultrasound. 2013;21(1):37–9.
23. Kucher N, et al. Randomized, controlled trial of ultrasound-assisted catheter-directed thrombolysis for acute intermediate-risk pulmonary embolism. Circulation. 2014;129(4):479–86.
24. Shammas N, Padaria R, Ahuja G. Ultrasound-assisted lysis using recombinant tissue plasminogen activator and the EKOS EkoSonic endovascular system for treating right atrial thrombus and massive pulmonary embolism: a case study. Phlebography 2015;30: 739–43.
25. Rose PS, Punjabi NM, Pearse DB. Treatment of right heart thromboemboli. Chest. 2002;121(3):806–14.
26. Donaldson C, et al. Thrombectomy using suction filtration and veno-venous bypass: single center experience with a novel device. Catheter Cardiovasc Interv. 2015;86(2):E81–7.
27. Chin AK, et al. Application of a novel venous cannula for en-bloc removal of undesirable intravascular material, Special topics in cardiac surgery (ed. C. Narin) ISBN: 978-953-51-0148-2, InTech, doi: 10.5772/25745. Available from: http://www.intechopen.com/books/special-topics-in-cardiac-surgery/application-of-a-novel-venous-drainage-cannula-for-en-bloc-removal-of-undesirable-intravascular-mate.
28. Mukharji J, Peterson JE. Percutaneous removal of a large mobile right atrial thrombus using a basket retrieval device. Catheter Cardiovasc Interv. 2000;51(4):479–82.
29. Beregi JP, et al. Right atrial thrombi: percutaneous mechanical thrombectomy. Cardiovasc Intervent Radiol. 1997;20(2):142–5.
30. Momose T, Morita T, Misawa T. Percutaneous treatment of a free-floating thrombus in the right atrium of a patient with pulmonary embolism and acute myocarditis. Cardiovasc Interv Ther. 2013; 28(2):188–92.
31. Rydman R, et al. Right ventricular function in patients with pulmonary embolism: early and late findings using Doppler tissue imaging. J Am Soc Echocardiogr. 2010;23(5):531–7.

Optical Coherence Tomography: Role in Percutaneous Coronary Intervention

12

David L. Ain, Robert Gallagher, and Ik-Kyung Jang

Abstract

Optical coherence tomography (OCT) is an imaging modality that utilizes back-reflection of near-infrared light. Superior resolution intra-coronary imaging, including assessment of plaque morphology and characteristics as well as imaging stents and post-stent complications have made OCT a powerful research tool, and more recently a clinical tool for guidance of PCI. Visualization of coronary lesions with OCT and their characterization as lipid-rich, fibrous, or fibro-calcific plaque can influence percutaneous coronary intervention (PCI) procedural planning. OCT has contributed significantly to the understanding of culprit lesion pathophysiology in acute coronary syndromes (ACS). ACS culprit lesions have been categorized by OCT features as resulting from plaque rupture, calcific nodule, or plaque erosion. Finally, OCT has proven to be an ideal imaging modality for ensuring optimal results after PCI. OCT can be used to assess for appropriate stent expansion and apposition of the stent with the vessel wall, and is an effective modality for the detection and assessment of stent-edge dissection, incomplete stent apposition, and in-stent tissue protrusion. The resolution of OCT allows for detection and assessment of in-stent neointima proliferation and neoatherosclerosis. A demonstrated safe and effective research instrument, OCT has shown great potential in this clinical role as an adjunctive imaging modality for PCI.

Keywords

Optical coherence tomography • Intra-coronary imaging • Acute coronary syndrome • Coronary artery disease • Intravascular ultrasound • Percutaneous coronary intervention • Plaque rupture • Calcific nodule • Plaque erosion • Instent restneosis • Neointimal proliferation • Neoatherosclerosis

Background

Optical coherence tomography (OCT) is an imaging modality that utilizes back-reflection of near-infrared light. OCT was initially developed at the Massachusetts Institute of Technology, and demonstrated ex vivo imaging of the retina as well as atherosclerotic plaque in 1991 [1]. Its intravascular use was subsequently developed in the late 1990s. For coronary imaging, OCT is performed using an intracoronary catheter that directs near-infrared light toward the coronary arterial walls and then measures the magnitude and echo time delay of the reflected light signal to generate an image. This is analogous to intravascular ultrasound

D.L. Ain, MD • R. Gallagher, MD
Cardiology Division, Massachusetts General Hospital, Boston, MA, USA
e-mail: dain@mgh.harvard.edu; rmgallagher@mgh.harvard.edu

I.-K. Jang, MD, PhD (✉)
Cardiology Division, Massachusetts General Hospital, Boston, MA, USA

Cardiology Division, Harvard Medical School, Boston, MA, USA
e-mail: ijang@mgh.harvard.edu

M.H. Picard et al. (eds.), *Intraprocedural Imaging of Cardiovascular Interventions*, DOI 10.1007/978-3-319-29428-5_12

(IVUS), which is being widely utilized in intracoronary imaging, except that OCT generates images by measuring the echo time delay and magnitude of backscattered light instead of sound [1]. OCT imaging has superior spatial resolution compared with IVUS, with current OCT systems providing an axial resolution of 10–15 μm and lateral resolution of 20–30 μm, but with tissue depth limited to 2–3 mm [2]. By comparison, IVUS has a spatial resolution of approximately 150–250 μm with tissue depth up to 10 mm [3]. A recently introduced Ilumien Optis OCT system utilizes a rapid automated pullback to image up to 75 mm coronary segments at a rate of 35 mm/s. OCT has been safely incorporated into cardiac catheterization procedures with low rates of complications [4]. Superior resolution coronary imaging, including assessment of plaque morphology and characteristics as well as imaging stents and post-stent complications have made OCT a powerful research tool, and more recently a clinical tool for guidance of percutaneous coronary interventions (PCI).

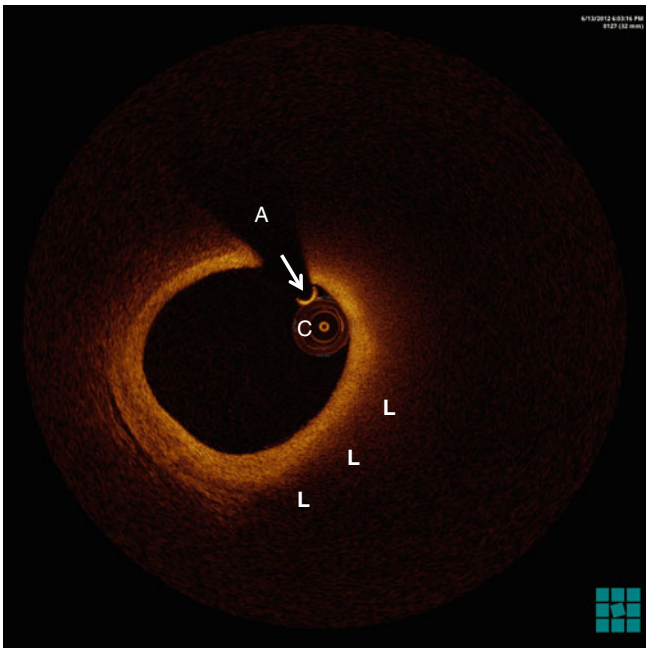

Fig. 12.1 Lipid-rich plaque (*L*) is characterized by a signal-poor region with diffuse borders. The OCT catheter (*C*) and coronary guidewire (*arrow*) can be seen within the artery lumen. The guidewire causes a backscatter imaging artifact (*A*) at the top of the image

OCT of Coronary Atherosclerosis

Practical application of OCT during coronary angiography in current cardiac catheterization procedures involves tracking of the OCT catheter into the coronary artery over a standard 0.014 in. coronary guidewire with image acquisition then performed during automated pullback of the imaging transducer within the OCT catheter. Because intraluminal blood produces significant scatter artifact on OCT images, image acquisition must be performed simultaneously with catheter injection of contrast, dextran, or saline to fully displace blood from the imaged coronary segments. For this reason, careful guiding catheter engagement for injection is critical to ensuring adequate image quality. Similarly, aorto-ostial segments of the left main and right coronary arteries are often difficult to adequately image with OCT, as imaging these locations prohibits full engagement of the guiding catheter, making displacement of blood by injection of these segments difficult. Once acquired, images are recorded and can be reviewed and manipulated in axial and longitudinal views to allow for analysis of the coronary anatomy and pathology, also facilitating measurements for guidance of PCI.

OCT has proven useful in identifying plaque characteristics with more accuracy and detail than other modalities, including IVUS [5–10]. Visualization of coronary lesions with OCT and their characterization as lipid-rich, fibrous, or fibro-calcific plaque (Figs. 12.1, 12.2, and 12.3) can

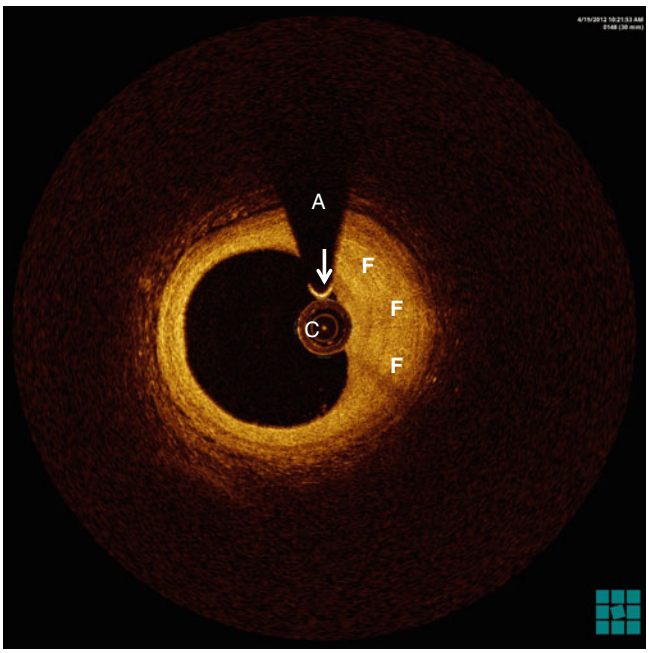

Fig. 12.2 Fibrous plaque (*F*) is characterized by a homogenous signal-rich region. Again, the OCT catheter (*C*) and coronary guidewire (*arrow*) can be seen within the artery lumen, with the guidewire causing characteristic backscatter imaging artifact (*A*)

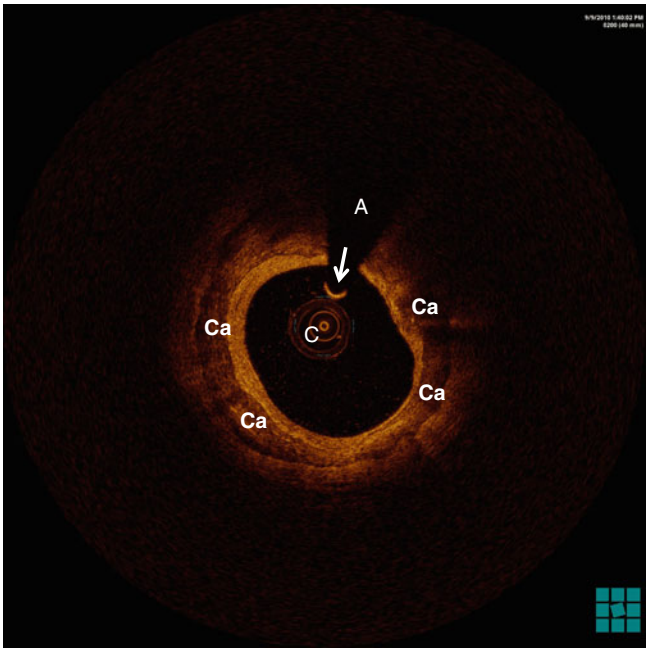

Fig. 12.3 Fibrocalcific plaque (*Ca*) is characterized by well-delineated, signal-poor regions with sharp borders. Circumferential calcification is seen in this image. Again, the OCT catheter (*C*) and coronary guidewire (*arrow*) can be seen within the artery lumen, with the guidewire causing characteristic backscatter imaging artifact (*A*)

influence PCI procedural planning. Furthermore, OCT has contributed significantly to the understanding of culprit lesion pathophysiology in acute coronary syndromes (ACS). ACS culprit lesions have been categorized by OCT features as resulting from plaque rupture, calcific nodule, or plaque erosion. Thrombus associated with culprit lesions is well visualized by OCT and can be characterized as platelet rich white thrombus or platelet poor red thrombus based on backscatter and attenuation characteristics (Fig. 12.4). Other non-traditional causes of ACS culprit lesions can also be well characterized by OCT. These include spontaneous coronary artery dissection, mural hematoma, and recanalized thrombus.

Although still primarily an area of research with a yet undefined clinical role, OCT imaging of vulnerable coronary plaques has been a vibrant area of research and discovery. Vulnerable plaques are those that have a high risk of rupture and resultant ACS. Histologic features of such vulnerable plaques include thin fibrous caps (<65 μm), large lipid cores (more than 40 % of overall plaque volume), and increased macrophage infiltration. OCT, with its resolution of 10–15 μm, is the only modality capable of visualizing the thin fibrous cap for identification of a thin cap fibroatheroma (TCFA) (Fig. 12.5). OCT identification of TCFA has been

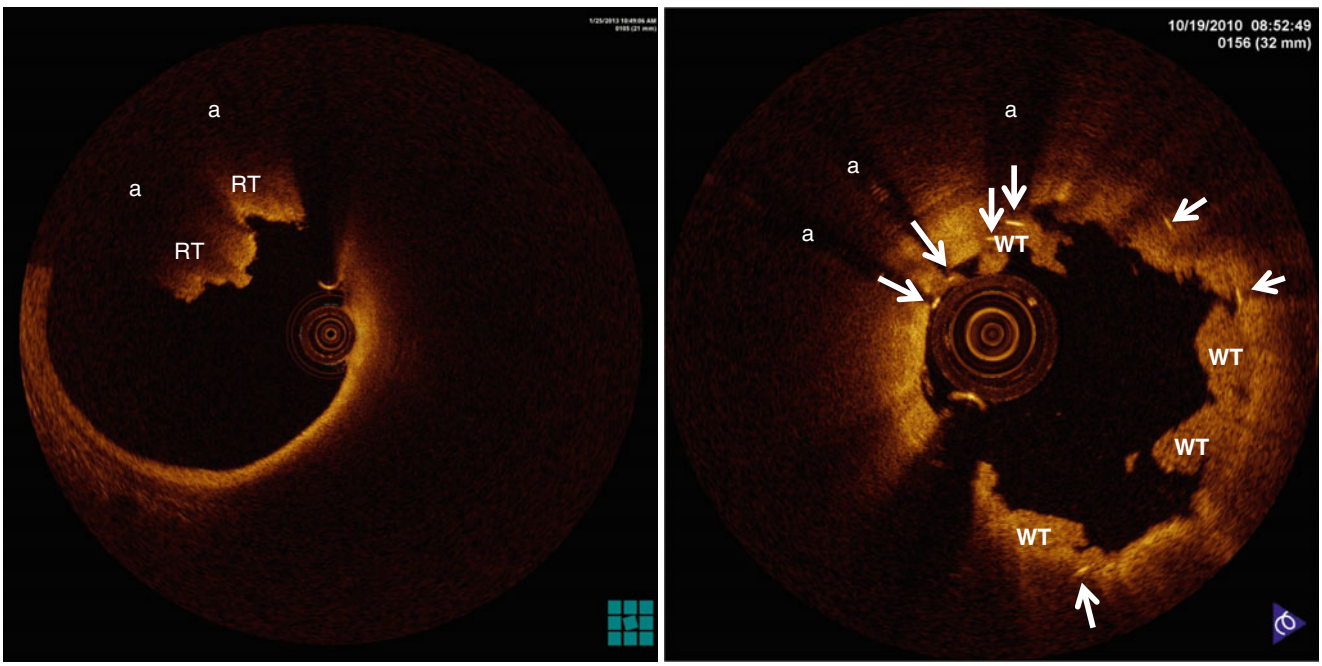

A: Red Thrombus **B: White Thrombus**

Fig. 12.4 Thrombus is clearly visible by OCT. (**a**) Red thrombus (*RT*) is erythrocyte-rich, platelet-poor and has a high degree of backscattering and attenuation (**a**). (**b**) White thrombus (*WT*) is platelet-rich and has homogenous backscatter and low attenuation. Structure including stent struts is visible behind thrombus. Metallic stent struts (*arrows*) are clearly visible and produce characteristic attenuation artifact (**a**)

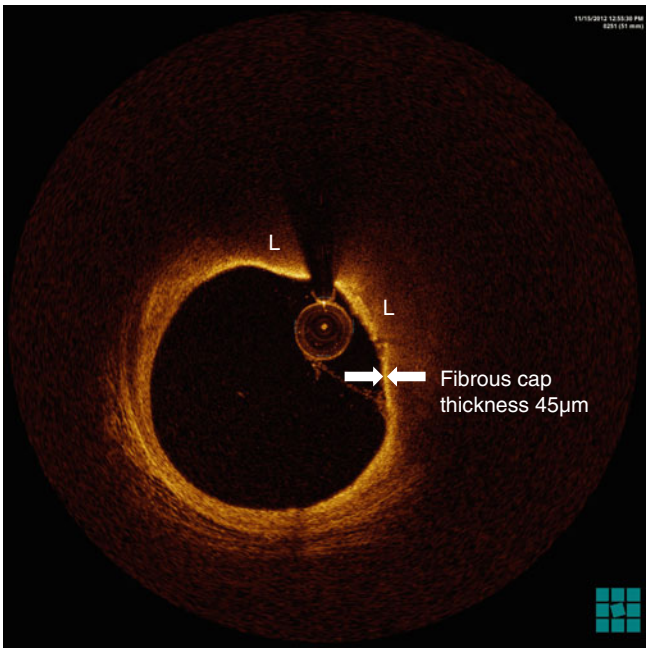

Fig. 12.5 Thin-cap fibroatheroma is characterized by a large lipid core (*L*) under a thin fibrous cap of <65 μm thickness

shown to correlate well with histology [11, 12]. Clinically correlated, patients with ACS are significantly more likely to have disrupted thin fibrous caps overlying their culprit lesions and thinner mean cap thickness compared with patients presenting with stable angina [9, 13].

OCT-Guided PCI

Before PCI, OCT can be used to accurately determine target vessel and lesion dimensions and characteristics to inform optimal stent sizing and procedural execution. If possible, OCT imaging can be performed prior to any manipulation of the target lesion, other than guidewire passage. In the event of a very severe stenosis or occlusive thrombus precluding OCT catheter passage, gentle balloon angioplasty pre-dilation can be performed to allow passage of the OCT catheter without gross disruption of the lesion if possible. Pre-PCI imaging is used to measure reference vessel diameter both proximal and distal to the target lesion, as well as lesion length (Fig. 12.6). These measurements are used to determine stent sizing, and a phantom-controlled study comparing OCT to IVUS for measurement of luminal dimensions found that OCT was more accurate and more reproducible than IVUS for making these measurements [14]. Lesion and reference vessel measurements are then used to select optimal stent diameter and length as well as appropriately size pre-dilation and post-dilation angioplasty balloons.

Plaque characteristics such as fibrous, lipid content and degree of calcification can also be determined on pre-PCI OCT imaging. These characteristics, as defined by OCT correlate with the risk of post-PCI complications [15–18]. These features may further influence choices regarding lesion preparation prior to stenting (i.e. use of pre-dilatation, cutting balloon, rotational atherectomy, etc.).

Minimal luminal area (MLA) of the target lesion can also be determined by OCT prior to any intervention (Fig. 12.6). OCT-derived MLA is moderately accurate, using fractional flow reserve (FFR) as the gold standard, in determining lesion severity, and similar in accuracy to IVUS [19]. OCT, although sensitive in this regard, has lower specificity and therefore limited positive predictive value for defining severe stenoses [20].

OCT for the Detection of Post-PCI Complications

While steady advances in PCI techniques and stent technology—including composition, design, and pharmacology—have made the field of interventional cardiology remarkably safe and effective, complications related to stent placement continue to limit procedural success in certain cases [21]. Understanding the mechanisms behind stent thrombosis and restenosis provides a potential opportunity to alter procedural elements in order to prevent adverse events. Intracoronary imaging has emerged as a key element in both defining stent complications and attempting to prevent untoward outcomes related to stenting. Research utilizing IVUS has laid the groundwork for this understanding, and IVUS has been the predominant mode of this type of imaging in clinical practice [22–27]. With its higher resolution and sensitivity, OCT has however emerged as an attractive modality for the characterization of both acute and chronic complications of intracoronary stenting.

Over the past decade, several studies have examined the feasibility of OCT for the detection of complications that arise post-PCI [28–31], and additional work has explored the connection between OCT-identified complications and adverse cardiac events [32]. OCT has proven to be an ideal imaging modality for ensuring appropriate stent expansion and evaluating apposition of the stent with the vessel wall [33, 34]. In addition to being an accurate tool for the evaluation of stent expansion and stent-vessel apposition, OCT has been demonstrated to be an effective modality for the detection and assessment of stent-edge dissection (disruption of the intima) (Fig. 12.7) [28, 30, 31, 35], incomplete stent apposition [28, 34] (Fig. 12.8), and in-stent tissue protrusion (protrusion of tissue between stent struts) [32, 36] (Fig. 12.9). More recent work has focused on the clinical implications of

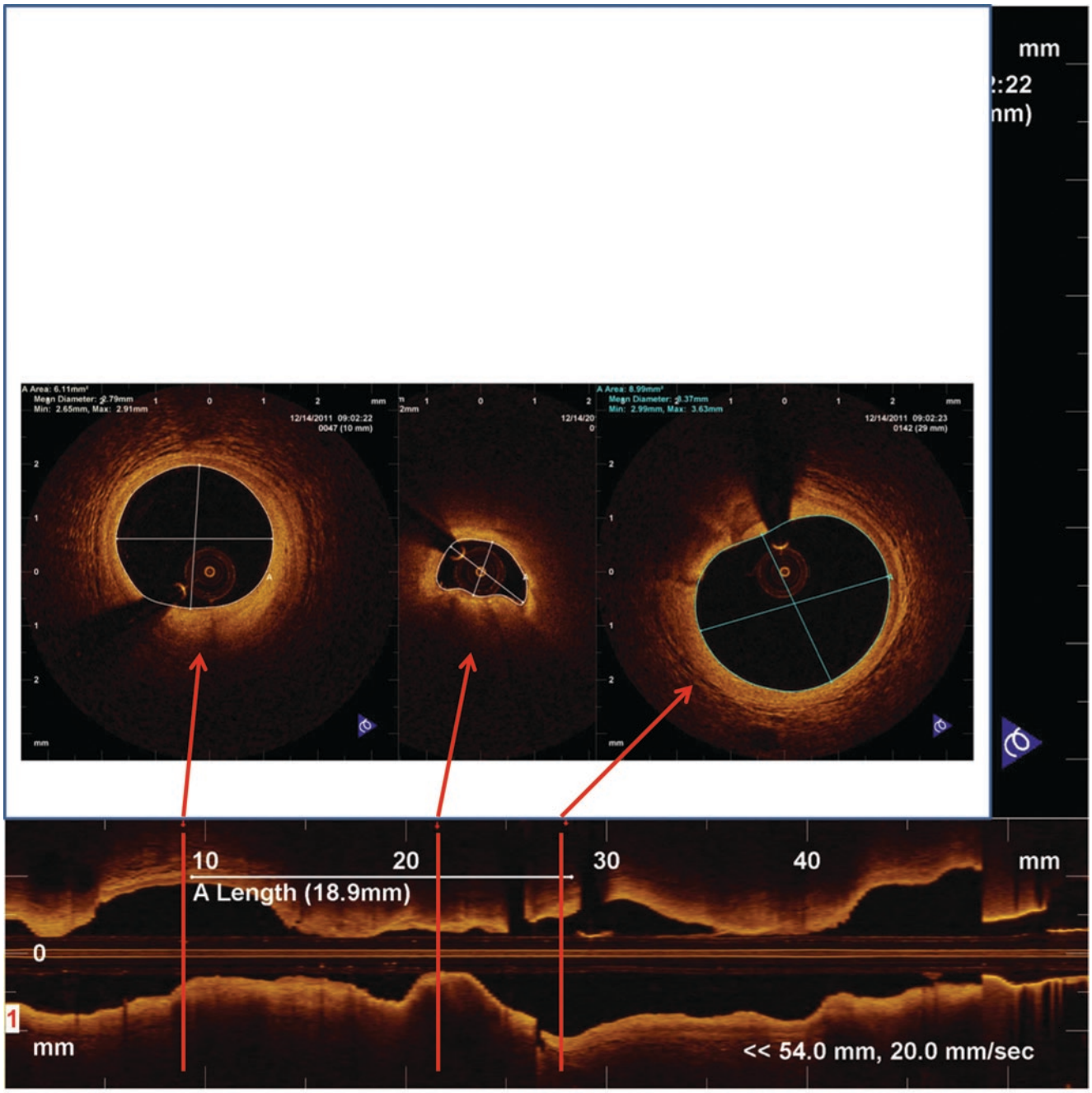

Fig. 12.6 OCT-guided PCI: lesion length is measured using the longitudinal view (*bottom*) and proximal (*right*) and distal (*left*) reference vessel diameters as well as MLA (*center*) are measured in the axial views. In this case the mean proximal reference vessel diameter is 3.37 mm and mean distal reference vessel diameter is 2.79 mm, with an MLA of 1.41 mm^2. Lesion length is 18.9 mm. Based on these OCT measurements, appropriate PCI for this lesion consisted of deployment of a 2.75 × 20 mm stent, followed by post-dilation to 3.5 mm in the proximal segment

OCT-identified complications that arise after PCI [37], and sought to identify stent complications that are associated with increased rates of adverse outcomes [32].

Measurement of minimal stent area is an important assessment that can be made with intravascular imaging. Accurate stent area measurements have been made with greater ease using OCT due to its high resolution and some system features such as automatic edge detection. There appears to be a clear association between small minimal stent area and restenosis [22–24], and stent underexpansion has been found to be an independent predictor of major adverse cardiac events and target lesion revascularization [32]. Research done with IVUS led to a range of cutoff values of 5.0–5.7 mm^2 to predict restenosis. A recent study of OCT-defined acute stent complications, the largest to date, found the best minimal lumen cutoff to predict

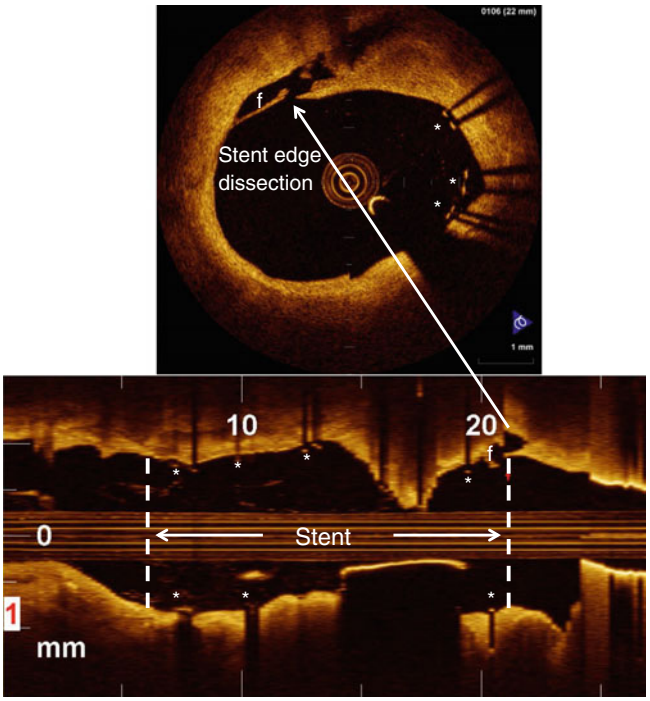

Fig. 12.7 Dissection flap (*f*) clearly visualized by OCT at the edge of a stent, both in the longitudinal view (*bottom*) and axial image (*top*). Groups of stent struts (*) are clearly seen in both views, with their characteristic attenuation artifact

target lesion revascularization by OCT is 5.0 mm^2, and smaller values were independent predictors of both major adverse cardiac events (MACE) and target lesion revascularization (TLR) [32].

Malapposition of the stent with the arterial wall is seen by OCT in anywhere from 10 % to 70 % of stents post-implantation [31–33], and incomplete apposition has been associated with late stent thrombosis [38–40]. OCT permits visualization of individual stent struts and determination of the distance of each strut from the vessel [33]. Research using OCT has demonstrated that reendothelialization occurs more slowly when stent struts are malapposed with the vessel wall [41]. Given what is known about the role of endothelialization in reducing exposure of the thrombogenic surface of the stent polymer and thereby preventing stent thrombosis, the effect of malapposition on late stent thrombosis may be a crucial one. Fortunately new stent scaffolds and enhanced antiplatelet therapy have drastically decreased the rate of serious adverse events after PCI; this will, however, make identifying technical factors that contribute significantly to clinical outcomes more difficult.

OCT's high image resolution allows for identification of dissections at the stent edge and within the stented segment. Because of the higher resolution, stent-edge

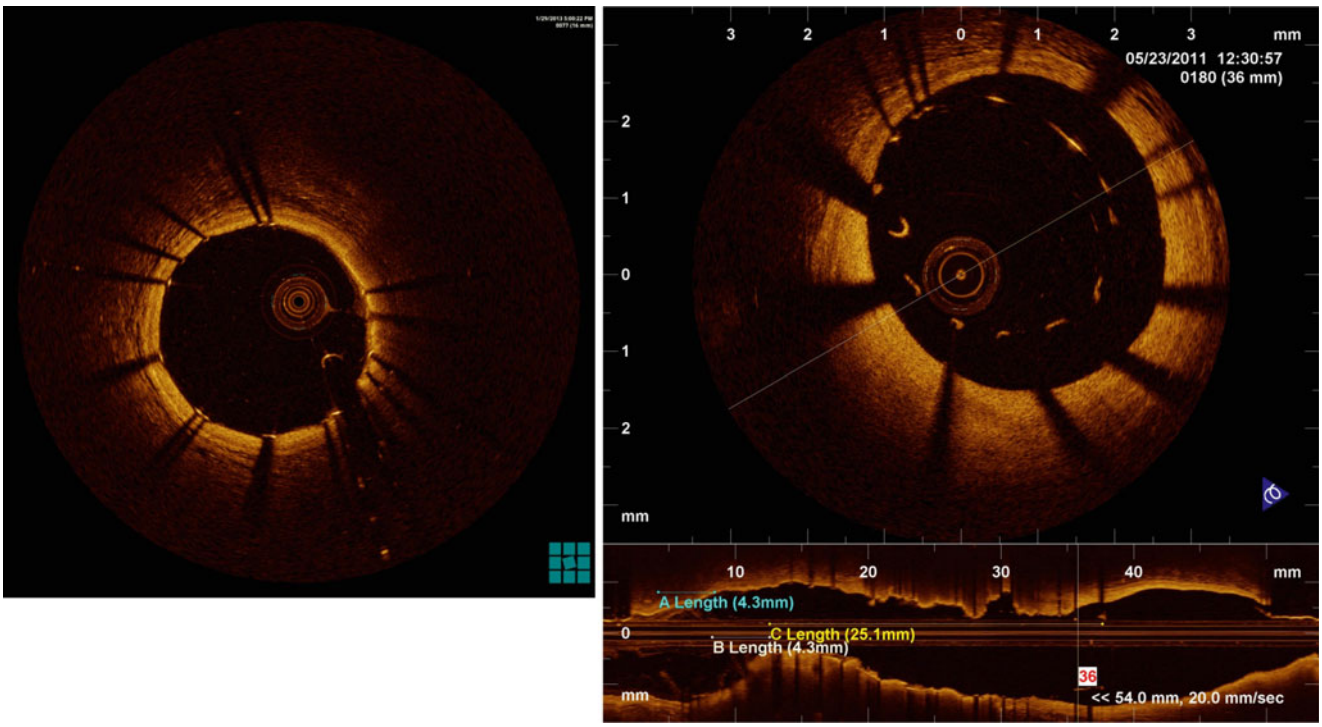

Fig. 12.8 (*Left*) A well-apposed stent with all struts in contact with the coronary intima. (*Right*) Malapposed stent struts with significant distance from the intima. Struts >320–350 μm from the intima are unlikely to become endothelialized and may be associated with adverse coronary events

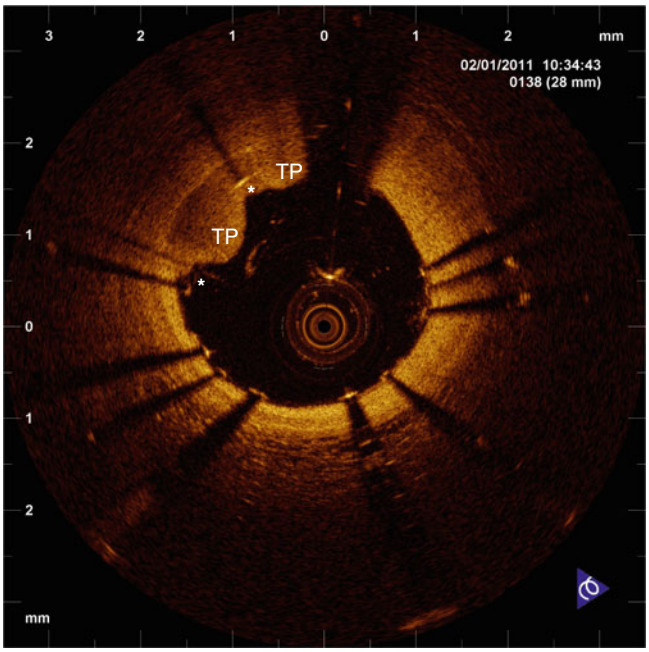

Fig. 12.9 In-stent tissue protrusion (*TP*) between stent struts (*)

dissection (SED) is found at least twice as often by OCT compared with IVUS [28, 31, 35]. OCT-detected SED is less likely to occur when the stent is expanded with its edge in a normal segment of artery compared with in an atherosclerotic plaque [42]. Additional research suggests that the type of plaque that the stent edge is placed in directly affects the risk of SED, with lipid and calcified plaques posing a much higher risk than fibrous plaques [29, 32]. While several studies have not shown a relationship between SED or in-stent dissection and clinical events [31, 32, 37, 43], the amount of lipid at the proximal stent edge has been shown to correlate with post-PCI creatinine kinase-MB elevation [44].

One under-investigated application of OCT is the detection and characterization of in-stent tissue prolapse or protrusion. Recent work suggests that when tissue protrusion is evaluated by OCT, the appearance of the protrusion correlates with the severity of vessel injury. Irregular protusion, suggesting moderate to severe vessel injury, was found to be an independent predictor of MACE and TLR.

Finally, OCT has the ability to identify thrombus within stents [45] (Fig. 12.4b). While the clinical significance of incidentally-discovered thrombus is unclear, it was found to be associated with longer stent length, smaller stent diameter, and absence of neointimal formation over stent struts. In general, small amounts of incidentally discovered in-stent thrombus need not prompt thrombus aspiration in the setting of good angiographic flow, but may influence the intensity of anti-thrombotic therapy.

Neointimal Hyperplasia and Neoatherosclerosis

The tendency of a neointima—composed of smooth muscle cells and extracellular matrix—to form within stents has been appreciated for years; indeed its presence is a surrogate for stent failure and vessel loss. The resolution of OCT allows for detection of neointima below the threshold of IVUS (Fig. 12.10). Three patterns of neointima have been described, based on the appearance by OCT: homogeneous (Fig. 12.11), heterogeneous (Fig. 12.12), and layered (Fig. 12.13) [46]. Small case series and case reports suggest that these OCT patterns of neoitima have histopathologic correlates, with the homogenous pattern identifying tissue with abundant smooth muscle cells and the other patterns signalizing extracellular matrix [47, 48].

In the last several years, post-mortem examination of coronary stents has demonstrated that atherosclerotic change within the neointima is a frequent occurrence, and it occurs earlier and nearly twice as often, in drug-eluting (DES), compared with bare metal stents (BMS) [49]. Neoatherosclerosis is a discrete pathologic process in which, months or years after stent implantation, foamy macrophages coalesce in the neointima around stent struts [31, 32]. When this process takes hold, these areas of neoatherosclerosis appear to be subject to the same fates as atherosclerotic plaques in native vessels. Calcium deposition occurs, as does formation of necrotic cores, leading to regions vulnerable to rupture and thrombosis [52]. This is a key mechanism underlying very late stent failure. Work has shown that neoatherosclerosis can be detected by OCT, and OCT has demonstrated that over time the neointima transforms into a lipid-rich tissue [50, 51] (Fig. 12.14). OCT-based research has corroborated the pathologic findings of earlier neoatherosclerosis with drug-eluting stents, but found that after 2 years, its frequency was the same in both drug-eluting and bare metal stents [53]. While evidence implicates incomplete endothelialization in late stent thrombosis, plaque rupture in the neointima has emerged as another mechanism. In the modern era of PCI, late stent thrombosis is a rare event, but a complete understanding of its pathogenesis may help avert this catastrophic occurrence. The degree of resolution afforded by OCT makes it an ideal modality for examining neointimal formation and assessing neoatherosclerosis.

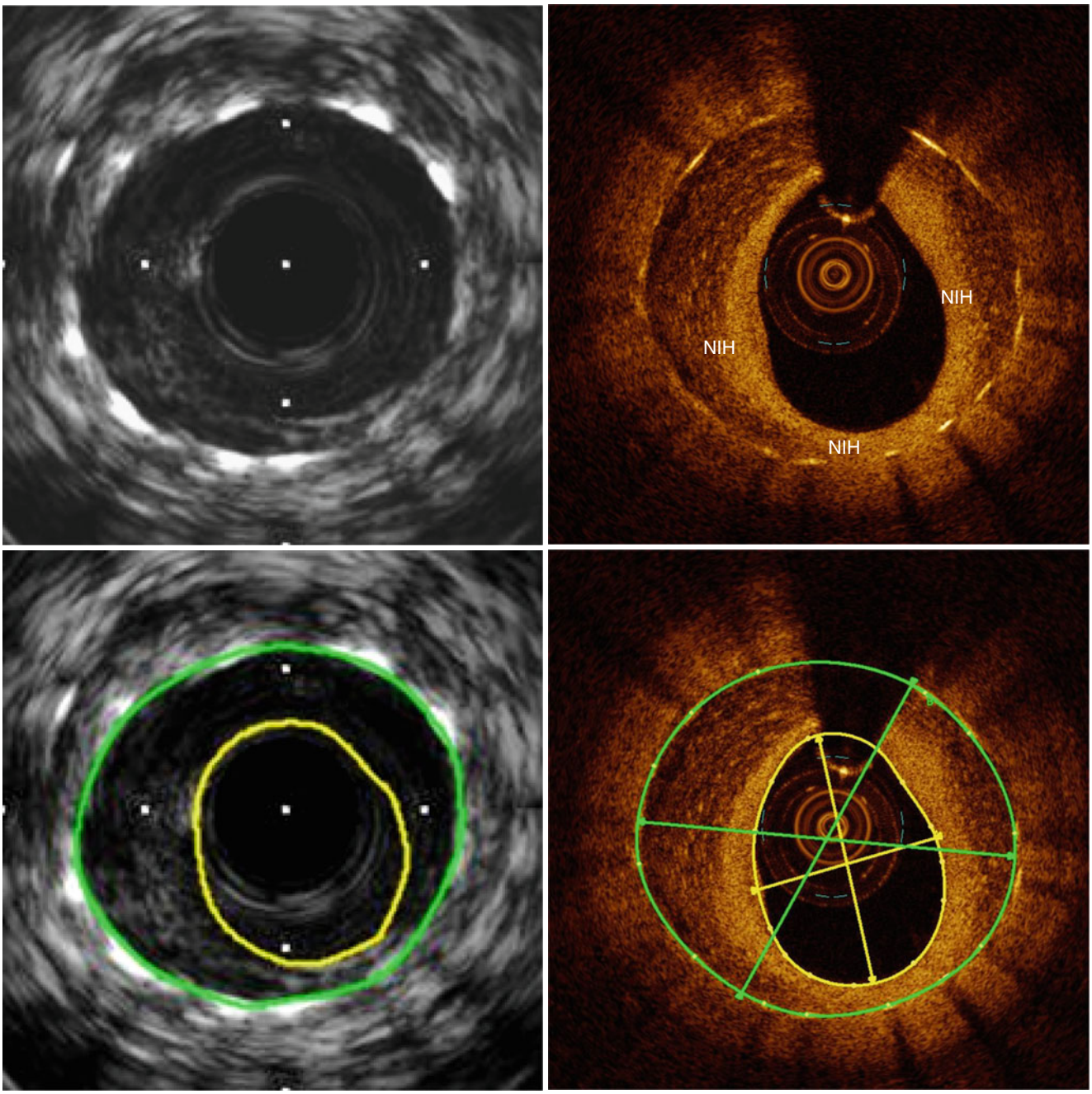

Fig. 12.10 Neointimal hyperplasia (*NIH*) within a stent is more clearly visualized by OCT (*right*) vs. IVUS (*left*), allowing more detailed tissue characterization as well as luminal and stent measurements (*bottom*)

OCT Evaluation of Bioabsorbable Vascular Scaffolds

Ongoing research has focused on the potential for a bioabsorbable vascular scaffold (BVS) to replace DES for intracoronary stenting. Because it is eventually absorbed, leaving no foreign body in the artery, BVS may reduce the risk of late stent thrombosis and other complications of PCI. Both animal and human outcomes studies have used intravascular imaging, including OCT, to evaluate the absorption of the polymer and the repopulation of BVS sites with cells. BVS currently under investigation appear different from metallic stents when imaged with IVUS; the struts are translucent, and OCT can completely image the strut thickness as well as the arterial wall behind the scaffold [54]. While BVS struts were no longer recognizable by IVUS after 2 years, some

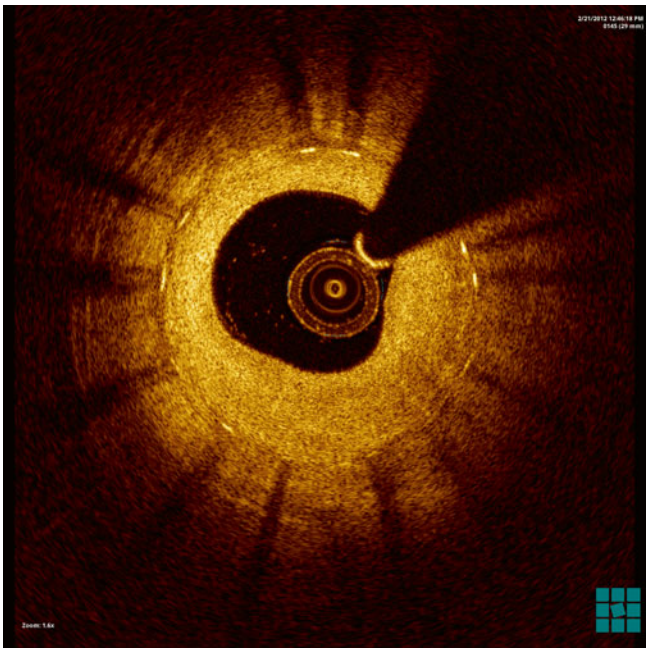

Fig. 12.11 Homogeneous neointimal hyperplasia

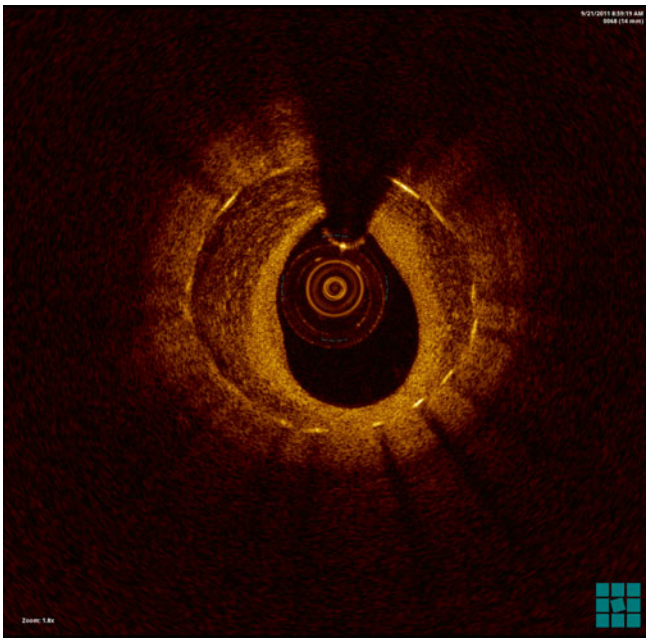

Fig. 12.13 Layered neointimal hyperplasia. The inner layer has high intensity signal, whereas the outer layer shows low signal material

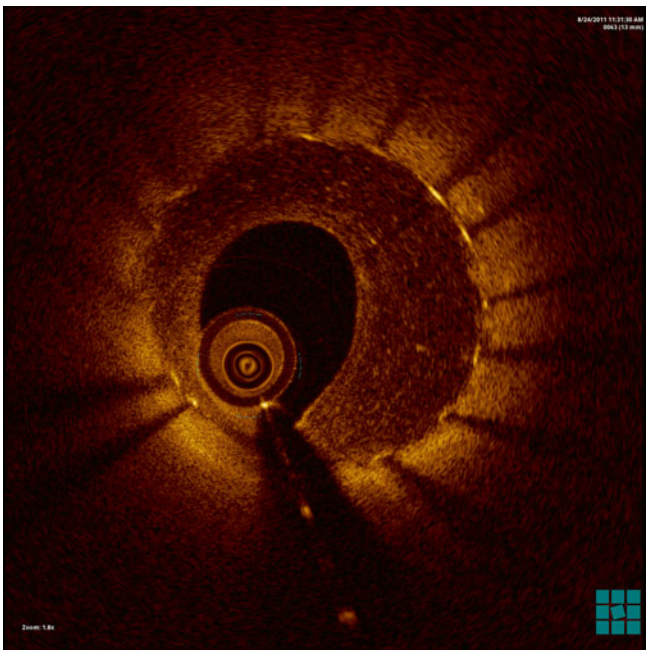

Fig. 12.12 Hetergeneous neointial hyperplasia

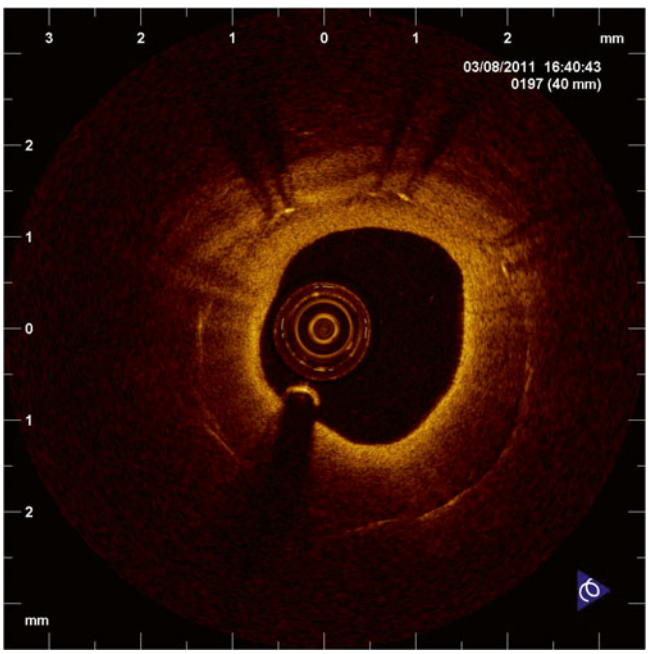

Fig. 12.14 Neoatherosclerosis within a coronary stent as characterized by OCT appears as a signal-poor regions (lipid laden) within stent struts

strut signals appeared to persist on OCT imaging in two thirds of cases. OCT was able to demonstrate a homogenous vessel wall at the site of the scaffold, suggesting endothelial healing [55]. Recent investigation employing serial OCT evaluation showed that, unlike BMS, self-expanding BVS expand over time, resulting in larger vessel diameters and preserved lumen size [56]. Potential applications of OCT continue to evolve with advances in both OCT technology

and stent design. Work with three-dimensional OCT has demonstrated the ability of reconstructions using this technology to evaluate vessel side branches jailed by BVS [57].

Conclusions

OCT is a safe and easily employed intravascular imaging modality with unmatched resolution and image quality of the coronary arteries. It has generated significant interest as a research tool for the evaluation of coronary vascular biology and atherosclerosis pathophysiology, but only recently has started to emerge into routine clinical practice for optimization of PCI. OCT shows great potential in this clinical role as an adjunctive modality for PCI, but is currently limited by the lack of clinical outcomes data supporting its routine clinical use. Similarly, routine IVUS-guided PCI had not been shown to improve hard clinical endpoints until recent meta-analysis of IVUS-guided DES implantation demonstrated significantly fewer adverse end points including death and MI in the IVUS-guided PCI group [40]. As OCT provides similar and possibly superior structural information upon which to guide PCI it may be reasonable to hypothesize that OCT-guided PCI may have similar clinical benefit. This has, however, yet to be rigorously studied and further outcome studies of OCT-guided PCI will be needed to differentiate the role of this promising technology in our clinical practice.

References

1. Huang D, Swanson EA, Lin CP, Schuman JS, Stinson WG, Chang W, et al. Optical coherence tomography. Science. 1991;254:1178–81.
2. Herrero-Garibi J, Cruz-Gonzalez I, Parejo-Diaz P, Jang IK. Optical coherence tomography: its value in intravascular diagnosis today. Rev Esp Cardiol. 2010;63:951–62.
3. Suh WM, Seto AH, Margey RJ, Cruz-Gonzalez I, Jang IK. Intravascular detection of the vulnerable plaque. Circ Cardiovasc Imaging. 2011;4:169–78.
4. Barlis P, Gonzalo N, Di Mario C, Prati F, Buellesfeld L, Rieber J, Dalby MC, Ferrante G, Cera M, Grube E, et al. A multicentre evaluation of the safety of intracoronary optical coherence tomography. EuroIntervention. 2009;5:90–5.
5. Suter MJ, Nadkarni SK, Weisz G, et al. Intravascular optical imaging technology for investigating the coronary artery. J Am Coll Cardiol Img. 2011;4:1022–39.
6. Low AF, Kawase Y, Chan YH, et al. In vivo characterization of coronary plaques with conventional grey-scale intravascular ultrasound: correlation with optical coherence tomography. EuroIntervention. 2009;4:626–32.
7. Kawasaki M, Bouma BE, Bressner J, et al. Diagnostic accuracy of optical coherence tomography and integrated backscatter intravascular ultrasoundimages for tissue characterization of human coronary plaques. J Am Coll Cardiol. 2006;48:81–8.
8. Garcia-Garcia HM, Gonzalo N, Regar E, et al. Virtual histology and optical coherence tomography: from research to broad clinical application. Heart. 2009;95:132–1374.
9. Kubo T, Imanishi T, Takarada S, et al. Assessment of culprit lesion morphology in acute myocardial infarction: ability of optical coherence tomography compared with intravascular ultrasound and coronary angioscopy. J Am Coll Cardiol. 2007;50:933–9.
10. Takano M, Jang IK, Inami S, et al. In vivo comparison of optical coherence tomography and angioscopy for the evaluation of coronary plaque charactistics. Am J Cardiol. 2008;101:471–6.
11. Kume T, Akasaka T, Kawamoto T, Okura H, Watanabe N, Toyota E, Neishi Y, Sukmawan R, Sadahira Y, Yoshida K. Measurement of the thickness of the fibrous cap by optical coherence tomography. Am Heart J. 2006;152(755):e751–4.
12. Raffel OC, Akasaka T, Jang IK. Cardiac optical coherence tomography. Heart. 2008;94:1200–10.
13. Jang IK, Tearney GJ, MacNeill B, Takano M, Moselewski F, Iftima N, Shishkov M, Houser S, Aretz HT, Halpern EF, et al. In vivo characterization of coronary atherosclerotic plaque by use of optical coherence tomography. Circulation. 2005;111:1551–5.
14. Kubo T, Takashi A, Shite J, et al. OCT compared with IVUS in a coronary lesion assessment. J Am Coll Cardiol Img. 2013;6:1095–104.
15. Yonetsu T, Kakuta T, Lee T, Takahashi K, Yamamoto G, Iesaka Y, Fujiwara H, Isobe M. Impact of plaque morphology on creatine kinase-MB elevation in patients with elective stent implantation. Int J Cardiol. 2011;146:80–5.
16. Lee T, Kakuta T, Yonetsu T, Takahashi K, Yamamoto G, Iesaka Y, Fujiwara H, Isobe M. Assessment of echo-attenuated plaque by optical coherence tomography and its impact on post-procedural creatine kinase-myocardial band elevation in elective stent implantation. JACC Cardiovasc Interv. 2011;4:483–91.
17. Lee T, Yonetsu T, Koura K, Hishikari K, Murai T, Iwai T, Takagi T, Iesaka Y, Fujiwara H, Isobe M, et al. Impact of coronary plaque morphology assessed by optical coherence tomography on cardiac troponin elevation in patients with elective stent implantation. Circ Cardiovasc Interv. 2011;4:378–86.
18. Porto I, Di Vito L, Burzotta F, Niccoli G, Trani C, Leone AM, Biasucci LM, Vergallo R, Limbruno U, Crea F. Predictors of periprocedural (type IVa) myocardial infarction, as assessed by frequency-domain optical coherence tomography. Circ Cardiovasc Interv. 2012;5:89–96. S81–86.
19. Gonzalo N, Escaned J, Alfonso F, Nolte C, Rodriguez V, Jimenez-Quevedo P, Banuelos C, Fernandez-Ortiz A, Garcia E, Hernandez-Antolin R, et al. Morphometric assessment of coronary stenosis relevance with optical coherence tomography: a comparison with fractional flow reserve and intravascular ultrasound. J Am Coll Cardiol. 2012;59:1080–9.
20. Stefano GT, Bezerra HG, Attizzani G, Chamie D, Mehanna E, Yamamoto H, Costa MA. Utilization of frequency domain optical coherence tomography and fractional flow reserve to assess intermediate coronary artery stenoses: conciliating anatomic and physiologic information. Int J Cardiovasc Imaging. 2011;27:299–308.
21. Garg S, Serruys PW. Coronary stents: current status. J Am Coll Cardiol. 2010;56(56):S1–42.
22. Choi SY, Witzenbichler B, Maehara A, Lansky AJ, Guagliumi G, Brodie B, et al. Intravascular ultrasound findings of early stent thrombosis after primary percutaneous intervention in acute myocardial infarction: a Harmonizing Outcomes with Revascularization and Stents in Acute Myocardial Infarction (HORIZONS-AMI) substudy. Circ Cardiovasc Interv. 2011;4(3):239–47.
23. Sonoda S, Morino Y, Ako J, Terashima M, Hassan AH, Bonneau HN, et al. Impact of final stent dimensions on long-term results following sirolimus-eluting stentimplantation: serial intravascular ultrasound analysis from the sirius trial. J Am Coll Cardiol. 2004;43(11):1959–63.

24. Hong MK, Mintz GS, Lee CW, Park DW, Park KM, Lee BK, et al. Late stent malapposition after drug-eluting stent implantation: an intravascular ultrasound analysis with long-term follow-up. Circulation. 2006;113(3):414–9.
25. Doi H, Maehara A, Mintz GS, Yu A, Wang H, Mandinov L, et al. Impact of post-intervention minimal stent area on 9-month follow-up patency of paclitaxel-eluting stents: an integrated intravascular ultrasound analysis from the TAXUS IV, V, and VI and TAXUS ATLAS workhorse, long lesion, and direct stent trials. JACC Cardiovasc Interv. 2009;2(12):1269–75.
26. Fujii K, Carlier SG, Mintz GS, Yang YM, Moussa I, Weisz G, et al. Stent underexpansion and residual reference segment stenosis are related to stent thrombosis after sirolimus-eluting stent implantation: an intravascular ultrasound study. J Am Coll Cardiol. 2005; 45(7):995–8.
27. Song HG, Kang SJ, Ahn JM, Kim WJ, Lee JY, Park DW, et al. Intravascular ultrasound assessment of optimal stent area to prevent in-stent restenosis after zotarolimus-, everolimus-, and sirolimus-eluting stent implantation. Catheter Cardiovasc Interv. 2014;83(6): 873–8.
28. Kume T, Okura H, Miyamoto Y, Yamada R, Saito K, Tamada T, et al. Natural history of stent edge dissection, tissue protrusion and incomplete stent apposition detectable only on optical coherence tomography after stent implantation: preliminary observation. Circ J. 2012;76:698–703.
29. Gonzalo N, Serruys PW, Okamura T, Shen ZJ, Garcia-Garcia HM, Onuma Y, et al. Relation between plaque type and dissections at the edges after stent implantation: an optical coherence tomography study. Int J Cardiol. 2011;150:151–5.
30. Gonzalo N, Serruys PW, Okamura T, Shen ZJ, Onuma Y, Garcia-Garcia HM, et al. Optical coherence tomography assessment of the acute effects of stent implantation on the vessel wall: a systematic quantitative approach. Heart. 2009;95:1913–9.
31. Kubo T, Imanishi T, Kibata H, Kuroi A, Ueno S, Yamano T, et al. Comparison of vascular response after sirolimus-eluting stent implantation between patients with unstable and stable angina pectoris: a serial optical coherence tomography study. JACC Cardiovasc Imaging. 2008;1:475–84.
32. Soeda T, Uemura S, Park S-J, Jang Y, Lee S, Vergallo R, et al. Incidence and Clinical Significance of Poststent Optical Coherence Tomography Findings: One-Year Follow-Up Study From a Multicenter Registry. Circulation. 2015;132:1020–9.
33. Bouma BE, Tearney GJ, Yabushita H, Shishkov M, Kauffman CR, DeJoseph Gauthier D, et al. Evaluation of intracoronary stenting by intravascular optical coherence tomography. Heart. 2003;89: 317–20.
34. Tanigawa J, Barlis P, Dimopoulos K, Dalby M, Moore P, Di Mario C. The influence of strut thickness and cell design on immediate apposition of drug-eluting stents assessed by optical coherence tomography. Int J Cardiol. 2009;134(2):180–8.
35. Fujino Y, Bezerra HF, Attizzani GF, Wang W, Yamamoto H, Chamié D, et al. Frequency-domain optical coherence tomography assessment of unprotected left main coronary artery disease-a comparison with intravascular ultrasound. Catheter Cardiovasc Interv. 2013;82(3):E173–83.
36. Jang IK, Tearney G, Bouma B. Visualization of tissue prolapse between coronary stent struts by optical coherence tomography: comparison with intravascular ultrasound. Circulation. 2001; 104:2754.
37. Kawamori H, Shite J, Shinke T, Otake H, Matsumoto D, Nakagawa M, et al. Natural consequence of post-intervention stent malapposition, thrombus, tissue prolapse, and dissection assessed by optical coherence tomography at mid-term follow-up. Eur Heart J Cardiovascular Imaging. 2013;14(9):865–75.
38. Cook S, Wenaweser P, Togni M, Billinger M, Morger C, Seiler C, et al. Incomplete stent apposition and very late stent thrombosis after drug-eluting stent implantation. Circulation. 2007;115: 2426–34.
39. Sawada T, Shite J, Shinke T, Tanino Y, Ogasawara D, Kawamori H, et al. Very late thrombosis of sirolimus-eluting stent due to late malapposition: serial observations with optical coherence tomography. J Cardiol. 2008;52:290–5.
40. Guagliumi G, Sirbu V, Musumeci G, Gerber R, Biondi-Zoccai G, Ikejima H, et al. Examination of the in vivo mechanisms of late drug-eluting stent thrombosis: findings from optical coherence tomography and intravascular imaging. JACC Cardiovasc Interv. 2012;5:12–20.
41. Gutierrez-Chico JL, Regar E, Nuesch E, Okamura T, Wykrykowska J, di Mario C, Windecker S, van Es GA, et al. Delayed coverage in malapposed and side-branch stents: in vivo assessment with optical coherence tomography. Circulation. 2011;124:612–23.
42. Chamié D, Bezerra HG, Attizzani GF, Yamamoto H, Kanaya T, Stefano GT, et al. Incidence, predictors, morphological characteristics, and clinical outcomes of stent edge dissections detected by optical coherence tomography. JACC Cardiovasc Interv. 2013;6(8):800–13.
43. De Cock D, Bennett J, Ughi GJ, Dubois C, Sinnaeve P, Dhooge J, et al. Healing course of acute vessel wall injury after drug-eluting stent implantation assessed by optical coherence tomography. Eur Heart J Cardiovasc Imaging. 2014;15(7):800–9.
44. Imola F, Occhipinti M, Biondi-Zoccai G, Di Vito L, Ramazzotti V, Manzoli A, et al. Association between proximal stent edge positioning on atherosclerotic plaques containing lipid pools and postprocedural myocardial infarction (from the CLI-POOL Study). Am J Cardiol. 2013;111:526–31.
45. Kim JS, Hong MK, Fan C, Kim TH, Shim JM, Park SM, et al. Intracoronary thrombus formation after drug-eluting stents implantation: optical coherence tomographic study. Am Heart J. 2010;159(2):278–83.
46. Gonzalo N, Serruys PW, Okamura T, van Beusekom HM, Garcia-Garcia HM, von Soest G, et al. Optical coherence tomography patterns of stent restenosis. Am Heart J. 2009;158:284–93.
47. Nagai H, Ishibashi-Ueda H, Fujii K. Histology of highly echolucent regions in optical coherence tomography images from two patients with sirolimus-eluting stent restenosis. Catheter Cardiovasc Interv. 2010;75:961–3.
48. Kume T, Akasaka T, Kawamoto T, Watanabe N, Toyota E, Sukmawan R, et al. Visualization of neointima formation by optical coherence tomography. Heart J. 2005;46:1133–6.
49. Nakazawa G, Otsuka F, Nakano M, Vorpahl M, Yazdani SK, Ladich E, et al. The pathology of neoatherosclerosis in human coronary implants bare-metal and drug-eluting stents. J Am Coll Cardiol. 2011;57(11):1314–22.
50. Takano M, Yamamoto M, Inami S, Murakami D, Ohba T, Seino Y, Mizuno K. Appearance of lipid-laden intima and neovascularization after implantation of bare-metal stents extended late-phase observation by intracoronary optical coherence tomography. J Am Coll Cardiol. 2009;55(1):26–32.
51. Hou J, Qi H, Zhang M, Ma L, Liu H, Han Z, et al. Development of lipid-rich plaque inside bare metal stent: possible mechanism of late stent thrombosis? An optical coherence tomography study. Heart. 2010;96(15):1187–90.
52. Yamaji K, Inoue K, Nakahashi T, Noguchi M, Domei T, Hyodo M, et al. Bare metal stent thrombosis and in-stent neoatherosclerosis. Circulation. 2012;5:47–54.
53. Kim JS, Kato K, Kim SJ, Xing L, Yeh RW, et al. Comparison of incidence and time course of neoatherosclerosis between bare metal stents and drug-eluting stents using optical coherence tomography. Am J Cardiol. 2012;110(7):933–9.
54. Serruys PW, Onuma Y, Dudek D, Smits PC, Koolen J, Chevalier B, et al. Evaluation of the second generation of a bioresorbable everolimus-eluting vascular scaffold for the treatment of de novo

coronary artery stenosis 12-month clinical and imaging outcomes. J Am Coll Cardiol. 2011;58:1578–87.
55. Serruys PW, Ormiston JA, Onuma Y, Regar E, Gonzalo N, Garcia-Garcia HM, et al. A bioabsorbable everolimus-eluting coronary stent system (ABSORB): 2-year outcomes and results from multiple imaging methods. Lancet. 2009;373: 897–910.
56. Bourantas CV, Serruys PW, Nakatani S, Zhang YJ, Farooq V, Diletti R, et al. Bioresorbable vascular scaffold treatment induces the formation of neointimal cap that seals the underlying plaque without compromising the luminal dimensions: a concept based on serial optical coherence tomography data. EuroIntervention. 2015;11:746–56.
57. Okamura T, Onuma Y, Garcia-Garcia HM, Regar E, Wykrzkowska JJ, Koolen J, et al. 3-dimensional optical coherence tomography assessment of jailed side branches by bioresorbable vascular scaffolds: a proposal for classification. J Am Coll Cardiol Intv. 2010;3:836–44.

Echocardiography in Mechanical Circulatory Support

13

Jorge Betancor, Antonio Perez, and Richard A. Grimm

Abstract

Echocardiography is the front line modality in the evaluation of advanced heart failure patients requiring mechanical circulatory support. The use of continuous-flow left ventricular assist devices (LVADs) continues to expand across numerous centers in the country, as both a bridge to transplantation and as destination therapy. Patients being evaluated for LVAD therapy require thorough pre-operative cardiac evaluation by echocardiography of biventricular function, the aortic, tricuspid and mitral valves, the ascending aorta, the atria and atrial septum. After LVAD implantation, echocardiography can effectively evaluate flow velocities into the apical inflow cannula and from the ascending aorta outflow cannula, left ventricular decompression, frequency of aortic valve opening, right ventricular function and degree of aortic, mitral and tricuspid regurgitation. Patients with suspected LVAD malfunction should undergo urgent echocardiography to help identify possible causes, including hypovolemia, valvular dysfunction, tamponade, thrombosis and cannula malposition. Echocardiography also plays a key role in the evaluation and management of patients with percutaneous catheter devices that provide temporary mechanical support in cardiogenic shock and during high risk cardiovascular procedures. It is important to become competent in the echocardiographic assessment of patients who are being evaluated for and receiving mechanical circulatory support, as they can develop critical complications that can be managed successfully if promptly diagnosed.

Keywords

Mechanical circulatory support • Left ventricular assist device (LVAD) • Percutaneous ventricular assist device • LVAD pump thrombosis • LVAD cannula malposition • Ramp study

Introduction

Echocardiography is the front line modality in the evaluation of advanced heart failure patients requiring mechanical circulatory support (MCS). It is portable, noninvasive and inexpensive, without exposure to radiation or nephrotoxic agents. Continuous-flow left ventricular assist devices (LVADs) are rapidly growing as therapy in patients for whom heart transplantation is not appropriate or not immediately available [1]. Temporary mechanical support therapies are also available for patients in cardiogenic shock, including percutaneous catheter devices and extracorporeal membrane oxygenation (ECMO). The International Society for Heart and Lung Transplantation (ISHLT) recommends the use of echocardiography in MCS patients [2], but there are currently no evidence-based guidelines to standardize its use. Significant variation in utilization and expertise continues to exist across hospitals nationwide. In this chapter, we will

J. Betancor, MD • R.A. Grimm, DO, FASE (✉)
Department of Cardiovascular Medicine,
Cleveland Clinic Foundation, Cleveland, OH, USA
e-mail: grimmr@ccf.org

A. Perez, MD, MBA
Department of Cardiovascular Medicine, Cleveland Clinic Foundation, Cardiovascular Imaging, Cleveland, OH, USA

M.H. Picard et al. (eds.), *Intraprocedural Imaging of Cardiovascular Interventions*, DOI 10.1007/978-3-319-29428-5_13

provide a clinically-focused review of the applications of echocardiography in the evaluation and management of patients receiving MCS therapy.

Anatomical Considerations Prior to LVAD Implantation

Prior to LVAD implantation, patients must undergo a thorough echocardiographic assessment of baseline anatomical characteristics that could potentially lead to poor outcomes and a protracted post-operative course. These include evaluation of the left ventricle (LV), right ventricle (RV), aortic valve, mitral valve, tricuspid valve and atrial septum. The LV should be assessed for signs of aneurysm, scar, hypertrabeculation and apical thrombus that could hinder placement of the inflow cannula or create dynamic inflow cannula obstruction. Presence or absence of aortic regurgitation (AR) and mitral stenosis (MS) must be characterized (Fig. 13.1a). Similarly, the ascending aorta needs to be examined in anticipation of placement of the outflow cannula. Aortic aneurysms, tortuosity, calcification and atheroma are common pathologies that can lead to post-operative complications.

RV dysfunction is an important relative contraindication to LVAD therapy. Post-LVAD RV failure results in substantial morbidity and mortality [3–5], with post-operative complications secondary to RV failure occurring in 13–40 % of LVAD implantations [6] (Fig. 13.1b). In the setting of pre-operative RV dysfunction, biventricular support has led to improved outcomes [7], provided RV pathology is recognized early. Although LVAD decompression improves RV afterload, greater venous return is believed to worsen preexisting RV dysfunction and tricuspid regurgitation by increasing RV volume [8–12].

Left atrial and left atrial appendage thrombi should be carefully ruled out on pre- and peri-operative TEE

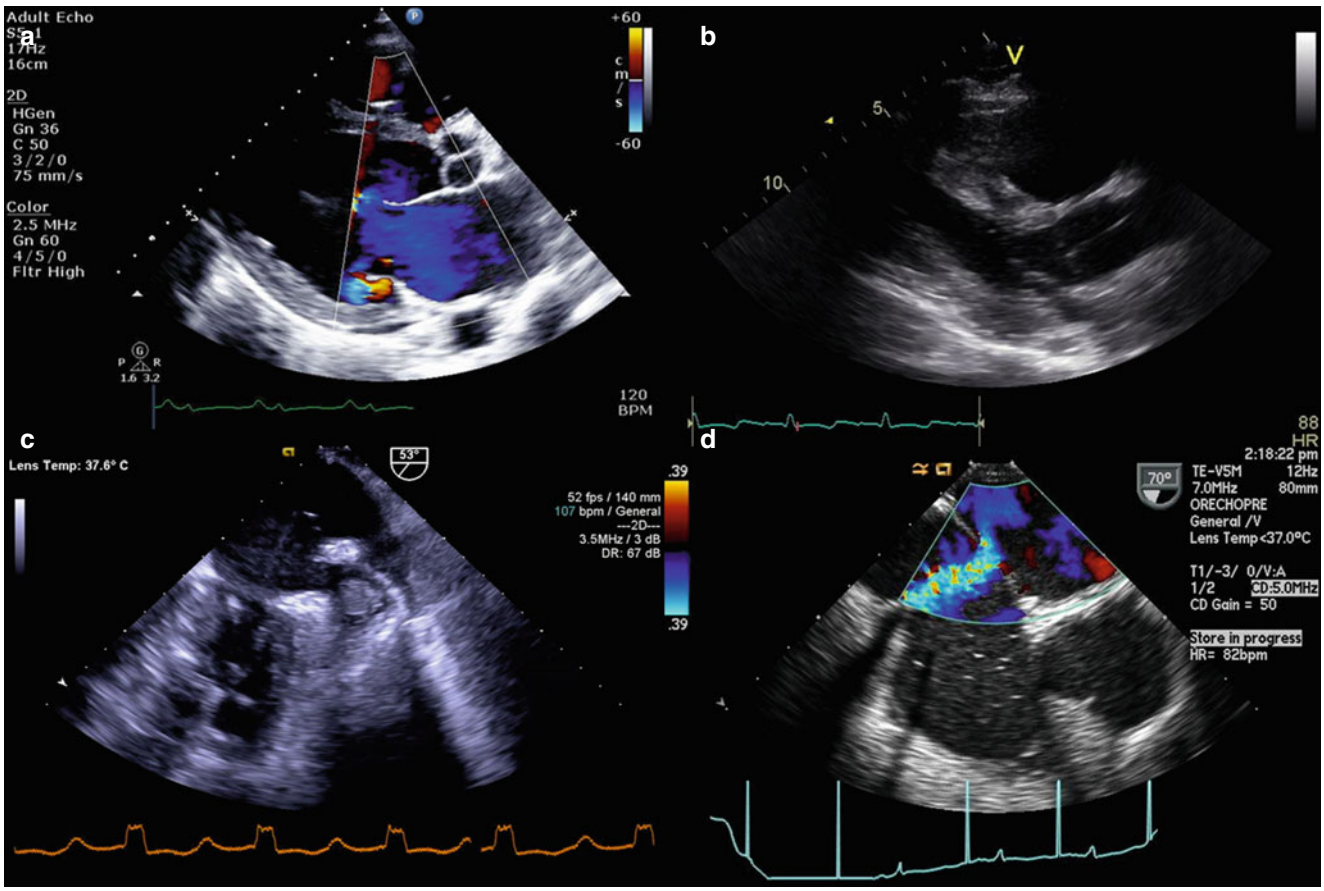

Fig. 13.1 (**a**) Parasternal long-axis TTE view during diastole with color Doppler sector over the LVOT, Mitral Valve and Left atrium, demonstrating the absence of Aortic Regurgitation and Mitral stenosis. It shows a dilated LV. (**b**) Parasternal long-axis TTE view showing a dilated and dysfunctional right ventricle. RV dysfunction is an important relative contraindication to LVAD therapy. (**c**) Mid-esophageal TEE view at 53° focused on the left atrium and left atrial appendage, demonstrating a thrombus. This was discovered during the pre-operative assessment of a candidate for LVAD implantation. (**d**) Mid-esophageal TEE view at 70° focused on the inter-atrial septum with color Doppler demonstrating evidence of left to right shunting. All intra-cardiac shunts should be repaired at the time of LVAD implantation

(Fig. 13.1c). Intravenous contrast can help discriminate between LAA thrombi and prominent pectinate muscle.

All intra-cardiac shunts should be repaired at the time of LVAD implantation to prevent right to left shunting in the supported heart [13] (Fig. 13.1d). In acute decompensated heart failure, many atrial septal defects can predominantly shunt left to right by color Doppler and agitated saline contrast. Even after Valsalva maneuvers, a high left atrial pressure may prevent passage of agitated saline across a patent foramen ovale (PFO). After LVAD decompression, however, lower left atrial pressure and increased right ventricular preload can potentially open a previously unidentified PFO and create right to left shunting [14, 15]. Meticulous search for elusive PFOs is therefore important prior to LVAD implantation [2, 16] and should be repeated in the OR at the time of surgery [15].

Pre-LVAD Implantation Valvular Assessment

Although LVAD decompression improves RV afterload, higher venous return is believed to worsen preexisting RV dysfunction and tricuspid regurgitation (TR) [8–12]. Therefore, repair or replacement of the tricuspid valve in moderate to severe TR should be strongly considered at the time of LVAD implantation [2, 17] (Fig. 13.2a).

Severe mitral regurgitation (MR) tends to improve with mechanical unloading of the left ventricle; therefore, mitral repair or replacement is not routinely required at time of LVAD implantation [2, 14] (Fig. 13.2b).

AR can be underestimated in end-stage heart failure with low systemic pressures and high LV diastolic pressures, as the aortic-to-LV pressure gradient may be artificially decreased [18–20]. AR can significantly worsen after LVAD implanta-

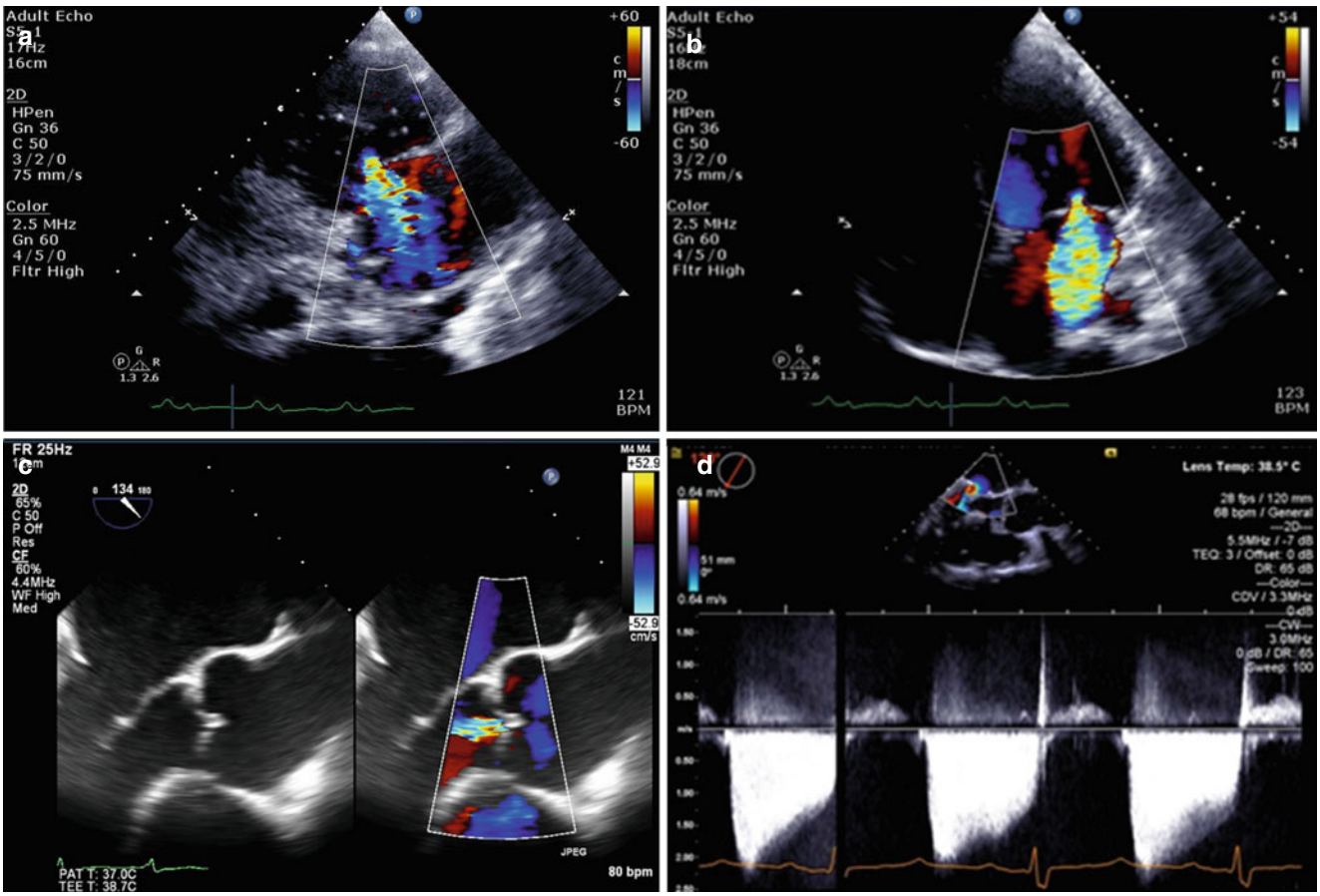

Fig. 13.2 (**a**) Parasternal RV inflow TTE view with color Doppler during systole demonstrating a moderately severe regurgitant tricuspid jet on the pre-LVAD assessment. There is evidence of PISA flow acceleration at an aliasing velocity of 0.6 m/s. (**b**) Apical four-chamber TTE view during systole with color Doppler sector over the mitral valve and left atrium demonstrating a moderately-severe regurgitant mitral jet with PISA flow acceleration at an aliasing velocity of 0.54 m/s. Severe MR tends to improve with mechanical unloading of the left ventricle. (**c**) Mid-esophageal long-axis TEE view at 134° focused on the aortic valve during diastole with the mitral valve open, demonstrating mild to moderate regurgitant flow by color Doppler. (**d**) Mid-esophageal long-axis TEE view at 120° with continuous wave Doppler cursor placed through the mitral valve inflow, demonstrating moderately-severe stenosis with high peak and mean gradients across the mitral valve

tion, due to negative pressure generated by the LVAD inflow cannula and the aortic diastolic pressure increase from blood flow return to the ascending aorta from the outflow cannula [21–23]. Therefore, AR that is moderate or greater in severity is considered an indication for valve replacement or oversewing at the time of surgery [2] (Fig. 13.2c). Similarly, aortic stenosis (AS) that is moderate or greater in severity should also be addressed at the time of implantation, as it can prevent adequate aortic valve opening. This can create increased risk of thrombus formation over the aortic valve leaflets.

MS that is moderate or greater in severity should be treated surgically at the time of implantation (Fig. 13.2d). Mechanical valves should be avoided given their thrombogenic potential.

Physiologic Changes Post-LVAD Implantation

While the LV in patients with end-stage systolic heart failure can be severely LV dilated with high sphericity index and rightward septal deviation, an appropriately functioning LVAD decompresses the ventricle by negative suction of blood into the inflow cannula implanted at the apex, decreasing LV dilatation. This can also cause a slight leftward septal shift (Fig. 13.3a, b).

After LVAD implantation, patients can experience decrease in MR, increase in AR, and increase in RV volume in setting of improved cardiac output. This increase in RV volume, however, can worsen RV function and TR (Fig. 13.3c) [3, 4, 6, 24–27].

Aortic regurgitation can be underestimated in end-stage heart failure with low systemic pressures and high LV diastolic pressure, as the aortic-to-LV pressure gradient may be artificially decreased [18–20]. AR can significantly worsen after LVAD implantation [21–23] (Fig. 13.3d). The presence of moderate or greater aortic regurgitation is considered an indication for valve replacement or oversewing at the time of surgery [2]. Similarly, moderate or greater aortic stenosis should also be treated surgically at the time of implantation, as can prevent adequate aortic valve opening. This increases risk of thrombus formation over the aortic valve leaflets.

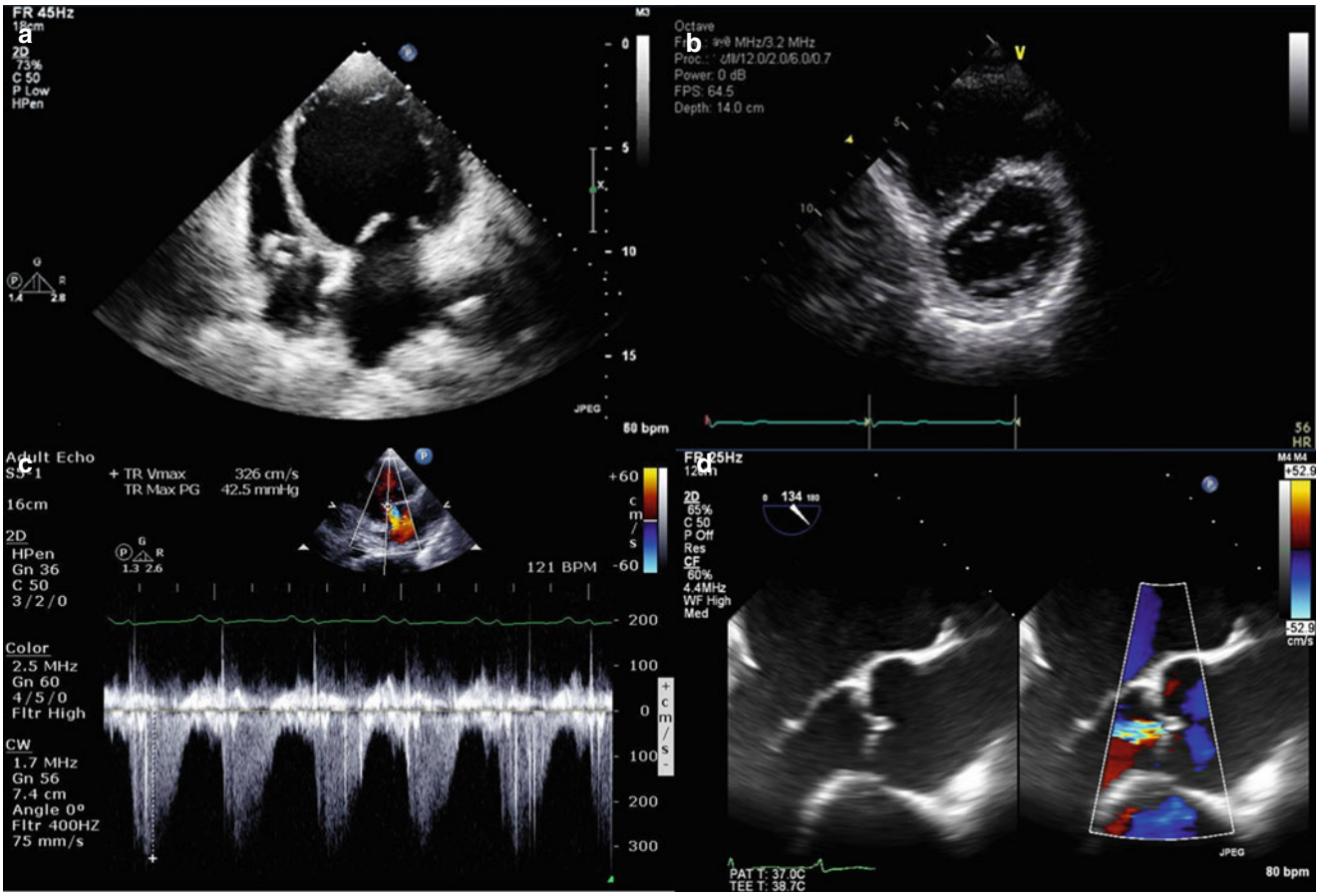

Fig. 13.3 (**a**) Apical four-chamber TTE view in a pre-LVAD patient during end diastole, demonstrating severe LV dilation, high sphericity index, and rightward septal deviation. (**b**) Parasternal short-axis TTE view of the LV at the mitral level in the same patient after LVAD implantation. RV appears moderately dilated on direct comparison; LV appears adequately decompressed with slight leftward septal shift. (**c**) Parasternal RV inflow TTE view in the same patient demonstrating worsening TR (maximum velocity 3.3 m/s) after LVAD implantation, with concomitant reduction in RV function and moderate RV dilation. (**d**) Mid-esophageal long-axis TEE view at 134° focused on the aortic valve during diastole with the mitral valve open, demonstrating mild to moderate regurgitant flow by color Doppler

Assessment of LVAD Cannulae Function

There are several important components to LVAD function assessment by echocardiography. The LVAD inflow cannula should be aligned with the mitral valve opening and oriented away from excessive trabeculations and ventricular walls (Fig. 13.4a, b). There should be laminar flow with normal filling velocities between 1 and 2 m/s. Partial inflow cannula obstruction will lead to increases in inflow pulse wave velocities and aliasing of color flow.

Cannula obstruction caused by malposition can manifest as leftward septal bowing due to excessive negative suction of the septum toward the inflow cannula and increased left ventricular end-diastolic volume caused by inadequate LV decompression. Current LVAD flow monitors trigger alarms when possible malfunction occurs. Echocardiography plays an important role in evaluating for causes of malfunction (e.g., hypovolemia, RV dysfunction, tamponade, pulmonary embolism, and pump thrombosis).

The outflow cannula is often difficult to image by TTE and is best visualized from right parasternal or upper left parasternal views or with TEE (Fig. 13.4c). Partial obstruction can lead to increases in outflow pulse wave velocity and color flow aliasing. Flow across the outflow cannula should be laminar with velocity between 1 and 2 m/s (Fig. 13.4d).

Assessment of Chamber and Valvular Function in LVAD Patients

Figure 13.5a–d show the ventricular size, aortic valve function and ventricular septal position with a normally functioning LVAD. The RV is often mildly dilated. The presence

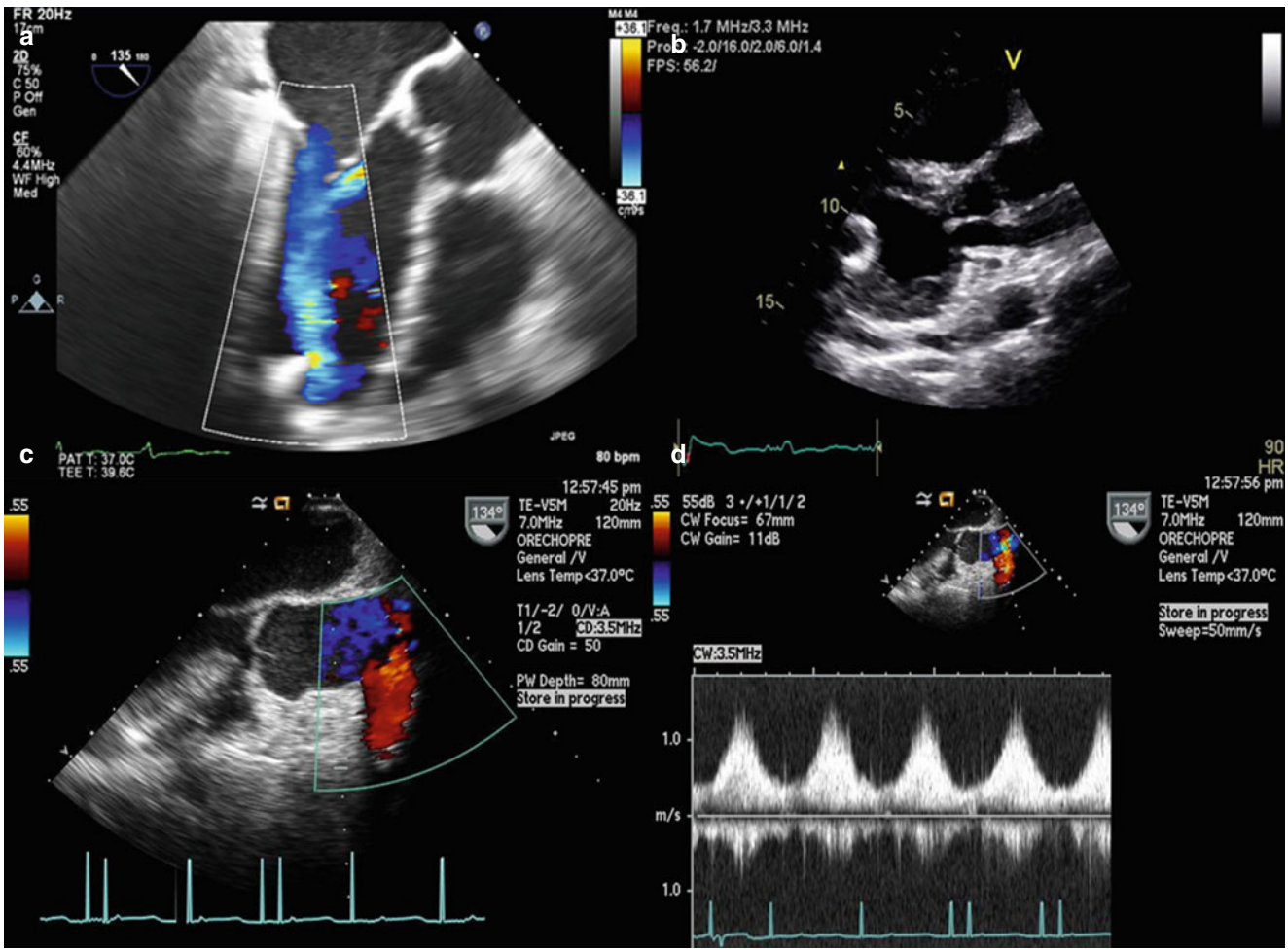

Fig. 13.4 (**a**) Mid-esophageal long-axis TEE view at 135° during diastole showing laminar flow across the mitral inflow tract and into the LV inflow cannula. The cannula orientation is slightly deviated towards the interventricular septum. (**b**) Parasternal Long-axis TTE view of an LVAD inflow cannula during diastole demonstrating adequate cannula orientation, which faces the mitral inflow tract directly across. (**c**) Mid-esophageal modified long-axis TEE view at 134° with color Doppler sector focused on the ascending aorta, demonstrating laminar unobstructed flow within the outflow cannula. (**d**) Mid-esophageal modified long-axis TEE view at 134° with continuous wave Doppler cursor across the outflow cannula that was implanted in the anterior aspect of the ascending aorta, demonstrating normal flow velocities (approximately 1.5 m/s)

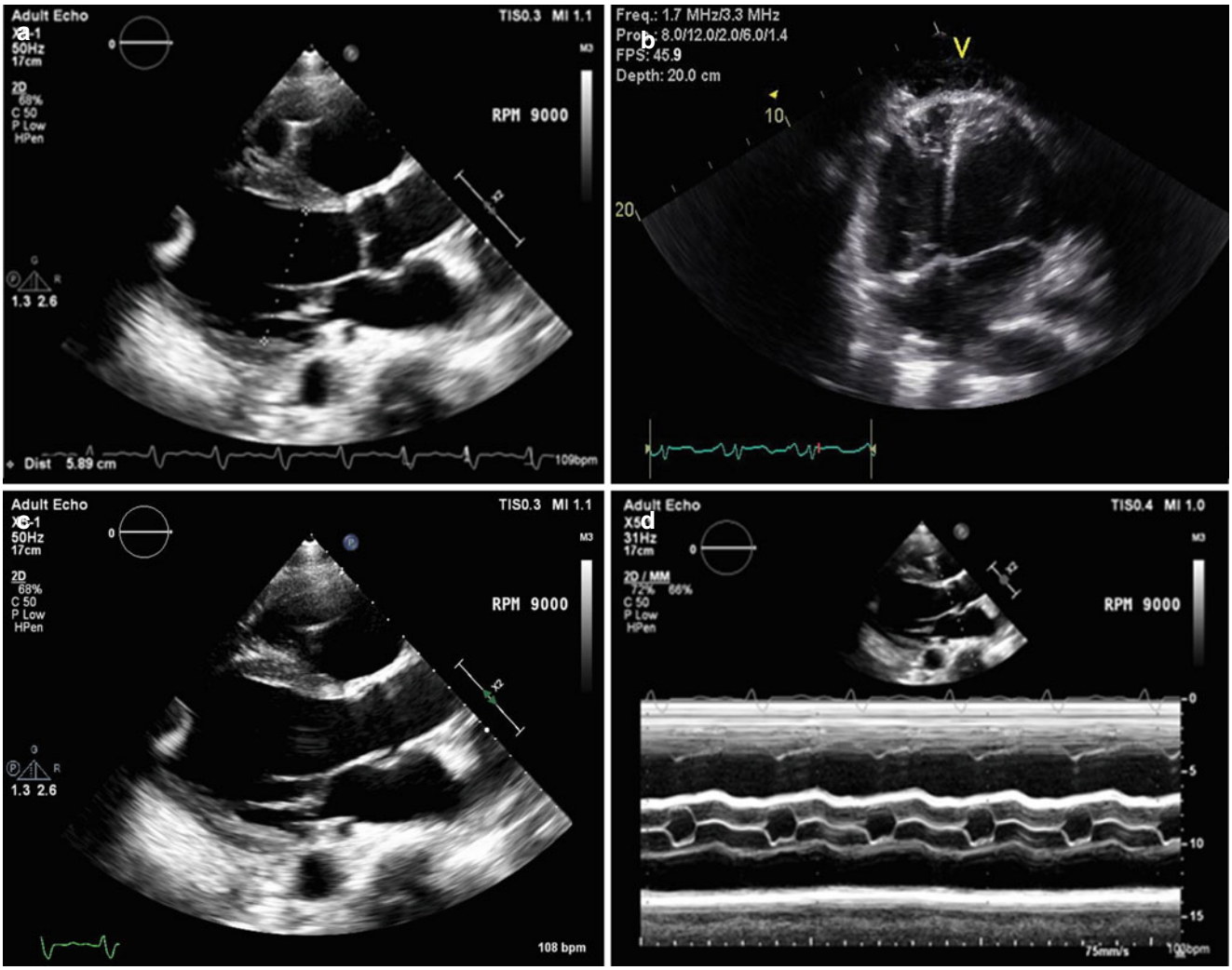

Fig. 13.5 (**a**) Parasternal long-axis TTE view at end diastole and LVAD pump rate of 9,000 RPMs, demonstrating mild RV dilation, adequate placement of LV apical inflow cannula, and optimal septal position with LV end diastolic dimension measured at 5.89 cm. (**b**) Apical four-chamber TTE view at end diastole showing mild RV dilation in an LVAD patient. LV apical inflow cannula is not well visualized in this image. (**c**) Parasternal long-axis TTE view during systole in an LVAD patient with pump set at 9,000 RPMs. Aortic valve appears to open with every ventricular contraction as demonstrated by this still frame and the M-mode Doppler in D. (**d**) Parasternal long-axis TTE view with M-mode Doppler cursor across the aortic valve in patient with LVAD programmed to 9,000 RPMs, demonstrating adequate opening and closing of the aortic valve with every LV contraction

and degree of aortic valve opening represents the degree of flow through the native circuit. Both native and bioprosthetic cusp fusion are recognized complications in LVAD patients [28–30]. There is a risk of thrombus formation when the aortic valve opens minimally [31]. M-mode and planimetry have been used to quantify degree of cusp separation. Aortic valve opening can be maintained by reducing LVAD RPMs. LVAD programming should aim to achieve an appropriate balance between adequate physiologic support by the LVAD and aortic valve opening. It may be possible that the risk of de novo aortic regurgitation is greater with persistent aortic valve closure [21, 32].

Complications After LVAD Implantation: Hypovolemia

If an LVAD is deployed in a patient who is hypovolemic, the LV cavity can become reduced to the point of obliteration. This can occur in the setting of major bleeding. Abnormal mitral lealflet position and persistent opening can also be noted (Fig. 13.6a, b). In such conditions the continuous wave Doppler velocity in the LVAD inflow cannula can be elevated if the LVAD cannula is partially obstructed by the distal septum in the collapsing LV (Fig. 13.6c, d). Repeat imaging after volume repletion and optimizing LVAD pump

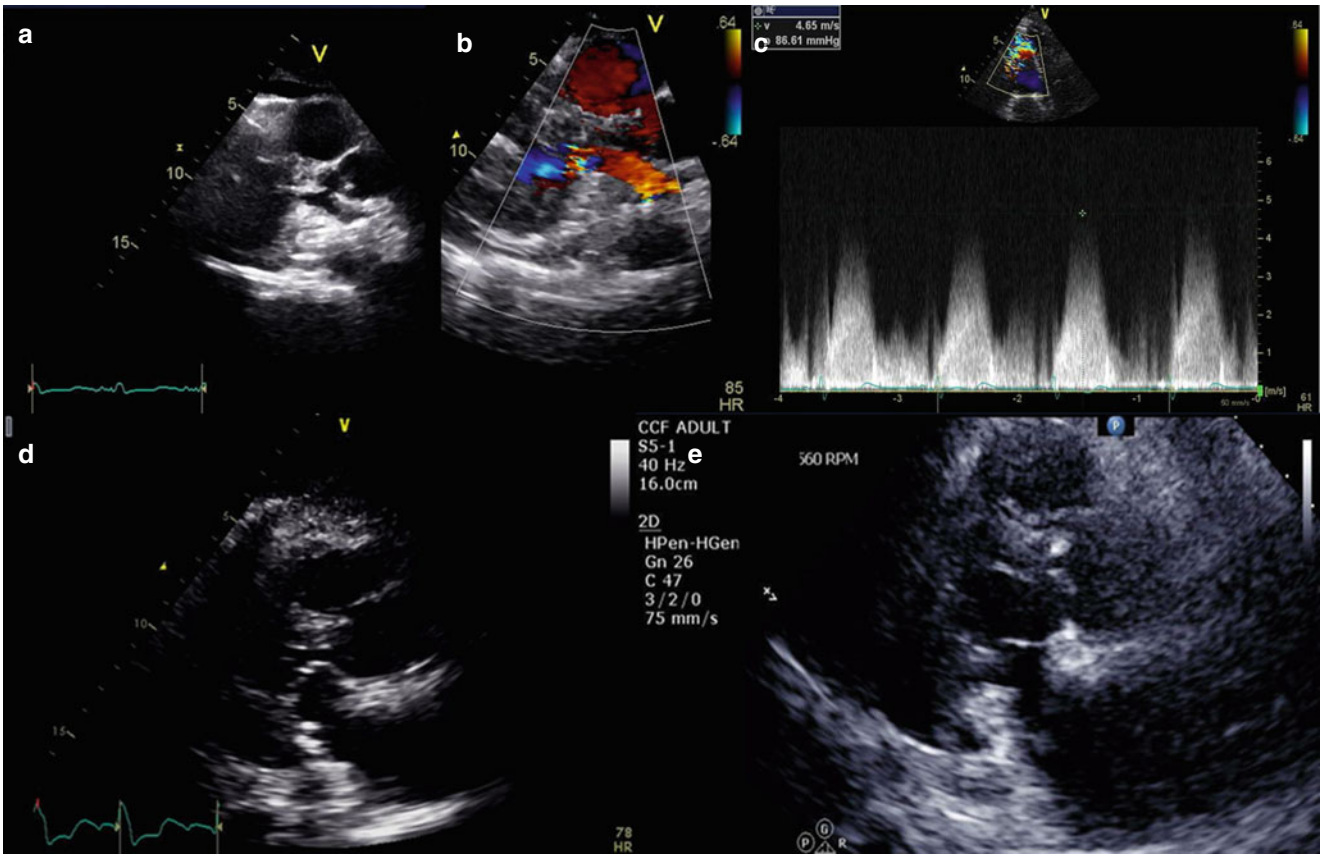

Fig. 13.6 (**a**) Parasternal long-axis TTE view demonstrating a reduced LV intracavitary size, resulting in anterior mitral leaflet "pulling" towards the interventricular septum in a hypotensive ICU patient who had recently undergone LVAD implantation. The patient was volume depleted, resulting in LV cavitary obliteration in setting of LVAD-mediated ventricular decompression. (**b**) Color Doppler sector over the mitral inflow tract demonstrating persistent opening of the anterior mitral leaflet during systole and diastole in setting of an intracavitary obliteration from hypovolemia in this same patient. (**c**) Continuous wave Doppler signal across the LVAD inflow cannula showing elevated peak velocities (4.65 m/s) in the same patient. The LVAD cannula is partially obstructed by the distal septum in the setting of hypovolemia and cavitary obliteration. The patient's hypotension and LV cavitary obliteration resolved with administration of intravenous fluids. Once euvolemic, the cannula was determined to be malpositioned on subsequent imaging, with persistently elevated peak inflow cannula velocities. (**d**) Parasternal long-axis TTE view in an LVAD patient who developed hypotension from major bleeding. The LV has the "suck-down" appearance, in which the anterior mitral valve leaflet lies in close proximity to the interventricular septum, the LV intra-cavitary size is diminished and the inflow cannula obstructs due to septal contact. (**e**) Parasternal long-axis TTE view in the same LVAD patient after volume resuscitation

rate can demonstrate normalization of LV size and inflow cannula function (Fig. 13.6e) [33].

Complications After LVAD Implantation: Right Ventricular Failure, Aortic Regurgitation and Tamponade

Although LV decompression by LVAD therapy improves RV afterload, higher venous return and leftward septal motion in setting of LVAD negative suction are believed to alter RV shape and efficiency of contraction, which in turn can worsen preexisting RV dysfunction and TR (Fig. 13.7a) [3, 4, 6, 24–27].

Aortic regurgitation can increase after LVAD deployment due to negative suction created by the LV apical inflow cannula and flow directed toward the aortic valve from the outflow cannula (Fig. 13.7b).

Pericardial hematoma and tamponade due to postoperative bleeding is also a complication of deployment of mechanical circulatory assist devices (Fig. 13.7c, d). Imaging of the effects of tamponade on cardiac structure can be difficult since the blood collections can be localized and only cause focal chamber compression or collapse. In addition, the functioning LVAD prevents Doppler assessment of respiratory variation in transmitral inflow velocities.

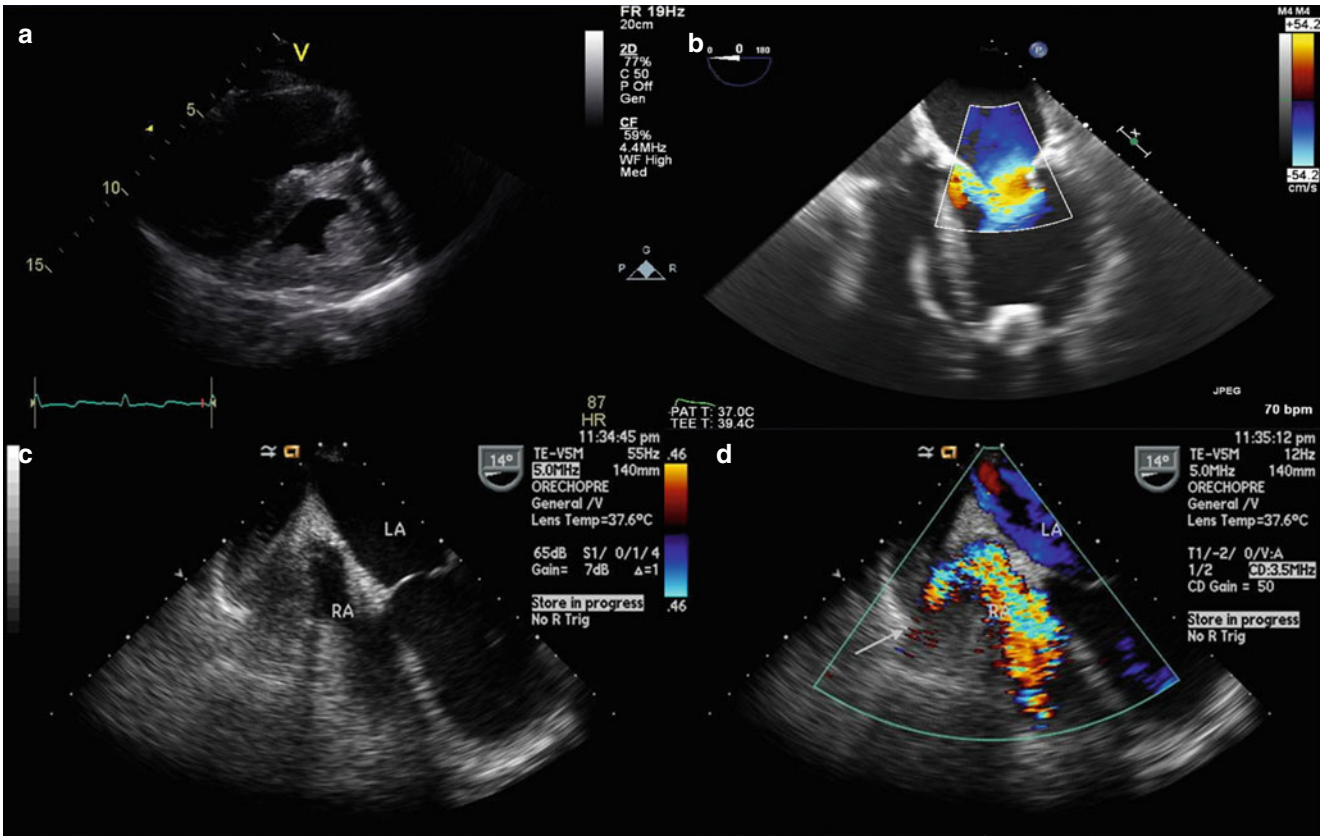

Fig. 13.7 (**a**) Parasternal short-axis TTE view of both ventricles, demonstrating severe right ventricular dilation in a patient who underwent LVAD implantation. Although LV decompression by LVAD therapy improves RV afterload, higher venous return and the leftward septal motion in setting of LVAD negative suction are believed to alter RV shape and efficiency of contraction, which in turn can worsen preexisting RV dysfunction and TR. B. Mid-esophageal four-chamber TEE view at 0° during diastole in a patient who developed moderately severe aortic regurgitation after LVAD implantation, in the setting of negative suction created by the apical inflow cannula. Color Doppler sector demonstrates an eccentric regurgitant jet in the LVOT that is directed posteriorly towards the anterior mitral valve leaflet. There is laminar flow across the mitral inflow tract. (**c–d**) Mid-esophageal four-chamber TEE view at 14° with and without color Doppler in an LVAD patient who developed tamponade post-operatively. There is RA and RV chamber collapse, caused by a large anterior pericardial hematoma. The LA and LV are both visualized in the posterior plane. There is flow acceleration at the junction of the IVC and RA, caused by compression from the focal hematoma. This patient required emergent surgery to evacuate the pericardial hematoma

Ramp Study to Assess LVAD Pump Thrombosis

Ramp studies, which involve serial monitored adjustment of LVAD flow rates, are performed to optimize LVAD flow, targeting maximal reduction in left ventricular dilatation while maintaining intermittent aortic valve opening. Ramp studies often involve assessment of LV function and aortic valve opening at different RPMs. Change in AR, MR, RSVP and RV dilatation are also assessed. In a normally functioning LVAD, higher speeds should reduce left ventricular size, decrease aortic valve opening, decrease MR and increase the transmitral Doppler deceleration time.

Pump failure from thrombosis is a common and high risk complication that occurs in LVAD patients, who often initially present with decompensated heart failure. Pump thrombosis can be challenging to diagnose, as there is rarely direct imaging evidence of thrombus formation [34]. Elevated LDH levels, high power "spikes" on LVAD interrogation along with imaging evidence of worsening LV dilatation, worsening MR, and increase in frequency of AV opening suggest possible pump thrombosis [35]. Failure to decompress and keep the aortic valve closed with increasing RPMs can also indicate pump obstruction [36, 37]. However, low grade, gradual, non-occlusive thrombus formation can be elusive, and small changes in LV function associated with pump thrombosis may be missed in ramp studies. Figure 13.8a–d display echocardiographic features observed during a ramp study in a patient with pump thrombosis.

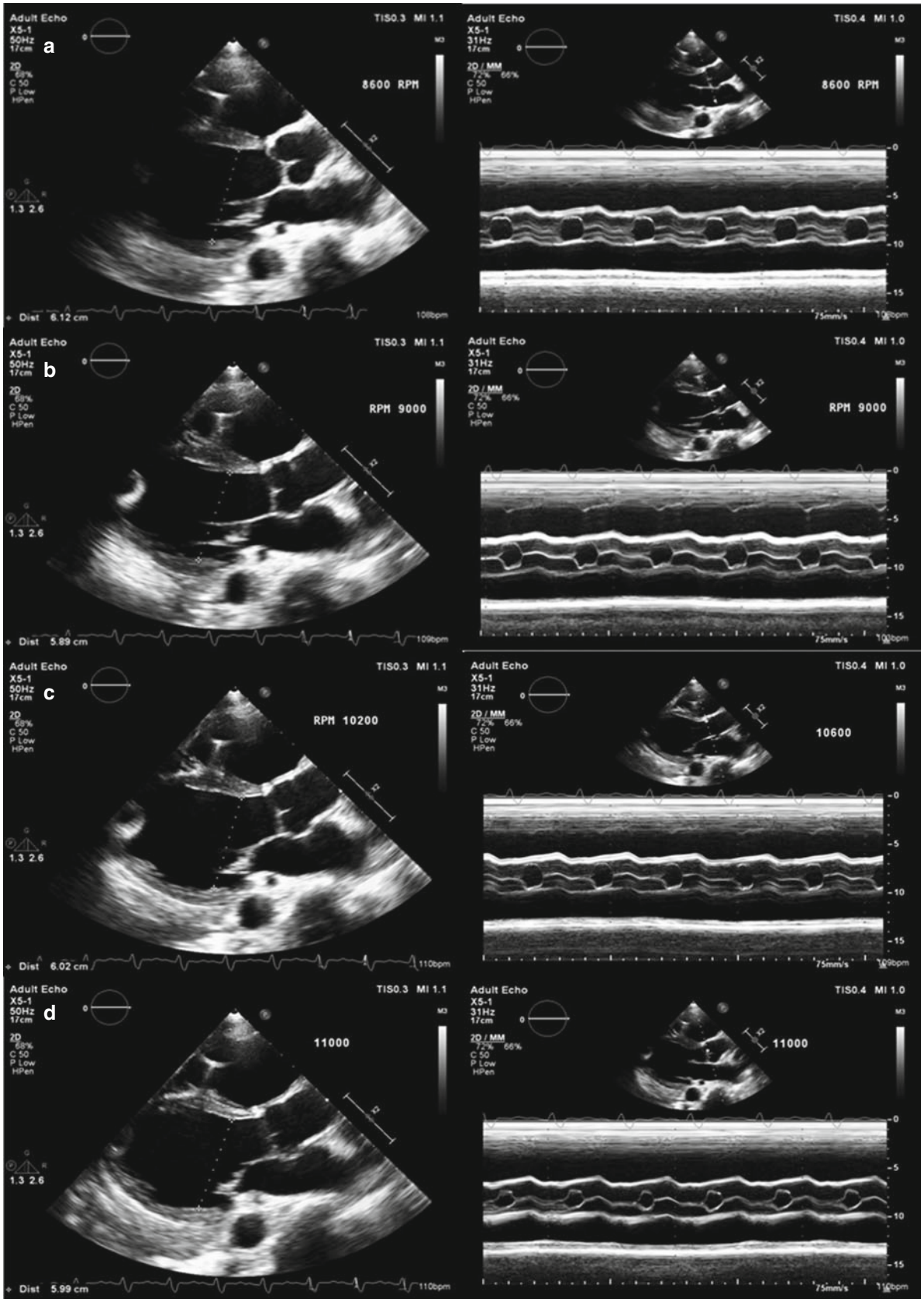

Fig. 13.8 (**a**–**d**) Serial parasternal long-axis TTE views in an LVAD pt with increasing RPMs, from 8,600 to 11,000 RPMs. In a normal ramp study, left ventricular end-diastolic dimension should decrease with increasing RPM. This series of still-frames shows inadequate LV decompression with increasing RPMs, with no significant change in LVEDd. This finding suggests underlying pump thrombosis, which was present in this patient with decompensated heart failure and elevated LDH

ECMO Weaning ("Turndown" Study)

Echocardiographic imaging is important in the determination of whether a patient can tolerate termination of mechanical support. In "turndown" studies, LVAD, ECMO or Impella mechanical support is gradually decreased and echocardiography is used to identify physiologic changes in cardiac and valvular function (Fig. 13.9a–d). In recovered myocardium, turning down mechanical circulatory flow increases preload and afterload, which can result in improved LV systolic function via Starling mechanisms while maintaining normal ventricular size. Conversely, ventricles that depend on mechanical circulatory support will dilate and fail after decreasing flows. During a successful wean, LV end diastolic dimension and systolic function do not worsen after decreasing LVAD or ECMO flow. Stroke volume by Doppler assessment of LVOT time velocity integral will also not significantly worsen in this scenario. These features suggests that the patient may tolerate discontinuation of the support. This approach is used to assess cardiac reserve prior to ECMO or Impella discontinuation in patients who may have recovered after acute cardiogenic shock and prior to LVAD explantation in the limited number of patients who experience significant myocardial recovery. In LVAD patients, some protocols propose the use of exercise or dobutamine stress testing after a favorable turndown study to provide further evidence of myocardial recovery [38].

Impella Percutaneous Ventricular Assist Device

Percutaneous ventricular assist devices can be used for short term support in patients undergoing high risk percutaneous coronary intervention or with refractory cardiogenic shock that is anticipated to be possibly reversed. The Impella catheter-based device is introduced via the femoral artery placed retrograde across the aortic valve into the left ventricle. The device removes blood from a distal port in the LV through the use of a miniaturized pump and then delivers the blood back to the ascending aorta through a more proximal port. The Tandem Heart device, a second type of percutaneous ventricular assist device, removes blood from the left atrium through a catheter delivered from the femoral vein across the

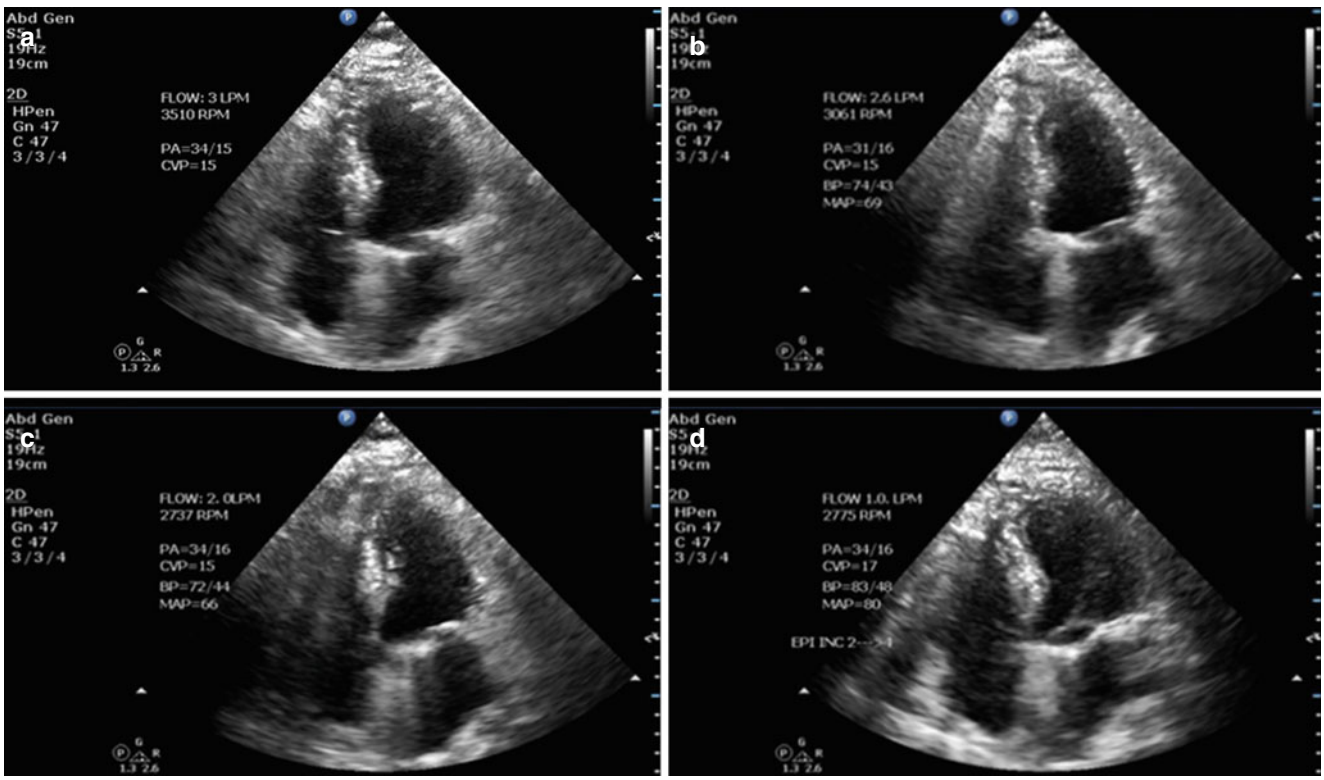

Fig. 13.9 (**a**–**d**) Apical four-chamber TTE views obtained in a patient receiving extracorporeal membrane oxygenation (*ECMO*) therapy in setting of cardiogenic shock. Serial images were obtained at decreasing levels of ECMO support: 3 L/min, 2.6 L/min, 2 L/min and 1 L/min, respectively. During this ECMO "turndown" study, LV end diastolic dimension and systolic function did not worsen after decreasing ECMO flow. This suggests patient may tolerate ECMO discontinuation

interatrial septum by use of an external pump and then delivers the blood back to the arterial circulation. Echocardiographic imaging is critical for appropriate positioning of each of these devices (Fig. 13.10a–f). For example, the inflow port at the tip of the Impella device should be 3–4 cm below the aortic valve and the outflow port should be 1.5–2 cm above the sinuses of Valsalva. The catheter should also be positioned in the mid LV

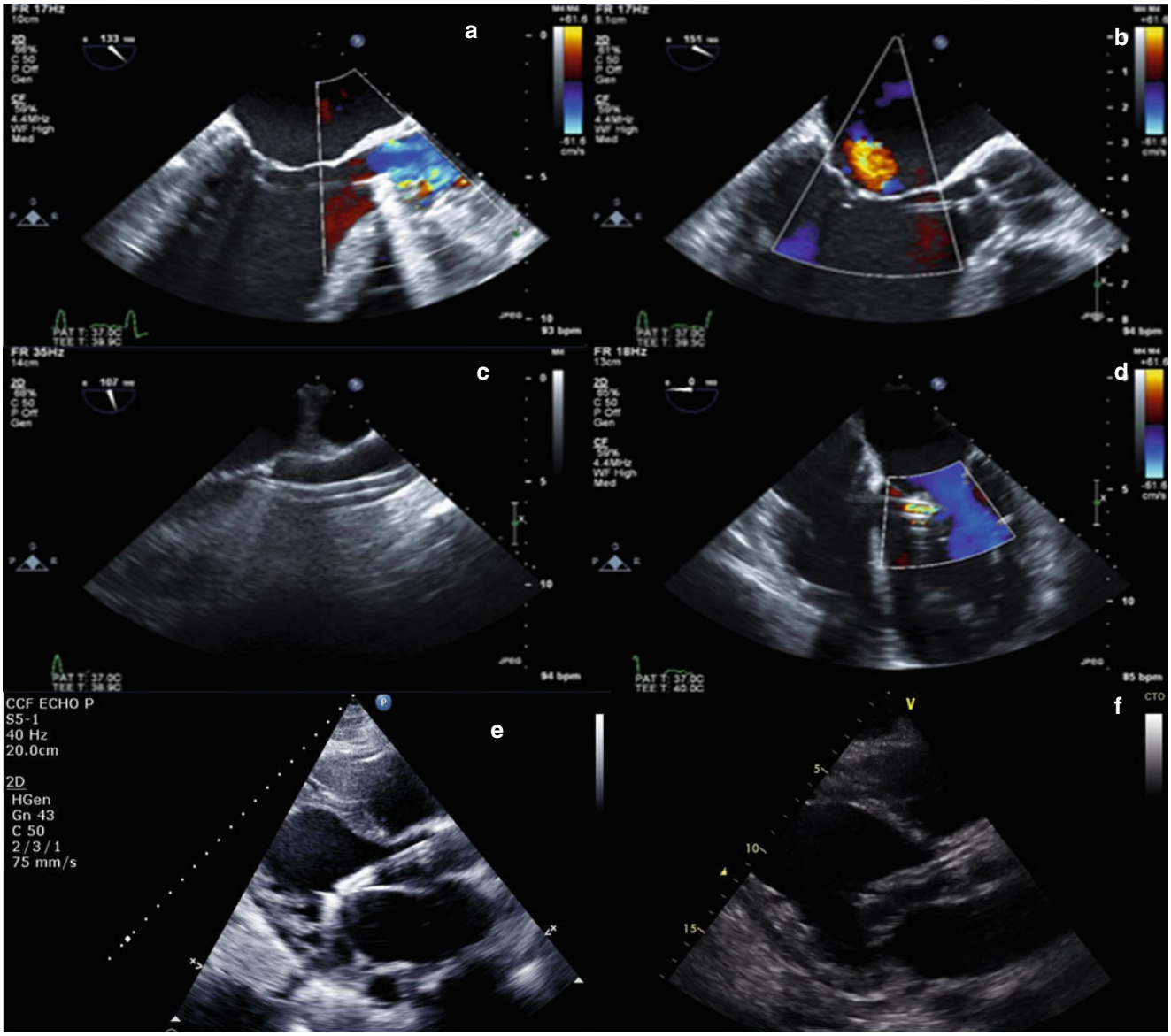

Fig. 13.10 (**a**) Mid-esophageal Long-axis TEE view at 133° during early systole showing an Impella percutaneous assist device inflow port in a suboptimal position in a patient with cardiogenic shock. The inflow port at the tip of the Impella device should be 3–4 cm below the aortic valve. The outflow port should be 1.5–2 cm above the sinuses of Valsalva. (**b**) Mid-esophageal Long-axis TEE view at 151° at end diastole showing the Impella inflow port disrupting the mitral valve leaflets resulting in diastolic mitral regurgitation. The Impella device can interfere with the chordal apparatus or the anterior mitral leaflet, leading to worsening mitral regurgitation. (**c**) Upper-esophageal Long-axis TEE view at 107° showing the Impella inflow port at the level of the aortic valve. (**d**) Mid-esophageal 4 chamber TEE view at 0° during diastole showing the Impella inflow port at the level of the Mitral valve without obstructing laminar flow at the mitral inflow. (**e**) Parasternal long-axis TTE view displaying an Impella device that is inappropriately positioned in a patient with non-ischemic cardiomyopathy who developed cardiogenic shock. The device was directed posteriorly in the ventricle with the inflow port abutting the mitral valve leaflets. The patient was at risk for disruption of the mitral leaflets by the Impella device. (**f**) Parasternal long-axis TTE view in the same patient after the Impella device was repositioned under fluoroscopy in the cardiac catheterization laboratory. The device is no longer abutting the mitral valve leaflets. The inflow port is appropriately positioned below the aortic valve and the outflow port is in the ascending aorta

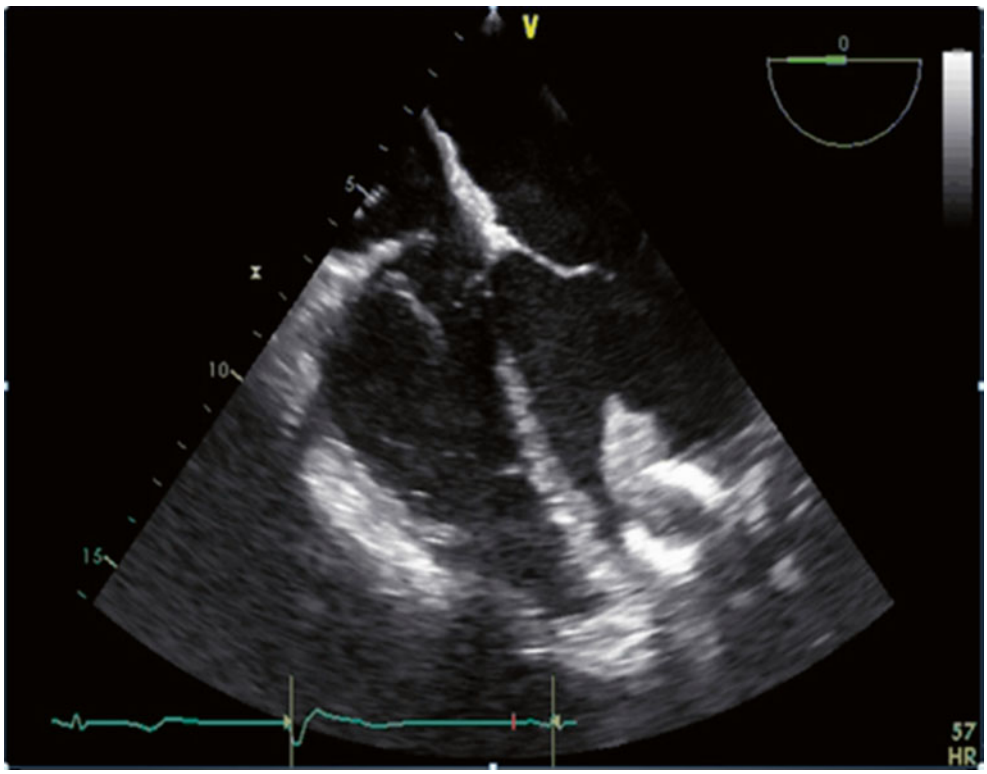

Fig. 13.11 Mid-esophageal four-chamber TEE view at 0° during end diastole showing a large mass with irregular borders attached to the LVAD inflow cannula consistent with thrombus. Anticoagulation had recently been held in this patient due to gastrointestinal hemorrhage

cavity away from the mitral valve leaflets, papillary muscles or ventricular wall. These can be assessed by TTE or TEE. TEE imaging of the Tandem Heart can guide the transeptal puncture and also insure that the catheter tip is in the mid left atrium away from pulmonary veins, left atrial appendage and mitral valve leaflets [39].

An Impella device can migrate after placement, which can significantly impair mechanical circulatory support. If a device migrates further into the ventricle, the outflow port may become positioned below the aortic valve. In a device that migrates into the aorta, the inflow port may become positioned outside of the left ventricle in the ascending aorta. In both examples, the Impella will not provide adequate mechanical circulatory support. In addition, use of Impella devices is contraindicated in moderate or greater aortic stenosis and regurgitation. The device should be used cautiously in patients with aortic root pathology, mitral stenosis, mitral regurgitation and ventricular septal defect.

Other Complications: Mobile Thrombus on LVAD Inflow Cannula

Thrombus formation on the LVAD inflow cannula will most often result in device malfunction (Fig. 13.11). Its presence can be assessed by TEE and if large, by TTE.

Transcatheter Aortic Valve Replacement for Severe Aortic Regurgitation in an LVAD Patient

As discussed above, the degree of aortic regurgitation in the patient with severe acute decompensated heart failure may be difficult to assess. In addition, it may worsen following deployment of LVAD (Fig. 13.12a). In such situations, transcatheter aortic valve replacement is an option to treat the significant aortic regurgitation which can result in cardiogenic shock despite the presence of mechanical circulatory support (Fig. 13.12b).

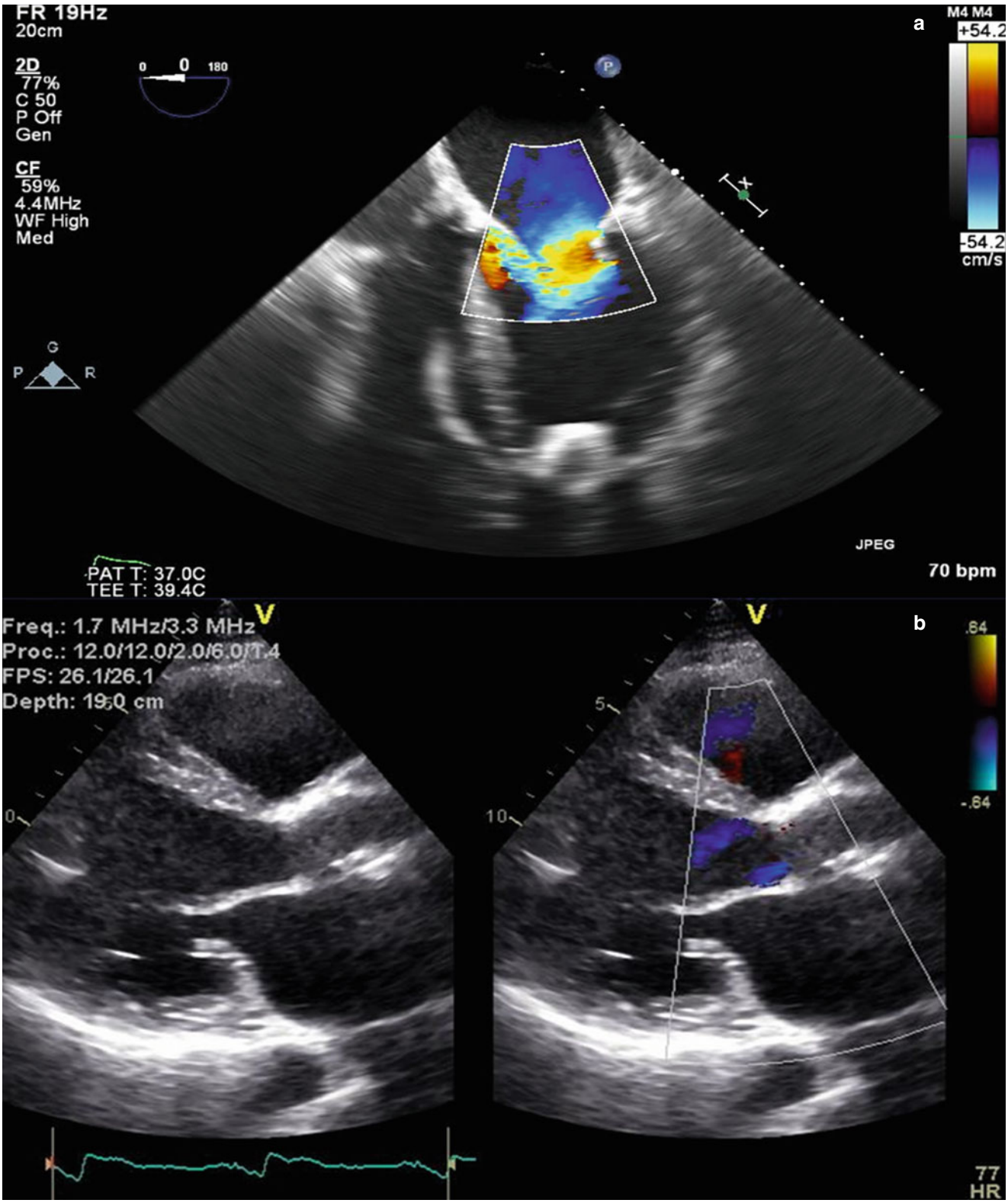

Fig. 13.12 (**a**) Mid-esophageal four-chamber TEE view at 0° during diastole in a patient who developed moderately severe aortic regurgitation post-LVAD implantation and cardiogenic shock. Laminar flow by color Doppler is seen across the mitral valve. The aortic regurgitation jet is eccentric and posteriorly-directed with increased turbulence, impacting the anterior mitral valve leaflet. The inflow cannula appears to have optimal orientation in reference to the adjacent myocardium and mitral valve. (**b**) Parasternal long axis TTE view during diastole with color comparison on the right demonstrating resolution of aortic regurgitation with absence of diastolic flow into the LVOT after transcatheter aortic valve replacement, which was performed via trans-femoral approach as a salvage procedure in an LVAD patient who developed cardiogenic shock from aortic regurgitation. Inflow cannula can be appreciated directly across from the mitral valve

References

1. Kirklin JK, Naftel DC, Pagani FD, Kormos RL, Stevenson LW, Blume ED, Miller MA, Timothy Baldwin J, Young JB. Sixth INTERMACS annual report: a 10,000-patient database. J Heart Lung Transplant. 2014;33(6):555–64.
2. Feldman D, Pamboukian SV, Teuteberg JJ, Birks E, Lietz K, Moore SA, Morgan JA, Arabia F, Bauman ME, Buchholz HW, Deng M, Dickstein ML, El-Banayosy A, Elliot T, Goldstein DJ, Grady KL, Jones K, Hryniewicz K, John R, Kaan A, Kusne S, Loebe M, Massicotte MP, Moazami N, Mohacsi P, Mooney M, Nelson T, Pagani F, Perry W, Potapov EV, Eduardo Rame J, Russell SD, Sorensen EN, Sun B, Strueber M, Mangi AA, Petty MG, Rogers J. The 2013 International Society for Heart and Lung Transplantation Guidelines for mechanical circulatory support: executive summary. J Heart Lung Transplant. 2013;32(2):157–87.
3. Slaughter MS, Pagani FD, Rogers JG, Miller LW, Sun B, Russell SD, Starling RC, Chen L, Boyle AJ, Chillcott S, Adamson RM, Blood MS, Camacho MT, Idrissi KA, Petty M, Sobieski M, Wright S, Myers TJ, Farrar DJ. Clinical management of continuous-flow left ventricular assist devices in advanced heart failure. J Heart Lung Transplant. 2010;29(4 Suppl):S1–39.
4. Rich JD. Right ventricular failure in patients with left ventricular assist devices. Cardiol Clin. 2012;30(2):291–302.
5. Patlolla B, Beygui R, Haddad F. Right-ventricular failure following left ventricle assist device implantation. Curr Opin Cardiol. 2013;28(2):223–33. doi:10.1097/HCO.0b013e32835dd12c.
6. Hayek S, Sims DB, Markham DW, Butler J, Kalogeropoulos AP. Assessment of right ventricular function in left ventricular assist device candidates. Circ Cardiovasc Imaging. 2014;7(2):379–89.
7. Fitzpatrick 3rd JR, Frederick JR, Hiesinger W, Hsu VM, McCormick RC, Kozin ED, Laporte CM, O'Hara ML, Howell E, Dougherty D, Cohen JE, Southerland KW, Howard JL, Paulson EC, Acker MA, Morris RJ, Woo YJ. Early planned institution of biventricular mechanical circulatory support results in improved outcomes compared with delayed conversion of a left ventricular assist device to a biventricular assist device. J Thorac Cardiovasc Surg. 2009;137(4):971–7.
8. Chen JM, Levin HR, Rose EA, Addonizio LJ, Landry DW, Sistino JJ, Michler RE, Oz MC. Experience with right ventricular assist devices for perioperative right-sided circulatory failure. Ann Thorac Surg. 1996;61(1):305–10; discussion 311-303.
9. Ochiai Y, McCarthy PM, Smedira NG, Banbury MK, Navia JL, Feng J, Hsu AP, Yeager ML, Buda T, Hoercher KJ, Howard MW, Takagaki M, Doi K, Fukamachi K. Predictors of severe right ventricular failure after implantable left ventricular assist device insertion: analysis of 245 patients. Circulation. 2002;106(12 Suppl 1):I198–202.
10. Matthews JC, Koelling TM, Pagani FD, Aaronson KD. The right ventricular failure risk score a pre-operative tool for assessing the risk of right ventricular failure in left ventricular assist device candidates. J Am Coll Cardiol. 2008;51(22):2163–72.
11. Farrar DJ, Compton PG, Hershon JJ, Fonger JD, Hill JD. Right heart interaction with the mechanically assisted left heart. World J Surg. 1985;9(1):89–102.
12. Maeder MT, Leet A, Ross A, Esmore D, Kaye DM. Changes in right ventricular function during continuous-flow left ventricular assist device support [corrected]. J Heart Lung Transplant. 2009;28(4):360–6.
13. Shapiro GC, Leibowitz DW, Oz MC, Weslow RG, Di Tullio MR, Homma S. Diagnosis of patent foramen ovale with transesophageal echocardiography in a patient supported with a left ventricular assist device. J Heart Lung Transplant. 1995;14(3):594–7.
14. Rasalingam R, Johnson SN, Bilhorn KR, Huang PH, Makan M, Moazami N, Perez JE. Transthoracic echocardiographic assessment of continuous-flow left ventricular assist devices. J Am Soc Echocardiogr. 2011;24(2):135–48.
15. Patangi SO, George A, Pauli H, O'Leary D, Roysam C, Butt T, Schueler S, Prabhu M, MacGowan G. Management issues during HeartWare left ventricular assist device implantation and the role of transesophageal echocardiography. Ann Card Anaesth. 2013;16(4):259–67.
16. Ferns J, Dowling R, Bhat G. Evaluation of a patient with left ventricular assist device dysfunction. ASAIO J. 2001;47(6):696–8.
17. Robertson JO, Grau-Sepulveda MV, Okada S, O'Brien SM, Matthew Brennan J, Shah AS, Itoh A, Damiano RJ, Prasad S, Silvestry SC. Concomitant tricuspid valve surgery during implantation of continuous-flow left ventricular assist devices: a Society of Thoracic Surgeons database analysis. J Heart Lung Transplant. 2014;33(6):609–17.
18. Kirklin JK, Naftel DC, Kormos RL, Stevenson LW, Pagani FD, Miller MA, Ulisney KL, Baldwin JT, Young JB. Second INTERMACS annual report: more than 1,000 primary left ventricular assist device implants. J Heart Lung Transplant. 2010;29(1):1–10.
19. John R, Mantz K, Eckman P, Rose A, May-Newman K. Aortic valve pathophysiology during left ventricular assist device support. J Heart Lung Transplant. 2010;29(12):1321–9.
20. Samuels LE, Thomas MP, Holmes EC, Narula J, Fitzpatrick J, Wood D, Fyfe B, Wechsler AS. Insufficiency of the native aortic valve and left ventricular assist system inflow valve after support with an implantable left ventricular assist system: signs, symptoms, and concerns. J Thorac Cardiovasc Surg. 2001;122(2):380–1.
21. Cowger J, Pagani FD, Haft JW, Romano MA, Aaronson KD, Kolias TJ. The development of aortic insufficiency in left ventricular assist device-supported patients. Circ Heart Fail. 2010;3(6):668–74.
22. Rajagopal K, Daneshmand MA, Patel CB, Ganapathi AM, Schechter MA, Rogers JG, Milano CA. Natural history and clinical effect of aortic valve regurgitation after left ventricular assist device implantation. J Thorac Cardiovasc Surg. 2013;145(5):1373–9.
23. Chapman CB, Allana S, Sweitzer NK, Kohmoto T, Murray M, Murray D, Johnson M, Rahko PS. Effects of the HeartMate II left ventricular assist device as observed by serial echocardiography. Echocardiography. 2013;30(5):513–20.
24. Lee S, Kamdar F, Madlon-Kay R, Boyle A, Colvin-Adams M, Pritzker M, John R. Effects of the HeartMate II continuous-flow left ventricular assist device on right ventricular function. J Heart Lung Transplant. 2010;29(2):209–15.
25. Kormos RL, Teuteberg JJ, Pagani FD, Russell SD, John R, Miller LW, Massey T, Milano CA, Moazami N, Sundareswaran KS, Farrar DJ. Right ventricular failure in patients with the HeartMate II continuous-flow left ventricular assist device: incidence, risk factors, and effect on outcomes. J Thorac Cardiovasc Surg. 2010;139(5):1316–24.
26. Dang NC, Topkara VK, Mercando M, Kay J, Kruger KH, Aboodi MS, Oz MC, Naka Y. Right heart failure after left ventricular assist device implantation in patients with chronic congestive heart failure. J Heart Lung Transplant. 2006;25(1):1–6.
27. Moon MR, Bolger AF, DeAnda A, Komeda M, Daughters 2nd GT, Nikolic SD, Miller DC, Ingels Jr NB. Septal function during left ventricular unloading. Circulation. 1997;95(5):1320–7.
28. Connelly JH, Abrams J, Klima T, Vaughn WK, Frazier OH. Acquired commissural fusion of aortic valves in patients with left ventricular assist devices. J Heart Lung Transplant. 2003;22(12):1291–5.
29. Mudd JO, Cuda JD, Halushka M, Soderlund KA, Conte JV, Russell SD. Fusion of aortic valve commissures in patients supported by a continuous axial flow left ventricular assist device. J Heart Lung Transplant. 2008;27(12):1269–74.
30. Baradarian S, Dembitsky WP, Jaski B, Abolhoda A, Adamson R, Chillcot S, Daily PO. Left ventricular outflow tract obstruction

associated with chronic ventricular assist device support. ASAIO J. 2002;48(6):665–7.
31. Rose AG, Connelly JH, Park SJ, Frazier OH, Miller LW, Ormaza S. Total left ventricular outflow tract obstruction due to left ventricular assist device-induced sub-aortic thrombosis in 2 patients with aortic valve bioprosthesis. J Heart Lung Transplant. 2003;22(5):594–9.
32. Deo SV, Sharma V, Cho YH, Shah IK, Park SJ. De novo aortic insufficiency during long-term support on a left ventricular assist device: a systematic review and meta-analysis. ASAIO J. 2014; 60(2):183–8.
33. Pagani FD, Miller LW, Russell SD, Aaronson KD, John R, Boyle AJ, Conte JV, Bogaev RC, MacGillivray TE, Naka Y, Mancini D, Massey HT, Chen L, Klodell CT, Aranda JM, Moazami N, Ewald GA, Farrar DJ, Frazier OH. Extended mechanical circulatory support with a continuous-flow rotary left ventricular assist device. J Am Coll Cardiol. 2009;54(4):312–21.
34. Bartoli CR, Ghotra AS, Pachika AR, Birks EJ, McCants KC. Hematologic markers better predict left ventricular assist device thrombosis than echocardiographic or pump parameters. Thorac Cardiovasc Surg. 2014;62(5):414–8.
35. Goldstein DJ, John R, Salerno C, Silvestry S, Moazami N, Horstmanshof D, Adamson R, Boyle A, Zucker M, Rogers J, Russell S, Long J, Pagani F, Jorde U. Algorithm for the diagnosis and management of suspected pump thrombus. J Heart Lung Transplant. 2013;32(7):667–70.
36. Uriel N, Morrison KA, Garan AR, Kato TS, Yuzefpolskaya M, Latif F, Restaino SW, Mancini DM, Flannery M, Takayama H, John R, Colombo PC, Naka Y, Jorde UP. Development of a novel echocardiography ramp test for speed optimization and diagnosis of device thrombosis in continuous-flow left ventricular assist devices: the Columbia ramp study. J Am Coll Cardiol. 2012;60(18): 1764–75.
37. Estep JD, Vivo RP, Cordero-Reyes AM, Bhimaraj A, Trachtenberg BH, Torre-Amione G, Chang SM, Elias B, Bruckner BA, Suarez EE, Loebe M. A simplified echocardiographic technique for detecting continuous-flow left ventricular assist device malfunction due to pump thrombosis. J Heart Lung Transplant. 2014;33(6):575–86.
38. Khan T, Delgado RM, Radovancevic B, Torre-Amione G, Abrams J, Miller K, Myers T, Okerberg K, Stetson SJ, Gregoric I, Hernandez A, Frazier OH. Dobutamine stress echocardiography predicts myocardial improvement in patients supported by left ventricular assist devices (LVADs): hemodynamic and histologic evidence of improvement before LVAD explantation. J Heart Lung Transplant. 2003;22(2):137–46.
39. Pretorius M, Hughes AK, Stahlman MB, Saavedra PJ, Deegan RJ, Greelish JP, Zhao DX. Placement of the TandemHeart percutaneous left ventricular assist device. Anesth Analg. 2006;103(6):1412–3.

Index

M.H. Picard et al. (eds.), *Intraprocedural Imaging of Cardiovascular Interventions*, DOI 10.1007/978-3-319-29428-5